University of Stuttgart
Germany

COMPARATIVE PHYSIOLOGICAL PARAMETERS FOR THE ANALYSIS OF H_2 PRODUCTION BY THE MICROALGA *CHLAMYDOMONAS REINHARDTII* AND THE PHOTOSYNTHETIC PURPLE BACTERIUM *RHODOSPIRILLUM RUBRUM*

Von der Fakultät Energie-, Verfahrens- und Biotechnik der Universität Stuttgart zur Erlangung der Würde einer Doktorin der Naturwissenschaften (Dr. rer. nat.) genehmigte Abhandlung

Vorgelegt von

Shreya Arun Shaw
aus Calcutta, (Indien)

Hauptberichter: Prof. Dr. Robin Ghosh

Mitberichter: PD Dr. Michael Schweikert

Tag der mündlichen Prüfung: 17th Dezember 2019

Institut für Biomaterialien und biomolekulare Systeme der Universität Stuttgart
Abteilung Bioenergetik
Pfaffenwaldring 57, 70569 Stuttgart

2019

Erklärung über die Eigenständigkeit der Dissertation

Ich versichere, dass ich die vorliegende Arbeit mit dem Titel:

"Comparative physiological parameters for the analysis of H_2 production by the microalga *Chlamydomonas reinhardtii* and the photosynthetic purple bacterium *Rhodospirillum rubrum*"

selbständig verfasst und keine anderen als die angegebenen Quellen und Hilfsmittel benutzt habe; aus fremden Quellen entnommene Passagen und Gedanken sind als solche kenntlich gemacht.

Declaration of Authorship

I hereby certify that the dissertation entitled:

"Comparative physiological parameters for the analysis of H_2 production by the microalga *Chlamydomonas reinhardtii* and the photosynthetic purple bacterium *Rhodospirillum rubrum*"

is entirely my own work except where otherwise indicated. Passages and ideas from other sources have been clearly quoted.

Name/Name: Shreya Arun Shaw

Unterschrift/Signed:

Datum/Date: Stuttgart, 04.10.2019

TABLE OF CONTENTS

Abbreviations

A_{660} (4 mm) or A_{882} (4 mm)	absorption (or optical density) at 660 nm (or 882 nm) taken with a 4 mm path-length cuvette
ABTS	2, 2'-azino-bis(3-ethylbenzthiazoline-6-sulfonic acid)
ACK	acetate kinase
alphaA	alpha amylase
Amp_{200}	200 μg/ml ampicillin concentration
AmyG	amyloglucosidase
AOX	alternative oxidase
ARS	aryl-sulfatase
BChla	bacteriochlorophyll a
βOG	*n*-octyl-ß-D-glucoside
BSA	bovine serum albumin
CFU	colony forming unit
Chl	chlorophyll
CIP	calf intestinal alkaline phosphatase
CM	cytoplasmic membrane
CNR	National Research Council (Italy)
COX	cytochrome oxidase
crt	carotenoid
Cyt c_2	cytochrome c_2
DCM	dichloromethane
EDTA	ethylenediamine tetraacetic acid
EM	electron microscopy
ETC	electron transport chain
EtOH	ethanol
FID	flame ionization detector

GC	gas chromatograph/ chromatography
GL	glass thread count
GOX	glucose oxidase
HPLC	high performance liquid chromatography
HRP	horseradish peroxidase
ICM	intracytoplasmic membrane
$I_{(av)}$	average light intensity
ITS	internal transcribed spacer regions
LB-Medium	Luria-Bertani medium
LHC I, II	light-harvesting complex I, II
LSJS	Laboratory Screw Joint systems
LDAO	lauryldimethylamine-N-oxide
MeOH	methanol
M2S	modified M-medium containing 40 mM succinate
M2SF	M2S medium + 0.3% (w/v) fructose
MS	mass spectroscopy
NCBI	National Center for Biotechnologial Information (USA)
NREL	The National Renewable Energy Laboratory (USA)
OD	Optical density
PAGE	polyacrylamide gel electrophoresis
PBS	phosphate buffered saline
PQ	plastoquinone
PSI, PSII	photosystem I, II
PMSF	phenyl methyl sulfonyl fluoride
RC	reaction centre
ROS	reactive oxygen species
SDS	sodium dodecylsulphate

SHAM	salicyl hydroxamic acid
RF	response factor
RT	room temperature
STP	standard temperature and pressure
TAE	Tris-acetate EDTA: 1×TAE: 40 mM Tris-acetate + 1 mM EDTA
TAP	Tris-acetate-phosphate
TCA	trichloroacetic acid
TCD	thermal conductivity detector
TCP	Tris-citrate phosphate medium
TE	Tris-EDTA: 10×TE: 100 mM Tris-HCl pH 8.0 + 10 mM EDTA,
Tet_4	4 μg/ml tetracycline-HCl concentration
Tet^R	tetracycline-resistant
TLC	thin-layer chromatography
UQ	ubiquinone
UQH_2	ubiquinol

Abstract

The main focus of this thesis in Part I is the investigation and establishment of growth benchmarks to enable better comparison of H_2 evolution in the microalga *Chlamydomonas reinhardtii* with other non-related bioH_2 producers, especially the purple bacterium *Rhodospirillum rubrum*. For *R. rubrum*, the physiological benchmarks have been worked out by the Ghosh group (Grammel, H., Gilles, E.D. and Ghosh, R. (2003). *Appl. Environ. Microbiol.* 69, 6577-6586.)

The major objectives adopted towards the fulfilment of our goal have been as follows: (1) the establishment of standard growth and aerobic culture conditions for *C. reinhardtii* strain SAG 18.79 (CC-1418) for establishment of biochemical benchmarks and (2) evaluating the H_2 production capacity of *C. reinhardtii* on the basis of biochemical benchmarks and culture volume considerations in cultures grown under sulphur depletion conditions. Extensive method development has been carried out to meet these objectives.

First, commercially available gas-tight (conducting) tubing and connections were used to construct professional small-scale gas sampling vessels. Secondly, the calibration of the apparatus was performed by measuring the H_2 evolved from the well-known reaction of $NaBH_4$ with water. With the H_2 evolution data, I demonstrated that, the application of gas laws enables determination of an unknown gas (here H_2) concentration by gas chromatography, in the absence of standard gas calibration mixtures. Thirdly, enzymatic and colorimetric assays were developed for the measurement of key substrates: (1) starch in *C. reinhardtii*; and (2) fructose in *R. rubrum*. A comprehensive protocol for the extraction and hydrolysis of starch from cells, and the assay of glucose by the glucose oxidase-horseradish peroxidase enzyme reaction along with chromogenic substrate 2,2'-azino-bis(3-ethylbenzthiazoline-6-sulfonic acid) (ABTS) has been described. For the determination of fructose, the well-known Kulka method was substantially modified and adapted to a small scale assay, presented in Part III of this thesis. The modified assay contains a smaller volume and a safer formulation (5.4 M) of HCl, than the original method, and is shown to be suitable for use in high-throughput systems biology or enzymatic applications. The assay was used for monitoring the consumption of fructose during growth experiments as well as during the H_2 production phase of *R. rubrum*. Additionally, the use of this assay has been extended for the rapid measurement of the phosphorylated sugar 1-deoxy-D-xylulose-5-phosphate, obviating the necessity of lengthy HPLC analysis. This work has now been published.

With the use of methodologies established above, we have determined a physiological dataset for *C. reinhardtii* which can be objectively compared to the reference data from *R.*

rubrum. For *C. reinhardtii*, we present a systematic comparison of "benchmark" parameters such as biomass units, cell number, chlorophyll, starch and protein content of cultures measured at two different light intensities. I show that, a simple measurable parameter, the culture turbidity, can be interconverted via linear curve fitting functions within the exponential growth phase to estimate any of the benchmark parameters at both light intensities. To our knowledge, no systematic correlation of growth parameters for *C. reinhardtii* has ever been published.

A comparison of the amounts and rates of H_2 produced by the *C. reinhardtii* strain SAG 18.79 has been made under both "intermediate" light intensity (70 µmol photons/m^2/s) and "very low" light intensity (5 µmol photons/m^2/s). The values obtained, have been compared to those of other bioH_2 producers in terms of culture volume and biomass wherever available.

The kinetics of H_2 accumulation in the bioreactor headspace for *C. reinhardtii* strain SAG 18.79 during sulphur depletion, showed a H_2 production phase lasting 40 - 75 h depending on the light intensity, followed by an equivalent H_2 uptake phase. For most of the widely studied strains, H_2 uptake has been observed only under special conditions. For the strain used here, H_2 uptake is considerable and may be a good model for studying this phenomenon.

A discussion of the present state of bioH_2 technology and the degree of improvement required to achieve conventional production levels have been calculated at the end of Part I.

In purple bacteria, H_2 production occurs primarily via the nitrogenase, which is only expressed at limiting [NH_4^+]. In Part II of the thesis, the effect of varied [NH_4^+] on *R. rubrum* growth and *nif* gene expression was examined under photosynthetic, anaerobic and dark, semi-aerobic conditions by the use of a newly developed, modified M2SF medium- here designated as M2NF medium. I show that *nif* gene expression in *R. rubrum* is regulated by [NH_4^+] within the concentration range of 0-10 mM. At the highest end of this concentration range, *nif* gene expression is totally repressed. At intermediate levels of [NH_4^+], *nif* gene expression occurs almost linearly at the expense of lower attainable cell densities, due to nitrogen limitation. This work forms the basis for further examination of *nif* gene regulation and consequently H_2 production by use of other N- sources such as amino acids.

Zusammenfassung

Im ersten Abschnitt (Teil I) dieser Dissertationsschrift richtet sich der Hauptfokus auf die Etablierung allgemeiner Vergleichs- und Referenzwerte (hier als Benchmarks bezeichnet) für physiologische Parameter der Grünalge *Chlamydomonas reinhardtii*. Diese Benchmarks sollten einen objektiven Vergleich der Wasserstoff-Produktionskapazität von *C. reinhardtii* mit der anderer, nicht verwandter H_2-Produzenten, hier vor allem des Purpurbakteriums *Rhodospirillum rubrum*, ermöglichen. Für *R. rubrum* sind die physiologischen Benchmarks bereits von der Ghosh-Gruppe etabliert worden (Grammel, H., Gilles, E.D. and Ghosh, R. (2003). *Appl. Environ. Microbiol.* 69, 6577-6586.)

Zum Erreichen dieses Ziels wurden (1) Standard-Wachstumsbedingungen für den *C. reinhardtii* Stamm SAG 18.79 (CC-1418) etabliert, um die biochemischen Benchmarks zu bestimmen und (2) die H_2-Produktionskapazität von *C. reinhardtii* unter Schwefel-limitierten Wachstumsbedingungen ermittelt. Hierfür wurden neue Analyse-Methoden entwickelt.

So wurden zunächst kommerziell erhältliche, gasdichte und leitfähige Schläuche und Verbindungsteile verwendet, um klein-skalige Gasproben-Entnahme-Gefäße zu konstruieren. Mit diesem Setup konnte, mit Hilfe der H_2-produzierenden Reaktion von Natriumborhydrid ($NaBH_4$) mit Wasser eine Kalibrierung der H_2-Messung durchgeführt werden. Es konnten thermodynamische Gasgesetze angewandt werden, um unbekannte Gaskonzentrationen (hier H_2) mittels Gaschromatographie bestimmen zu können, ohne auf käufliche Gas-Kalibrierungs-Mischungen zurückgreifen zu müssen. Außerdem wurden enzymatische und kolorimetrische Tests zur Messung der wichtigsten Nährsubstrate - Stärke in *C. reinhardtii* und Fruktose in *R. rubrum* - entwickelt. Ein verbessertes Protokoll zu Stärke-Extraktion aus Zellen, Hydrolyse und anschließendem Glukose-Test mit Hilfe der Glukose Oxidase / Meerrettich Peroxidase Enzymreaktion und dem chromogenen Substrat 2,2'-Azino-bis(3-ethylbenzthiazolin-6-sulfonsäure) (ABTS) wird hier beschrieben. Zur Fruktose-Bestimmung wurde die bekannte Kulka-Methode modifiziert, was in Teil III dieser Arbeit beschrieben wird. Unser modifizierter Kulka-Assay kann mit kleineren Volumen durchgeführt werden und ist sicherer als die Original-Methode (da er nur 5,4 M HCl anstelle konzentrierter HCl verwendet). Der Fruktose-Assay wurde verwendet, um den Fruktose-Verbrauch von *R. rubrum* während Wachstums- und H_2-Produktions-Experimenten zu beobachten. Außerdem wurde der Assay an die Messung des phosphorylierten Zuckers 1-Deoxy-D-xylulose-5-phosphat, der sonst nur mittels zeitaufwendiger HPLC-Analyse quantifiziert werden kann, angepasst. Eine Publikation zu dieser Arbeit wurde veröffentlicht.

Mit Hilfe der oben beschriebenen Methoden wurde für die physiologischen Parameter von *C. reinhardtii* ein Datensatz entwickelt, der nun objektiv mit den Referenzwerten von *R. rubrum* verglichen werden kann. Diese Arbeit zeigt einen systematischen Vergleich der für *C. reinhardtii* ermittelten Benchmark-Parameter, wie z.B. Referenzwerte für die Biomasse, die Zellzahl und den Chlorophyll-, Stärke- und Protein-Gehalt, die für Kulturen bestimmt wurden, die unter zwei verschiedenen Lichtintensitäten inkubiert wurden. Für Kulturen in der exponentiellen Phase können nun, mit Hilfe dieser Benchmarks, aus einem einfach zu messenden Parameter - der Trübung der Kultur - alle anderen Parameter durch lineares Fitting ermittelt werden. Unseres Wissens nach ist diese Art der systematischen Korrelation verschiedener Wachstumsparameter für *C. reinhardtii* bislang nicht veröffentlicht worden.

In dieser Arbeit stelle ich einen Vergleich der H_2-Mengen und -Produktionsraten vom *C. reinhardtii* Stamm SAG 18.79 vor, der unter den zwei verschiedenen Wachstumsbedingungen *"intermediate" light intensity* (70 µmol Photonen/m^2/s) und *"very low" light intensity* (5 µmol Photonen/m^2/s) inkubiert wurde. Die Messung der Kinetik der H_2-Akkumulation im Gasraum (*headspace*) der *C. reinhardtii* SAG 18.79 Kulturflasche während Schwefel-limitierter Wachstumsbedingungen zeigte eine H_2-Produktionsphase, die, je nach Lichtintensität, zwischen 40 und 75 Stunden andauerte, und eine darauffolgende H_2-Wiederaufnahmephase. Bei den meisten untersuchten Stämmen wurde bislang H_2-Aufnahme nur unter sehr speziellen Bedingungen beobachtet. In dem hier verwendeten Stamm gab es allerdings eine beträchtliche H_2-Aufnahme, was diesen Stamm zu einem guten Modellsystem für dieses Phänomen machen könnte.

Teil II dieser Arbeit beschäftigt sich mit der H_2-Produktion in Purpurbakterien, die hauptsächlich durch die Nitrogenase vermittelt wird. Die Nitrogenase wird allerdings nur unter limitierenden NH_4^+-Konzentrationen exprimiert. Hier wurde daher die Wirkung verschiedener [NH_4^+] auf das Wachstum und die Expression der Nitrogenase (*nif*) Gene von *R. rubrum* unter verschiedenen Wachstumsbedingungen (anaerob/photosynthetisch bzw. semi-aerob im Dunkeln) untersucht, und dabei ein neues, modifiziertes M2SF-Medium (M2NF) verwendet. Die Regulation der *nif* Genexpression fand dabei innerhalb eines NH_4^+ Konzentrationsbereichs von 0-10 mM statt. Bei 10 mM NH_4^+ ist die *nif* Genexpression komplett reprimiert. Im mittleren Konzentrationsbereich steigt die *nif* Genexpression nahezu linear mit sinkender NH_4^+ Konzentration. Die Stickstoff-Limitierung führte hier allerdings zu niedrigeren Zelldichten. Die vorliegende Arbeit soll als Basis für weitere Untersuchungen der *nif* Genregulation und damit der H_2-Produktion mit Hilfe anderer Stickstoff-Quellen (z.B. Aminosäuren) dienen.

PART I.

Establishment of physiological "benchmarks" for H_2 evolution in *Chlamydomonas reinhardtii*

1. INTRODUCTION

1.1. Overview of the physiology of *Chlamydomonas reinhardtii*

C. reinhardtii is a unicellular eukaryotic photosynthetic alga that has been described as the ''unicellular yeast'' (See Rochaix, 1995). It possesses a simple life-cycle where haploid cells can be rapidly vegetatively propagated. This has contributed to its widespread utility as a model organism for studying eukaryotic photosynthesis, chloroplast biogenesis, flagellar motility as well as for biotechnological applications (See Harris, 2001). Wild-type cells are oval-shaped and typically of the dimensions of 10 µm x 3 µm, and possess two anterior flagella. The cells contain a single cup-shaped chloroplast. The wild-type cells have a total volume of 122 μm^3 where the chloroplast accounts for 30% of the total (Hummel *et al.*, 2012). The pyrenoid, a distinct body contained within the chloroplast, is the site of CO_2 fixation and the dark reactions of photosynthesis.

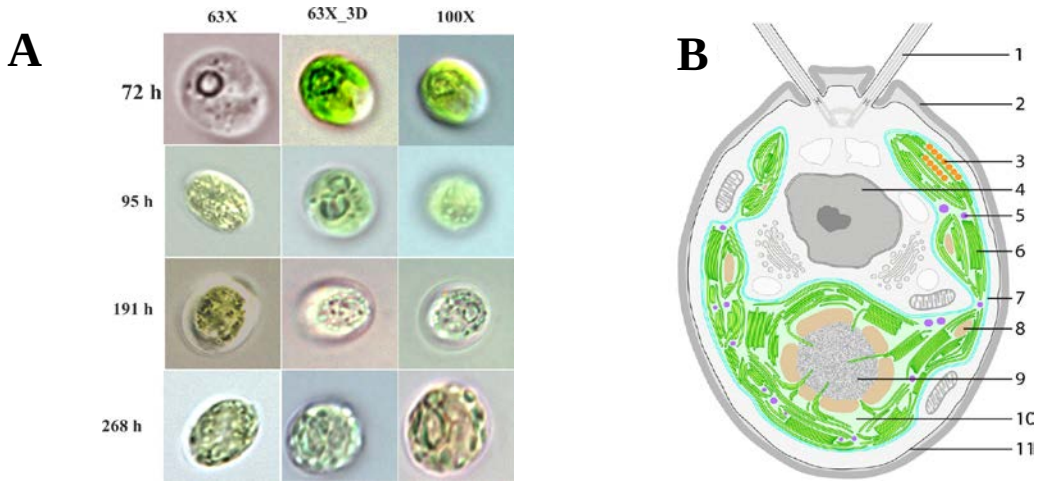

Fig. 1.1. (A) Phase contrast microscopy image of a *C. reinhardtii* cell taken at a total magnification of 630x and 1000x **(B)** Cross-section diagram of a *C.* reinhardtii cell. The chloroplast is shown in green: (1) flagellum, (2) cell wall, (3) eyespot, (4) nucleus, (5) plastoglobule, (6) thylakoids, (7) chloroplast envelope, (8) starch granule, (9) pyrenoid, (10) chloroplast stroma, (11) plasma membrane (taken from Engel *et al.*, 2015)).

C. reinhardtii contains three genetic systems: (1) the 120 Mb nuclear genome (Merchant *et al.*, 2007) present on 17 haploid chromosomes, (2) the 0.2 Mb chloroplast

genome (Maul *et al.*, 2002) and (3) the 15.8 kb mitochondrial genome (Gray and Boer, 1988). All three chromosomes are amenable to genetic manipulation via DNA transformation.

C. reinhardtii grows photoautotrophically (CO_2 as sole C-source) and also photoheterotrophically (acetate as C-source), as well as photomixotrophically (CO_2 plus acetate as C- source). These varied modes of nutrition make it a valuable organism for the study of mutants defective in photosynthetic metabolism. *C. reinhardtii* is also unusual for a photosynthetic eukaryote in that glycolysis is compartmented (Klein, 1986), occurring partly in the chloroplast stroma and partly in the cytoplasm. In addition, it also expresses the four major enzymes for fermentative metabolism of pyruvate (Mus *et al.*, 2007) which include pyruvate formate lyase (PFL1), pyruvate ferredoxin oxidoreductase (PFR1), lactate dehydrogenase, and pyruvate decarboxylase (PDC1), which are characteristic of anaerobic prokaryotic metabolism, and can thus show fermentative growth both in light and dark (heterotrophic growth) conditions, where H_2 and formate, respectively, are the major fermentative end products (Gfeller and Gibbs, 1984; Gibbs *et al.*, 1986).

1.1.1. Overview of photosynthesis in *C. reinhardtii*

C. reinhardtii performs oxygenic photosynthesis including the water-splitting reaction using a Z-scheme, analogously to higher plants (Fig. 1.2). The primary process takes place in the thylakoid membrane and a light-independent Calvin cycle occurs in the chloroplast stroma.

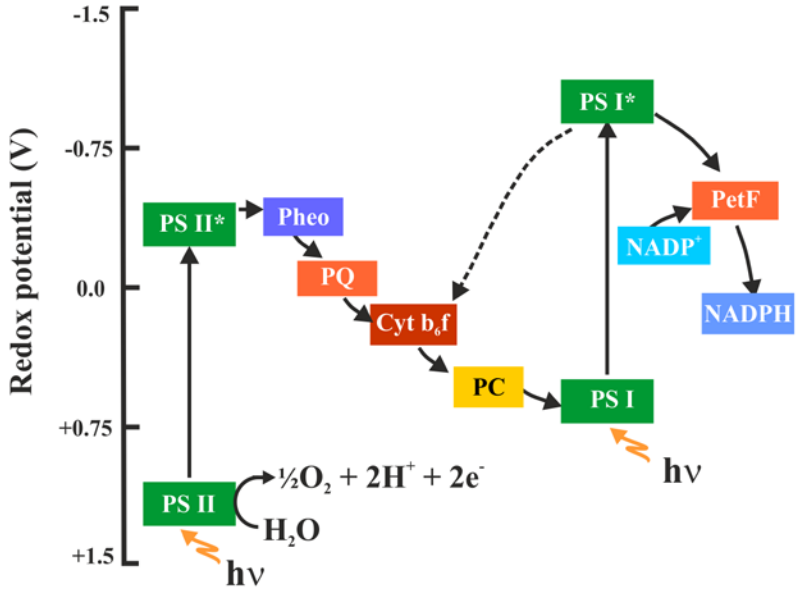

Fig. 1.2. The classical Z-scheme of photosynthesis. The light-induced water-splitting reaction and NADPH formation are performed by PSII and PSI, respectively. For abbrvns. see main text. The pathway of cyclic electron flow is shown by the dotted line.

In the primary process of photosynthesis, photosystem II (PSII) is initially excited by a 680 nm photon to generate the high energy chlorophyll (Chl) excited state Chl*. The electron is then passed to PSII-bound pheophytin (Pheo) and subsequently to the electron transfer components (plasoquinone (PQ), cytochrome b_6f (b_6f), plastocyanin (PC)) and finally to photosystem I (PSI). Subsequent excitation of PSI with a 700 nm photon generates the PSI-Chl excited state, allowing electrons to be passed via PetF (a ferredoxin) to ferredoxin-NADPH reductase (FNR), thereby allowing the formation of NADPH. A second 680 nm excitation of PSII allows water splitting and oxygen evolution (at the PSII-bound Mn-complex) to occur (Fig. 1.2 and Fig. 1.3).

The physical organization of the thylakoid membrane and the photosynthetic components are shown in Fig. 1.3.:

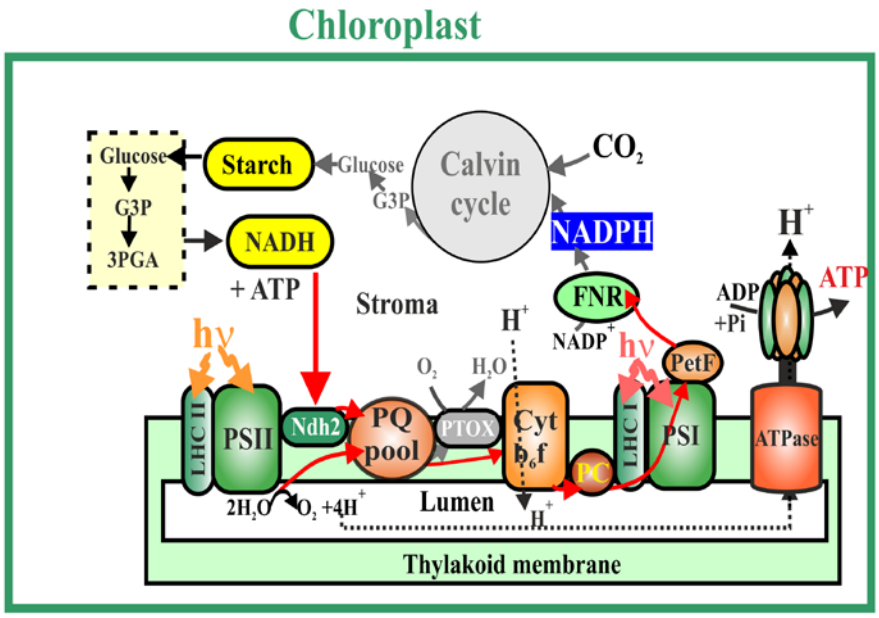

Fig. 1.3. Schematic representation of organization of the components of the Z-scheme in the thylakoid membrane of *C. reinhardtii*. The diagram also shows the dark reactions in the stroma and the inclusion of an ATPase for proton pumping. The PTOX (plastid terminal oxidase) only has a role in chlororespiration (see main text for details).

Some of the energy released during the downhill transport of electrons along the ETC, drives pumping of H^+ from the stroma into the thylakoid interior, building up a H^+ gradient as the thylakoid inner membrane is otherwise impermeable to H^+. The protons arising from water splitting reaction also contribute to the proton motive force (PMF).

The ATP and NADPH formed in the light reactions, fuel the Calvin cycle. Six turnovers of the Calvin cycle are required to produce 6 moles CO_2, 18 moles ATP and 12 moles NADPH and one mole of glucose.

Additionally, cyclic electron flow, which favours ATP generation but prevents NADPH formation due to recycling of electrons between the PQ pool and the cyt b_6f complex, occurs when the ratio of NADPH to $NADP^+$ is high.

1.1.2. Respiration in *C. reinhardtii*, the pathways of O_2 consumption

Three separate respiratory pathways for O_2 consumption exist in *C. reinhardtii*, two of which are located in the mitochondrial membrane, as in higher plants: (1) the cyanide-sensitive cytochrome oxidase (COX) pathway; and (2) the cyanide-insensitive alternative oxidase (AOX) pathway (myxothiazol- or salicyl hydroxamic acid- (SHAM) sensitive). Although, the COX pathway accomplishes most of the ATP production in plant mitochondria, the electron flux through AOX increases when the cytosol and mitochondria are overreduced (see Raghavendra and Padmasree, 2003). In *C. reinhardtii*, cyanide-resistant respiration is especially pronounced during nutrient deficiency (Weger and Dasgupta, 1993).

In addition, a third respiratory pathway which is propyl gallate-sensitive, exists in the *C. reinhardtii* chloroplast. This pathway involves two components (Fig. 1.3), a type II NADPH dehydrogenase (Ndh2) (Jans *et al.*, 2008) which transfers electrons into the PQ pool, and the plastid terminal oxidase (PTOX1 and PTOX2 of which PTOX2 is the major oxidase) (Houille-Vernes *et al.*, 2011) which uses these electrons to directly reduce O_2 to form H_2O (Benoun, 1982). This alternative pathway is known as chlororespiration.

1.1.3. Special case of anaerobic photosynthesis; the production of H_2 by *C. reinhardtii*

In 1942, Gaffron and Rubin reported transient H_2 production upon anaerobic induction of the oxygenic photosynthetic microalga *Scendesmus obliquus*. H_2 production was also subsequently reported upon anaerobic induction of cultures of *C. reinhardtii* (Ben-Amotz and Gibbs, 1975; Greenbaum, 1979; McBride *et al.*, 1977) growing in the light. The reverse phenomenon of H_2 uptake with concomitant CO_2 evolution by anaerobically adapted cells of *S. obliquus* in the dark, was already known in 1939 (Gaffron 1939; 1944). The amount of H_2 produced by *C. reinhardtii* in the light was very small, occurring only as long as anaerobiosis could be maintained in the culture by flushing with inert gases. H_2 production was abolished when concomitant photosynthetic O_2 production occurred (Ghirardi *et al.*, 1997). However, biotechnological interest in *C. reinhardtii* as a potential source of industrial bio-H_2 for clean

energy gathered momentum only 60 years after the initial discovery, when a major breakthrough methodology of the sulphur depletion (S-depletion) protocol (Melis *et al.*, 2000) for sustained photobiological H_2 production was developed which induced anaerobiosis in cultures by reversible inactivation of O_2 evolution. Much of the research and development exploring the use of *C. reinhardtii* as a H_2 producer came after the publication of this protocol. More recently, Mg^{2+} depletion has been successfully used to achieve prolonged H_2 production in *C. reinhardtii* (Volgusheva *et al.*, 2015).

1.1.4. Metabolic regimes in *C. reinhardtii* with respect to H_2 production

1.1.4.1. H_2 production as a case of photofermentation

In the laboratory environment, anoxia may be induced by sparging cultures with an inert gas in the dark and by employing the S-depletion method (see section 1.1.5) in light. Following the shift to anaerobiosis, massive starch build-up of up to 10 times that of aerobic cultures, is observed in the initial hours. Starch, which is confined to the chloroplast, is subsequently degraded and oxidized to pyruvate via glycolysis (Gfeller and Gibbs, 1984). From this point onwards, the steps of dark and light fermentation differ.

In the light, starch breakdown decreases 2-4 fold over dark conditions, and H_2 production increases manifold, acting as the major alternative electron sink and with a general inability to produce ethanol. Formate is produced as a fermentative end product and the oxidative C-metabolism (TCA cycle) is able to produce CO_2 from exogenous acetate uptake (Gfeller and Gibbs, 1984). Light enables the water splitting reaction of photosynthesis to occur, as well as continuous respiratory and photosynthetic ATP generation (Arnon, 1961; Melis, 2007). Thus, H_2 production in *C. reinhardtii* is a case of photofermentation.

In the process of dark fermentation (Fig. 1.4) in *C. reinhardtii*, formate, acetate and ethanol are major end products due to the action of pyruvate formate lyase (PFL1), NADH-dependent acetaldehyde and alcohol dehydrogenases, phosphate acetyl transferase (PAT) and acetate kinase (ACK). The PFL1 converts pyruvate to formate and acetyl-CoA which is subsequently converted to ethanol. Alternatively, acetyl CoA may be converted to acetate and ATP via PAT (Ohta, 1987).

Under both light and dark conditions, the Calvin cycle, which is the normal electron sink under photoautrophic conditions, remains inoperative.

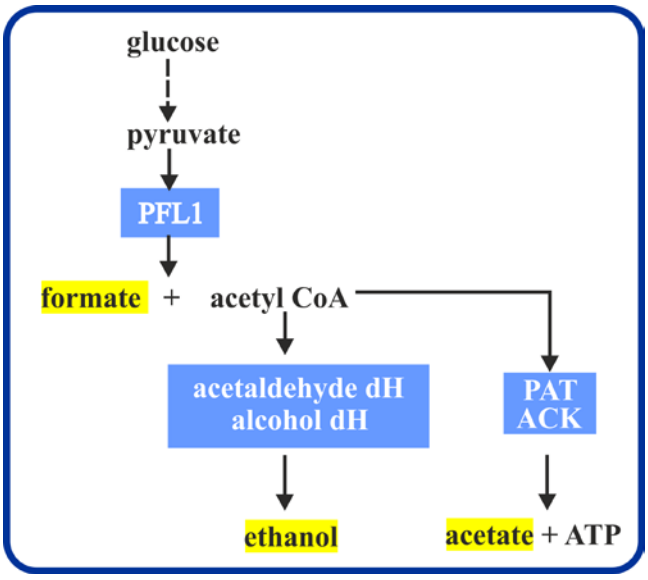

Fig. 1.4. The process of dark fermentation in *C. reinhardtii*, where formate, acetate and ethanol are major end products (Ohta, 1987). (See text for abbreviations)

This ability to produce ethanol in the dark and H_2 in light under anaerobic conditions, provides an evolutionary advantage to the algae, that ensures cell survival. The transient hydrogenase (H_2ase) activity shortens the lag phase of re-activation of oxygenic photosynthesis and contributes to restoring the ATP to NADPH ratio suitable for the start of CO_2 assimilation in anaerobically adapted algae (Ghysels *et al.*, 2013).

1.1.4.2. Altered photosynthesis leading to H_2 production in *C. reinhardtii*

The H_2ases (HydA1 and HydA2) catalyze reversible reduction of H^+ to H_2 by using electrons derived from the photosynthetic electron transport chain via PetF. HydA1 is the major H_2ase with the HydA2, being responsible for less than 25 % of the H_2 production (Meuser *et al.*, 2012). Under aerobic photosynthetic conditions, $NADP^+$ is the terminal electron acceptor of the photosynthetic electron transport chain (ETC), with NADPH subsequently entering the Calvin cycle. Under periods of anoxia, when Rubisco is degraded, the Calvin cycle is inoperative and the electron flow through FNR is blocked. Under these conditions, PetF donates electrons from the ETC to HydA1and HydA2. The subsequent H_2 production, which diffuses out of the cells and is 95% pure (Kruse *et al.*, 2005a), functions as an alternate electron sink which prevents over-reduction of the photosynthetic complexes.

In *C. reinhardtii*, there are two sources of electrons for the reduction of protons to H_2: (1) direct photolysis or photochemical water-splitting by PSII, which releases electrons,

protons and O_2 and where the electrons are directly funneled to the H_2ases via the electron transport chain (Melis and Happe, 2001; Melis *et al.*, 2000). Although this is the predominant electron source with the highest photon conversion efficiency, the co-evolution of O_2, which inhibits H_2ase, is a major limitation. (2) An indirect process where solar energy is first converted to chemical energy in the form of endogenous substrates like starch, which is then oxidized to release electrons that feed into the photosynthetic plastoquinone pool (PQ) for H_2 production and CO_2 evolution (Gfeller and Gibbs, 1984; Gibbs *et al.*, 1986), thus being a PSI dependent but PSII independent process. 80% of the H_2 is derived from the PSII activity and the rest from the endogenous starch breakdown (Volgusheva *et al.*, 2013). In both cases, the electrons enter the photosynthetic ETC, initially via the PQ pool, and are subsequently channeled through the PetF to the H_2ases for H^+ reduction. Thus, PetF may function as a bifurcating valve as it can donate electrons equally to HydA1 and to FNR (Jacobs *et al.*, 2009).

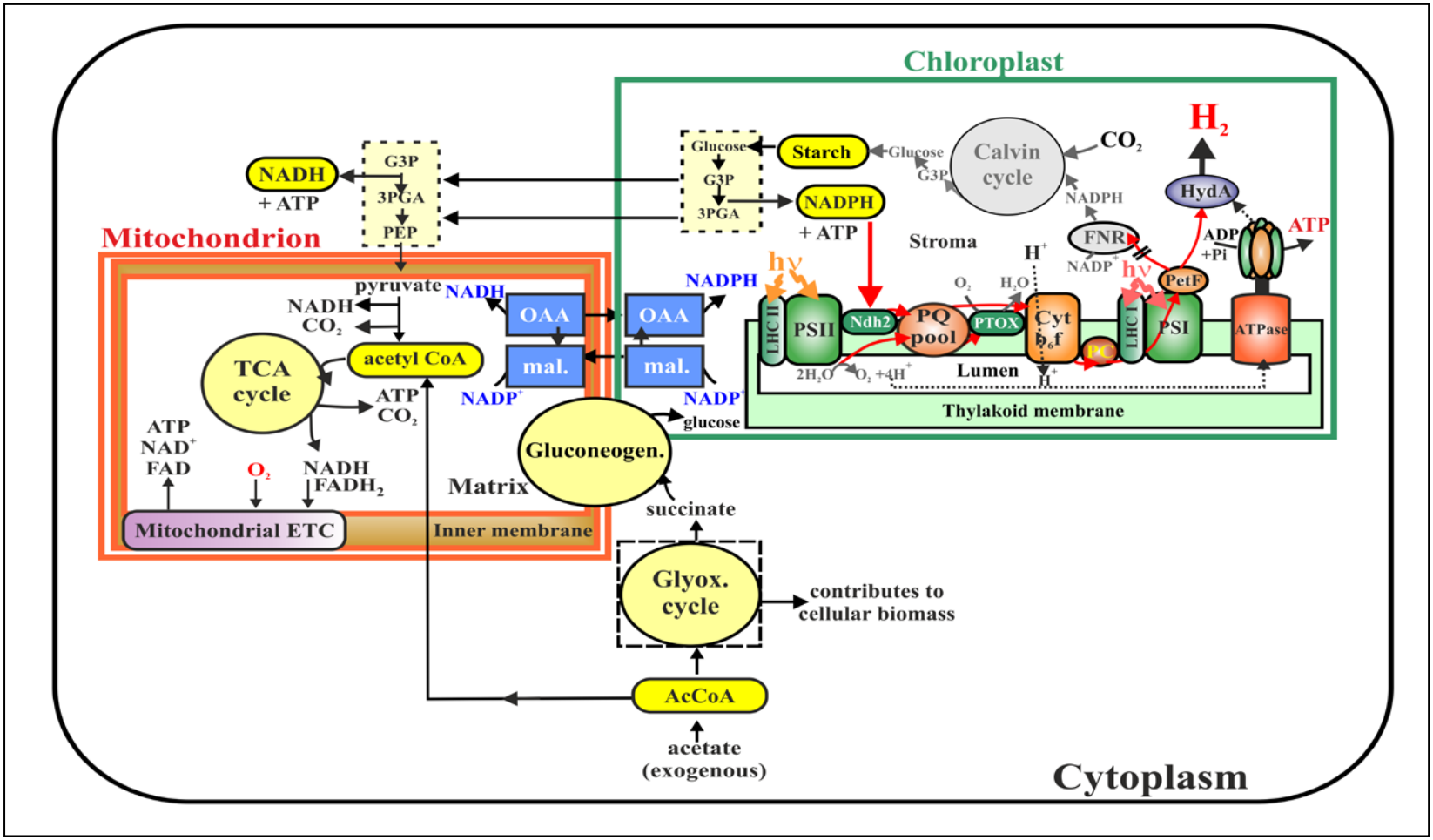

Fig. 1.5. Overview of photosynthesis, H_2 production and the associated C-metabolism in *C. reinhardtii* under S-depletion: The e^- and H^+ transfer in the chloroplast is indicated in solid red and dotted black arrows respectively. e^- transfer to FNR and Calvin cycle (shaded grey) is suppressed. The pathway of uptake of exogenous acetate is indicated and the bi-directional malate shunt is shown in blue.

1.1.4.3. C- metabolism and H_2- production in *C. reinhardtii*

During photomixotrophic or photoheterotrophic growth mode, the acetate supplied in the growth medium is incorporated into the cells as acetyl CoA under aerobic conditions, ultimately feeding into the TCA cycle or into gluconeogenesis for synthesis of longer C-chain compounds (see Johnson and Alric, 2013), thereby enhancing cellular respiration.

Starch reserves in the chloroplast function as an alternative source of electrons for H_2 production, but must be first degraded to glucose via starch degradation enzymes, and subsequently converted to NADH via glycolysis. Interestingly, in *C. reinhardtii*, compartmentalization of glycolysis is observed (Klein, 1986, see Johnson and Alric, 2013), as shown in the Fig 1.5 with the consequence that the NADH ultimately released inside the chloroplast can shunt electrons directly into the PQ pool of the photosynthetic ETC, via the thylakoid membrane-bound class II- type NADH dehydrogenase (Ndh2 or Nda2) (possibly nucleus-encoded) (Mus *et al.*, 2005).

1.1.5. S-depletion as a method for H_2 production

The condition of "anaerobic" oxygenic photosynthesis, implies culture conditions with high mitochondrial and chloroplastic (see Section 1.3) respiration rates which consume O_2 more rapidly than the rate of photosynthetic O_2 production (Kessler, 1966). Thus, "anaerobic" conditions are maintained during photosynthesis, and cells remain in an almost passive cell maintenance mode with limited cell division. The S-depletion method is performed by suspending actively growing cells in S-limited Tris-acetate-phosphate (TAP) medium in a closed culture bottle.

Under these conditions, S- depletion limits the biosynthesis of the methionine-rich D1 protein of PSII (the D1 and D2 polypeptides of photosystem II are functionally analogous to the integral membrane L and M polypeptides of the reaction centers in the purple non-sulphur bacteria, (Margulies, 1991)) which leads to photooxidative damage (Wykoff *et al.*, 1998). S-limitation reduces the number of active PSII complexes by as much as 75% (Volgusheva *et al.*, 2013). The decrease of PSII, reduces the rate of photosynthesis. Consequently, since the rate of O_2 uptake by respiration remains unaffected, the net pO_2 in the culture becomes almost negligible. At this point, both H_2ase enzymes are expressed and H_2 production begins, H_2 production continues until the damage to PSII leads to loss of essential functions (Volgusheva *et al.*, 2013).

Fig. 1.6 shows an example of a previously published gas evolution profile of a S-depleted *C. reinhardtii* culture (Hemschemeier *et al.*, 2005). The progression of the gas profile can be understood by the help of three reference points, which will be applied later to our results:
(1) the O_2 "turnaround" point, where the rate of respiration overtakes the rate of photosynthetic O_2 production. This can be judged by the net appearance of CO_2 and occurs at 20 h in this example,

(2) the point of total O_2 consumption which occurs close to 100 h here. H_2 production ensues when O_2 is sufficiently depleted to approximately 3% by volume, and continues until 220 h.

(3) the maximal H_2 accumulation, which is seen here at 220 hrs. No uptake of H_2 was documented in the publication of Hemschemeier *et al.* (2005).

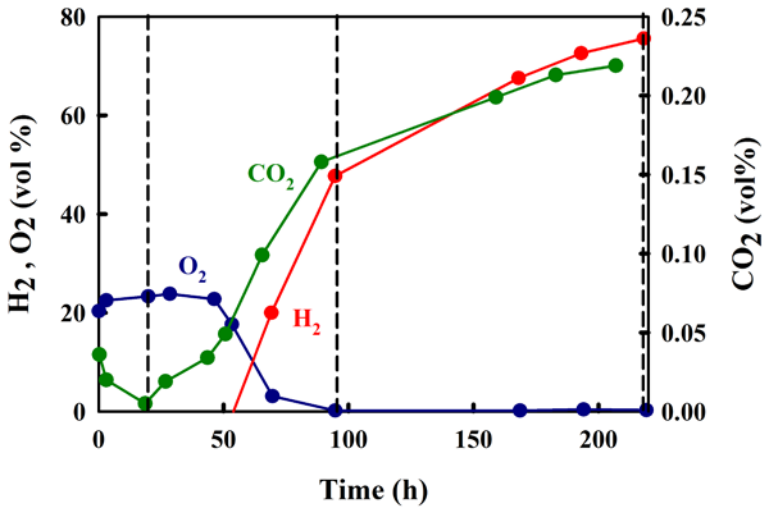

Fig. 1.6. The data (from Hemschemeier *et al.*, 2005) shows the gas composition in the headspace of a resuspended S-depleted *C. reinhardtii* culture (14 µg Chl/ml) which had been sealed in flat glass bottles and illuminated at 100 µmol photons/m^2/s. The measured gases are indicated in the figure. Note the reduced scale for CO_2. The horizontal dashed lines indicate the three reference points in order.

The acetate supplied in the TAP medium serves as the direct substrate for respiration (Laurinavichene *et al.*, 2004) contributing to rapid establishment of anaerobiosis. Both acetate and CO_2 are required for the rapid inactivation of PSII and the highest levels of H_2 production, although H_2 production with S-depletion has been achieved under photoautotrophic, photomixotrophic and photoheterotrophic growth conditions (Kosourov *et al.*, 2007).

S-depletion causes significant changes in gene expression, metabolism, protein composition and function (Winkler *et al.*, 2002; Matthew *et al.*, 2009; Nguyen *et al.*, 2008). Apart from a decline in photosynthetic electron transfer, S-depletion induces starch biosynthesis enzymes leading to almost a tenfold accumulation of starch (Zhang, 2002) and a rapid increase in PTOX1 transcript coding for the alternative chlororespiratory oxidase (Zhang, *et al.*, 2004). An extracellular aryl sulfatase (ARS) is also expressed in response to S-depletion, allowing hydrolysis and assimilation of soluble SO_4^{2-} esters present in the medium (Lien and Schreiner, 1975).

Metabolomic analysis has suggested that the build-up of toxic fermentative products of starch breakdown such as, ethanol and formate during S-depletion eventually slows H_2 production even though the bulk of the endogenous substrates or energy reserves such as starch and triacylglycerides remain unused (Matthew *et al.*, 2009; Kosourov *et al.*, 2003).

1.2. A general overview of hydrogen production by microorganisms

H_2 metabolism (production as well as uptake) has been reported in various methanogenic, acetogenic, nitrogen-fixing, photosynthetic, sulphate-reducing bacteria, cyanobacteria and microalgae (Adams *et al.*, 1981; Adams, 1990). In general H_2 production is carried out by one or more of these three enzyme systems; (1) H_2ase (2) nitrogenase (N_2ase) and (3) formate hydrogen lyase (FHL). The H_2ases are a family of iron-sulphur (Fe-S) proteins (Stephenson and Stickland, 1931), which catalyze the following reaction:

$$H_2 \quad \leftrightharpoons \quad 2H^+ + 2e^- \qquad (1)$$

to either provide reducing power from H_2 oxidation or acting in the reverse direction as electron sinks, balancing the redox potential of the cell as required (see Lubitz *et al.*, 2014). They may also be involved in establishing transmembrane proton gradients (Vignais *et al.*, 2001).

Organism	H_2ase types	Organism	H_2ase types
E. coli	NiFe	***C. reinhardtii***	FeFe
Desulfovibrio fructosovorans	NiFe	*Clostridium pasteurianum*	FeFe
Desulfovibrio gigas	NiFe	*Methanocaldococcus jannaschii*	Fe
R. rubrum	NiFe	*Methanopyrus kandleri*	Fe
Proteus vulgaris	NiFe	*Methanothermobacter marburgenesis*	Fe
Allochromatium vinosum	NiFe	*Chlorella vulgaris*	Fe
Ralstonia eutropha	NiFe	*Desulfovibrio vulgaris*	Fe
Salmonella enterica	NiFe	*Desulfovibrio vulgaris*	NiFe
		Desulfovibrio vulgaris	NiFeSe
		Desulfovibrio baculatum	NiFeSe

Table 1.1. A list of microorganisms and their corresponding H_2ases (Meyer, 2007)

In bacteria, H_2ases are generally localized in the periplasm or cytoplasm, in soluble or membrane-bound forms, whereas in eukaryotes, they are usually localized in specialized compartments. For instance, in *C. reinhardtii*, the H_2ases are localized in the chloroplast stroma (Vignais *et al.*, 2001). In anaerobic bacteria, growing on glucose, pyruvate is a key intermediate in H_2 production. In facultative microorganisms such as *E. coli* and *K. aerogenes*, formate is the key metabolite which is utilized by the FHL system. The H_2ases in sulphate reducing bacteria like *Desulfovibrio* sp. use H_2 to reduce sulphate, sulphite and thiosulphate to sulphide. Methanogenic bacteria reduce CO_2 with H_2 to produce methane and *Clostridia* reduce CO_2 by H_2 to yield acetic acid (see Krasna, 1979) (See Table 1.1 for a list of H_2 producers).

1.3. Structural aspects of microlagal H_2ases

H_2ases (cytochrome c_3 oxidoreductase, EC 1.18.99.1) are classified into two major families on the basis of the metal content of their catalytic centers (see Frey, 2002):

(1) the NiFe H_2ases;

(2) the FeFe H_2ases.

Although all H_2ases are reversible, NiFe-H_2ases are more inclined in the direction of hydrogen oxidation and FeFe-H_2ases towards hydrogen production. Moreover, NiFe-H_2ases are approximately 10 - 100 -fold less active, show 100-fold higher affinity for H_2, and are less sensitive to inhibition by oxygen and carbon monoxide than FeFe-H_2ases (Adams, 1990). An additional metal-free H_2ase, found in methanogenic bacteria, catalyzes the reversible reduction of a methenyl-tetrahydromethanopterin (methenyl-H_4MPT) methanogenic cofactor with H_2 to form methylene-H_4MPT and a proton during methane formation from CO_2 and $4H_2$ (Thauer *et al.*, 1996; Geierstanger *et al.*, 1998).

H_2ases vary in their O_2-sensitivity. H_2ases of facultative microorganisms may be reversibly inactivated by O_2, while those of obligate anaerobes such as *Clostridium sp*. are irreversibly inactivated in the presence of O_2, which can be a limiting factor in biotechnological application. In general, FeFe H_2ases are more O_2 sensitive than the NiFe H_2ases. The structural basis for O_2 sensitivity has been extensively studied (see Lubitz *et al.*, 2014; Fritsch *et al.*, 2013; Shafaat *et al.*, 2013). A special [4Fe-3S] 6Cys cluster, such as the one in *Hydrogenovibrio marinus, E. coli* and *Ralstonia eutropha* H16 close to the catalytic site of NiFe H_2ases, is able to scavenge O_2 and convert it to water by rapid electron transfer. It has therefore been proposed that these H_2ases can also function as oxidases (see Lubitz *et al.*, 2014).

In *C. reinhardtii*, H_2 production is catalyzed by a reversible FeFe-type H_2ase. The predominant H_2ase, HydA1 of *C. reinhardtii* was purified and shown to be a monomeric enzyme with a molecular mass of 48 kDa (Happe and Naber, 1993). The enzyme is encoded by the nucleus and is expressed with a transit peptide of 56 amino acids which targets the protein to the chloroplast stroma. The mature stromal polypeptide contains 441 amino acids (Happe *et al.*, 1994; Happe and Kaminski, 2002). A paralogue of HydA1, HydA2, is responsible for less than 25 % of the H_2 production (Meuser *et al.*, 2012). H_2 evolution in *C. reinhardtii* is extremely sensitive to the presence of O_2 (Abeles, 1964; Erbes et al., 1979). The transcription of the H_2ase genes are induced only after anaerobic adaptation of the cells (Stirnberg and Happe, 2004) with the earliest H_2ase (HydA1/HydA2) proteins being detected 15 min after anaerobic adaptation (Happe and Kaminski, 2002). However, contradictory observations were made by Nguyen *et al.* (2008), who showed *hydA* (*hydA1*/*hydA1*) transcript induction in S-starved cultures, before anaerobiosis sets in.

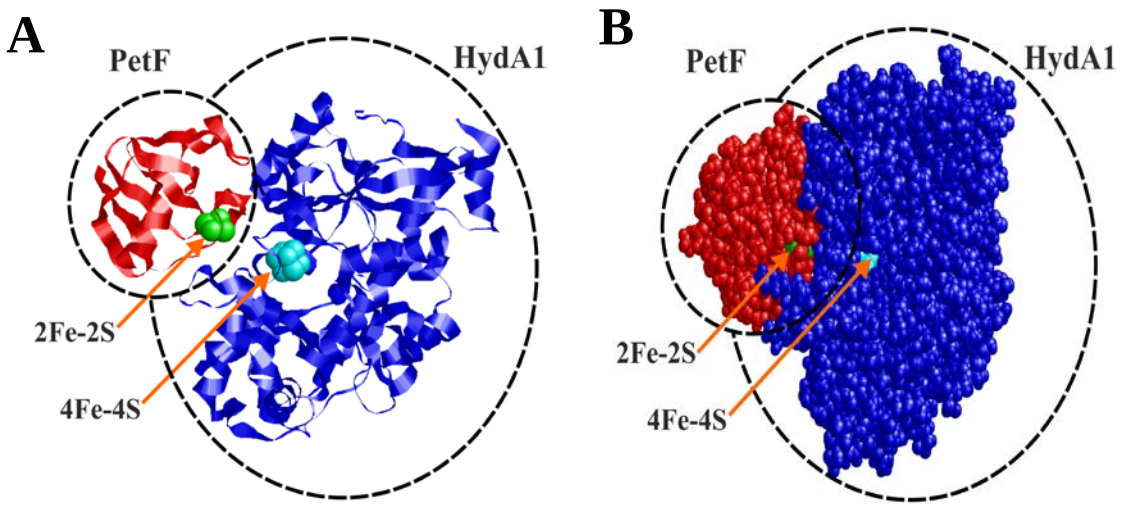

Fig. 1.7. NMR structural model (PDB: 2N0S) (Berman *et al.*, 2000) of the PetF and [FeFe]-H_2ase complex (HydA1) from *C. reinhardtii*. (Rumpel *et al.*, 2015), (image generated with RasWin (http://www.openrasmol.org/) (Sayle and Milner-White, 1995)). The 4Fe-4S and the 2Fe-2S clusters are shown in cyan and green, respectively. **(A)** cartoon and **(B)** spacefilling representations.

The active site of the enzyme, a complex bridged 4Fe-4S subcluster bridged to a 2Fe subcluster (the H-cluster) is coordinated by four cysteine residues at the highly conserved C-terminal domain and lacks the N-terminal domain usually associated with other FeFe-H_2ases (Vignais *et al.*, 2001). The absence of additional redox clusters or a second subunit suggests direct electron transfer from PetF to HydA (Happe and Kaminski, 2002). O_2-mediated inactivation of HydA involves the diffusion of the gas into close proximity of the catalytic site and subsequent redox and chemical reactions with the H cluster which leads to breakdown of the 2Fe subcluster site. However, long-term or high concentration of O_2 exposure always precedes complete H cluster breakdown (Swanson, 2015).

Like ferredoxins, FeFe-H_2ases are one of the metalloproteins for which the catalytic cofactor can be synthesized chemically and incorporated into the apo-protein (Esselborn *et al.*, 2013; Bergerren *et al.*, 2013; see Lubitz *et al.*, 2014), thus enabling manipulation of both the protein and the H- cluster. This will be beneficial for the development of more oxygen-resistant H_2ases (see Lubitz *et al.*, 2014).

1.4. H_2 metabolism in *R. rubrum* and the role of nitrogenase in H_2 production

Amongst the prokaryotes, light-dependent production of H_2 was first observed in the photosynthetic purple non-sulphur bacterium *Rhodospirillum rubrum* (Gest and Kamen, 1949). Photosynthesis in *R. rubrum* is an anaerobic process with no water splitting or O_2 evolution, involves a cyclic electron flow, and results in ATP production via the ATP synthase and NADH production by reverse electron transport.

R. rubrum grows in the light, anaerobically, in a defined medium consisting of organic substrates, mineral salts including ammonium chloride, and a trace of biotin (Hutner, 1946). However, *R. rubrum* grown photosynthetically on certain oxidized substrates, such as C-4 dicarboxylic acids with glutamate or aspartate instead of ammonia as a nitrogen source, produces both CO_2 as well as large amounts of H_2 (Gest *et al.*, 1962). The N_2ase system is the primary means of H_2 production under photosynthetic nitrogen-limiting conditions in many photosynthetic bacteria, including *R. rubrum* however multiple H_2ase activities in various anoxygenic photosynthetic bacteria have also been reported (Adams *et al.*, 1981; Llama *et al.*, 1981; Gogotov, 1984). *R. rubrum* seems to be extremely versatile in its modes of H_2 metabolism with three distinct H_2ase activities, (1) the uptake H_2ases (Ormerod and Gest, 1962; Adams and Hall, 1977; 1979), (2) the formate-linked H_2ase (Schön and Voelskow, 1976; Gorrell and Uffen, 1977; Voelskow and Schön, 1980), and (3) the carbon-monoxide linked H_2ase (Uffen, 1981, Bonam *et al.*, 1984). These three H_2ase enzymes of *R. rubrum* can be expressed singly or conjointly depending on growth conditions, and the presence of inhibitor or inducer (Maness and Weaver, 2001). For instance, the CO-linked H_2ase is expressed only when *R. rubrum* is grown with CO as an energy and C-source, and is therefore an unimportant pathway under normal growth conditions. Cells growing photosynthetically can convert acetate, succinate, fumarate and malate almost quantitatively to CO_2 and H_2.

The N_2ase enzyme complex also catalyzes H_2 evolution in bacteria and cyanobacteria. This reaction is ATP-dependent and irreversible, in contrast to the H_2ase reaction. N_2ase consists of two distinct proteins, the dinitrogenase and dinitrogenase reductase which reduces N_2 to NH_3 accompanied by an obligatory reduction of protons to H_2 as seen in the overall reaction:

$$N_2 + 16ATP + 8e^- + 8H^+ \Rightarrow 2NH_3 + H_2 + 16ADP + 16P_i \quad (2)$$

N_2ases are known to occur in strict anaerobes, facultative aerobes, microaerophilic organisms, and strict aerobes. The enzyme is extremely O_2-sensitive and organisms possessing them have evolved mechanisms to protect against O_2 inhibition. In filamentous

cyanobacteria, about 10% cells differentiate into heterocysts, which are thick walled cells which limit gaseous influx, and have evolved to lose the O_2 producing PSII complex. Unlike vegetative cells, heterocysts undergo genetic rearrangements (Golden *et al*., 1988; see Burris, 1991) to activate nitrogen fixing genes, such that N_2 fixation and H_2 production can occur. Thus, in laboratory conditions, cyanobacteria or filamentous blue-green algae were found to be less sensitive to O_2 (Benemann and Weare, 1974), but high levels of H_2 production was incumbent upon anaerobic (flushing with an inert gas such as argon) and low light conditions with water as the source of H_2.

With *R. rubrum*, a continuous H_2 production rate of 180 ml/l/h has been achieved (Zürrer and Bachofen, 1982), comparatively, a rate of 30 ml/l/h has been reported for blue green algae *Anabaena sp*. (Weissman and Benemann, 1977) and a rate of 2.5 ml H_2/l/h is common for a *C. reinhardtii* wild-type culture in S-depleted medium (Laurinavichene *et al.*, 2006). Since the separation of H_2 from O_2 is a prerequisite for the usage of H_2 as a fuel, the coevolution of CO_2 with H_2, in purple non-sulphur bacteria, is advantageous over cyanobacterial systems where O_2 is co-produced.

1.5. The measurement of gases in the bioreactor headspace

1.5.1. Principle of gas chromatography

The gas chromatograph (GC) is used to separate, identify and quantify individual components of gas mixtures. Like all other chromatographic techniques, the GC creates a temporal separation of each injected component by passing the gas through a column material (stationary phase) that retards some components more than others. A gas chromatographic system consists of: a pure carrier gas (usually helium or nitrogen or argon-mobile phase) which moves the sample through the GC column contained within an oven to carefully regulate the temperature of separation. Either a flame ionization detector (FID) or thermal conductivity detector (TCD) responds to the passage of each component by changing its electrical output with respect to the reference gas electrical output, which is eventually seen as a chromatogram. The amount of a gas is inferred from the corresponding chromatogram peak area.

The response factor (RF) or calibration factor for any standard gas, is calculated by dividing a known amount of a component by the size of the peak it produces and makes two important assumptions, that the amount/size line is linear and that it passes through the origin

i.e. null amount of any gas should not have a detectable peak area. Both assumptions must be demonstrated experimentally by performing a calibration series.

1.5.2. Principle of the thermal conductivity detector (TCD)

All gases conduct heat but differ in their thermal conductivities (See Table 1.2). When a voltage is applied to a filament, it heats up. The steady-state temperature of the filament depends on the applied voltage, the resistance of the filament, and the rate at which the filament loses heat to its surroundings. When a filament is immersed in a gas stream, any change in the thermal conductivity of the gas causes a change in filament temperature and the resistance of the filament. The electronics senses this change and adjusts the power to the filament to keep the temperature constant and this change in the supplied voltage is represented in the form of a chromatogram (mV vs. retention time).

Gas	**Thermal conductivity (mW/mK)**
Air	24
O_2	26
H_2	187
Ar	18
CO_2	17
N_2	26
He	157

Table 1.2. Thermal conductivities of gases (Assael, 2010), the high thermal conductivity of H_2 implies that the detection limit for H_2 is lower than for other gases with a TCD detector.

1.5.3. Instrumental factors affecting separation of gas components

Important factors influencing component separation in the GC are:

(1) the vapour pressure of the compound,
(2) the polarity of the stationary phase,
(3) temperature and length of the column and
(4) carrier gas flow rate.

The boiling point of a compound is related to its polarity: the lower the boiling point, the higher is the vapor pressure which leads to a shorter retention time.

A high column temperature results in very poor separation as the differences in retention times are not as pronounced anymore. The best separations are seen when temperature gradients are deployed, because the differences in polarity and in boiling points come into play. A high flow rate also reduces the retention times, but gives a poor separation as the components have very little time to interact with the stationary phase and are just being propelled through the column. A longer column generally improves separation as it increases the time of interaction with gas components and a significant peak broadening is observed which is inversely proportional to the flow rate.

Ideally, the peaks in the chromatogram display a symmetric shape (Gaussian curve) (Fig. 1.8). If too much of the sample is injected, poorer separation occurs and the peaks show a significant tailing. Most detectors are relatively sensitive and under standard conditions only 1-2 % of the compound injected into the injection port passes through the column because most GC instruments are operated in split-mode to prevent overloading of the column and the detector.

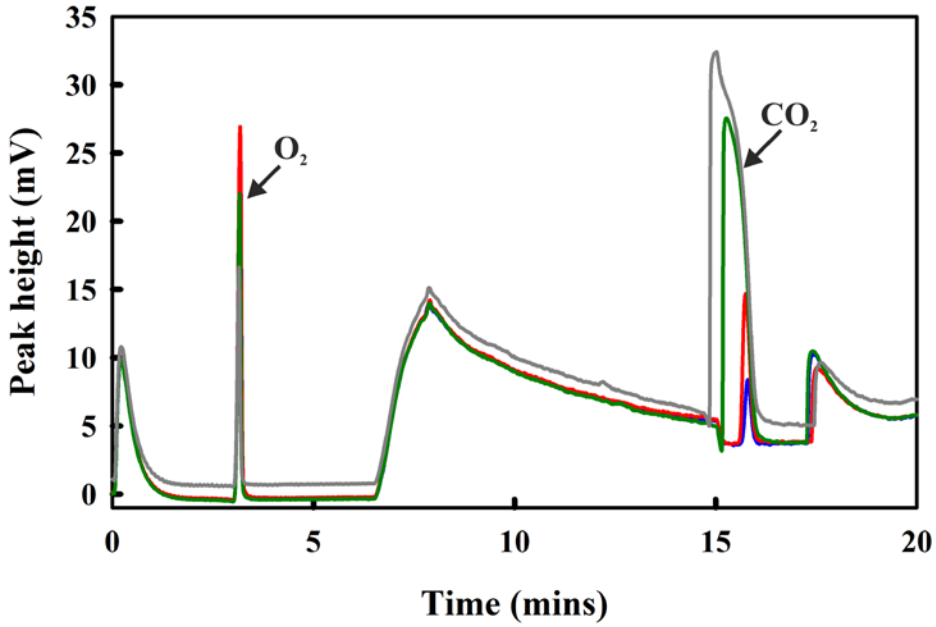

Fig. 1.8. GC chromatograms, showing peak tailing vs. symmetric peak for increasing volumes of CO_2 (0.1 ml (blue), 0.2 ml (red), 0.5 ml (green) and 1 ml (gray)) headspace from carbonated bottled-water sampled, shows peak shape becoming non-Gaussian at high CO_2 levels.

2. MATERIALS AND METHODS

2.1. Chemicals and Materials

In general, chemicals and enzymes were obtained from Roth (Karlruhe, Germany), Sigma-Aldrich (Darmstadt, Germany). Organic solvents were HPLC grade.

Components required for the construction of the closed setup apparatus used for the H_2 production experiments for *C. reinhardtii* and *R. rubrum* were obtained from BOLA® (Bohlender, Grünsfeld, Germany) and Swagelok® (Solon, Ohio, USA). Gas-tight syringes and needles for gas sampling by gas chromatography (GC) were obtained from SGE Syringe (Trajan Scientific, Australia) and Hamilton (Switzerland), respectively.

2.2. Preparation of culture media

TAP and Luria Bertani (LB) medium (see Appendix 2) were made according to Gorman and Levine (1965) and Sambrook and Russell (2001), respectively. Culture media were sterilized by autoclaving at 121°C for 20 min. at 1.2 bar. For solid agar medium, 7.7 g agar was added to 500 ml medium and autoclaved at 121°C for 15 min at 1.2 bar.

2.3. Culture conditions and strain storage

2.3.1. Growth of *C. reinhardtii:*

The strain of *C. reinhardtii* used is designated as CC-1418 by the *Chlamydomonas* Resource Center, located at the University of Minnesota and as SAG 18.79 by the Culture Collection of Algae at the University of Göttingen, abbreviated as the SAG (Sammlung von Algenkulturen der Universität Göttingen). *C. reinhardtii* SAG 18.79 strain was cultivated photomixotrophically on TAP medium (Gorman and Levine, 1965, see Appendix 2) pH 7.0, at 21°C at one of two light regimes: (1) very low light (VLL) intensity of 5 µmol photons/m^2/s (from fluorescent 58 W neon tube-lights); or (2) intermediate light (IL) intensity of 70 µmol/m^2/s (obtained with an LED light source from Emil Lux GmbH, (retailed at OBI, Germany). Culture stocks were maintained by monthly streaking of *C. reinhardtii* on TAP medium plates. In general, 100 ml pre-cultures (in 250 ml Erlenmeyer flasks) were inoculated directly from TAP plate colonies, and then grown at 130 rpm on a rotary shaker or with a magnetic stirrer. 100 ml TAP medium was also inoculated using 1 ml of a late logarithmic phase pre-culture. Cultures were periodically checked for contamination by streaking onto LB agar plates and TAP medium plates, followed by incubation at 30°C (first plate) and 37° C (second plate) for up to one week. In addition, cultures were also checked using optical microscopy.

For growth using the S-depleted TAP medium for the induction of anaerobic conditions, 100 ml of a mid-to-late-logarithmic phase culture (IL: 0.45 – 0.57 approx. OD; VLL: 0.32 - 0.4 approx. OD value measured with a 4 mm path length cuvette), was grown in normal TAP medium, harvested (under sterile conditions) by centrifugation at 2,500 rpm (590 x g) for 5 min. The harvested cells were washed once in S-depleted TAP medium, and then resuspended to the desired optical density or Chl concentration in 110 ml S-depleted TAP medium. The suspended cells were placed into 130 ml bottles (total volume) (Schott, Germany), closed with the sampling assembly cap (see Fig. 2.3), and then illuminated with either VLL or IL light with continuous stirring.

2.3.2. Growth of *R. rubrum*

R. rubrum S1 was cultivated phototrophically in closed Pyrex bottles at 30°C in M medium (Sistrom, 1960, see Appendix 2). For semi-aerobic growth, *R. rubrum* strains were cultivated in modified M medium: either M2S medium (containing 40 mM NH_4^+-succinate as C- and N-source) or M2SF medium (containing 40 mM NH_4^+-succinate and 16.7 mM (0.3%) fructose as an additional C-source) (Ghosh *et al.*, 1994, see Appendix 2).

For quantitative semi-aerobic growth experiments with *R. rubrum*, 4 ml of a culture grown photoheterotrophically with M medium were used to inoculate 100 ml of M2SF medium (present in 250 ml baffled Erlenmeyer flasks), and the culture was shaken at 150 rpm (2 cm throw) at 30°C in the dark. The A_{660} (4mm) and A_{882} (4mm) values of the culture at different time points were measured using a single-beam spectrophotometer with a 4 mm path length cuvette. It has been shown previously (G.S. Wang and R. Ghosh, manuscript in preparation) that the A_{660} (4mm) correlates linearly with the dry weight up to an A_{660} (4mm) of 1.4. Above this value the culture must be diluted as appropriate.

Glycerol cultures were used for long-term storage of S1. In this procedure 10 ml fresh culture was pelleted by centrifugation at 4000 rpm (1,940 × g) and 4°C for 10 min. The supernatant was removed and the pellet was re-suspended with 1 ml M medium (*R. rubrum*) or 1 ml LB medium (*E. coli*). The suspended pellet was transferred to a cryotube and 1 ml sterile 87% (v/v) glycerol was added and mixed thoroughly, followed by a 10 min incubation on ice. Finally, the cryotube was flash-frozen in liquid N_2 and transferred to the -80°C freezer.

2.4. Analytical techniques

2.4.1. Turbidity and cell count

Culture turbidity of *C. reinhardtii* at A_{561} (4 mm) was measured in a single beam spectrophotometer (Biochrom) in 4 mm path length cuvettes against a TAP medium blank. Cell counts of *C. reinhardtii* were recorded by using a Thoma cell counter (Assistent®, Glaswarenfabrik Karl Hecht, Rhön, Germany) with a chamber volume of 0.1 µl. Cell samples were incubated on ice prior to making the counts, in order to sufficiently immobilize the cells to enable accurate counting. Every reported cell count is an average of 4 measurements.

2.4.2. Determination of protein

Total cellular protein was determined using the modified Lowry method (Peterson, 1979) using bovine serum albumin as a standard. Generally, 100 µl or 50 µl aliquots of cell cultures were used for protein determination. Phenylmethylsulfonyl fluoride (PMSF) was added to about 1 mM to prevent proteolysis prior to the trichloroacetic acid (TCA) precipitation step.

2.4.3. Determination of Chl

Chl was extracted in 80% (v/v) buffered aqueous (final conc. of 2.5 mM Na-phosphate buffer from a stock solution at pH 7.0) acetone (Porra *et al.*, 1989), from approximately 1 ml or 0.5 ml culture volume by vortexing. Cell pellets were extracted in a total volume of 1 ml buffered aqueous acetone till the pellet turned grey and colourless. The absorbance values of the extracted sample were determined at 647 nm, 664 nm, and 750 nm (1 cm path length) against an 80% acetone blank. Acetone extracts were diluted 1:10 in buffered aqueous acetone if A_{664} (1 cm) values were higher than 1.4.

2.4.4. Spectral analysis of whole cells

The absorption spectra of intact cells were determined with a Jasco V-560 UV/VIS spectrophotometer (Jasco, Japan) equipped with a photodiode detector for turbid samples. Culture aliquots were first pelleted in an Eppendorf centrifuge (3 min, 13,000 rpm) and the pellet was resuspended in TAP medium containing 80% (v/v) glycerol. Absorption spectra between 300 - 900 nm were obtained using 2 mm path length cuvettes. For comparisons of relative amounts of photosynthetic complexes in cells between the unmodified TAP grown versus S- depleted TAP cells, equal cell amounts (judged from the A_{561} (4 mm) values) were pelleted at 13,000 rpm for 5 min at 4° C in a 1.5 ml Eppendorf tube, and the pellets were then resuspended in 100 µl TAP medium at 4°C. The resuspended pellet was then mixed with 400

µl of 100% glycerol, transferred to a 2 mm quartz cuvette and the spectra taken as described above.

2.4.5. Determination of dry weight from culture aliquots

For the measurement of the dry weight of culture aliquots, samples from three replicate 250 ml cultures (growing in 500 ml flasks) exhibiting an A_{561} (4 mm) of about 0.35, were passed through pre-weighed glass microfiber filters (Whatman®, GE Healthcare Life Sciences, Little Chalfont, UK) using a vacuum glass filtration apparatus (Sartorius Stedim Biotech, Germany). The filters were then dried in an 80°C oven until they reached a constant weight.

2.4.6. Thin-layer chromatography (TLC)

Preparation of samples for TLC was performed as follows. 80 ml of log phase cells were centrifuged at 5000 rpm at 4°C for 15 min. The pellet was resuspended and washed in 20 ml cold 50 mM Na-phosphate buffer at pH 7.0, centrifuged, washed once more with 20 mM Tris-HCl buffer at pH 8.0 followed by resuspension in 15 ml water. The resuspended cells were homogenized with a precision glass homogenizer with a Teflon plunger (Sartorius AG, Germany) and after a short equilibration in ice (10 min), the cell suspension was centrifuged for 15 min as mentioned above, and the pellet extracted twice in 16 ml methanol (MeOH) by vortexing, followed by centrifugation for 15 min. The remaining bulk of the pellet was extracted twice in 5 ml hexane by vortexing and centrifuging for 15 min. All extraction, resuspension and centrifugation steps were performed in the dark. The MeOH and hexane extracts were dried under a stream of N_2 gas and dissolved in 3 ml dichloromethane (DCM)/hexane (1/1(v/v)). Approximately 10 µl of the extracted samples were spotted onto silica gel TLC plates (DC-Fertigplatten SIL G-25, Merck) and developed using one of two solvent systems: (1) pentane/EtOH (100:2 (v/v)); (2) $CHCl_3$,/MeOH/H_2O ((80:30:4 (v/v/v)). Iodine staining was used to visualize hydrophobic substances e.g. fatty acids and pigments.

2.4.7. Enzymatic determination of starch

The starch content of cells was measured by the amount of glucose present after enzymatic hydrolysis of the starch-containing pellet obtained after ethanol extraction (Hendricks *et al.*, 2003). The glucose in the hydrolysate was assayed by the coupled reaction of glucose oxidase (GOX) and horseradish peroxidase (HRP) with 2,2'-azino-bis(3-ethylbenzothiazoline)-6-sulphonic acid (ABTS) as the chromogenic substrate (see Appendix 4). Briefly, a cell culture volume of 2 ml was pelleted in 1.5 ml screw-cap tubes (Sarstedt, Germany) for 5 min. at 13,000 rpm at room temperature, and the pellets were extracted by vortexing in 1 ml of 90%

(v/v) ethanol. The colourless ethanol-insoluble pellet obtained was vortexed and washed in 1 ml 100% ethanol, and then suspended in 1 ml of 0.1 M NaOH. Alkaline hydrolysis was performed by incubating the sample at 95°C for 30 min. After cooling to room temperature, 50 µl of 0.5 M Na-phosphate buffer pH 7.0 and 45-50 µl of 1 M HCl were added to neutralize the pH. Subsequently, enzymatic hydrolysis of the dissolved starch was performed overnight at 37°C with the addition of 2.2 U of fungal amyloglucosidase (dissolved in 100 mM Na-phosphate buffer, pH 7.0) and 2 U of fungal α-amylase. Each 1.1 ml hydrolysate sample was de-ionized by addition of a small number of mixed bed ion exchange resin AG 501-X8 beads (pre-adjusted to neutral pH) to the tube followed by vigorous mixing at 1500 rpm for 1 h in a shaker (Peqlab, Germany). The supernatant was used for glucose estimation.

The assay buffer used to perform glucose determination was 100 mM Na-phosphate pH 7.0, with GOX (0.025 U) and HRP (1.25 U) and with 2.5 mM (ABTS) (Bateman and Evans, 1995) (see Appendix 4 for more details of the glucose assay.) For the Michaelis-Menten calibration curve, a glucose (substrate) concentration of 0-125 mM, in a final volume of 1 ml was employed. Optical rate measurements were performed at 25°C using a 1 cm path length cuvette in a Jasco V-560 spectrophotometer. The rate of glucose consumption (in ΔAbs/min) was measured at 414 nm for a time course of 360 s. For cellular starch samples, the assay was performed at 50 mM buffer strength with 700 µl of hydrolysate as substrate in a 1 ml assay volume. An example of the glucose calibration assay is shown below. The derived Michaelis- Menten equation with a K_m value of 18.4 and a V_{max} (ΔAbs/min) value of 0.89 at 25 °C was used to estimate unknown glucose samples.

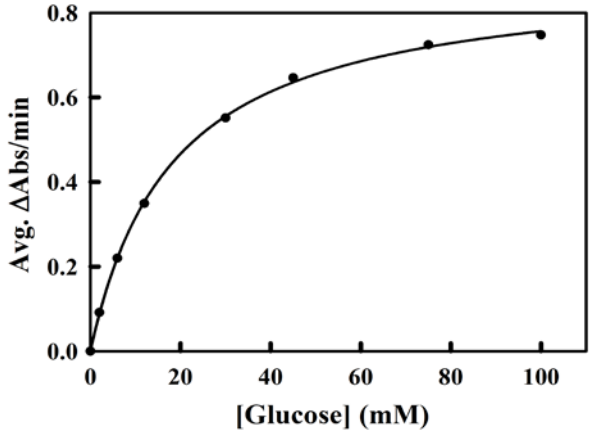

Fig. 2.1. The Michaelis- Menten calibration curve of for glucose determination estimated by the GOX/HRP enzyme assay at 25°C. Measurements were performed in triplicates, with the average values plotted to obtain the curve.

2.5. Quantitative analysis of gases

2.5.1. The gas chromatograph protocol

Gases were quantitated by GC using a Thermo Fisher Scientific Trace 1300, (Waltham, USA) gas chromatograph equipped with a thermal conductivity detector (TCD). Gases in the experimental setups were sampled (usually with a 1.5 ml gas volume) using a 2.5 ml fixed Luer Lock gas-tight SGE syringe, equipped with a 23 gauge, 51 mm length, point style 5 Hamilton needle (Reno, USA), and injected into a 1 ml GC sample loop. The loop overfill ensured that the residual loop gas is washed out prior to re-filling. The gas sample was chromatographed using two 1/16 inch x 2 m micropacked (ShinCarbon ST packing material) columns (Restek GmBH, Germany), connected in series. TCD detection was performed for signal analysis. The GC run was performed with a temperature ramp of 10°C/min. from 35°C - 170°C starting from 6.5 min. after sample injection to 20 minutes. N_2 gas (5.0 grade) was as the mobile phase used and the detector filament maintained at 200°C. Data analysis was performed using the proprietary Chromeleon 7.2 software package (Thermo Fisher Scientific, Waltham, USA).

Routinely, the GC was flushed each day with two air samples before beginning with gas measurements to eliminate spurious signals due to the accumulation of dirt.

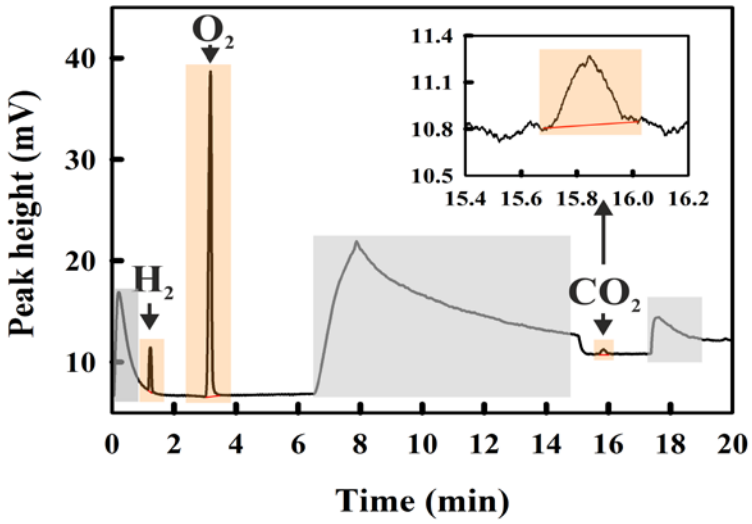

Fig. 2.2. A typical GC chromatogram for a gas sample containing H_2, O_2 and CO_2 (orange shaded regions) with retention times 1.4 min, 3.18 min, and 15.8 min respectively. The inset shows an expanded view of the 15-16 min. region. Grey shaded regions indicate the background chromatogram output which appears irrespective of the gas sample injected. The rise in peak height from 6.5 min. corresponds to the start of temperature ramp applied from 35°C to 170°C at the end of 20 min. The drop of the baseline output signal at 15 min is due to a valve switching event.

2.5.2. BOLA and Swagelok components and connections used for constructing gas sampling assemblies (See Appendix 3. for individual component descriptions)

Explosion proof and high pressure resistant BOLA caps and connections were used to connect the Schott bottles used for H_2 evolution experiments with the Swagelok gas sampling port and N_2 gas flushing tube. All connections were made of chemically inert but conductive materials.

The BOLA *Laboratory Screw-Joint* system consisting of four components (screw cap, sealing, tapered and V-ring) was used to build connections between all *Zebra tubing* and *Tube fittings*. The Schott bottles with a neck size GL-45 were sealed with a GL-45 BOLA screw cap containing multiple (three) distributors each with GL-14 threaded necks. These distributors were used for withdrawing or introducing gaseous or liquid components. The ports were connected to transparent *Zebra* explosion proof tubing (6 mm and 4 mm outer and inner diameter, respectively) through the BOLA *Laboratory Screw Joint System* (LSJS). All fittings were autoclavable up to 121 °C and can withstand pressures up to 6-10 bar, with the *Zebra tubing* having a burst pressure of 57 bar.

Two-way valves (stop-cocks) were fixed in place by means of *GL Tube fittings* and *Screw joints* to either seal the vessel contents or allow gas exchange with the surroundings. A two-way BOLA *Universal Coupling* adapter was used to connect the GL 14 BOLA Screw joint connection to the ¼ inch metallic Swagelok gas sampling assembly.

2.5.3. Use of N_2 gas reservoir for gas dilution (the gas dilution bottle)

A small glass tube (Pyrex, USA) (17 ml) or bottle (260.16 ml) capped with a SubaSeal (Sigma-Aldrich, Darmstadt, Germany) was employed as a reservoir of N_2 gas for filling up residual volumes of pure N_2 in the syringes used to perform GC calibration experiments with the standard gases O_2 and CO_2. N_2 flushing was performed for 5 min by flushing N_2 from a N_2 (5.0) supply line through a 21 gauge, 100 mm long needle (Supra, Misawa Medical Industry Co. LTD, Japan) using a 21 gauge, 40 mm long needle (Sterican®, B. Braun, Germany) acting as an outlet. The N_2-filled bottle was maintained at positive pressure by removing the outlet needle before removal of the inlet needle at the end of the 5 min. period.

All gas-tight bottles were checked for gas tightness with the Snoop liquid leak detector (Swagelok, USA). The Pyrex tube with the SubaSeal used as N_2 gas reservoir or H_2 dilution vessel was tested for gas tightness by immersing the N_2-filled tube in water and checking for air bubbles.

2.5.4. GC calibration of O_2 using an air standard

Atmospheric air has a near constant composition and is thus useful for calibrating the O_2 signal in GC measurements. At standard temperature (298K) and pressure (1 atm = 1.013 x 10^5 Pa), the composition of air at sea level is given in Table 1:

Using the ideal gas equation (which is sufficiently accurate for the experimental conditions):

$$PV = nRT \qquad (3)$$

we calculate that 3.46 moles of air are present in 83.3 litres at a standard pressure and a temperature of 294 K (this value corresponds to the average lab temperature during the period of the measurements). Thus, **1 ml air contains 8.68 μmoles O_2 at 294 K**. This is the starting point for the GC calibration (see Results for a detailed description).

Composition of air at sea level at 294K and 1 atm. press.						
		100 g normal air			**1 ml sample air**	
Gas	**Mass (g)**	**Weight (g)**	**n (moles)**	**x**	**n (μmoles)**	**mole fraction x**
N_2	28	75.53	2.698	0.781	32.365	0.781
O_2	32	23.16	0.724	0.209	8.684	**0.209**
Ar	39	1.27	0.033	0.009	0.391	0.009
CO_2	44	0.047	0.001	0.000	0.013	0.000
			3.455		**41.452**	

Table 2.1. The relevant parameters for the composition of at sea level at 294 K and standard pressure. The data has been shown with a precision of three decimal places. However, at the attainable sensitivity of the GC only two decimal places are relevant, thus allowing us to ignore the [CO_2] for the calibration calculations.

2.5.5. GC calibration of the signal arising from H_2

The GC signal arising from H_2 was calibrated using the $NaBH_4$ reaction:

$$NaBH_4 + 2H_2O \Rightarrow NaBO_2 + 4\ H_2 \qquad (4)$$

A pellet (0.23 ± 0.01 g) of $NaBH_4$ (Sigma) (purity: 90% by weight) doped with a cobalt catalyst, was placed in 40 ml H_2O in a 1 litre Schott bottle, which was closed immediately with a gas-tight bottle cap assembly (constructed with BOLA cap and Swagelok (Solon, USA) components (Fig. 2.3)). The bottle assembly was stirred magnetically to aid dissolution of the pellet.

Sampling (1.5 ml gas samples) was started after 5 min and the kinetics of H_2 evolution within the bottle was followed by GC until a constant value was obtained. The amount of H_2 generated in the reaction vessel was calculated by inverse correlation to the depression of the O_2 peak area. At every time point, a 1-2 ml gas sample from the BOLA reaction bottle was diluted into the 260.16 ml gas dilution bottle, and after short period to allow mixing, a 1.5 ml gas sample from this reservoir was withdrawn for the GC measurement.

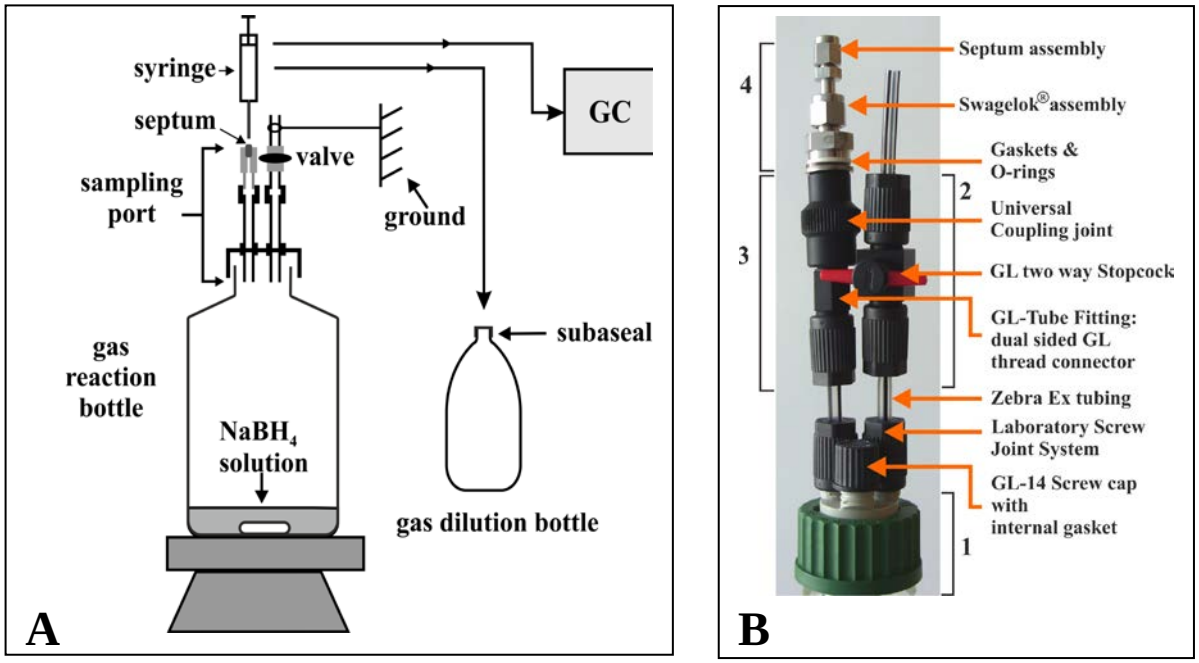

Fig. 2.3. (A) Schematic diagram of the BOLA®-Swagelok® bottle assembly used for the production of H_2 from defined amounts of $NaBH_4$. Gas sampling was facilitated by a home-made Swagelok assembly containing a gas-tight septum connected via electrically conducting BOLA tubing which was earthed manually. Gas samples were diluted by injecting sampled gas into a smaller gas bottle fitted with a Suba Seal® septum. **(B)** A photograph of the BOLA/Swagelok apparatus (1) the GL-45 cap with 3 GL-14 threaded distributors on its head. The unused port is sealed with GL-14 screw-cap; (3) the sampling connection assembly; and (4) the sampling assembly. All components are listed in Appendix 3. (The apparatus was designed by Dr. Caroline Autenrieth, Dept. of Bioenergetics, IBBS.)

2.5.6. Calibration of the GC signal arising from CO_2

A custom-filled gas cylinder containing a precise defined H_2/CO_2 (vol %) ratio (6 % H_2 and 2 % CO_2) was obtained commercially (Kraiss and Fritz, Stuttgart). The 6% H_2/ 2 % CO_2 (the rest is N_2, which is not observable here) gas mixture (initially under pressure) was used to flush a 100 ml bottle for 2 min, then the cap tightened during flushing. The cap was then loosened briefly to release the excess pressure and then tightened immediately. A 1 ml sample was then taken using the septum described in the $NaBH_4$ experiment above.

2.6. O_2 consumption experiments by use of glucose oxidase (GOX) with glucose as substrate

Oxidation of glucose by GOX (from *Aspergillus niger*, Fluka (Sigma Aldrich) Missouri, USA) consumes O_2 as electron acceptor and produces gluconic acid, and H_2O_2. Equimolar O_2 and glucose are consumed by this reaction. In preliminary experiments, the consumption of dissolved and atmospheric O_2 was measured in 2 ml cuvettes, with 1.8 ml of headspace, sealed by means of SubaSeal(s). The gaseous O_2 conc. in the cuvette headspace was measured by withdrawing 0.5 ml air from the headspace and filling the rest of the 1.5 ml syringe volume with N_2 from the N_2 reservoir bottle. The reaction was performed overnight and gaseous samples were withdrawn only once from each cuvette. 100 mM glucose (~ 5 times K_m = 18.18 mM), and 10U/ ml assay mix GOX (2U) was mixed in a 200 µl volume assay in 100 mM Na-phosphate buffer pH 7.0 and stirred overnight with a magnetic stirrer. All measurements were done in duplicates.

The final scaled-up GOX-mediated O_2 consumption experiment with S-depleted *C. reinhardtii* was carried out with the standard BOLA S-depletion bottle, where the headspace of the setup was connected via tubing to the headspace of a sealed 500 ml reservoir bottle (Setup II) containing 50 ml reaction mixture (O_2 consumption system) of 1000 U of GOX, and 100 mM glucose in 100 mM Na-phosphate buffer such that total headspace volume of the system is ~90%.

2.7. Measurement of oxygen production and consumption using a Clark-type electrode

Oxygen exchange activities were measured with a Clark-type oxygen electrode (Hansatech, Norfolk, UK). A late log-phase *C. reinhardtii* culture was concentrated ten-fold and triplicate sets of 100 µl and 200 µl aliquots were re-suspended in fresh TAP medium in a final volume of 1.5 ml into the reaction cuvette of the electrode. Respiratory oxygen uptake was detected in the dark, and photosynthetic oxygen evolution was measured with a focused beam lamp as

light source. The rate of each process was recorded until a straight line appeared on the output sheet. The oxygen electrode was calibrated with air saturated TAP medium (= 100 % oxygen) and Na-dithionite treated TAP medium (0 % oxygen). The concentration of dissolved O_2 was determined by using Henry's Law:

$$P_{o2} = x_{o2} K_H \qquad (5)$$

where P_{O2} is the partial pressure of O_2, K_H is Henry´s constant for O_2 (4.4×10^9 Pa), and the mole fraction x_{O2} is approximated (in dilute solution) as:

$$x_{o2} = \frac{n_{o2}}{n_{H2O}} \qquad (6)$$

where n_{O2} and n_{H2O} are the mole numbers for O_2 and H_2O respectively. Since P_{O2} and K_H are known, the concentration of dissolved oxygen can be readily calculated assuming that n_{H2O} = 55.5 moles (≡ 1 litre H_2O).

The temperature of the cuvette was maintained at 21°C (the *C. reinhardtii* growth temperature). The path-length, incident light intensity and temperature were held constant throughout the experiment.

3. RESULTS

3.1. Method development for this study

3.1.1. Basic experimental considerations for the use of the GC for gas measurement

3.1.1.1. The effect of temperature variation upon the GC measurement of gas concentrations

Since the GC is operating in a laboratory with varying ambient temperature, we thought it necessary to consider the accuracy of the measurement with temperature variation. A plot of the micromolar volume with temperature, calculated using the ideal gas equation (equation (3)) is shown below (Fig. 3.1):

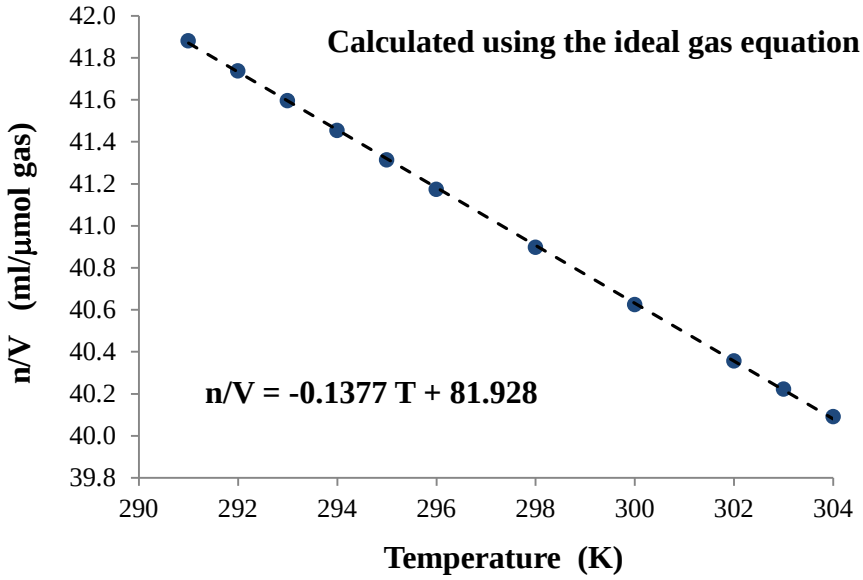

Fig. 3.1. Temperature variation of the micromolar gas volume, calculated from the ideal gas equation. A value of 1 atm. (1.01325×10^5 Pa) was used for the ambient pressure.

The numerical values indicate a maximum of 4% error over the complete ambient temperature range encountered for the measurements reported here. This error is small and probably similar to the accuracy of the volume drawn into the syringe. Nevertheless, a temperature (measured with a digital thermometer (Voltcraft, Germany)) correction of the GC data was performed routinely.

3.1.1.2. The effect of pressure variation upon the GC measurement of gas concentrations

The injection of samples into the GC sample loop occurs at atmospheric pressure. However, in many cases the samples in the experimental setup are at slightly elevated pressure. This complicates the interpretation of the GC measurement, since although higher sampling pressures will not change the gas composition they ***will*** affect the absolute gas concentration injected into the loop.

Initially, we attempted to compensate for the pressure effect by diluting the syringe volume with N_2 directly. However, unacceptable large errors were introduced with this method. After some trials, we devised an alternative methodology which obviates the pressure effect.

The sampling protocol:

(1) the sample was obtained from experimental setup (calibration bottle or cell culture gas) and injected into the gas-tight 216.17 ml ***gas dilution bottle*** (see Materials and Methods);

(2) the gas-tight syringe was rinsed three times with ambient air;

(3) A 1.5 ml sample (now pressure-equalized) was withdrawn from the gas dilution bottle and used for the GC measurement directly. The dilution factor was used to correct the concentration value obtained by GC.

(4) Between each sampling event, the gas dilution bottle was flushed thoroughly with air to remove residue from the previous sample.

3.1.1.3. O_2 contamination of the N_2 supply line

A standard in-house N_2 supply line was used to fill up the SubaSeal(ed) bottle to create a N_2 gas reservoir for use in O_2 and CO_2 calibration experiments (see Materials and Methods). Although the N_2 source is O_2-free, the connection line in the laboratory allows a small amount of O_2 to enter. This explains the small O_2 peak that appears on the GC chromatograms of pure "N_2" gas. It was found that, the N_2 supply line is contaminated with an average of 26 µl air/ml of N_2, or contains 0.54% by volume O_2 (with a standard deviation of 0.1%) or 0.230 µmol O_2 per ml at 20 °C. GC measurements reported here were routinely corrected to eliminate this baseline value.

3.1.1.4. Use of GC sample loop overfill

The GC was equipped with a 1 ml sample loop and in trial experiments a 1 ml injection volume of gas was used for making measurements. Trial runs of the GC showed that an average of 5% by volume or 58 µl air found its way into the GC column resulting in a small O_2 peak (no detectable CO_2 peak) when sample loops were left empty. This demonstrates that, unfilled or insufficiently filled loops tend to draw in some air externally (possibly through the sample vent), and to overcome this dilution effect, loops were routinely filled completely by injecting 1.5 ml total sample in the loop. Thus, the standard deviation for the O_2 peak area was only 1.4 % when 1.5 ml air samples were used compared to 2.7 % when 1 ml air samples were injected.

3.1.1.5. Determination of the GC conversion factor for O_2 calibration

Experiment (1) (high [O_2]): A calibration series was performed with four different concentrations (21%, 14%, 10.5 %, and 7%) of O_2, derived by mixing air and N_2 gas in ratios of (1:0), (2:1), (1:1) and (1:2), respectively, and the samples quantified by GC analysis. All measurements were performed in triplicate. The results (Fig. 3.2) show convincing linearity between the GC peak area (1.7% standard deviation) and the injected volume.

O_2 conversion factor = 2.67 µmol O_2/mV.min.

Experiment (2) (low [O_2]): A second experiment was performed using a lower range of O_2 concentrations. The lower [O_2]s (0.5%, 0.8%, 1.1%, 1.7%, 2.3%, 2.8%, 3.5%, 4%) were obtained by spiking a 17 ml N_2-filled SubaSeal(ed) Pyrex tube with varying volumes of air. As above the GC area was shown to be linear with the injected volume (Fig. 3.2), and the conversion coefficient was essentially identical to the above.

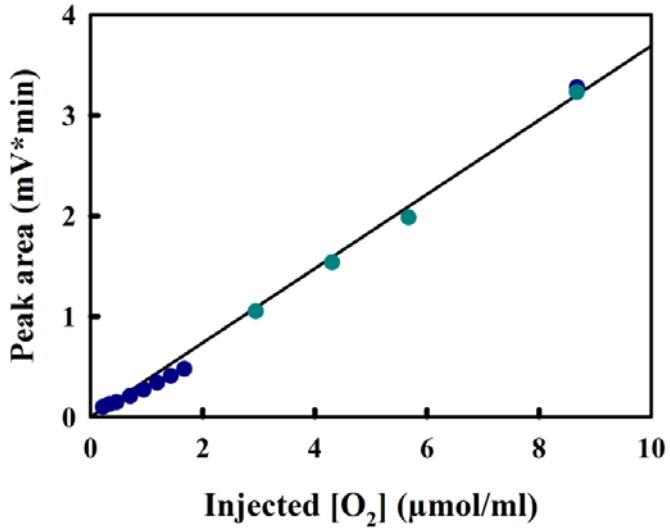

Fig. 3.2. Linearity of the GC signal to the [O_2]: light blue points (experiment 1), the high concentration range; dark blue points (experiment 2), the low concentration range. The standard deviations are within the diameter of the data points shown.

3.1.1.6. Determination of the GC conversion factor for H_2 calibration

The determination of the GC-conversion factor for O_2 now allows us to determine the GC-conversion factor for H_2 by a straightforward application of Dalton's law:

$$P_{tot} = P_{O2} + P_{CO2} + P_{N2} + \sum P_i \qquad \text{(no } H_2\text{)} \qquad (7)$$

and

$$P'_{tot} = P'_{O2} + \boldsymbol{P_{H2}} + P'_{CO2} + P'_{N2} + \sum P'_i \qquad (+ H_2) \qquad (8)$$

where each P_i corresponds to the partial pressure of the gas *i*. The Σ P_i term indicates the values of the trace gases, which are not considered here explicitly. In the presence of H_2 in the same closed system, the total pressure (P_{tot}) is increased to P'_{tot} and all of the partial pressures other than hydrogen will be decreased accordingly (represented by P'_i).

To perform this procedure, we need only to generate a defined amount of H_2 in the same closed system used for the determination of the O_2 conversion factor, determine the modified [O_2] by GC and then use this value to determine the GC conversion coefficient for H_2. This calculation is described in detail below.

We generated molecular hydrogen using the $NaBH_4$ hydrolysis reaction as described in Materials and Methods. Thus, according to equation (4), a 0.23 g $NaBH_4$ pellet (doped with 10% (w/w) Co^{2+} catalyst) dissolved in 40 ml H_2O should yield **21.88 mmol H_2** (corresponding to an excess pressure of 0.47 atm) assuming that the reaction goes to

completion. The position of completion was determined by following the production of H_2 in the closed bottle following dissolution of $NaBH_4$:

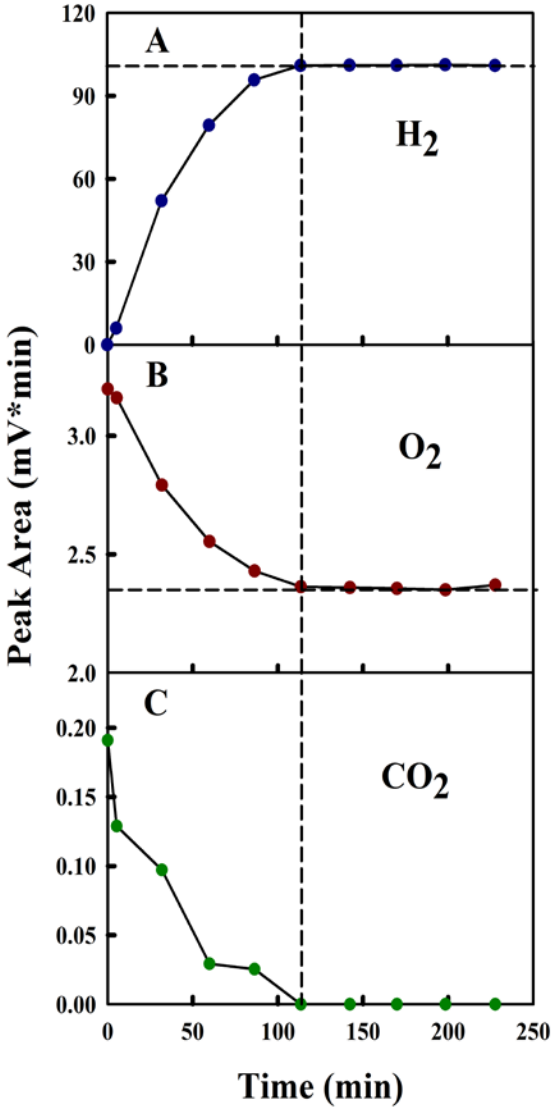

Fig. 3.3. The measured peak areas obtained in a $NaBH_4$-H_2 evolution experiment performed at 294K. The zero time point refers to the time after addition of $NaBH_4$ pellet to water and sealing of the vessel. The reaction is essentially complete after 120 min. Note that from our calculations in Table 3.1 that the reaction probably only goes to 72% completion, due to competing side reactions.

If this reaction is performed in a closed bottle previously filled with ambient air, the molar values of the other components (e.g. O_2, CO_2, N_2) will remain unchanged (the reaction of H_2 with O_2 at room temperature in the absence of a Pt catalyst is negligible). However, the total pressure in the bottle will rise above atmospheric pressure **solely due to the presence of H_2**. When a sample from the experimental bottle is now injected into the GC at atmospheric pressure, the decrease of pressure in the total sample (in the sample loop) will also decrease the partial pressure due to O_2 due to the reduced molar fraction (x'_{O2}).

$$P'_{O2} = P'_{total} x'_{O2} \qquad (9)$$

Now since we have already determined a conversion factor for O_2, we can use this to calculate the number of moles of O_2 in the H_2-containing 1 ml sample, and from the ideal gas equation, calculate the effective pressure (P'_{total}) in the H_2 containing bottle. A typical dataset is shown below (Table 3.1):

	Initial sample, T = 294 K (21°C)								
	1 ml ambient air				**1 ml (air + H_2)**		**GC measurement**		
Gas	**n_i (μmoles)**	**x_i**	**Peak area (mV.min)**	**T_1 (expt) (K)**	**n_i (μmoles)**	**x_i**	**Peak area (mV.min)**	**n_i' (μmoles)**	**x_i'**
N_2	32.365	0.7808			32.365	0.52919		24.102	0.58144
O_2	**8.684**	0.2095	**3.2470**	**294**	**8.68**	**0.14193**	**2.418**	**6.467**	**0.15601**
Ar	0.391	0.0094			0.391	0.00639		0.291	0.00702
CO_2	0.013	0.0003	0.22770		0.013	0.00021		0.01	0.00023
H_2	0.000	0.0000	0.00000	294.4	**14.21**	**0.32227**	**99.239**	**10.582**	0.25529
	41.452			**Total**	**55.663**				
P (Pa) =	**101325**			**P (Pa) =**	**136064**				

Table 3.1. A typical dataset for calibration of the GC for H_2 and O_2. 19.7 μmol/ml corresponds to 21.88 mmol H_2 liberated from a 0.23 g pellet of $NaBH_4$ (90% by weight) in 1110 ml bottle volume. Note that at 1 atm. pressure and 292 K, the volume occupied by 21.88 mmol H_2 is 524 ml. If the reaction goes to 72% completion, this would yield about 377 ml H_2, which corresponds reasonably well to the value of ~ 500 ml H_2 evolution/pellet reported in the Sigma-Aldrich catalogue.

Step 1: from the GC-O_2 conversion factor we calculate that the peak area (PA) of O_2 for the H_2-containing sample (PA(air+H_2)) corresponds to **6.464 μmoles O_2**. However, the molar value of O_2 (n_{O2}) in the H_2-containing closed bottle is unchanged (i.e. 8.68 μmoles (PA(O_2)). The pressure (P_T') in the H_2-containing bottle is now calculated as:

$$P_T' = \gamma P_T \qquad (10)$$

where:

$$\gamma = \frac{PA(O_2)}{PA(H_2+O_2)} = \frac{3.247}{2.418} = 1.342 \qquad (11)$$

which yields the value of 136064 Pa for P_T'. The justification for this calculation is given in the box below (Formalism of gas equation provided by R. Ghosh):

Justification for equations (9) and (10)

In the closed bottle in the **absence** of $NaBH_4$-induced H_2, we can write the gas pressures with Daltons's law:

$$P_T V = (P_{O_2} + P_{N_2} + P_{CO_2} + \sum_i P_i)V \qquad \text{(J1)}$$

which can also be written as:

$$P_T(air) = \boldsymbol{n_{O_2}} \frac{RT}{V} + n_{N_2} \frac{RT}{V} + n_{CO_2} \frac{RT}{V} + \sum_i n_i \frac{RT}{V} \qquad \text{(J2)}$$

In the **presence** of $NaBH_4$-induced H_2, the total pressure increases to P_T', and equation (J2) is modified:

$$P_T'(air + H_2) = \boldsymbol{n_{H_2}} \frac{RT}{V} + \boldsymbol{n_{O_2}} \frac{RT}{V} + n_{N_2} \frac{RT}{V} + n_{CO_2} \frac{RT}{V} + \sum_i n_i \frac{RT}{V} \qquad \text{(J3)}$$

If 1 ml of this gas is filled in the GC sample loop, P_T' will once again be reduced to P_T by a factor γ:

$$P_T(air + H_2) = \gamma^{-1} P'_T = \frac{RT}{V}\left(\boldsymbol{\gamma^{-1} n_{H_2}} + \boldsymbol{\gamma^{-1} n_{O_2}} + \gamma^{-1} n_{N_2} + \gamma^{-1} n_{CO_2} + \sum_i \gamma^{-1} n_i\right) \quad \text{(J4)}$$

or

$$P_T(air + H_2) = \gamma^{-1} P'_T = \frac{RT}{V}\left(\boldsymbol{n'_{H_2}} + \boldsymbol{n'_{O_2}} + n'_{N_2} + n'_{CO_2} + \sum_i n_i'\right) \qquad \text{(J5)}$$

Since we have the GC-O_2 conversion factor, we can calculate n'_{O2} ($= \gamma^{-1} n_{O2}$) from the measured peak area for O_2. In the table, the O_2 peak area ($PA(O_2 + H_2)$) of the H_2-containing sample

= 2.418 mV.min ≡ 6.467 µmoles O_2. However, since the peak area is proportional to the gas concentration, we can calculate γ directly from the GC peak areas:

$$\gamma = \frac{PA(O_2)}{PA(H_2 + O_2)} = \frac{3.247}{2.418} = 1.342$$

Step 2: we note that factor γ is the same for all gaseous components in the H_2-containing sample. Thus:

$$\boldsymbol{n'_{H_2}} = \frac{n_{H_2}}{\gamma} = \frac{14.21\ \mu moles\ H_2}{1.342} = 10.582\ \mu moles\ H_2 \qquad (12)$$

This now allows the GC-H_2 conversion factor (CF) to be calculated from the corresponding peak area:

$$GC - CF\ for\ H_2 = \frac{n'_{H_2}}{PA\ (H2)} = \frac{10.582\ \mu moles\ H_2}{99.239\ mV.min} = 0.106\ \mu moles\ H_2.(mV.min^{-1}) \qquad (13)$$

Thus:

H_2 conversion factor = <u>0.106 µmol H_2/mV.min</u>

3.1.1.7. Determination of the GC conversion factor for CO_2 calibration

To determine the CO_2 conversion factor 1 ml of a commercially supplied defined gas mixture (in vol.%) of 6% H_2/2% CO_2 (the rest is N_2, which is not observable here) was injected into the GC and the respective peak areas from H_2 and CO_2 measured. The peak areas were:

6% H_2: 28.148 mV. min. and **2 % CO_2: 2.9478 mV.min**.

The apparent GC conversion factor for H_2 can now be calculated easily:

6 % H_2 in a 1 ml volume ≡ 0.06 ml H_2

Since 24.04 ml H_2 ≡ 1 mmol H_2 at 293 K, **0.06 ml H_2 ≡ 2.496 µmol H_2**

Thus, the coefficient determined here is **0.0887 µmol H_2/mV.min**., which is 16.3 % lower than that reported above. However, we cannot be sure that during the pressure release of the sampling bottle that some air exchange occurred, which would decrease the absolute amount of H_2 loaded into the GC, or indeed whether some positive pressure still existed in the bottle, which would again decrease the measured peak area. We have therefore chosen to use the H_2 conversion coefficient calculated from the $NaBH_4$ experiment above. Thus, we calculate the H_2 amount in the GC to be (0.106 x 28.147) **2.983 µmol**. Since the ratio of gas volumes is proportional to the molar volumes, then:

3 x 2.9478 mV.min. = 8.8434 mV.min. ≡ 2.983 µmol CO_2.

consequently;

CO_2 conversion factor = <u>0.337 µmol CO_2/mV.min</u>

3.1.2. Development of protocol for starch assay

The starch content of cells was measured by the assaying the amount of glucose present after enzymatic hydrolysis of the starch-containing pellet. The protocol for ethanol extraction of the cell pellet was adapted from Hendricks *et al.* (2003), while the assay conditions used to perform glucose determination was adapted from Bateman and Evans (1995) (see Appendix 4 for more details of the glucose assay). Potato starch and subsequently *C. reinhardtii* cells were used for preliminary experiments for standardization of the starch hydrolysis protocol. The enzymatic hydrolysis of the dissolved starch to glucose was found to be more efficient at 37°C than at 55°C. A mixture of both enzymes α– amylase and amyloglucosidase were found to be most reliable for reproducible results of starch hydrolysis, even though amyloglucosidase alone showed upto 97 % activity as when both enzymes were used (see Fig. 3.4). α–amylase showed an average of 85% of the total activity at 37°C.

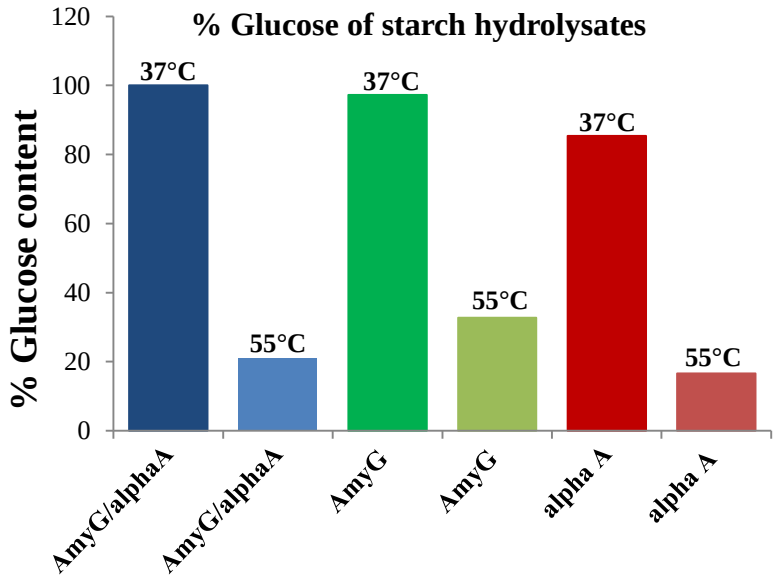

Fig. 3.4. The average percent yields of glucose from starch hydrolysates for a combination of α- amylase (alphaA) and amyloglucosidase (AmyG) incubated at 37°C and 55°C overnight. Duplicate measurements were performed.

A final deionization and centrifugation step was added to the protocol, to help remove small charged ions and phosphorylated sugars and other charged molecules as well as any large macroscopic debris.

For the assay of *C. reinhardtii* cell samples, the use of large volumes of hydrolysate was deemed necessary, especially for cells grown at VLL and samples from the initial growth

phases of IL growth, as the glucose yields were very low. A total of 2 ml sample of cells were pelleted and hydrolyzed and 700 µl of this hydrolysate was used per assay, with a final buffer strength of 50 mM Na-phosphate buffer (50 µl of 0.5 M stock) to obtain measurable results.

3.2. Establishment of physiological "benchmarks" for H_2 evolution in *C. reinhardtii*

3.2.1. Preliminary considerations

3.2.1.1. Light intensity and light quality

The goal of this study is to provide phenotypic "benchmarks", which facilitate comparisons between H_2 production experiments involving *C. reinhardtii*, as well as with purple bacteria (here *R. rubrum*) and cyanobacteria. To our knowledge, all H_2 production studies to date involving *C. reinhardtii* have employed photosynthetically growing cultures, so that light intensity and light quality are important variables. Since most studies involving *C. reinhardtii* have involved different light intensities, as well as different culture dimensions (which modify the luminous efficacy of a given light intensity), a "standardized" light intensity cannot be defined unequivocally. However, a recent systems biology study (Mettler *et al.*, 2014), has shown that the single chloroplast of *C. reinhardtii* exhibits only small variations in its photosynthetic pigment proteins in response to varying light intensity, so it may only be necessary to establish benchmark parameters in a light regime which is within commonly used ranges. An upper limit to this range is probably 500 µmol photons/m^2/s, at which the photosystems are saturated and the electron transport systems show no further increase with increasing light intensity (Kosourov *et al.*, 2007). However, this very high light (VHL) intensity has been seldom employed for H_2 production, partly due to the high energy demand, but also because cells exhibit significant phototoxic stress under these conditions.

More commonly, H_2 production studies (see Discussion for more details) have been performed in the range employed in the Mettler *et al.* (2014) study of between 145 µmol photons/m^2/s (here designated as "high light" (HL) and 41 µmol photons/m^2/s. (here designated as "low light" (LL)). In our study, due partly to technical limitations, we have mainly employed light sources yielding 70 µmol photons/m^2/s, which we consider to be an "intermediate light" (IL) intensity. For some experiments, however, we have also examined effects at "very low" light (VLL) intensities of 5 µmol photons/m^2/s, given by illuminating the cultures with commercial 58 W neon tubes used for general room illumination. A schematic summary of the light intensities used in the literature is shown in Fig. 3.5.

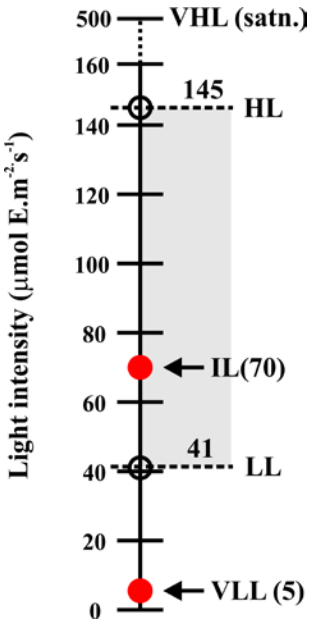

Fig. 3.5. A schematic summary of the light intensities commonly used in the literature. The grey shaded region indicates the HL - LL range defined by Mettler *et al.* (2014). The present study was performed using IL and VLL intensities. The light intensity employed by Hemschemeier *et al.* (2005) (see main text) is also indicated (orange point).

For any photosynthetic organism, the light quality is determined by the wavelength range of the incident light and its overlap with the active photosynthetic pigments. For *C. reinhardtii* and the purple bacterium *R. rubrum*, these requirements are completely different. As indicated in Fig. 3.6, whereas "daylight" LED light sources are perfectly adequate for *C. reinhardtii*, they are completely inappropriate for *R. rubrum*.

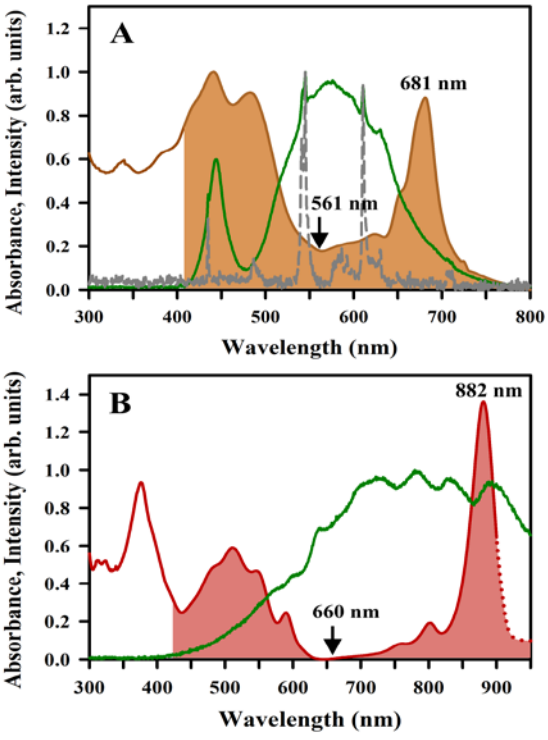

Fig. 3.6. The relationship between light quality and photosynthetic availability. **(A)** absorption spectrum of *C. reinhardtii* (brown line) and its overlap (shaded) with the intensity profile from the "daylight" LED source (green line) used in this study, as well as that of a 58W neon tube light (dashed grey line) commonly used for room illumination; **(B)** absorption spectrum of *R. rubrum* (red line) and its overlap (shaded) with the intensity profile from an incandescent tungsten 40W light source. Useful wavelengths, relevant to this study are also indicated.

3.2.1.2. Choice of wavelength and optical path length for turbidity measurements

The optical measurement of culture turbidity is a useful and rapid indicator of physiological state. However, for photosynthetic organisms, the presence of optically absorbing pigments, which may vary during growth, dictate that the wavelength for turbidity measurements should be chosen to minimize phenotypic variability. For *R. rubrum*, it is now well-established (Ghosh *et al.*, 1994, Grammel *et al.*, 2003, Wang *et al.*, 2012) that 660 nm is optimal for turbidity measurement, since pigment absorption is essentially absent at this wavelength (Fig. 3.6 B). Unfortunately, for *C. reinhardtii*, no analogous wavelength can be detected, since the carotenoid spectral bands overlap significantly with those of Chl. Nevertheless, for this study we have chosen to employ 561 nm for turbidity measurements, as this seems to be the absorption minimum between the two types of pigments (Fig. 3.6A).

Finally, we routinely use 4 mm path length cuvettes (which also have an alternative 1 cm path length face), since we have shown previously (for *R. rubrum*), that the dynamic range of this path length remains linear until a turbidity of 1.4 (effectively equivalent to an A_{561} (1 cm) = 3.5, which cannot be estimated accurately using a 1 cm path length cuvette). Beyond this value, culture samples must be diluted.

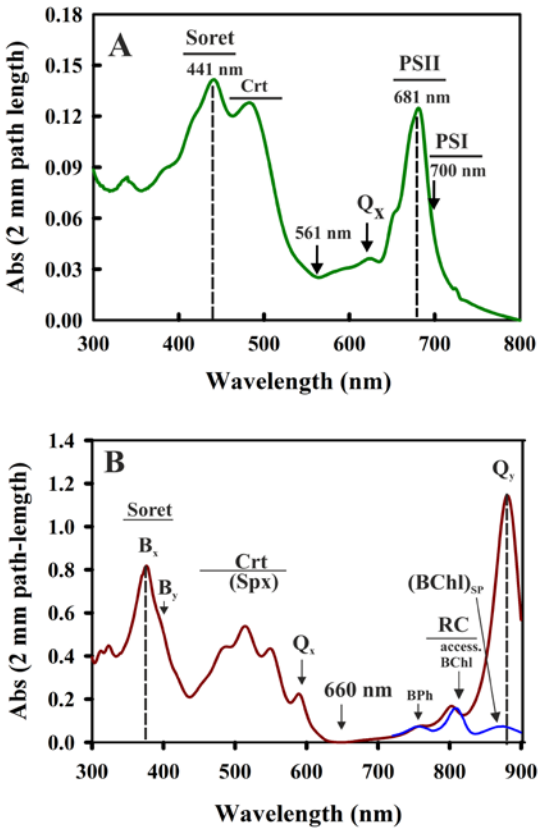

Fig. 3.7. Whole cell absorption spectrum of *C. reinhardtii* **(A)** showing the spectral characteristics of the PSI and PSII complexes with a shoulder at 655 nm for Chl b absorbance. The Soret band region and carotenoid peaks are indicated. **(B)** the whole cell spectra of *R. rubrum* S1 (red line). The absorption peaks due to carotenoids, the $(BChl)_{SP}$ special pair with λ_{max} of 870 nm, the Q_x and Q_y corresponding to the BChl absorption maxima, and Soret bands (B_x, B_y) are indicated. The spectrum shown in blue corresponds to that of purified RC in reduced form.

3.2.2. Growth dynamics of *C. reinhardtii*

3.2.2.1. *C. reinhardtii* growth in TAP medium

In *C. reinhardtii*, growth depends on photosynthetic C-fixation, which can be altered by changes in the light intensity. When *C. reinhardtii* is cultured photoheterotrophically with acetate as a carbon source in TAP medium, it is able to achieve high rates of photosynthesis and accumulation of C-reserves, leading to an increase in the growth rate at IL intensity over VLL intensities. Light intensity differences determine the specific growth rates and the final ODs reached at the end of exponential growth. We note that, since all cultures were inoculated with a 1% (by volume) inoculum from a late-log phase pre-culture grown at the respective light intensities, the number of cells in the inoculum will be therefore higher for IL cultures than for VLL cultures.

In the widely-used TAP medium, which employs 20 mM Tris to buffer the system at pH 7.0, the counter ion is acetate. From the Henderson-Hasselbalch equation, one can calculate that the weak base Tris (pKa = 8.08) is present to about 93 % in the protonated form at pH 7.0, whereas acetic acid (pKa = 4.36) is present almost exclusively in the ionized form. Thus, at pH 7.0, the Tris-acetate ion pair can be considered as to be perfectly matched. However, since acetate is also a substrate for growth, acetic acid uptake results in the depletion of the buffer capacity of the medium and a rise in pH to 8.5 -9.0 towards the end of the exponential growth phase (phase (a) in Fig. 3.8A). A stationary phase is established, though an asymptote or decline in OD is not seen (phase (b) in Fig. 3.8A). Instead, at about 75 h after attainment of the “stationary” phase, the turbidity continues to rise slowly but steadily. This turbidity increase is probably not primarily due to cell growth, since only a minimal increase in the cell number is observed for this phase (see Fig. 3.12), but may be due to other factors:

(1) self-shading in the culture due to increased turbidity, which leads to progressively poor light penetration and the onset of growth limitation;

(2) appearance of light-scattering cellular inclusion bodies (e.g. starch granules and/or lipid droplets);

(3) changes in grana stacking due to the late growth phase physiology;

(4) utilization of metabolic fermentation products in the late phase of growth following the expression of the appropriate enzymes.

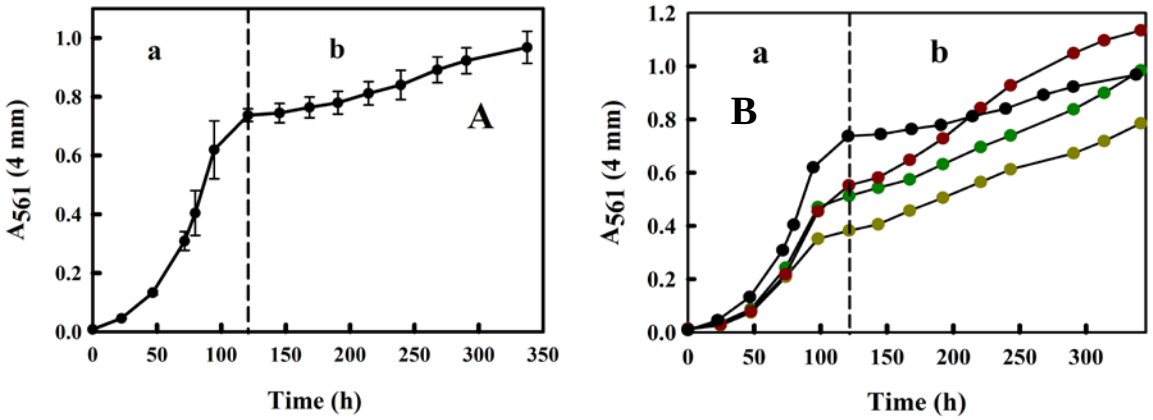

Fig. 3.8. (A) The growth curve of *C. reinhardtii* in standard TAP medium, under IL light, with the exponential (a) and stationary phases of growth (b) indicated. **(B)** The growth kinetics of *C. reinhardtii* in TCP medium under IL intensities. [Na-acetate]: yellow, 8 mM; green, 12 mM; and red, 15 mM. The growth kinetics in TAP medium containing 17.5 mM Na-acetate (from (A)) are also shown (black circles).

For cultures grown at both VLL and ILL intensities, the growth kinetics appear identical, with the completion of phase (a) occurring at about 100 h. However, the attainable cell density at IL intensities was about twice that observed for VLL intensities.

In order to test the effect of acetate as a buffer, we performed a growth experiment using a buffer system where citrate replaces acetate as a counterion (TCP medium) and defined amounts of Na-acetate are added after the buffer had been adjusted. Although citrate is a tricarboxylic acid with three pKa's (3.13, 4.76, 6.4), only the pKa value of 6.4 is relevant for a pH 7.0 buffer system, so that the total [citrate] in TCP medium should be equivalent to that of acetate in TAP medium.

Growth in TCP medium under IL conditions yielded an interesting result. Whereas the initial growth phase (phase (a)) kinetics were qualitatively identical to those of TAP medium, with the “stationary” cell densities approximately proportional to the [Na-acetate], the phase (b) kinetics deviated significantly (see Discussions).

However, for further growth and H_2 production experiments, the use of TCP medium was not adopted to ensure conformity to published literature and to prevent an additional experimental variable.

3.2.2.2. The relationship between [protein] and [Chl] changes under IL and VLL growth conditions

The fundamental relationships between the growth kinetics under both IL- and VLL-grown cultures and characteristic physiological parameters (e.g. protein content, [Chl], and cell number) determined in this study are shown below (Fig. 3.9):

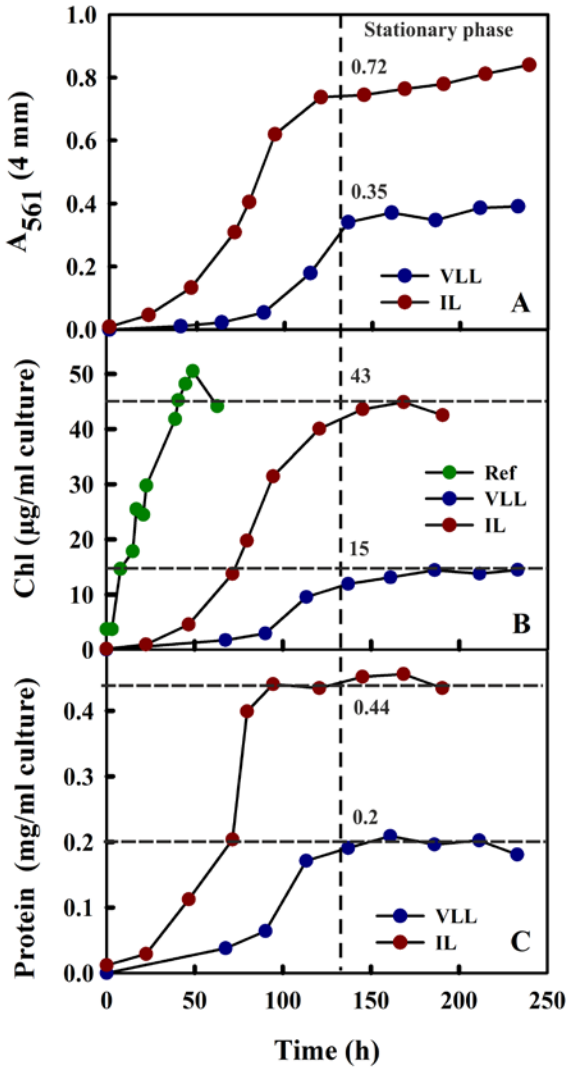

Fig. 3.9. Comparative physiological parameters of turbidity, Chl content and protein content with time, for *C. reinhardtii* growing under IL (red circles) and VLL (blue circles) intensities. "Ref" or reference, corresponds to Chl accumulation in CC-124 cultures grown at 140 µmol photons/m^2/s light intensity by Torzillo *et al.* (2009) shown here for comparison. The stationary phase is marked by the vertical dashed line, with the values of the respective parameters at the stationary phase (horizontal dashed lines) mentioned therein.

The data can be summarized as follows:

(1) the overall growth kinetics of both IL- and VLL-grown cultures is essentially identical, with the "stationary" phase being attained in the same time period (about 120 h). However, the final cell densities in VLL-grown cultures is about half that of IL-grown cultures. This is slightly surprising since it might be expected that low light levels only affect the growth rate and not the final yield. Possible reasons for this result will be examined in the Discussion section.

(2) The total protein content of the cells largely corresponds to the cell density (Fig. 3.10).

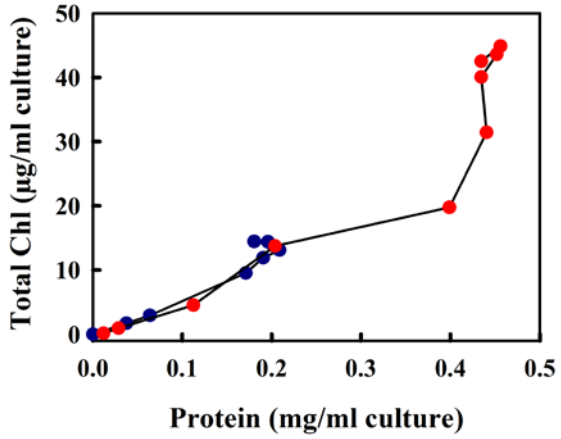

Fig. 3.10. Comparative physiological parameters of Chl content per volume culture plotted against the protein content for *C. reinhardtii* growing under IL (red circles) and VLL (blue circles) intensities.

(3) The [Chl] corresponds well with the cell densities of the cultures grown under both IL and VLL conditions, respectively. This indicates that the single chloroplast is replicated faithfully without significant changes of photosynthetic pigment composition (also the PSI/PSII ratio) during cell growth. However, the [Chl]/[protein] ratio of the VLL culture is only about 74 % of the IL culture, indicating that chloroplast biosynthesis is modulated by the light intensity, as expected from many studies of photosystem expression in *C. reinhardtii* (Malnoë *et al.*, 1988; Rochaix, 1996; Teramoto *et. al.*, 2002). Nevertheless, the variation of this factor is far below that observable in many plant systems. Interestingly, with respect to the total [Chl] attainable, the IL data also corresponds closely to the data of Torzillo *et al.* (2009) which also employed strain CC-124 but grown under HL (140 µmol photons/m^2/s) conditions.

(4) A more detailed insight into the chloroplast composition during growth can be obtained by measuring the amounts of Chl *a* and Chl *b*, since these pigments are unequally distributed between PSI and PSII, as well as their associated LHCs (see Discussion). The values of total Chl as well as Chl *a* and Chl *b*, show stable ratios to each other throughout the exponential and stationary growth phases, with the amounts rising linearly during the exponential phase

(Fig. 3.11). The ratio of Chl *a* to Chl *b* lies between the narrow range of 2.3 to 2.7, throughout the rise in total chlorophyll amounts or culture turbidity. Cultures at VLL intensities show similar behaviour (not shown here). The relatively constant ratios of Chl *a* to Chl *b* indicate a stable PSI to PSII ratio throughout the exponential and stationary phases of aerobic growth at both IL and VLL intensities.

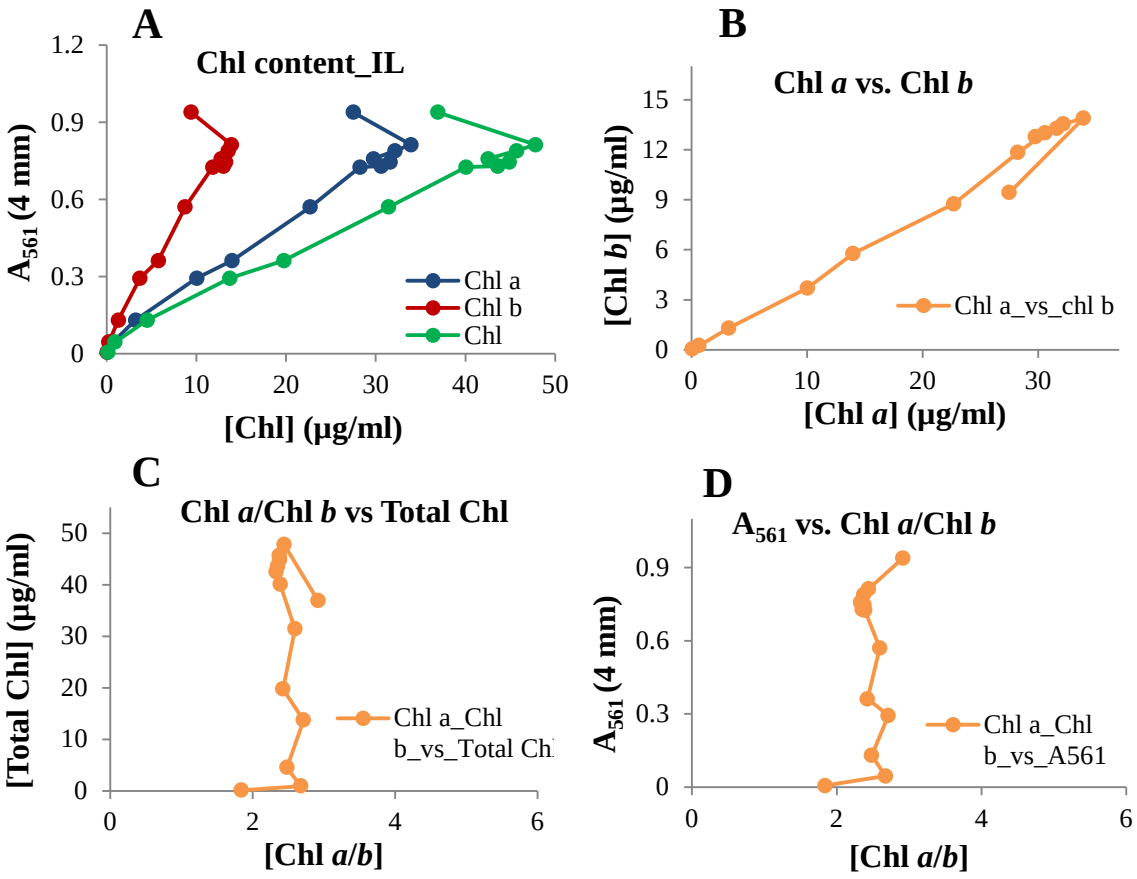

Fig. 3.11. (A) Variation of A_{561}(4mm) vs. the total Chl and the Chl *a* or Chl *b* species, respectively **(B)** Variation of Chl *a* with Chl *b* during the growth curve; **(C)** Total Chl plotted against the ratio of Chl *a*/*b*. **(D)** The A_{561} plotted against the ratio of Chl *a*/*b*.

Interestingly, although the cellular proteins are encoded by three different genomes (nucleus, chloroplast, mitochondrion), the total protein content also showed a near linear rise with turbidity. However, at equal values of turbidity, cells at VLL intensity contain half the amount of Chl and 75% of the protein as those grown at IL intensities.

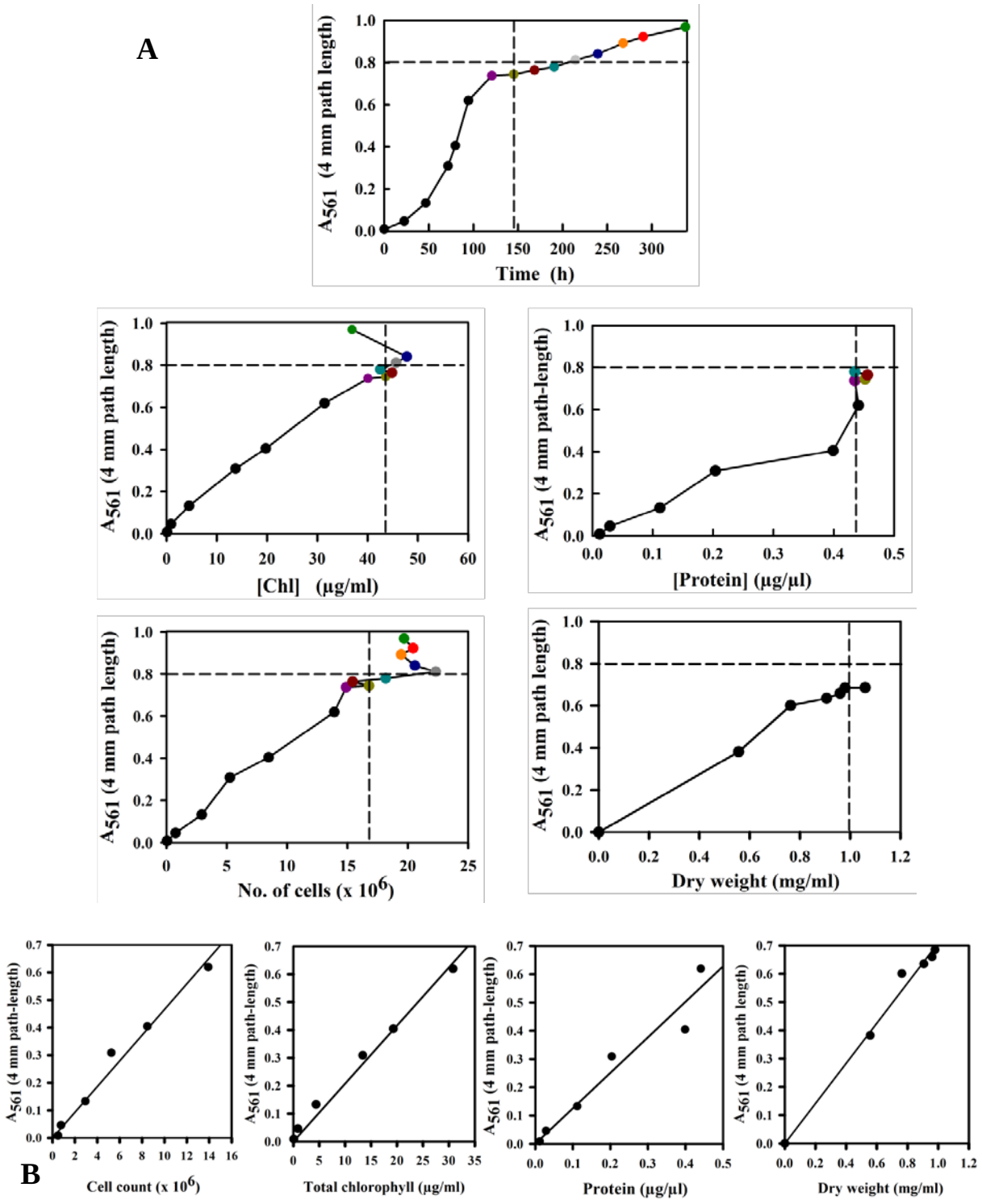

Fig. 3.12. **(A)** The physiological parameters at IL intensities of cell count, Chl content, protein and dry weight plotted vs. turbidity (A_{561} (4 mm)), with the black dotted lines indicating the OD where exponential growth gives way to the stationary phase. The values below the dotted lines were used to derive the linear correlations of the type y = m.x +c, where c is 0 as the lines pass through the origin. **(B)** The linear portions (only) of the plots are shown.

Using linear curve fitting functions within the exponential growth phase, coefficients of conversion between culture turbidity and each physiological parameter measured could be established both under IL and VLL intensities. Turbidity measured at A_{561} was also correlated to A_{600} (a commonly used wavelength for turbidity measurements of bacterial cultures) (Fig. 3.13).

Our results provide a roadmap for establishing similar coefficients of microalgal growth. The use of turbidity values to describe other physiological growth benchmarks has been routinely used in the field of microbiology, but a systematic correlation between parameters has been absent in *C. reinhardtii* literature. The derived correlations were consistent in subsequent experiments.

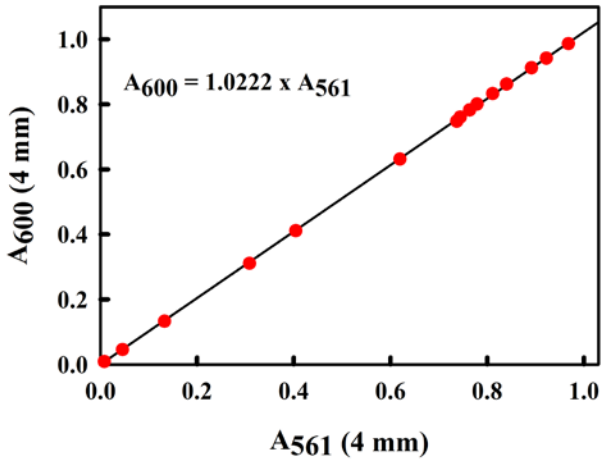

Fig. 3.13. The correlation of *C. reinhardtii* turbidity measured at 561 nm and 600 nm in a 4 mm path length cuvette. The turbidity at 600 nm is 1.022 times the turbidity at 561 nm.

3.2.2.3. *Benchmarks for C. reinhardtii* grown at IL intensity of 70 µmol photons/m^2/s

(1) A_{561}(4 mm) = 0.0473*(no. of cells x 10^{-6}/ml); 1 x 10^6 cells/ml ≡ A_{561} =0.0473; **A_{561} = 0.473 ≡ 1 x 10^7 cells/ml**

(2) A_{561}(4 mm) = 0.0184*(total Chl in µg/ml); 1 µg/ml total Chl ≡ A_{561} = 0.0184; **A_{561} = 1 ≡ 54.35 µg/ml Chl**

(3) A_{561}(4 mm) =0.0259* (Chl *a* in µg/ml); 1 µg/ml total Chl *a* ≡ A_{561} = 0.0259; **A_{561} = 1 ≡ 38.61 µg/ml Chl *a***

(4) A_{561}(4 mm) = 0.0638*(Chl *b* in µg/ml); 1 µg/ml total Chl *b* ≡ A_{561} = 0.0638; **A_{561} = 1 ≡ 15.67 µg/ml Chl *b***

(5) A_{561}(4 mm) = 1.5546*(total protein in mg/ml); 1 mg/ml total protein ≡ A_{561} = 1.5546; **A_{561} = 1 ≡ 0.643 mg/ml protein**

(6) A_{561}(4 mm) = 0.7007*(cell dry weight (DW) in mg/ml); 1 mg/ml DW ≡ A_{561} = 0.701; **A_{561} = 1 ≡ 1.43 mg/ml DW**

All coefficients are only valid up to A_{561}(4 mm) = 0.72; A_{561} (1 cm) = 1.8

Final interconversion "benchmark" coefficients at IL intensity

(1) **A_{561}(4 mm) = 0.473 ≡ 1 x 10^7 cells/ml ≡ 0.304 mg/ml protein**

(2) **A_{561}(4 mm) = 0.473 ≡ 1 x 10^7 cells/ml ≡ 0.676 mg/ml DW**

(3) **A_{561} = 1 ≡ 54.35 µg/ml total Chl ≡ 1.43 mg DW; 1 µg Chl ≡ 0.026 mg DW**

(4) **A_{561} = 1 ≡ 30.61 µg/ml Chl *a***

(5) **A_{561} = 1 ≡ 15.67 µg/ml Chl *b***

(6) **A_{561} = 1 ≡ 0.643 mg/ml protein ≡ 1.43 mg/ml DW; 1 mg/ml protein = 2.224 mg/ml DW**

(7) **A_{561} (4 mm) = 1 ≡ 1.43 mg/ml DW**

All coefficients are only valid up to A_{561}(4 mm) = 0.72; A_{561} (1 cm) = 1.8

3.2.2.4. Benchmarks for *C. reinhardtii* grown at VLL intensity of 5 µmol photons/m^2/s

(1) A_{561}(4 mm) = 0.0394* (no. of cells x 10^{-6}/ml); 1 x 10^6 cells/ml ≡ A_{561} =0.0394; **A_{561} = 0.394 ≡ 1 x 10^7 cells/ml**

(2) A_{561}(4 mm) = 0.0375*(total Chl in µg/ml); 1 µg/ml total Chl ≡ A_{561} = 0.0375; **A_{561} = 1 ≡ 26.64 µg/ml Chl**

(3) A_{561}(4 mm) =0.0557* (Chl *a* in µg/ml); 1 µg/ml total Chl *a* ≡ A_{561} = 0.0557; **A_{561} = 1 ≡ 18.9 µg/ml Chl *a***

(4) A_{561}(4 mm) = 0.115*(Chl *b* in µg/ml); 1 µg/ml total Chl *b* ≡ A_{561} = 0.115; **A_{561} = 1 ≡ 7.8 µg/ml Chl *b***

(5) A_{561}(4 mm) = 2.0531*(total protein in mg/ml); 1 mg/ml total protein ≡ A_{561} = 2.0531; **A_{561} = 1 ≡ 0.49 mg/ml protein**

All coefficients are only valid up to A_{561} (4 mm) = 0.35; A_{561} (1 cm) = 0.875

Interconversion coefficients at VLL intensity

(1) **A_{561}(4 mm) = 0.394 ≡ 1 x 10^7 cells/ml ≡ 0.19 mg/ml protein**

(2) **A_{561} = 1 ≡ 26.64 µg/ml total Chl ≡ 0.48 mg/ml protein; 1 µg Chl ≡ 0.0180 mg protein**

(3) **A_{561} = 1 ≡ 18.9 µg/ml Chl *a***

(4) **A_{561} = 1 ≡ 7.8 µg/ml Chl *b***

All coefficients are only valid up to A_{561} (4 mm) = 0.35; A_{561} (1 cm) = 0.875

3.2.3. Additional aspects of *C. reinhardtii* physiology relevant to the present study

Both starch content and dark respiration rates are intricately linked to H_2 production physiology of *C. reinhardtii*, contributing to the extent of H_2 being produced and the time required to establish anaerobiosis in S- depleted cultures.

3.2.3.1. Glucose content of *C. reinhardtii* cells

The levels of starch accumulation (measured as glucose units) at the end of exponential growth was 4-fold increased under IL conditions compared to those observed under VLL conditions. The pattern of starch accumulation follows the growth kinetics of the culture under IL conditions, with similar exponential rise of turbidity and starch content until the stationary phase is reached. This is not quite the case at the VLL intensities, where the rise in starch levels are very gradual, increasing well into the stationary phase. At an A_{561} (4 mm) of 0.3 at VLL conditions, 0.015 µmol glucose was detected per ml culture, while at IL, the glucose content was 0.214 µmol/ml culture, at equivalent turbidity. The starch content in the stationary phase increases with time of incubation at VLL intensity. The starch accumulation pattern is similar to that of the Chl and protein accumulation, with large differences in the amounts measured between the two light conditions.

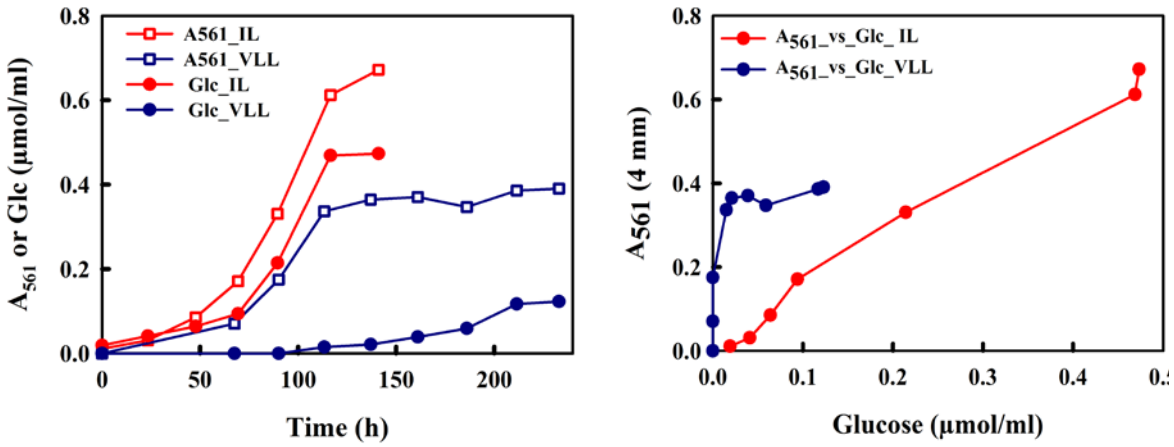

Fig. 3.14. The starch accumulation pattern with time **(A)** and as a function of culture turbidity **(B)** at IL and VLL conditions. **(A)** The growth curves at both IL and VLL are shown in red and blue open square symbols and the corresponding starch contents in filled circles respectively.

3.2.3.2. Investigations into rates of dark respiration

Dark respiration and photosynthetic O_2 evolution rates were determined directly by measurement of the rate of consumption and production of dissolved O_2 (dO_2) in culture in the dark and in light, respectively. Instantaneous changes in dO_2 content occurred upon dark and light incubation.

The average dark respiration rate measured at both sample turbidities of A_{561} (4 mm) = 0.46 and 0.89, was found to be identical when rates were normalized to the same number of cells, with the rate being a direct function of the cell number or turbidity, doubling when twice the number of cells in the same volume were measured (See Table 3.3). The average dark respiration rate for 10^6 cells was 0.10 % O_2 saturation per min with a standard deviation of 0.021 across all samples.

The rate of photosynthetic O_2 production was not proportional to the cell number as observed with the respiration rates. When normalized to the same number of cells (10^6 cells) the rate was half at the higher A_{561} (4 mm) of 0.89 than at 0.46, with the overall rates of O_2 production for the total number of cells in 1.5 ml volume remaining identical at both cell densities. Thus, the rate of photosynthesis per cell was found to be inversely proportional to culture turbidity or Chl content, at constant incident light intensity. This effect is due to the efficiency of light penetration into turbid cultures.

	Rates at respective A_{561} (4 mm)			**Rates per 10^6 cells**			
A_{561} (4mm)	**Dark respirn. rate (%O_2 sat./ min)**	**Net ps [O_2] prodn. rate (% O_2 sat./min)**	**No. of cells/1.5 ml (x 10^7)**	**Dark respirn. rate (% sat.O_2/min)**	**Net. [O_2] prodn. (% O_2 sat./10^6 cells/min)**	**Dark respirn. (nmol/1 0^6 cells /h)**	**Net. [O_2] prodn. rate (nmol/10^6 cells/h)**
0.46	1.47	1.33	1.44	0.102	0.09	24.80	22.39
0.89	2.79	1.35	2.82	0.099	0.05	24.03	11.61

Table 3.3. Measured rates of dark respiration and photosynthetic O_2 consumption in *C. reinhardtii* cultures re-suspended in fresh TAP medium. O_2 consumption was determined with a Clark-type electrode. The rates were measured at two culture densities.

3.3. H_2 production in *C. reinhardtii* cultures

3.3.1. Setup assembly used for studying gas evolution in the head-space of *C. reinhardtii* sealed cultures grown under illuminated S-depleted conditions

H_2 evolution under S-depleted culture conditions requires that late-log phase cells growing actively in normal TAP medium, are pelleted by centrifugation, washed in S-depleted TAP medium, and then resuspended in the same medium in a gas-tight bottle under illumination (see Materials and Methods for details). After a short adaptation period, the culture becomes anaerobic due to PSII-D1 protein degradation and O_2 consumption via the mitochondrial ETC, H_2 evolution begins. Thus, the experimental setup assembly must be both gas-tight to H_2 (which passes though many materials, including silicon tubing (albeit slowly)) and must also allow gas sampling from the culture headspace.

For the small-scale laboratory experiments reported here, we employed the same BOLA/Swagelok bottle cap assembly used for the $NaBH_4$ experiments above. The bottle cap allows a 1.5 ml syringe sample to be taken from the headspace, which can be analyzed by GC as described above. In our experiments, the culture volume was maintained at 110 ml, which allows a fixed headspace volume of 23 ml headspace.

Fig. 3.15. An image of the bottle assembly setup used here for the S-depletion experiments described here. The bottle was wrapped in plastic foil to minimize the danger of explosion. The fittings were always grounded via an (here orange-brown) earthing wire (for safety). The image shows a typical *C. reinhardtii* cell density used for the S-depletion experiments.

Sampling of the culture for Chl, protein and starch content was only performed before sealing the bottle and after the completion of the experiment.

3.3.2. H_2 evolution by *C. reinhardtii* growing under S-depleted IL conditions

Fig. 3.16 shows typical gas evolution kinetics in the headspace of a *C. reinhardtii* culture growing under S-depletion at IL intensities.

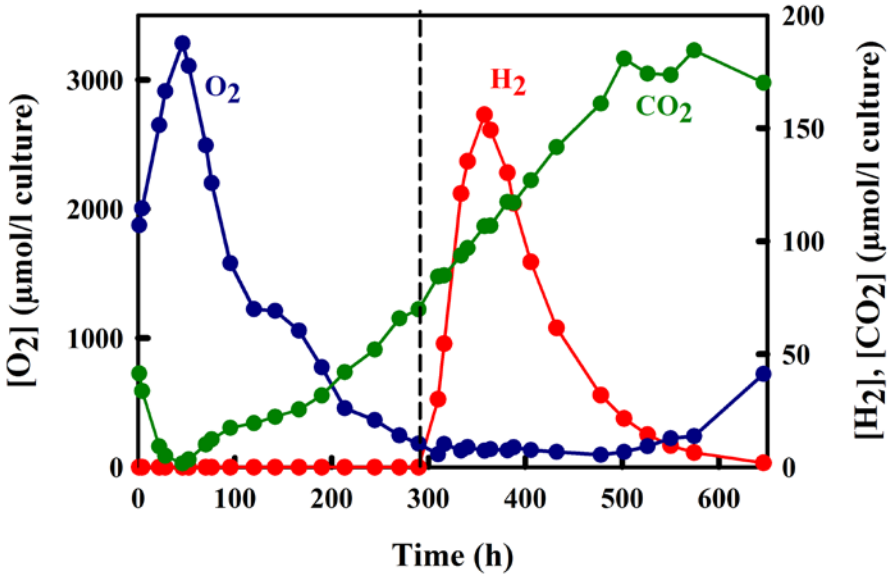

Fig. 3.16. The kinetics of gas evolution in the headspace of an S-depleted culture of *C. reinhardtii* under IL intensities. The culture was initially resuspended at an A_{561} (4 mm) = 0.407. The gas components are indicated, as well as the start of the H_2 production phase (dashed line). Note, the scales for H_2 and CO_2 are different from that of O_2.

The characteristic features of the gas phase kinetics differ significantly from the data of Hemschemeier *et al.* (2005) discussed in the Introduction, even though the cell densities were comparable (Hemschemeier: 14.7 µg/ml Chl; this study: 12.75 µg/ml Chl). In detail:

(1) the time point for the O_2 "turnaround" point between PSII-mediated O_2 production and the ETC-mediated O_2 consumption was longer in this study (Hemschemeier: about 25 h; this study: 70 h);

(2) the time for the complete removal of O_2 was longer (Hemschemeier: 100 h; this study: 300 h);

(3) in this study, a sharp peak in H_2 production was observed, which was not reported in the Hemschemeier *et al.* (2005) data.

We believe that the differences in the gas evolution profile can partly be reconciled with the different experimental configurations in the two studies. In particular, the Hemschemeier setup displaced gas into a measuring cylinder. This not only removes H_2 from the headspace, thereby lessening H_2 uptake, but also displaces O_2 in the early stages of the

experiment. Also, Hemschemeier *et al.* (2005) employed significantly higher light intensities (100 μmol photons.m^{-2}.s^{-1}) than those employed here. The higher light intensity produced more O_2 from PSII, and consequently more singlet oxygen, thus accelerating the loss of PSII protein.

Secondly, a major difference between the two studies is the *C. reinhardtii* strain used. This will be discussed more extensively in the Discussion section.

For our experiments at IL intensity, with the culture resuspended to 12.75 μg Chl/ml culture in Fig. 3.16, O_2 levels continued to rise until 46 h after S-depletion, reaching 1.5 times the atmospheric O_2 level (from 1804 μmol/l culture to 3176 μmol/l culture). The maximum O_2 level coincided with the attainment of the minimum CO_2 levels at 46 h.

Subsequent lowering of the O_2 concentration leads to progressive degradation of Rubisco (Zhang *et al.*, 2002) and non-performance of the Calvin cycle, suppressing CO_2 uptake and accounting for the high CO_2 levels measured during the remainder of the experiment. The O_2 production phase is succeeded by the O_2 consumption phase, which, interestingly, was found to proceed through two distinct sub-phases. Initially, a rapid initial consumption phase lasting from 45 -120 h with a maximum uptake rate of 45 μmol O_2 /l/h was observed, which reduced O_2 levels to 13% by volume (1184 μmol/l). This was followed by a second phase with an average consumption rate of 7 μmol O_2/l/h which appeared to be induced when O_2 falls below a certain threshold value (13%) and continued until 300 h when the O_2 levels were around 1% (176 μmol/l culture).

After 300 h, when sufficiently anaerobic conditions were reached, H_2 production was observed for a period of about 68 h. Thereafter, the decrease in H_2 concentration, representing the uptake of H_2 by the reversible hydrogenase of *C. reinhardtii*, was measured until only traces remained. The appearance of H_2 indicates that photosynthetic electron flow continues with the Calvin cycle being replaced by H_2 production as the alternative electron sink. H_2 was produced at an average rate of 2.3 μmol/l/h and a total of 3.5 ml H_2/l or 156 μmol H_2/l culture was detected at 357 h. The amount of photosynthetic O_2 evolved was found to vary with the Chl content. Experiments with higher (20 μg/ml culture) and lower (7 μg/ml culture) Chl contents could not successfully establish anaerobic conditions in cultures at IL intensities, hence no H_2 production was observed (data not shown). Thin cultures, were generally not able to respire fast enough to establish anaerobiosis, whereas at higher Chl contents too much O_2 was produced to allow anaerobiosis to occur before the medium was exhausted.

3.3.3. H_2 evolution by *C. reinhardtii* growing under S-depleted VLL conditions

Contrary to the observations at IL intensity, at VLL intensities, an initial net O_2 evolution phase was not observed, but the cells were observed to directly pass into the O_2 consumption phase. Fig. 3.17 shows the headspace gas profile for a culture suspended at 9.4 µg Chl/ml culture, where no net O_2 evolution was observed. At such low light conditions, photosynthesis appears to be low enough for respiration to dominate and establish an average rate of O_2 consumption at 40 µmol/l/h, such that the initial atmospheric level of O_2 (1800 µmol/l culture) is reduced to ~30 µmol/l in a time span of 40 h, after which H_2 production ensues with a maximum rate of 0.617 µmol H_2 /l/h reaching 12.5 µmol H_2/l culture in the next 40 h. The low level of O_2 was maintained until 150 hours after S-depletion, rising thereafter. Anaerobiosis, the essential pre-condition for H_2ase activity was maintained for both the H_2 production as well as H_2 consumption phase at both light intensities, indicating H_2ase-mediated active uptake of H_2.

The length of the H_2 production phase at VLL intensities remained between 41 - 49 h for resuspension turbidities between 0.2 - 0.22 and a Chl content between 6.5 - 9.5 µg/ml culture.

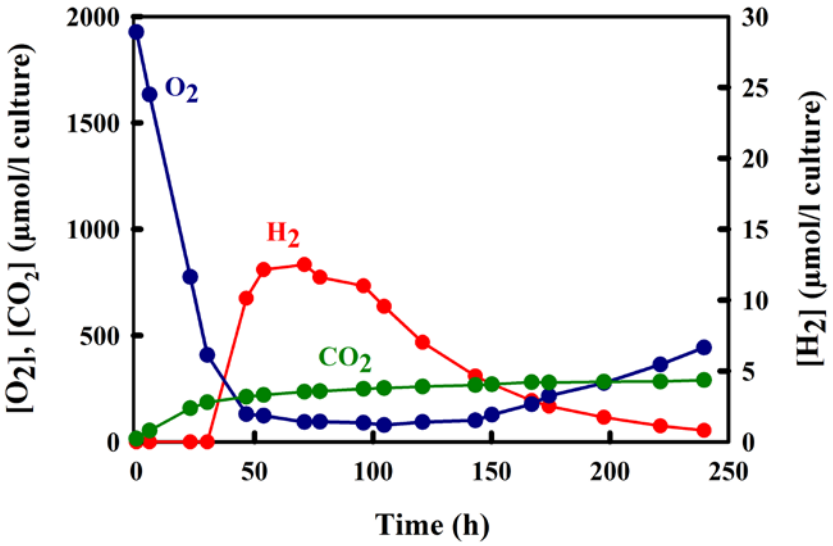

Fig. 3.17. The kinetics of gas evolution in the headspace of an S-depleted culture of *C. reinhardtii* under VLL intensities. Note, the differences in scale for H_2 than for O_2 and CO_2. The cells were resuspended at an initial A_{561} (4 mm) of 0.222. The data are summarized in Table 3.4. The dashed line indicates the commencement of H_2 production.

The salient parameters of H_2 production under IL and VLL conditions, respectively, are summarized in Table 3.4.

Table. 3.4. Summary of the H_2 production data shown in Fig. 3.16 and Fig. 3.17.

H_2 production amounts and rates		
	VLL	**IL**
Length of H_2 production phase (h)	41	68
Time for onset of H_2 prodn. (h)	40	290
Initial no. of cells (x 10^6)	5.6	8.6
Initial [Chl] (µg/ml culture)	9.39	12.7
Initial protein (mg/ml)	0.08	0.23
Initial A_{561} (4 mm)	0.222	0.407
Max. H_2 production rates		
Highest rate of H_2 prodn. (ml H_2/l/h)	0.0138	0.09
Highest rate of H_2 prodn. (µmol H_2/µg Chl/h)	0.066	0.316
Highest rate of H_2 prodn. (µmol H_2/l/h)	0.617	4.009
Highest rate of H_2 prodn. (ml/mg protein/h)	0.0068	0.017
Avg. H_2 production rates		
Avg. rate of H_2 prodn. (µmol H_2/l culture/h)	0.305	2.3
Avg. rate of H_2 prodn. (ml H_2/l culture/h)	0.0068	0.051
Avg. rate of H_2 prod. (µmol H_2/µg Chl/h)	0.033	0.157
Avg. rate of H_2 prod. (µmol H_2/mg protein/h)	0.0034	0.0099
Total H_2 produced		
Amount of H_2 prodn. (ml H_2/l)	0.28	3.494
Amount of H_2 prodn. (µmol H_2/l culture)	12.5	156
Amount of H_2 prodn. (µmol H_2/10^6 cells)	0.0022	0.018
Amount of H_2 prodn. (µmol H_2/µg Chl)	1.331	12.283
Amount of H_2 prodn. (µmol H_2/mg protein)	0.139	0.678
O_2 production/consumption rates		
Highest rate of O_2 consumption. (µmol O_2/l/h)	51	45
Avg. rate of O_2 prodn. (µmol O_2/l/h)	37.5	27
Amount of photosynthetic O_2 produced (µmol O_2/l culture)	0	1371.42

3.3.4. H_2 production at VLL intensities: the special case

In some experiments at VLL intensities, H_2 production was found to commence as soon as 2 or 5 h after resuspension in S-depleted medium, well before anaerobiosis was established in the culture. In the plot shown in Fig. 3.16, the maximum rate of O_2 consumption established was 83 µmol/l/h, which was the highest O_2 consumption rate recorded amongst all S-depletion experiments performed here. This rate of O_2 consumption was the closest to the dark respiration rates (24 nmol/h for every 10^6 cells or 134 µmol/l/h for this experiment). The initial H_2 production at 5 hours occurred when O_2 has been reduced to only 15% (1300 µmol/ml culture) by volume from 21%. Also, the O_2 concentration never reached below 8.6% by volume or 800 µmol/l culture. The total H_2 produced, however, was only 6 µmol/l culture, much lower than in experiments where anaerobiosis (below 2% by volume O_2 in Fig. 3.17) is established (12.5 µmol H_2/l culture) at VLL intensities.

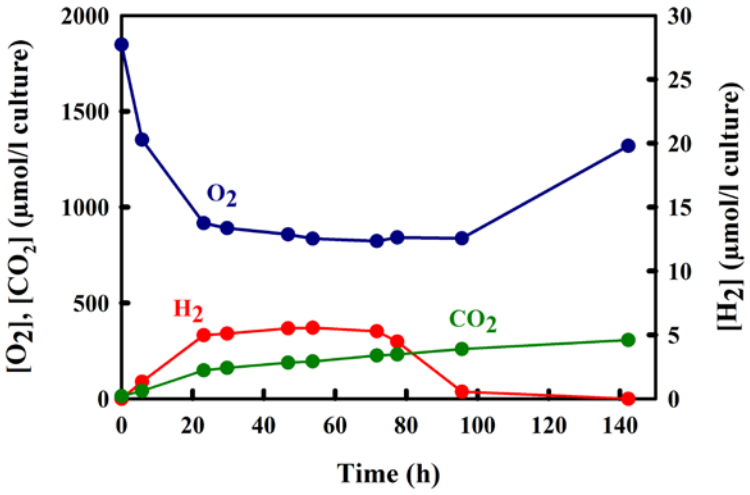

Fig. 3.18. The kinetics of gas evolution in the headspace of an S-depleted culture of *C. reinhardtii* under VLL intensity. Cells were resuspended at an initial A_{561} (4 mm) of 0.207. This profile is representative of a special case which was found to occur at VLL intensities, where H_2 production starts soon after S-depletion and continues even though anaerobic levels of O_2 (usually < 2% by volume O_2 in the headspace) is not established (see text for details).

In all of the experiments conducted at VLL intensities, an initial uptake of CO_2 was not observed, instead a continuous rise of CO_2 was observed. This observation fits well with the absence of the initial net O_2 production phase. However, photosynthetic electron transport does occur at these light intensities, albeit at a much lower rate than for ILL intensities, otherwise the H_2ase induction as the alternate electron sink would not occur. The VLL intensity creates a special condition where photosynthesis is very low, net O_2 consumption is rapidly established and damage to PSII is minimal, and as a consequence of low levels of photosynthesis, H_2 production is also low compared to the rates at IL intensities (see Discussion).

3.3.5. Summary of the effects of S-depletion on cellular physiology

The three key physiological parameters, [Chl], protein content, and starch production, which are often reported in the literature (Melis *et al.*, 2000; Kosourov *et al.*, 2003), are summarized for IL in VLL intensities in Fig. 3.19.

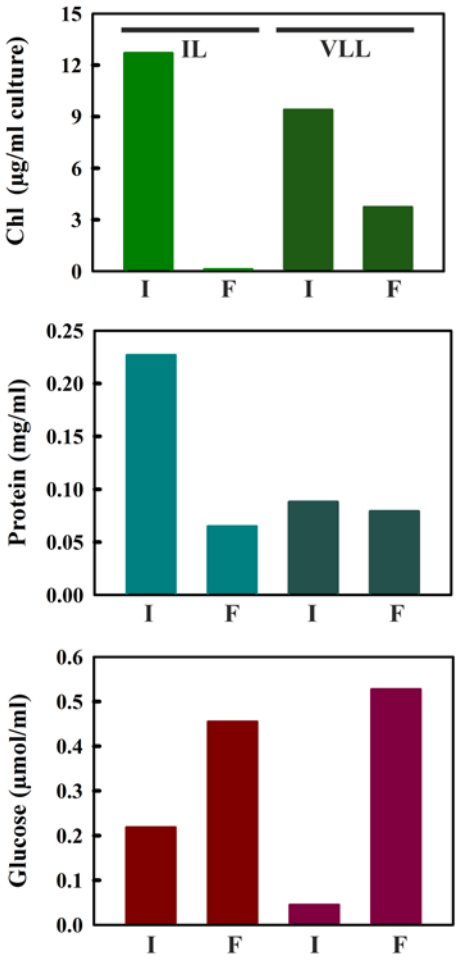

Fig. 3.19. Histograms showing the initial (at resuspension) and final (end of S-depletion phase) concentrations of cellular Chl, protein and glucose (starch) as measured for the IL and VLL experiments depicted in Fig. 3.16 and 3.17 respectively. I and F indicate the initial and final levels measured at the two light intensities. The black bar overhead indicates the IL and VLL experiments.

In our experiments (see Fig. 3.16) strain CC-1418 had a significantly longer S-depletion phase at IL intensities than other strains reported in literature (see Appendix 6). This longer length of the S-depletion phase reflects the larger, almost complete loss of Chl, with only between 1 - 20% of the initial Chl remaining towards the end. Cultures at VLL intensities retained up to 40 - 70 % of initial Chl. The extent of losses was found to correlate proportionally with the magnitude of H_2 produced by the culture along with the length of the S-depletion phase.

Proteins remained near resuspension levels, decreasing or increasing slightly, between 80 - 120% of initial values under VLL intensities and undergoing significant decrease (30% of initial value) under IL intensities with experiments exceeding 600 h. Unlike the above physiological parameters, starch was accumulated manifold during the initial aerobic phase of S-depletion, before being degraded for H_2 production. Cellular glucose (starch) remained at fairly high levels until the end of S-depletion at VLL intensities (at least 10-fold over initial levels). Although net initial CO_2 uptake and assimilation was not observed under VLL conditions, the accumulation of starch occurred by almost 20-fold over initial aerobic levels. For the experiment shown in Fig. 3.16 (the VLL condition indicated in Fig. 3.19), the starch levels at the end of the H_2 production experiment was 0.7 µmol glucose/ml culture, increasing from 0.05 µmol glucose/ml at resuspension in S-depleted medium. Similarly, the experiment depicted in Fig. 3.17 showed a 12-fold increase between the final and initial starch levels (the IL condition indicated in Fig. 3.19). The extent of starch breakdown, reflects the extent of H_2 production at the two light intensities, with more starch being channelled into H_2 production at IL than at VLL intensities. This is indicated by the lower final levels of starch under IL conditions than at VLL intensities. This difference in final starch levels between the two light intensities might also be a consequence of the longer duration (600 h as compared to 250 h) of the IL intensity experiments, which would naturally lead to more pronounced damage to cellular machinery, than at VLL intensities as significant amounts of ethanol and formate (photofermentative products) are produced (Winkler *et al.*, 2002). Although, the accumulation of starch in the first hours of S-depletion is attributed to the high initial CO_2 uptake rates (Melis *et al.*, 2000; Zhang *et al.*, 2002), the higher than 20-fold accumulation of starch at VLL intensities suggests that starch accumulates to high levels even when cells directly pass on to net production of CO_2.

3.3.6. Variation in the harvesting times of cultures dictates the chlorophyll content of cells and yields differences in the headspace GC profile

A major factor contributing to variation amongst experimental replicates resulted from differences in the harvesting time of aerobic *C. reinhardtii* cultures at VLL intensities, prior to their resuspension in S-depleted medium. The increase in turbidity (A_{561}) slowed down significantly at the end of the exponential growth phase at both IL and VLL intensities, though cells continued to accumulate Chl, protein and starch. Within the exponential growth phase, the turbidities were well correlated to the cellular Chl and protein contents, although this correlation was less pronounced in the stationary phase. However, beyond the exponential phase of growth, Chl and protein content of cells at the same values of turbidity were variable. Reproducible amounts of H_2 were obtained by harvesting cultures at similar time points in their growth and resuspending to the same Chl content. Since parameters such as Chl, protein, glucose content and cell number change progressively as the experiment proceeds, the amounts and rates of H_2 produced were calculated only on the basis of their initial concentrations at the time of resuspension.

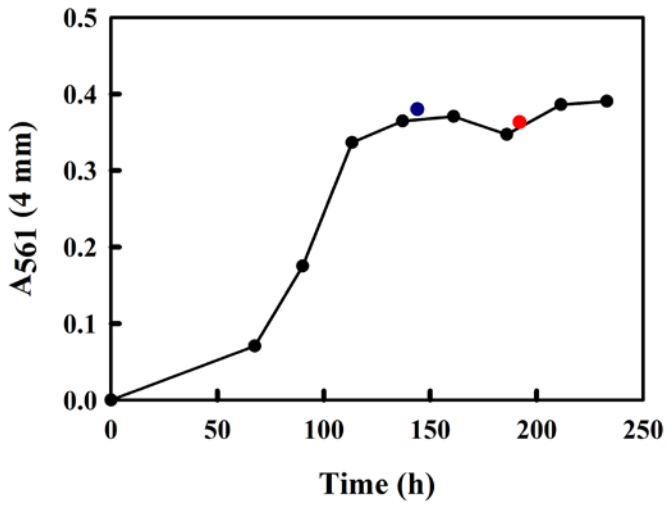

Fig. 3.20. A representative growth curve of *C. reinhardtii* cells in aerobic TAP medium under VLL conditions. The blue (VLL_(a)) and red symbols (VLL_(b)) represent time points at which aerobic cultures were harvested for resuspension into S-depleted medium at the same initial A_{561} (4 mm path length) of 0.222. The resulting differences in length of lag phase and rate of O_2 consumption due to varying chlorophyll amounts in the gas profiles are summarized in Table 3.5.

3.3.7. A comparative survey of the amounts and rates of H_2 produced by *C. reinhardtii* under conditions of S-depletion.

H_2 production amounts and rates in this study		
Resuspension parameters	**VLL Intensity**	
	VLL_(a)	**VLL_(b)**
Initial no. of cells (x 10^6)	5.6	5.6
Initial Chl (µg/ml culture)	*7.36*	*9.39*
Initial protein (mg/ml)	0.09	0.08
Initial A_{561} (4 mm path length)	*0.222*	*0.222*
Length of H_2 production phase (h)	41	41
Time for onset of H_2 prodn. (h)	*24*	*40*
Max. H_2 production rates		
Highest rate of H_2 prod. (µmol/H_2 µg Chl/h)	0.13	0.12
Highest rate of H_2 prodn. (µmol H_2/l/h)	0.96	1.12
Avg. H_2 production rates		
Avg. rate of H_2 prodn. (µmol H_2/l/h)	0.57	0.56
Avg. rate of H_2 prodn. (µmol H_2/µg Chl/h)	0.078	0.059
Total H_2 produced		
Amount of H_2 prodn. (µmol H_2/l)	20.6	22.8
Amount of H_2 prodn. (µmol H_2/10^6 cells)	0.0037	0.004
Amount of H_2 prodn. (µmol/µg Chl)	2.8	2.4
Amount of H_2 prodn. (µmol H_2/mg protein)	0.26	0.25
O_2 production/consumption rates		
Highest rate of O_2 consumption. (µmol O_2/l/h)	72	51
Avg. rate of O_2 prod. (µmol/l/h)	49	37.5

Table 3.5. The H_2 production and O_2 consumption amounts and rates for two S-depletion experiments conducted at VLL intensities. Differences in the times of harvesting may be responsible for the observed differences in H_2 evolution and uptake.

3.3.8. Optimization strategies for reduction of lag phase for H_2 production

The time required to achieve anaerobiosis following S-depletion increased drastically at IL intensities, from an average of 25 hours at VLL to 300 hours at IL, due to higher photosynthetic O_2 production. Additional strategies were devised, to help accelerate the consumption or diffusion of the evolved O_2 by means other than just the respiratory capacity of the cells. The study of Melis *et al.* (2000), which first described the S-depletion protocol, used a setup which was left unsealed until the rate of cellular respiration was found to overtake the rate of photosynthesis, allowing the diffusion of evolved O_2 to near atmospheric levels and decreasing the amount of O_2 for the cellular machinery to process, thereby shortening the lag phase of H_2 production.

By utilizing the Setup II (see Materials and Methods section 2.6), the equilibration of gases out of the culture bottle, into a second evacuated reservoir was achieved. Equilibration of gases between the two chambers connected by tubing was observed to occur only when a negative pressure was maintained in the reservoir and positive pressure in the culture bottle due to evolution of gases drove the gases into the reservoir. Surprisingly, in the absence of a pressure differential, gas equilibration between chambers was inefficient.

Another method of decreasing the O_2 was the use of a GOX enzyme solution within the reservoir bottle of Setup II provided with substrate glucose as an O_2 consuming reaction. In preliminary experiments performed in 2 ml cuvettes (~90% headspace volume) (see Material and Methods section 2.6) a reduction of 50% of the O_2 volume was measured over control experiments at the end of 24 h at 21°C with a reaction rate of 18 µmol O_2 consumed per hour (Fig**.** 3.21). Active consumption of 36% of the O_2 volume at 17 h to 50% of the O_2 vol. at 24 h demonstrates that the enzyme is active at 21° C at the end of 1 day of incubation.

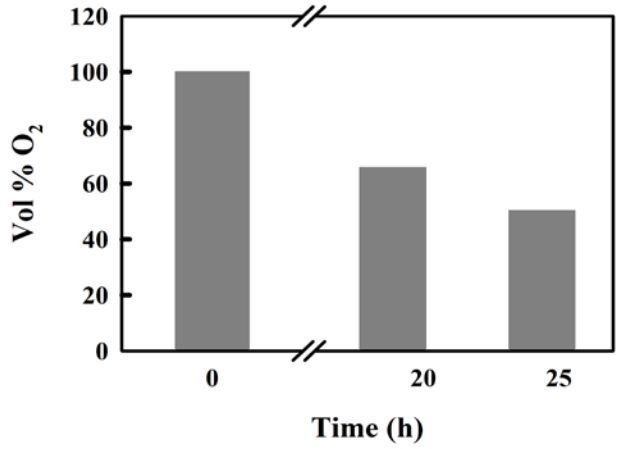

Fig. 3.21. Results showing the reduction in the GOX-mediated O_2 concentration vs. time. The reaction was performed in a 2 ml sealed cuvette (see main text for details).

In a scaled up S-depletion experiment with Setup II, the gas kinetic profile obtained was compared to a control experiment (performed in a standard setup, at IL intensity, see Fig. 3.16) performed at identical initial Chl contents.

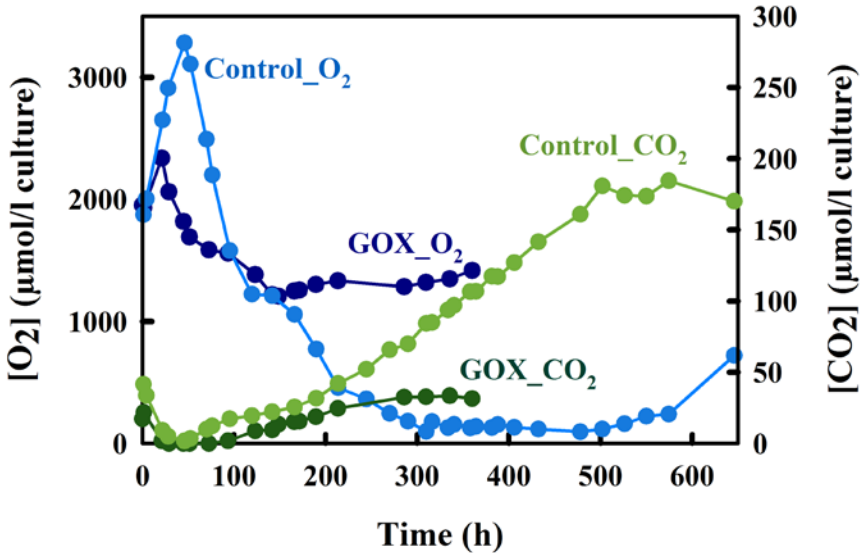

Fig. 3.22. Bioreactor headspace profiles comparing the O_2 (blue circles) and CO_2 (green circles) concentrations, respectively, from two experiments performed at IL intensities. The gas profiles from the experiment conducted in Setup II with an O_2-consuming trap (50 ml of GOX-glucose assay mix contained in the reservoir bottle) is marked as GOX_O_2 and GOX_CO_2. Control_O_2 and Control_CO_2 are the same as in Fig. 3.16. Both cultures were resuspended to a [Chl] of 12.75 µg/ml.

The gas profiles measured indicated that the GOX-glucose system actively consumed large volumes of O_2 evolved by the culture. The high O_2 levels attained in the control were not reached, and by the second day, the O_2 concentration was already below the atmospheric level. That this effect is not solely due to the respiratory uptake of O_2 by the culture, is indicated by the fact that the O_2 maxima (21 h) does not correlate with the CO_2 minima (28 to 72 h). The diffusion of CO_2 into the reservoir is also a possibility, which may account for the prolonged length of time that the CO_2 remains undetectable (28 - 72 h) and why the rise in CO_2 levels is significantly lower than the control values. The metabolic event of the respiration rate overtaking the rate of photosynthesis, is not clearly indicated as in the control (46 h), and may lie between 28 and 72 h. The connection of the culture bottle with the reservoir bottle was not closed after the initial O_2 consumption, thus anaerobiosis was not established and H_2 was not produced.

However, the ideal time to seal off the culture vessel from the reservoir bottle would be after the CO_2 levels reach the minimum value, and the O_2 concentration falls below atmospheric levels (45 h), to allow the cellular respiration to establish anaerobic oxygenic photosynthesis and subsequent H_2 production undisturbed by external factors. Since the extent of damage to the PSII centers should be the same as in the control, similar pattern of H_2 production would be expected.

Leaving the vessel unsealed, however, encourages backflow and equilibration of the O_2 and CO_2 between the two vessels, and prevents O_2 levels from decreasing further, with the consequence that anaerobiosis is not established. Consequently, the Calvin cycle remains functional (CO_2 uptake continues) and an alternate electron sink is not required. Additionally, the GOX-glucose enzyme assay mix is not stable at 21°C for very long periods of time (the activity remains for about 30 h) and the accumulation of H_2O_2 as a byproduct of the enzyme reaction may have an adverse effect upon cell viability. At 285 h, the cells have lost most of their Chl and turned grey in colour. This is an additional consideration to seal the culture vessel by day 2 of the experiment, which ensures enough time for optimal removal of O_2, establishment of anaerobic oxygenic photosynthesis and H_2 production while ensuring the least damage to cells.

The GOX-mediated O_2-consuming setup appears feasible for laboratory scale experiments, but prohibitively expensive at larger scales. Therefore, use of an evacuated Setup II (at negative pressure) without the GOX-glucose assay mix, seems to be the most economical method to achieve diffusion of O_2 during S-depletion.

4. DISCUSSION

4.1. Summary of the objectives of this chapter

The goals of this chapter were:

(1) to examine procedures for measuring and analyzing gas production, particularly hydrogen, in closed culture vessels. This is relevant for both the *C. reinhardtii* system studies here as well as for parallel studies in the laboratory employing the purple bacterium *R. rubrum*. Gas analysis is not a challenge for the engineering environment. However, in a typical biological laboratory, much of the technical infrastructure and know-how is not available. This is quite apparent in the bioH_2 literature, where many of the measurement procedures are mentioned only cursorily and where the small-scale experimental setups often employ silicon tubing and stoppers, both of which are well-known to be suboptimal for H_2 collection and measurement.

We could show that, with the recently available BOLA gas-tight (conducting) tubing and connections, merged with well-established Swagelok components, professional small-scale gas collection vessels can be easily constructed without special know-how or tools. We have also shown that calibration of the apparatus can be easily performed using the $NaBH_4$ reaction and a knowledge of the gas laws, provided that the appropriate corrections are made.

(2) The major goal of the chapter was to establish "benchmark" comparative parameters which allow the H_2-production capacity of *C. reinhardtii* (as well as other green algal systems as mentioned in Wang *et al.*, 2012) to be compared objectively to that of other non-related organisms (e.g. purple bacteria such as *R. rubrum, Rps. palustris, Rb. sphaeroides*, as well as cyanaobacteria (e.g. see Bandyopadhyay *et al.*, 2012). Typically, in a growth experiment, physiological parameters include growth turbidity, cell number, pigment content and more. Even in the *C. reinhardtii* literature there seems to have been no common ground rule for reporting these parameters, which is necessary for an objective comparative assessment of bioH_2 production. In addition, from our extensive perusal of the literature, no systematic correlation of growth parameters seems to have been published.

In the following sections, we discuss the results obtained in the context of the known physiology of *C. reinhardtii* as available in the literature.

4.2. The parameter "light intensity"

C. reinhardtii grows by photosynthesis and all studies of bioH_2 production with this organism have been performed under light conditions. In general, in studies of photosynthesis it is usual to consider "high light and" "low light" conditions. It is very common to define light intensity

for a particular organism from an experimentally observable point of view. In particular, definitions of “low” and “high” light intensities usually reflect the change of the appropriate photosystems. Thus, “low” light intensities usually maximize expression of photosystems delivering photonic energy to dark metabolism whereas at “high” light intensities the reverse is true. For *C. reinhardtii*, different light intensities have been employed in the bioH_2 literature, and those employed in several key studies are summarized in Fig. 4.1 below:

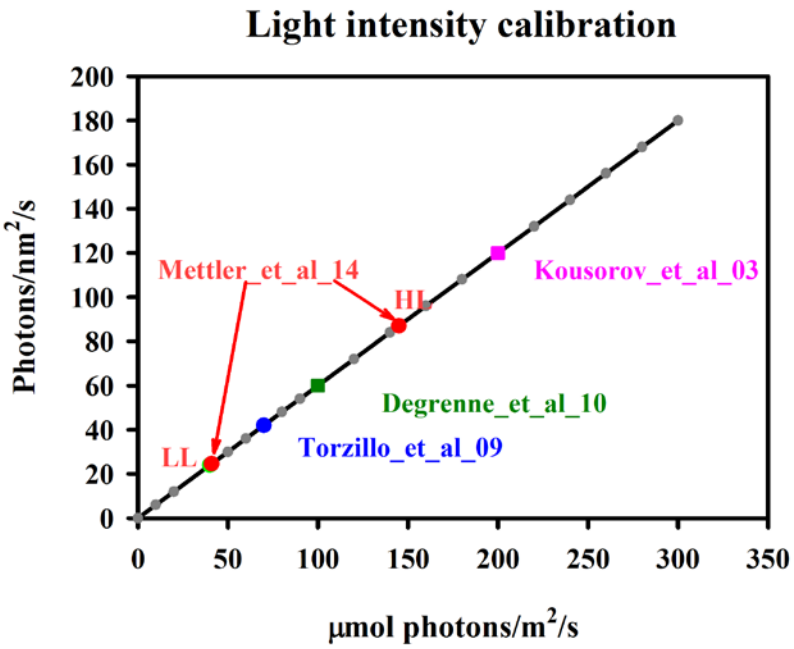

Fig. 4.1. Light intensities used by several key studies of the bioH_2 production with *C. reinhardtii*.

The study of Mettler *et al.* (2014) is perhaps the most detailed study of system-wide variation of physiological parameters (metabolomics, transcriptomic profiles, variation of protein and PSI and PSII contents, respectively) under defined light conditions in continuous steady state cultures of *C. reinhardtii*. In this study, only low culture densities in thin cells were employed, thus eliminating many effects due to self-shading. The results from this study will be discussed in the context of our results below.

Fig. 4.1 shows the relation of the commonly used light intensity unit (µmol photons/m^2/s) to units which are more relevant for calculating the efficiency of light excitation of photosynthetic complexes such as PSI and PSII, when photons strike the effective cross-sectional area of these complexes. Since the structures of some of the key photosystems are known, it is possible to calculate an estimate of the effective light intensity at the molecular level.

The structures and calculated dimensions of the PSI and PSII surfaces are shown in Fig. 4.2 (A). For the purposes of computing their surface area, they may be considered as an elliptical shaped structure with equivalent area as calculated by the formula Area= πab (a and b are radii of width and length, respectively). The PSI was calculated to have an area of 114 nm^2 and the PSII an area of 174 nm^2.

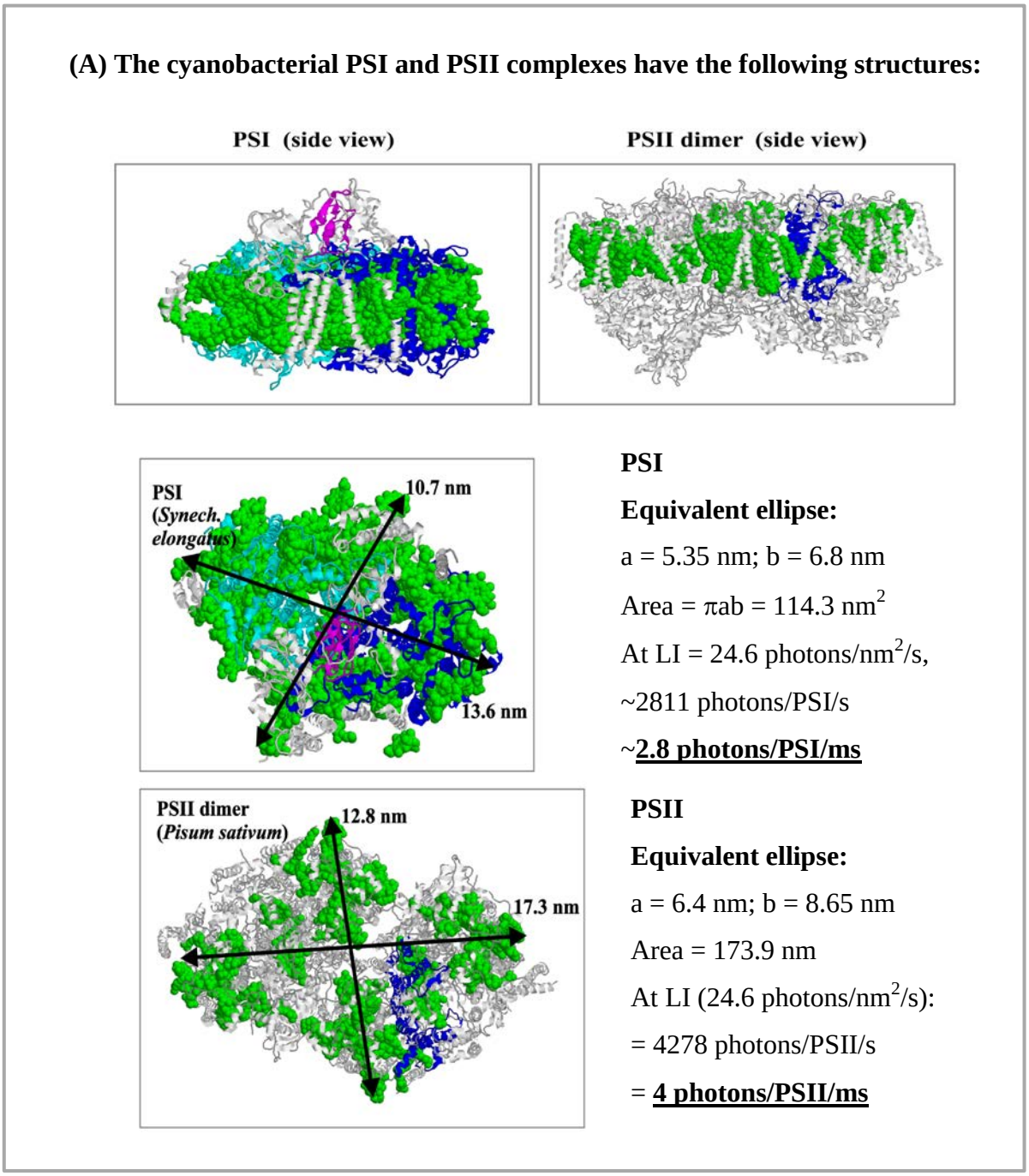

Fig. 4.2. (A) The dimensions of cyanobacterial PSI and pea PSII and representative examples for calculation of light experienced by these complexes. (Figures conceived by R. Ghosh.)

(B) Light intensity for *C. reinhardtii* illumination

Low irradiance (LL): **41 μmol photons.$m^{-2}.s^{-1}$** (Mettler *et al.*, 2014)

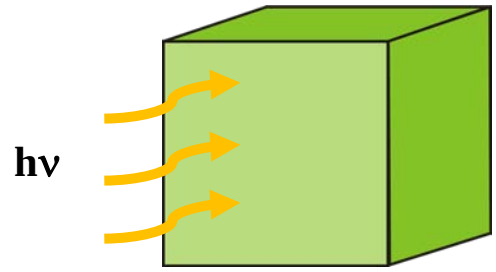

$1m^2 = 100\ cm \times 100\ cm = 10^4\ cm^2$

LI = 41 x 10^{-4} x 10^{-6} mol photons/cm^2/s = **41 x 10^{-10} mol photons/cm^2/s**

In terms of nos. of photons:

LI = 41 x 10^{-10} x 6 x10^{23} = 246 x 10^{13} photons/cm^2/s = **2.46 x 10^{15} photons/cm^2/s**

$cm^2 = 10\ mm \times 10\ mm = 10^2\ mm^2 = 10^4\ \mu m \times 10^4\ \mu m = 10^8\ \mu m^2$

$10^8\ \mu m^2 = 10^7\ nm\ 10^7\ nm = 10^{14}\ nm^2$

Thus:

LI = 2.46 x 10^{15} x 10^{-14} photons/nm^2/s = **24.6 photons/nm^2/s**

In 1 ms (about the time for cyclic electron transport):

LI = 0.0246 photons/nm^2

In other words, for a 100 nm^2 area (about the size of the photosynthetic complexes), 1 ms is required for a single photon to arrive.

Similarly, at HL = **145 μmol photons/m^2/s** = **87 photons/nm^2/s**

Fig. 4.2. (B) The calculations for converting the standard unit of light intensity into smaller molecular dimensions of photons/nm^2/s. (R. Ghosh, unpublished)

From Fig. 4.2 (B) an area of 1 m^2 is equivalent to 10^{14} nm^2, such that LL intensity is equivalent to 24.6 photons falling per nm^2/s or 0.0246 photons/nm^2/ms. In other words, for a 100 nm^2 area, ~ 1 ms is required for a single photon to arrive. The light intensity falling on the

C. reinhardtii chloroplast (10 μm^2), which occupies ~ 30% of the cell volume, is thus estimated to be 2.46 x 10^8 photons/s.

Similarly, the HL intensity of 145 $\mu mol/m^2/s$ is equivalent to 87 photons/nm^2/s, the VLL intensity is equivalent to 3 photons/nm^2/s and the IL intensity equals 42 photons/nm^2/s. Light intensities of more than 200 μmol photons/m^2/s or 120 photons/nm^2/s are inhibitory to high levels of H_2 production, due to light saturation effects. At full sunlight or under HL, the rate of absorption of photons by the chlorophyll antennae far exceeds the rate at which they can be utilized for photosynthesis, with the excess photons being dissipated in the form of heat or fluorescence. When exposed to excess light in nature, *C. reinhardtii* responds by moving away by negative phototaxis, and by re-ordering the LHC antennae, by altering electron transport and through thermal dissipation of excess light. Over a long exposure time, adaptive gene expression occurs.

The established knowledge indicates that *C. reinhardtii* grown at very high light intensities (450 μmol photons/m^2/s or greater) grow faster, produce more biomass and have 50% lower chlorophyll per cell than those grown at IL or HL intensities, though such intensities are counterproductive for H_2 production. Cells were not only found to halve their chlorophyll content upon exposure to very high light intensities but also to increase the amounts of carotenoids and lutein twofold for enhanced photoprotection (Shapira *et al.*, 1997).

4.3. Growth under IL and VLL conditions

Growth with acetate is predominantly photoheterotrophic. Adding a bicarbonate component in medium, such as that used for *R. rubrum* growth, appears to be a more convenient solution to achieving photomixotrophic growth than aeration with CO_2-enriched air, as cultures grown in cotton-plugged flasks become rapidly growth-limited as CO_2 runs out.

The growth at both light intensities in the TAP medium as measured by the A_{561} (4 mm), show a biphasic pattern of growth, with an exponential rise lasting approximately 125 h under both conditions, followed by a stationary phase, where the cell numbers hardly increased. However, the levels of final turbidity achieved at the end of exponential growth at VLL intensity was only half (0.35) that at IL intensity (0.72).

Physiologically, one would expect that the presence of equal [acetate] in the TAP medium should result in equivalent final culture turbidities, with growth at VLL intensity progressing at a slower rate, hence requiring a longer time to achieve the same final turbidity as reached under IL conditions. However, such an effect was not observed.

That growth at VLL would result in such a drastic lowering of culture turbidity despite an equivalence of respiratory substrate acetate at the two illumination conditions may be understood as follows:

(1) VLL intensity represents a highly limiting growth condition, which severely limits the contribution of oxygenic photosynthesis to cellular growth, with cultures experiencing self-shading due to lower light penetration. However, normal household (dark) metabolic activities proceed at the same rate as under IL conditions, thereby exhausting resources at low cell densities.

(2) Light limitation may lead to activation of fermentative pathways, leading to accumulation of acidic end products resulting in pH changes, both being detrimental to growth and imposing a higher metabolic cost of cell division at VLL intensities than at higher light intensities.

We know that microalgal species tend to exhibit a maximum saturating growth rate at certain high light intensities, which is not influenced or limited by additional substrate addition. Growth rate saturation can occur at a much lower light intensity than photosynthesis saturation, and once the growth rate saturates, cells may photosynthesize more rapidly, but are unable to grow more rapidly. Thus, saturating light intensities also impose a higher metabolic burden on cell turnover. This indicates that, cells have definite physiological limits beyond which they may not be manipulated by external factors such as the amounts of respiratory substrates available, at both very limiting light intensity that VLL intensity represents and at saturating light intensities.

Multiple growth experiments confirm that growth profiles are highly reproducible if both media and inoculum size are carefully controlled at the designated light intensity, a result also demonstrated by Lee and Fiehn (2008). Thus, physiological benchmarks derived by us can be compared across experiments, if performed under similar conditions. Alternatively, cell counts can be used to measure the status of cultures prior to inoculation (Lee and Fiehn, 2008). This is both time-consuming and unnecessary, as they may be reliably calculated from turbidity interconversion coefficients as demonstrated by our results. Such correlations will simplify procedures in the future and enable comparison of H_2 production rates and amounts across species as well.

Finally, we have successfully used the interconversion coefficients determined for strain SAG 18.79 (Table 4.1) to calculate the published physiological parameters described in H_2 production experiments performed with strains derived from CC-124. Thus, we believe that the coefficients described are applicable to *C. reinhardtii* strains in general.

4.4. Apparent diauxic growth of *C. reinhardtii* in TCP medium

Microalgae have been reported to exhibit diauxic growth behaviour when the culture medium contains a mixture of carbon sources (Chalima *et al.*, 2017; Baroukh *et al.*, 2017). Growth of *C. reinhardtii* in TCP medium at IL intensity provides a useful contrast to growth in TAP medium. With citrate replacing acetate as the counter ion in the Tris buffer system, the uptake of acetate as a substrate should no longer destabilize the medium buffer during exponential growth. The uptake of dissolved carboxylic acids by microalgae has been known for a long time (Bollman and Robinson, 1977), with the annotated di- and tri- carboxylic acid carrier (DCT1) in the *C. reinhardtii* genome (JGI database) being possibly responsible for uptake of citrate as a respiratory substrate.

Therefore, with a stable buffer system and two respiratory substrates, growth in TCP medium at IL intensities was found to be distributed across two phases representing the uptake of acetate and citrate respectively. The first phase with acetate uptake was similar to exponential growth in TAP medium (phase a) with the exponential phase giving way to a second, slightly slower growth phase b (citrate uptake). In this second phase, doubling of turbidity is observed. This second phase differs significantly from phase b kinetics of TAP medium growth, which is essentially the stationary phase.

Since all TCP medium cultures all have equal [Na-citrate], but unequal [Na-acetate] (increasing from 9 - 15 mM through the experiments), the differences in the growth kinetics and the final turbidities achieved in phase b confirm expectations, that the pathways of citrate utilization, presumably the TCA cycle, must be linked to the co-utilization of acetate. This co-dependence explains why higher turbidities are achieved in phase b (citrate dependent growth) with increasing [acetate] but at equivalent [citrate].

The role of citrate as an inhibitor of the enzyme phosphofructokinase (PFK) of glycolysis, as explained by the Pasteur affect (Gans and Rebeille, 1990) leads to slower growth on citrate than on acetate. Interestingly, since glycolysis is partly localized in the chloroplast stroma and partly in the cellular cytoplasm, the consequence of this compartmentalization on cell growth and H_2 production would be interesting to learn.

4.5. The “benchmark” interconversion coefficients of *C. reinhardtii* growth parameters

In *C. reinhardtii*, optical density measurements have seldom been reported as a standalone value or been linked to other measured parameters representing the physiological status of a culture, contrary to the prevalent use of culture turbidity in the field of microbial (bacterial) physiology.

Mettler *et al.* (2014) used instruments in the range of 840 to 910 nm for turbidity measurements, while Laurinavichene *et al.* (2004) used instrumentation in the range of 400 to 750 nm, both without reporting any real values of turbidity or mentioning the actual wavelength where turbidity was measured. Strangely, the former range lies beyond the UV-VIS absorption spectrum of *C. reinhardtii* cells measured by us. Doebbe *et al.* (2007) measured turbidity at 750 nm. Publications in the field of biodiesel and feed stock generation from *C. reinhardtii* have reported turbidities at 680 nm, which is the PSII absorption maximum (Kong *et al.*, 2010; Kropat *et al.*, 2011). The choice of such a wavelength for measuring turbidity is questionable, since the cell density may not necessarily correlate to the amount of photosystems present.

The lack of clarity in literature about the measurement of this basic parameter of *C. reinhardtii* physiology was overcome by our systematic measurement of whole cell absorption spectra of *C. reinhardtii* (see Results) which indicated the optimal wavelength for turbidity measurements.

Our rationale for using A_{561} was based upon the fact that this wavelength has the least contribution from both PSI and PSII, while still being close to the 660 nm position commonly used for turbidity measurement of purple bacteria. However, we also showed that the turbidity at 600 nm (commonly used in many microbiological studies for bacterial turbidity measurements) correlates linearly with A_{561} throughout the growth curve. The usefulness of A_{561} as sufficient indicator of cellular physiology including cell number, chlorophyll content, protein content and dry weight has been demonstrated by our results and the range of usefulness of this parameter carefully delineated (within exponential phase of growth). Our methodology maybe adapted to the study of physiology for other microalgae at various conditions of growth, and represents a very convenient way forward for routine laboratory work with microalgae, reducing the need for subsequent time-consuming measurements of cell number or Chl prior to resuspension in S-depleted medium, and requiring only the interconversion of simple turbidity measurements.

4.6. The variation of Chl and protein content throughout the aerobic, photosynthetic growth curve

The proteins accumulating in cells have three possible origins of expression, the nuclear genome, chloroplast genome and the mitochondrial genome, each regulated by their respective ribosomes. This provides a broader scope for variation in cellular protein content.

Under both illumination conditions tested, the protein content generally correlates to the cell count, albeit with a steep rise towards the mid to end log phase at IL conditions.

Fig. 3.9 shows that despite the lower cell densities obtained at VLL, the protein content/cell was approximately equivalent in both VLL- and IL-grown cells. However, in the late exponential phase of IL-grown cells, there seems to be non-proportional increase of proteins with respect to the cell density. This may be due to "preparation" for the stationary phase, where a new set of proteins must be synthesized to ensure cell maintenance.

Our results confirm the conclusion of Mettler *et al.* (2014), who showed that the shift from LL to HL conditions did not increase the total protein concentration per unit volume (Calvin cycle components were found to be equal at both conditions, and only small decreases in protein content at HL were observed for some ribosomal proteins), as they are able to invest in maintenance of surplus proteins or ribosomes, thus enabling them to rapidly adapt to shifts in light intensity.

Chloroplasts also degrade gradually in response to stress (Xie *et al.*, 2015; Zienkiewicz *et al.*, 2016), characterized by a disorganization of the thylakoid membranes (Warakanont *et al.*, 2015). Growth at VLL intensity can be considered as a light-stressed condition, leading to a substantial reduction in the amount of cellular Chl.

The variation of the Chl content in *C. reinhardtii* is limited to the variations in chloroplast size and content only, unlike in higher vascular plants where the number of chloroplasts per cell can be drastically regulated in response to growth conditions, leading to a much larger capacity for Chl variation. The presence of a simpler chloroplast regulation is reflected in the rise of Chl which closely follows cell count, with absolute amounts of Chl per ml at IL intensity rising to three times that at VLL intensity. In addition, the Chl *a* /Chl *b* ratio remains almost constant, varying only within a narrow range of 2.3 - 2.7 at IL intensities and between 1.9 – 2.0 at VLL intensities, within the exponential phase. From the data presented in Table 4.1 the Chl content per 10^7 cells saturates at around 30 µg Chl/ml, irrespective of light intensity being used.

Culture conditions				
Author	**Light Int (µmol photons/ m^2/s)**	**Temp. °C**	**Strain**	**Chl content (µg/ml) of (1 *10^7 cells/ml)**
Hemschemeier *et al.*, 2009	~ 80	-	CC-124 ($137c^-$)	30.77
Melis *et al.*, 2000	200	25	CC-125 ($137c^+$)	24
Oncel and Sukan, 2011	40*2	27	CC-124 ($137c^-$)	30
	50*2			27.6
	70*2			31.8
	80*2			30.03
	100*2			29.7
Kosourov *et al.*, 2003	200	25	CC-124 ($137c^-$)	24
Tortillo *et al.*, 2008	70*2	28	CC-124 ($137c^-$)	-
			L159I-N230Y	-
IL (this work)	70	21	SAG 18.79 or CC-1418($^+$)	**25.7**
VLL (this work)	5	21	SAG 18.79 or CC-1418 ($^+$)	**10.5**

Table 4.1. A table showing the calibration between Chl content and number of cells as collected from various references under varying light intensities as well as the value measured by us under IL and VLL conditions. The asterisk indicates that the culture vessel was illuminated from two sides with the light intensity given by the first number.

In plants and algae, the Chl *a*/Chl *b* ratios of 2 - 3 have often been reported under ambient growth conditions. Chl *a* is the primary pigment in photosynthesis, is present in both PSI and PSII core complexes, whereas Chl *b* has a role of an accessory pigment being confined to LHC antennae (also containing Chl *a*). In plants, diverse ratios of chlorophyll between PSI and PSII (ranging from 0.54 to 1.4 (Wientjes *et al.*, 2017)) have been reported with differences even amongst different axes of the leaf blades. The *C. reinhardtii* PSI core unit has been reported to contain ~95 molecules of Chl *a* and the PSII unit 37 units of Chl *a*. (Glick and Melis, 1988; Zouni *et al.*, 2001) with the Chl *a*/*b* containing LHCs increasing the number of pigment molecules associated with the reaction centers to up to 250 for PSI and

300 for PSII respectively (Melis and Anderson, 1983; Smith *et al.*, 1990; Melis, 1991). Despite these large changes, our results confirm that the ratios of the complexes remain relatively constant during growth.

4.7. Effect of S-depletion on physiology

Nutrient deficiency (N, P, S) is a commonly pursued strategy in *C. reinhardtii* lipid production for biofuel generation and H_2 production. These methods severely affect photosynthesis and limit cell growth. S-deficiency in microalgae affects Chl formation and S-depletion causes the loss of Chl, as our results confirm. Melis *et al.* (2000), using a light intensity of 200 µmol photons/m^2/s with the CC-124 strain, observed that 70% of the cells undergo doubling during the initial aerobic phase of S-depletion, before decreasing thereafter, but still remaining well above the initial value at resuspension. The cells were also observed to undergo a gradual continuous decline in their Chl content, losing ~ 50% of their Chl by the end of the S-depletion phase.

At the same light intensity, Kosourov *et al.* (2003) reported that the glucose content of cells increases at least 10-fold before declining to initial levels at the end of the phase. Protein content per volume of culture also underwent a near doubling (reflecting the concurrent doubling of cell number) following which they decreased to reach near initial levels.

Our own experiments (see Fig. 3.16) had a significantly longer S-depletion phase at IL intensities than those reported in literature (see Fig. 1.6). The longer length of the S-depletion phase reflects in the larger, almost complete loss of Chl per volume culture. The extent of losses was found to correlate proportionally with the magnitude of H_2 produced by the culture along with the length of the S-depletion phase. Proteins remained near cell resuspension levels, decreasing or increasing slightly, between 80 - 120% of initial values under VLL intensities and undergoing significant decrease under IL intensities with experiments exceeding 600 h (30% of initial values).

Cellular glucose remained at fairly high levels until the end of S-depletion at VLL intensities (at least 10-fold over initial levels). This indicates that, large amounts of starch was accumulated at the onset of S-depletion, some of which was degraded and chanelled towards the production of H_2. The extent of glucose utilization at IL intensities were much higher, therefore the final levels of glucose assayed were much lower at IL than at VLL. This indicates greater channeling of starch for H_2 production at IL intensities. The difference in starch accumulation between the two light intensities might also be a consequence of the longer duration (600 h as compared to 250 h) of the IL intensity experiments, which would

naturally lead to more pronounced damage to cellular machinery, than at VLL intensities as significant amounts of ethanol and formate (photofermentative products) are produced (Winkler *et al.*, 2002b). Although, the accumulation of starch in the first hours of S-depletion is attributed to the high initial rates of CO_2 uptake (Melis *et al.*, 2000; Zhang *et al.*, 2002), the nearly 20-fold accumulation of starch at VLL intensities suggests that starch accumulates to high levels at the onset of S-depletion, even when cells directly pass on to net production of CO_2, bypassing the initial CO_2 uptake stage normally seen under IL conditions.

This longer length of aerobic and S-depleted growth of our strain CC-1418 was the reason for considering strategies for reduction of the initial aerobic O_2 evolving phase to hasten the onset of H_2 production (see Results section 3.3.8).

4.8. H_2 production and uptake by *C. reinhardtii* strain SAG 18.79 or CC-1418

Our experiments clearly indicate that for the SAG 18.79 strain H_2 uptake is considerable, which is not observed usually for bioH_2 production in the literature using strain CC-124 or CC-125.

H_2 uptake in the green alga, *Scenedesmus sp*. was first demonstrated more than 70 years ago (Gaffron, 1942). Since that time very little has been resolved regarding the metabolic pathways of the H_2 uptake reaction.

Thus far, the H_2 uptake reaction in CC-124 has been reported to be a response to high H_2 concentrations, occurring after prolonged incubation in the light as well as in sudden darkness (Scoma and Hemschemeier, 2017). H_2 uptake mechanisms were found to be activated in *C. reinhardtii* cells at H_2 partial pressures > 5% (Kosourov *et al.*, 2012) when H_2 gas was injected into the headspace of S-depleted and H_2 producing cells to reach a concentration of 30%.

Generally, H_2 uptake as described in literature involves the reduction of ferredoxin through the H_2ases and subsequent NADPH formation via FNR. Two downstream pathways have been proposed to be involved subsequently, either the photoreduction of CO_2 in low light or the oxy-hydrogen reaction in the dark (Chen and Gibbs, 1992; Gaffron, 1942). However, we presume that the RuBisCo mediated anaerobic CO_2 photoreduction (Gaffron, 1942; 1944; Kessler, 1974), should be unlikely in S-depleted conditions where the Calvin cycle is inoperative. H_2 can also be taken up in an oxy-hydrogen reaction, whereby at low O_2 concentrations in the dark (Russell and Gibbs, 1968; Kessler, 1974; Maione and Gibbs, 1986a, b) ferredoxin facilitates reduction of the PQ pool (directly or indirectly) (Maione and

Gibbs, 1986a) which reduces O_2, resulting in the uptake of both H_2 and O_2. This reaction appears to be similar to chlororespiration.

We note that all of our S-depletion GC datasets obtained at both IL and VLL intensities have consistently shown both a H_2 production and a H_2 uptake phase. At VLL intensities, the H_2 accumulates and plateaus for a considerable amount of time before uptake commences, though at IL intensities, uptake swiftly follows peak H_2 accumulation. Such uptake profiles have been thus far absent or unreported by groups working in this area. The reason for this omission might be due to differences in sampling methodology or reactor design, but is more likely to be due to the strain used in this study. The strain CC-125 (137 c^+) or strain CC-124 (137 c^-) has been universally adopted by most laboratories working on *C. reinhardtii* H_2 production since the establishment of the breakthrough S-depletion protocol by Melis *et al.* (2000) (see Appendix 6 for a list of common strains in literature). The use of strain CC-125 over other wild type strains for studying H_2 production seems to originate from the work of Greenbaum (1979). Other reasons have not been addressed specifically by any group. Neither have we carried out the S-depletion of *C. reinhardtii* strains other than SAG 18.79 (CC-1418).

The standard *C. reinhardtii* strains all derive from a single zygote isolated in 1945 by G.M. Smith in Massachusetts (Harris, 1989) and were subsequently ordered into three subgroups. CC-1418 however, was isolated by L. Provasoli (of Yale University, USA) from a fresh-water sample in Florida in 1977 originally labelled as “red tide Florida”. Attempts have been made to use genome-wide analysis of nuclear internal transcribed spacer regions (ITS) (Pröshold *et al.*, 2005) and whole genome sequencing (Gallaher *et al.*, 2015) to correctly identify strains. The ITS sequence of strain CC-1418, was found to be identical to other standard strains (Pröshold *et al.*, 2005), with identical endonuclease restriction fragment pattern of plastid DNA (Harris, 1998) and similar distribution of copies of the Gulliver transposon (Ferris, 1989). However, the whole genome sequence of CC-1418 is not available, hence bioinformatic comparison with CC-124 or CC-125 cannot be carried out.

It may be that H_2 uptake activity is enhanced in strain CC-1418, while being absent or undetectable in strain CC-124 or CC-125 (also in strain SAG 11/32b, see Appendix 6) or that they may have a defect in H_2 uptake. This property has made the latter a serendipitously better strain for producing H_2. We are not aware of bioH_2 production in other wild type *C. reinhardtii* strains. However, other strains and species such as *Anabaena sp*., *Chorella sp*., *Oscillatoria sp*., *Scenedesmus sp*. and their mutants have been used for H_2 production (see Vijayaraghavan *et al.*, 2010).

Our study shows that strain SAG 18.79 exhibits significant H_2 uptake under both VLL and IL conditions, with the activity in both production and uptake directions of the H_2ases being proportional to the light intensity. We have shown that H_2 uptake occurs even when H_2 accumulates to levels well below partial pressures of 5%. This may indicate that the same H_2ase enzymes are responsible for the reaction in both directions. This H_2ase turnaround point is probably dictated by the physiological requirements of the cells for production or consumption of reducing equivalents.

Additionally, the special case of H_2 production before the onset of anaerobiosis at VLL intensities, has not been reported previously for S-depleted cultures of *C. reinhardtii*. The appearance of H_2 at high O_2 concentration of 15% by volume seems to support the observation of Nguyen *et al.* (2008) that *hydA* (*hydA1*/*hydA2*) transcripts (see Introduction section 1.3) were induced soon after S-starvation, and long before onset of anaerobiosis, although anaerobiosis enhances *hydA* transcription. Although the observations of Nguyen *et al.* (2008) were made for cultures illuminated at 250 - 450 µmol photons/m^2/s light, there are currently no published reports of such a phenomenon occurring at very low light intensities, other than our own. Low initial photosynthetic rates, overtaken almost immediately by respiration have also been reported in a Rubisco-deficient strain (CC-2803, which does not accumulate starch) where H_2 is produced immediately within a few hours upon sealing the culture (Hemschemeier, 2005). Hydrogen evolution of this strain is mainly dependent on PSII activity.

4.9. The role of dark respiration in inducing anaerobiosis

Respiratory O_2 consumption in *C. reinhardtii* occurs through two mitochondrial oxidases, the cytochrome c oxidase, and an alternative oxidase (AOX) and one chloroplastic plastid terminal oxidase (PTOX). The rates of respiration are dependent on the availability of reducing equivalents channeled through the TCA cycle and photosynthetic PQ pool, respectively. Acetate in TAP medium serves to enhance respiratory rates by donating flux into the TCA cycle. Thus, under uniform experimental conditions of darkness, temperature, and nutrient availability, equal numbers of cells would be expected to show equivalent rates of respiration (at least initially) with rates being proportional to the cell density. Thus, respiration rates are a function of cell number (density), and the rate per cell is more or less constant in the dark. This is confirmed by our experiments measuring dark respiration rates in *C. reinhardtii* (see Results).

In the case of photosynthetic O_2 evolution by PSII, as measured by the Clark-type electrode, turbidity differences and Chl content affect the rates of photosynthesis even when the incident light intensity was unvaried. At higher ODs, more self-shading and lesser light penetration decrease the average light intensity experienced by the culture. Consequently, higher photosynthetic rates (per cell) would be established at lower cell densities than at higher cell densities for equal number of cells. Thus, in the early stages of growth, the rate of photosynthesis per cell is inversely proportional to culture turbidity or Chl content, when the incident light intensity remains constant.

Additionally, respiration continues in the cells in the presence of light, so that the measured rate of photosynthetic O_2 production should be considered as a net rate. This net production rate is reversed in the direction of net consumption in *C. reinhardtii* upon induction in S-depleted TAP medium. Exposure to light is known to cause some inhibition of respiration by relation to the photosynthetic processes (Graham, 1980; Turpin and Weger, 1990). A higher photosynthetic rate should result in a greater availability of ATP and NADPH (Turpin and Weger, 1990), thus decreasing the demand for respiratory energy. Therefore, it seems likely that there will be a positive relationship between the degree of light inhibition of respiration and photosynthetic rate (Villar *et al.*, 1995). Thus, the ratio of photosynthesis to dark respiration measured here may not correspond exactly to physiological ratios of cultures growing in light. The maximum recorded rate of O_2 consumption amongst all experiments is 83 µmol/l/h which is the highest O_2 consumption rate recorded amongst all S-depletion experiments performed. This rate of O_2 consumption is the closest to the dark respiration rates (24 nmol/h for every 10^6 cells or 134 µmol/l/h calculated for the experiment shown in Fig. 3.18).

Interestingly, our results at VLL intensities, show a similar phenomenon, though the amount of light is extremely limiting rather than saturating. Instead of increasing cellular Chl content to capture as much light as possible, the cells were found to decrease their Chl content by about 16% of that observed at IL intensities, whereas the protein content per cell was similar to that observed at IL intensities. These results are significant in that they may indicate the response of *C. reinhardtii* to a frequently occurring natural environmental condition. Additionally, the rapid onset of anaerobiosis at VLL intensities upon S-depletion and the start of H_2 production even before the establishment of anaerobiosis is significant in that, VLL intensities are frequently encountered in nature, for instance at dusk or dawn, or by cells significantly below the water surface. In such circumstances, anaerobiosis may be rapidly established in local environments around cell clusters and the switch from normal aerobic

photosynthesis to anaerobic oxygenic photosynthesis with the use of uptake H_2ases as alternative electron sinks may be a commonly occurring physiological condition.

4.10. The measurement of H_2 and the present status of bioH_2 production

4.10.1. The rationale for the use of H_2 as a fuel source

Fossil fuels have reliably provided for our increasing energy needs since the industrial revolution in the 18th and 19th centuries, with the unfortunate consequence of the release of harmful combustion products and the highest levels of atmospheric CO_2 ever recorded in human history. Before the industrial revolution in the 19th century, the global average CO_2 was about 280 ppm. Today, the values have surpassed 400 ppm and the rate of CO_2 increase is more than 100 times faster than that which occurred when the last ice age ended (data from Earth System Research Laboratory, U.S. Department of Commerce, https://www.esrl.noaa.gov/). Renewable fuels such as bio-ethanol or butanol burn cleaner than fossil fuels, although their use presents no obvious difference in their CO_2 emissions. Nuclear fission reactors provide clean energy, but the problem of radioactive waste disposal raises risks. The destruction of the Fukushima Daiichi power plant in March 2011 in Japan, has led to contamination of soil, ground and ocean water, with radioactive waste entering the food chain and increasing chances of bioaccumulation in animal and human organs. In contrast, the use of H_2 as a fuel with H_2O being the only combustion by-product presents none of the above disadvantages.

Biofuels such as H_2, offer environmental sustainability, a large energy density of 121 kJ/g, easy storage and conversion to electricity via fuel cells and no emissions other than H_2O. Microalgae, as well as other photosynthetic microorganisms such as purple bacteria and cyanobacteria, offer the added advantage of being able to utilize solar energy to drive bioH_2 production in a photosynthesis dependent process. In principle, the energy in sunlight received by the earth in a single day, is enough to power our energy need for an entire year, and is therefore the most convenient source of renewable energy available.

4.10.2. Present state of the art: limitations to upscaling of *C. reinhardtii* H_2 production

C. reinhardtii possesses considerable metabolic flexibility, with the presence of photosynthetic, heterotrophic and fermentative pathways enabling the production of H_2 under anoxic conditions. However, due to the anoxic nature of the H_2-producing process, and the difficulties associated with up-scaling of a light-dependent reaction, large-scale commercial

success in bioH_2 production has been evasive. Despite the extensive literature available on *C. reinhardtii* H_2 production, there is still no clear consensus on the biotechnological optimization required for the process. An absence of basic physiological data for *C. reinhardtii* is widely observed in this field. Culture turbidity, a parameter universally used to define the physiological state of liquid microbial cultures due to ease of measurement and reliability, has hardly ever been reported in this field.

Ensuring uniform distribution of light in bulk cultures is difficult and expensive, especially when solar conversion efficiencies are low. Flat panel glass reactors have been found to be more suited to H_2 production than the use of round bottles. There is some consensus that light intensities beyond 200 µmol photons/m^2/s is limiting to H_2 production (Oncel and Sukan, 2011). Hahn *et al.* (2004) reported that, irrespective of Chl content of cells, the production of H_2 increases with light intensity, reaching a maximum at 100 µmol photons/m^2/s, while Laurinavichene *et al.* (2004) reported the value of 30-40 µmol photons/m^2/s as the optimum light intensity for H_2 production, while 140 µmol photons/m^2/s with 10^8 cells has also been reported for best rates of H_2 production (see Esquivel *et al.*, 2011). These differences in results may be attributed to the differences in the design of the photobioreactor and also in the Chl content and turbidity of the cultures. In fact, the importance of the "average light intensity" (I_{av}) experienced by the culture as a more relevant parameter influencing H_2 production than the "incident light intensity" has been discussed so far only by Laurinavichene *et al.* (2004). Laurinavichene *et al.* (2004) defined an average light intensity as an important parameter to predict optimal conditions for H_2 production in photoheterotrophic conditions, and showed that H_2 production varied with the Chl concentration and the thickness of the photobioreactor. They suggested that I_{av} is the parameter that more faithfully represents the physiological characteristics of cultures without reflecting the technical details of experiments. The I_{av} includes within its considerations, the incident light intensity, the radius of the photobioreactor, and the optical density of the culture at various concentrations of Chl.

Other reaction parameters, such as optimum temperature, have not been defined and a range of temperatures between 20 - 30°C have been used for experimental studies. Kosourov *et al.* (2003) reported an initial pH of 7.7 for the S-depleted TAP medium to be optimal for H_2 production. However, it should be noted that the pH of the medium in the batch culture changes with time, increasing during the O_2 production and O_2 consumption stages due to photosynthetic consumption of dissolved CO_2 and utilization of acetate (Kosourov *et al.*, 2002) and decreasing slightly during the anaerobic and H_2 production phase, as a result of

CO_2 release (Kosourov *et al.*, 2002) and fermentative accumulation of acetate and formate (Tsygankov *et al.*, 2002).

The wash step for aerobic cells in S-depleted TAP medium prior to resuspension also represents a challenge for process up-scaling. Here too, considerable variation exists in the literature with some groups washing once, three times (Kosourov *et al.*, 2003) or up to five times (Kosourov *et al.*, 2002), before resuspending in S-depleted TAP medium. Five wash steps would be highly unfeasible and also time-consuming if this process is to be scaled up.

Finally, the initial cell densities (often estimated from the initial Chl at resuspension) optimal for resuspension have not been systematically studied for large-scale processing. At the small lab scale, the range of initial [Chl] at resuspension used in literature has varied between 9-30 µg/ml with 12-16 µg/ml being reported more often (see Table 4.2).

Unlike bacterial systems, *C. reinhardtii* physiology is more sensitive to variations in culture conditions, especially the bioreactor dimensions, and obtaining reproducible results from one group to another is quite difficult. Often, the rates of H_2 production are measured by indirect means, by withdrawing samples from bulk culture and incubating in gassed and evacuated vials with small volumes and measuring the gas phase therein (e.g., Hemschemeier, 2005). Such indirect measurements, calculated for extremely small culture volumes, are then extrapolated by calculation to apply to larger bulk volumes and often result in a much higher calculated rate of production than is achievable in real bulk cultures. Rates and amounts of H_2 are also generally reported on a volume basis of the culture rather than biomass, because S-depletion causes significant physiological changes. However, comparison of these rates and amounts with those from other bioH_2 producers, necessitates the calculation on biomass or Chl basis. Our results are always calculated in terms of the initial amounts of Chl, protein or biomass at the time of resuspension.

Our studies of bioH_2 production with strain SAG 18.79 indicate an important conclusion. On the one hand, the benchmark conversion coefficients described above for SAG 18.79 are directly applicable to actively (photosynthetically) growing cultures of CC-124, as indicated by conversion of literature values reported for the latter strain. This is not unexpected, since both strains correspond to the same species and only a single chloroplast is present in both. On the other hand, the kinetics of H_2 production under S-depleted near-stationary growth conditions are significantly different between the two strains, indicating significant physiological phenotypes in the anaerobic growth mode. At least for the SAG 18.79 strain, although the growth kinetics were highly reproducible, we could not achieve completely reproducible kinetics of H_2 production under both VLL and IL intensities. Thus,

we have not presented averaged data sets for the gas phase composition of S-depleted H_2 producing cultures.

4.10.3. A comparative survey of the amounts and rates of H_2 produced by *C. reinhardtii* under S-depletion conditions

A large number of published datasets on *C. reinhardtii* S-depletion and H_2 production were collated. Most of these experiments were conducted using the CC-124 strain at temperatures above 25° C. The cell number and Chl content at harvesting and at resuspension in S-depleted medium were widely reported figures. It should be noted that the experiments were conducted at various incident light intensities in the non-saturating range. These data points along with others have been reported in Table 4.2 and Fig. 4.3.

The amounts and rates of H_2 production have been presented on a concentration (µmol) and volume basis (ml), and where available, on the basis of physiological parameters such as Chl content. It should be noted that rates and amounts of H_2 reported on a volume basis can be converted to a concentration basis or vice versa by using the gas laws at the appropriate growth temperature. Certain values have been converted to more convenient units, such as the [Chl] of 7.7 nmol/ml culture (Melis *et al.*, 2000) which was recalculated as 7.15 µg/ml using our conversion coefficients. Our highest rate of H_2 production is still ~10 fold smaller than those reported in literature. Note that, unlike the Melis group and some (but not all) others, we have not employed an inverted water column to trap the gases emanating from the bioreactor, but instead kept the gases sealed within the bioreactor. This possibly affects the behavior of the culture and might be responsible for the H_2 uptake phase recorded. Additionally, the differences in culture conditions, such as whether lighting was provided from one or both directions, or whether different light/dark cycles were employed, and the length of the H_2 production phase, significantly impact results. For instance, the large amounts of total H_2 reported by Oncel and Sukan (2011) were collected over 27 days of dark/light growth cycles. The amounts and rates are presented in tabular form, and as figures (Table 4.2 and Fig. 4.3).

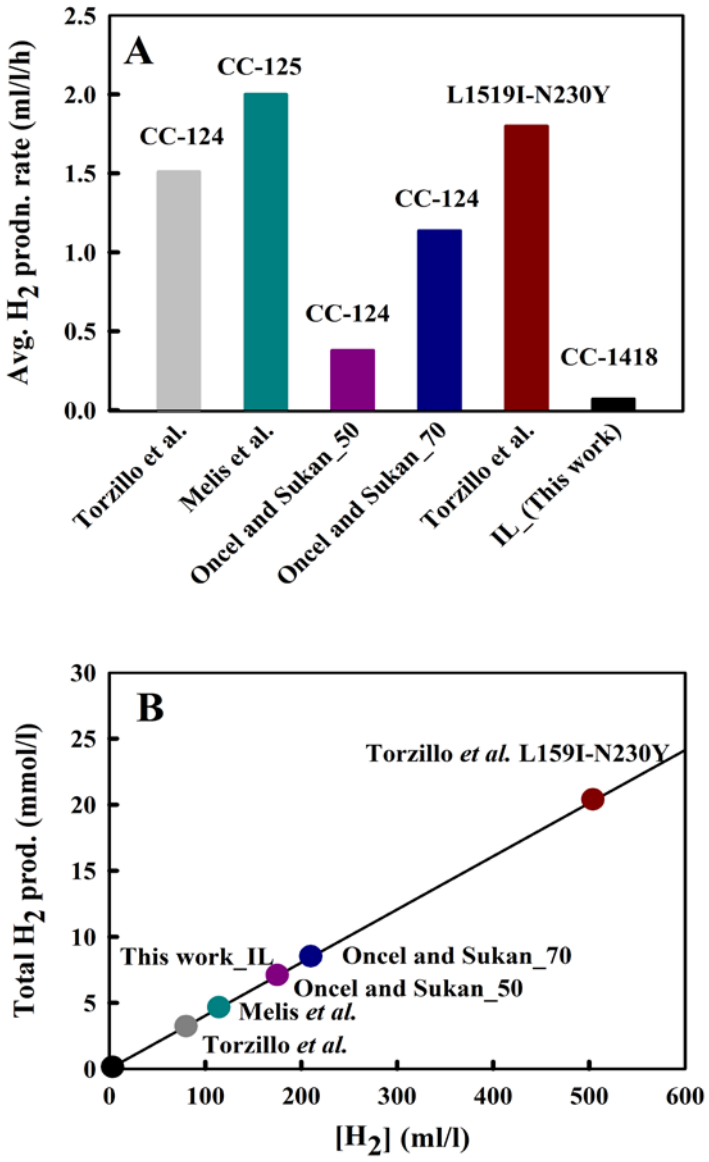

Fig. 4.3. (A) A graphical representation of the average H_2 production rates and **(B)** the total amounts of H_2 evolved in experiments reported in literature. Our results for strain CC-1418 are also shown. This data is also expanded in Table 4.2. Colour code: (1) grey, Torzillo *et al.* (2008) for strain CC-124; (2) cyan, Melis *et al.* (2000) for strain CC-125; (3) purple, Oncel and Sukan (2011) for strain CC-124 at light intensityof 50 µmol photons/m^2/s and (4) dark blue, Oncel and Sukan (2011) for strain CC-124 at light intensity of 70 µmol photons/m^2/s; and (5) brown, Torzillo *et al.* (2008) for strain L159I-N230Y; and (6) black, IL intensity, this work for strain CC-1418.

Culture conditions						S- depletion conditions				H_2 production amounts and rates					
Author	**Light Int (µmol photons/ m^2/s)**	**Temp. °C**	**Strain**	**pre-culture Chl (µg/ml)**	**Chl content (µg/ml) of (1 *10^7 cells/ml)**	**Resuspension Chl**	**Bottle Path-length (cm)**	**Culture volume (ml)**	**Bioreactor volume (ml)**	**H_2 prod. lag time (h)**	**Avg. H_2 accumulation rate (ml/l/h)**	**Max. H_2 prod. Rate**	**Time of prod.**	**Total H_2 (mmol/l)**	**Total H_2 (ml/l)**
Hemschemeier *et al.* 2009	~ 80	20	CC-124 (137c$^-$)	20	30.77	20-25	5	100	120	50	-	-	50 to 200 h		
						15	~10	290	320		-	-			
Melis *et al.* 2000	200	25	CC-125 (137c$^+$)	7.43	24	7.15	3-5	1000	-	40	2	-	42 to 120 h	6	150
Oncel and Sukan, 2011	40*2	27	CC-124 (137c$^-$)	24	30	12	5.6	1100	1,100		-	-	-		
	50*2			20+-1	27.6	12	5.6	1100		24	0.379	-	27 days	7.1	175.45
	70*2			24+-1	31.8					26	1.136	-		8.53	210.91
	80*2			25+-1	30.03					26	1.06	-		7.5	187.27
	100*2			26+-1	29.7					28	0.83	-		7.72	190
Kosourov *et al.* 2007	25	28	CC-124 (137c$^-$)	14-18	-	14-16	-	-	1,500	25-30	-	-	-	0.9 +-0.8	22.24
Kosourov *et al.* 2003	200	25	CC-124 (137c$^-$)	-	24	9-12	4	1200	1,200	35	-	9.4 µmol (mg Chl)$^{-1}$h^{-1}		7.66 (pH 7.7)	187.3 (per bioreactor)
Torzillo *et al.* 2008	70 *2	28	CC-124 (137c$^-$)	-	-	12	5		1,100	16	1.51	2.09 ml/l/h	53 h	3.24	80
			L159I-N230Y	-	-	12				37	1.81	5.77 ml/l/h	285 h	20.4	504
IL (this work)	70	21	SAG 18.79 or CC-1418	30.6	25.69	12.7	5.3	110	133	290	0.051	0.09 ml/l/h	68 h	0.156	3.494

Table 4.2. A comparative summary of the H_2 production experiments conducted with the CC-124 strain (Hemschemeier *et al.*, 2009, Melis *et al.*, 2000, Oncel and Sukan, 2011, Kosourov *et al*,. 2007, Kosourov *et al.*, 2003, Torzillo *et al.*, 2008) and the IL intensity experiment outlined in Fig. 3.16.

4.10.4. Present status of bioH_2 production technology and strategies for the future

Though bioH_2 represents a highly desirable solution to our energy needs and emission problems, current research in this field unfortunately shows that we are far from achieving the levels of H_2 required for practical everyday use. This can be demonstrated by the following calculations.

We calculated the amounts of H_2 reported in literature from bioH_2 producers by normalizing the culture volumes to 100 l for convenient comparison (Table 4.3). For this calculation, we have ignored the practical matters of differences in light intensities used, the number of days required to produce the reported amount of H_2 and the culture volumes used.

A typical German household, requires on average, energy equivalent to 1.374×10^{11} J/year or 3 MJ/day. With an energy density of 121 kJ/g H_2 or 0.121 MJ/g H_2, a household would require 3140 g H_2/day or 1570 mol H_2/day. From Table 4.3, we can conclude that, the present state of bioH_2 technology, would be realistically unable to supply such high energy demands. Even at the highest levels achieved to date, 70,000 l of *C. reinhardtii* culture or 47,000 l of *Cyanothece* culture, or 8,000 l of *R. rubrum* culture will be required to produce the 1570 mol H_2 that a household requires daily.

At least a 10 – 100-fold increase over present day *R. rubrum* H_2 production technologies or a 100 – 1000-fold increase over present day *C. reinhardtii* H_2 production technologies would be required before we can realistically consider bioH_2 as a reliable source of energy. Therefore, extensive physiological, transcriptomic, genetic, and metabolomics data is available for *R. rubrum*. Additionally, biochemical benchmarks, light intensities, and growth conditions are already well optimized, unlike for *C. reinhardtii*. A breakthrough in biotechnology was the development of "dark photosynthesis" in *R. rubrum* by means of the M2SF medium (for details see Appendix 2 and Part II of the thesis) whereby they may be grown to reach ODs (A_{660}) as high as 160 in the dark. The combinatorial use of these very high cell densities, and genetic modifications which activate multiple routes of H_2 production and growth medium which ensures de-repression of N_2ase, can very realistically lead to a 10 - 100 fold enhancement over present day numbers. This may allow *R. rubrum* to become a favoured system over microalgal organisms such as *C. reinhardtii*.

Literature	Strain	Light-intensity ($\mu mol.m^{-2}s^{-1}$)	Culture volume (ml)	Time for H_2-Prodn. (h)	Total H_2 (mol) /100 Liter culture	Total vol. H_2 (l) /100 Liter culture
Melis *et al.* (2000)	$137c^+$	200	1000	100	0.6	15
Winkler *et al.* (2002)	$137c^+$	150	200	100	0.8	20
Kruse *et al.* (2005)	Stm6	100	?	338	2.22	54
Doebbe *et al.* (2007)	Stm6Glc4	110	?	250	1.5 x increase over Stm6	(assumed) 81
Torzillo *et al.* (2009)	L159I-N230Y	140 (70 x 2)	1100 (PBR)	285	2.02	50
Torzillo *et al.* (2009)	WT	140 (70 x 2)	1100 (PBR)	80	0.12	2.9
Torzillo *et al.* (2009)	$137c^-$	140 (70 x 2)	1100 (PBR)	29	0.32	8
Bandopadhyay *et al.* (2010)	Cyanothece 51142	100	25	?	3.336	83
Hilmer & Gest (1977a,b)	*Rb. capsulatus* WT	6.5 kLux	60	40	30	750
Zürrer & Bachofen (1979)	*R. rubrum* WT	14	40000	240	1.54	38.4
Kim *et al.* (2008b)	*R. rubrum* Δ*glnB*Δ*glnK*	7	10	120	20	500

Table 4.3. H_2 production by *C. reinhardtii* (strain names in black lettering), purple bacterium (purple lettering) and cyanobacterium (green letters) scaled up for 100 l cultures volumes. (PBR (photobioreactor volume)).

Genetic engineering of *C. reinhardtii* has delivered promising enhancements and is realistically the only route to enhance bioH_2 production in this organism. Genetic manipulation in *C. reinhardtii* aims at improving the efficiency of photosynthesis by decreasing the Chl antennae sizes, improving the O_2 tolerance of the *C. reinhardtii* hydrogenases by either restricting O_2 diffusion into the protein or by replacing them with a more O_2-tolerant hydrogenase from other microorganisms, or by increasing respiration rates for higher O_2 sequestration. (For a detailed review see Navarro *et al.*, 2010). Unfortunately, increasing the cell density of *C. reinhardtii* is counterproductive to H_2 production rates, unlike in *R. rubrum*.

Additionally, in the field of *C. reinhardtii* H_2 production, more has to be done to adapt the processes to biotechnological requirements. A systematic reporting of units must be adopted by the community to make comparisons with other bioH_2 producers easier, though volumetric considerations are also important and should not be left out when reporting rates and amounts of H_2 being produced. Starting with modification of the TAP medium, and optimization of growth parameters, large scale screening for super-producing mutants is urgently required. Also systems biology-guided approaches to genetic engineering of *C. reinhardtii* may yield significant increases in bioH_2 levels.

PART II

M2NF growth medium: a new medium for high-level cell density and photosynthetic membrane production under conditions of nitrogen source variation.

1. INTRODUCTION

1.1. Discovery of H_2 production and nitrogen fixation genes in photosynthetic bacteria

H_2 production in anoxygenic photosynthetic purple bacteria was first discovered when *R. rubrum* was grown in mineral salts with glutamate and fumarate. H_2 production was light-dependent, and was found to be inhibited by N_2 (Gest and Kamen, 1949; Kamen and Gest, 1949). This inhibitory effect of N_2 on H_2 evolution was interpreted as a competition for reductants between the two and the incorporation of ^{15}N into cellular nitrogenous compounds (Kamen and Gest, 1949; Lindstrom *et al.*, 1949) in *R. rubrum*, which effectively showed the presence of nitrogen fixation genes in photosynthetic bacteria for the first time. Furthermore, H_2 evolution and the nitrogenase (N_2ase) activity were found to be affected by a common set of physiological conditions such as, inhibition by NH_4 and O_2, which led to the hypothesis that both H_2 evolution and N_2ase activity in *R. rubrum* were catalyzed by the same enzyme complex (Ormerod and Gest, 1962). Burns and Bulen (1965) were able to co-purify the N_2ase and ATP dependent H_2 production activities from *Azotobacter vinelandii* cell extracts.

Apart from *R. rubrum*, *Rhodobacter capsulatus* (*Rb. capsulatus*) has been widely used for investigations into N_2ase regulation (see Kranz and Foster-Hartnett, 1990; Hübner *et al.*, 1991; Masepohl *et al.*, 1988).

Nitrogen fixation by the N_2ase reaction is highly energy intensive:

$$N_2 + 8\,H^+ + 16\,MgATP + 8\,e^- \Rightarrow 2\,NH_3 + H_2 + 16\,MgADP + 16\,Pi \qquad (1)$$

H_2 evolution via N_2ase represents an alternative e- transfer pathway and prevents excess ATP build-up in cells, while under conditions of N_2ase inhibition, reducing power and ATP are directed more towards biosynthesis. Thus, the ATP/ADP ratio in cells could possibly determine which pathway the e^- take (Ormerod and Gest, 1962).

1.2. Elucidation of the *nif* genes responsible for nitrogen fixation

In purple bacteria, two types of N_2ases have been widely reported:

(1) MoFe- N_2ase (encoded by *nifHDK*);

(2) the alternative Fe- N_2ase (encoded by *anf*HDGK, (Brigle *et al.*, 1985; Joerger *et al.*, 1989)).

Additionally, a third type of N_2ase is important for N_2 fixation in environments where Mo is limiting (Joerger *et al.*, 1988).

(3) a VFe- N_2ase (encoded by *vnfH*-Fd and *vnfDGK* (Joerger *et al.*, 1990)), has also been documented. All three types of N_2ases are found in *A. vinelandii* (Chisnell *et al.*, 1988) whereas purple bacteria contain only the Mo- and Fe- N_2ases (Davis *et al.*, 1996; Schneider *et al.*, 1991).

1.2.1. The MoFe-N_2ase

The organization of the nitrogen fixation (*nif*) genes has been studied most extensively in *Klebsiella pneumoniae* because of its similarity to *E. coli* (Ausubel and Cannon, 1980; Brill, 1980; see Ausubel, 1984). The N_2ase enzyme has been purified from many species. It consists of two main structural components: component I (diN_2ase), a Mo-Fe protein complex, a 230-kDa $\alpha_2\beta_2$ tetramer of the *nif*D and *nif*K gene products and component II (diN_2ase reductase), a Fe protein composed of a 64-kDa α_2 dimer of the *nifH* gene product (Mortenson and Thorneley, 1979).

The *nifHDK* genes have been highly conserved in evolution, permitting the identification and cloning of *Rhizobium nifHDK* genes using *K. pneumoniae nifHDK* genes as hybridization probes (Ruvkun and Ausubel, 1980). The *Rb. capsulatus nifHDK* genes comprise a single expression unit, with the same organization and polarity as found in *K. pneumoniae*. However, the *Rb. capsulatus nifHDK* operon does not complement the corresponding *Klebsiella* genes, and the reciprocal relation is also true (Avtges, 1983).

Approximately 36 genes encoding both structural and regulatory proteins have been identified as *nif* genes in *Rb. capsulatus* (Klipp, 1990). Functions for some of the *nif* genes have been demonstrated directly or inferred from sequence homology with genes from *K. pneumoniae* (see Gussin *et al.*, 1986; Arnold *et al.*, 1988). In all microbes studied, the direct electron donor to N_2ase is either a ferredoxin (Fd) or a flavodoxin (Fld). The electron transfer complex FixABCX, bifurcates electrons from NADH to generate reduced quinone and reduced Fd or Fld in *R. rubrum* (Edgren and Nordlund, 2006), and is required for electron transfer to N_2ase (Huang *et al.*, 2010).

Gene	Phenotype
nifH	Fe-protein (diN_2ase reductase). Electron donor to FeMo- protein (diN_2ase). Required for FeMo-cofactor biosynthesis and FeMo-protein maturation.
nifD	α subunit of FeMo- protein. Forms $\alpha_2\beta_2$ tetramer along with β subunit.
nifK	β subunit of FeMo protein.
nifT	Unknown.
nifY	In *K. pneumoniae*, aids in insertion of FeMo-co into apoFeMo- protein.
nifE	Forms $\alpha_2\beta_2$ tetramer with NifN. Required for FeMo-co synthesis.
nifN	Required for FeMo-co synthesis.
nifX	Involved in FeMo-co synthesis.
nifU	Involved in mobilization of Fe for Fe-S cluster synthesis and repair.
nifS	Involved in mobilization of S for Fe-S cluster synthesis and repair.
nifV	Homocitrate synthase, involved in FeMo-co synthesis.
nifW	Involved in stability of FeMo- protein. Proposed to protect from O_2 inactivation.
nifZ	Unknown.
nifM	Required for the maturation of NifH
nifF	Flavodoxin. Electron donor to NifH.
nifL	Negative regulatory element.
nifA	Positive regulatory element.
nifB	Required for FeMo-co synthesis. Specific Fe and S donor to FeMo-co.
fdxN	Ferredoxin. In *Rb. capsulatus*, e^- donor to N_2ase.
nifQ	Involved in FeMo-co synthesis.
nifJ	Pyruvate:flavodoxin (ferrodoxin) oxidoreductase. Involved in electron transport to N_2ase.
fixABCX	Bifurcates electrons from NADH to generate reduced quinone and reduced Fd or Fld. Required for electron transfer to N_2ase.

Table. 1.1. A list of *nif* genes and their respective known or proposed functions (adapted from Rubio and Ludden, 2005).

1.3. Regulation of *nif* gene expression by N-status of cell and O_2

In both *Rb. capsulatus* and *K. pneumoniae*, two levels of control exist: the first involves at least five proteins which act in a cascade to sense and relay the N-status of the cell (Kranz *et al.*, 1990; Kranz and Foster-Hartnett, 1990). Upon nitrogen deficiency, genes involved in the second level of control are activated whose gene products (NifA and RpoN/ σ^{54}) further activate all other *nif* genes.

In both organisms, the nitrogen status of the cell is sensed as a ratio of the concentrations of glutamine to α-ketoglutarate (αKG). A low ratio, indicating N-limitation, is sensed by the uridyltransferase (UTase) via allosteric modifications, which transmits this information via sequential phosphorylations of the GlnB, NtrB and NtrC proteins. The NtrC further activates the *nifLA* operon along with RpoN (in *Rb. capsulatus*, the RNA polymerase sigma factor (σ^{54}), not RpoN is used) (see Gussin *et al.*, 1986; see Kustu, 1989). The *nifA* gene product is the transcriptional activator required for the expression of all *nif* operons except its own (Buchanan-Wollaston *et al.*, 1981). NifA activates the RNA polymerase holoenzyme positioned at the *nifHDK* promoter by catalyzing the formation of transcriptionally active, open complexes (Morett and Buck, 1989) between the holoenzyme and the promoter. This activation is enhanced by the integration host factor (IHF), a small heterodimeric protein (Nash and Robertson, 1981), which binds to a site between the upstream binding site for NifA and the promoter and induces DNA looping. This IHF-induced loop facilitates interactions between NifA and the σ^{54}-holoenzyme (Hoover *et al.*, 1990) (Fig.1.1A).

The gene products of the regulatory genes *nifA* and *nifL*, are required for the positive and negative control (Merrick *et al.*, 1982) of *nif* structural gene transcription, respectively. The *nif*L product appears to antagonize the action of the *nif*A product in the presence of O_2 (Buchanan-Wollaston and Cannon, 1984) or at low concentrations of fixed N_2. Under such conditions, the *nifLA* operon is still activated by NtrC, though the *nifL* gene product inactivates the *nifA* gene product (Merrick *et al.*, 1982) and therefore transcription of other *nif* operons is also repressed.

An additional mechanism of O_2-based regulation, is the control of *nif* gene transcription by the action of DNA gyrase and DNA topoisomerase I. Oxygen appears to prevent the adoption of a DNA conformation necessary for *nif* gene transcription (Kranz and Haselkorn, 1986). The expression from the *nifH* promoter is possibly the most O_2-sensitive step (see Hill, 1988).

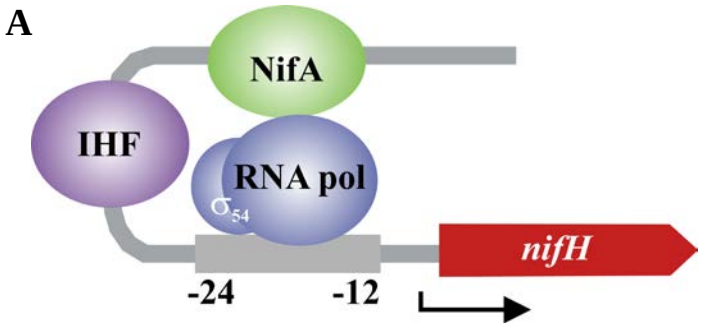

B

```
                1         10        20        30        40        50        60
rr_PnifH  GGGGATCCCAAGGAGGGACCCTCCGTCCTGACCAAGAACTGTGCGTTCGTGTTTTCGCCC
rc_PnifH  ------------------------AGTTCATCCCGCGCGATGAAGACGTGATGGTGC--

               61        70        80        90        100       110       120
rr_PnifH  ATTCCTTTATCACCGATCGGGCGGCGACGGGAAGGGCGTTCTGGGCAGTAGCGCACCATC
rc_PnifH  ATTTCACCGGCACC--CCCGGCGGC----------TCGGTCTGAA-ACCGCCGCAAGGAC

               121       130       140       150       160       170       180
rr_PnifH  GCGCATAGCGTCGCGCCGCCCGCTGTTGGGTCCG----CGACAGGGTTTTGGGGCGTTG
rc_PnifH  -CGGAAAACGCCGCGCTGGCGGGGTTTTTCATTTCCTCCCGACAGAGGGCCCGACAAAAC

               181       190       200       210       220       230       240
rr_PnifH  TCGCGTTTGCGACACGGTTGAAAATA-ACCCTACATTCCTTGTTAGATAGATTATTCCT
rc_PnifH  CCCGCC---CGACACCGCAGGCCCTACAATTTGTCGGCCTTGTTCCAT---TTCGTAACAA

                                                          -24
               241       250       260       270       280       300
rr_PnifH  TTGATTAAAAACGATAATTTTCAA--AAAAATCGGCAAATCAGGTTTGGCACGCTGGGT
rc_PnifH  AACCTTCAACACCATGATTTCGCGTCATTATTTCGAAAATTCCGGTTGGCACGATGGCT
-12
               310       320       330       340       350       360
rr_PnifH  GCATTA-ACGGGGTGAGCGTGGCGGTGGAGCTTCCCCGCCTTAGGACCGGATCACGAAGA
rc_PnifH  GCTGTAGAAGCTGTGAGCCCGGTTAGGAACCGTCTCGATATTCGTGAAGCACCA--ACCC

               361       370       380       390       400       410       420
rr_PnifH  AAAGGATTGATTCCATGAGCGCACTGCGTCAGATCGCGTTCTACGGCAAGGGCGGTATCG
rc_PnifH  CAAGGAGCCACCACATGGGCAAACTCCGTCAGATCGCCTTCTACGGCAAAGGTGGTATCG
```

NifH coding region

Fig. 1.1. (A) A schematic representation (R. Ghosh, unpublished) of the NifA – IHF- σ^{54} RNA polymerase holoenzyme interaction at the *nifH* promoter (promoter region DNA indicated in grey) and the IHF induced DNA bending. The σ^{54} RNA Pol binds at the -24 and -12 bp position upstream of the start site. NifA binding is centered at -132 relative to the transcriptional start site. **(B)** The DNA sequence of *nifH* gene and upstream promoter elements for both *R. rubrum* (rr) and *Rb. capsulatus* (rc), red boxes denote the -12 to -24 *nifH* promoter regions, orange boxes indicate the IHF binding sites and green boxes indicate the NifA binding sites. Experimental determination of IHF binding sites for both (rr) and (rc) by Hoover *et al.* (1990).

In some bacteria (e.g. *R. rubrum* and *Rb. capsulatus*, *Azospirillum brasilense* and *Azospirillum lipoferum* (microaerophilic, associative bacteria), and *Chromatium vinosum*) an additional level of N_2ase regulation is present, to prevent nitrogen fixation during energy-limiting or nitrogen-sufficient conditions (Ludden and Roberts, 1989). The N_2ase complex is rapidly and reversibly inactivated by ADP-ribosylation of the Fe-protein. This post-translational N_2ase regulation was first identified in *R. rubrum*. The NAD^+-dependent enzyme, diN_2ase reductase ADP-ribosyltransferase (DRAT), and its partner, diN_2ase reductase-activating glycohydrolase (DRAG) catalyze the ADP-ribosylation and ADP de-ribosylation of the Fe- protein, inactivating and activating the Fe- protein complex respectively (Halbleib *et al.*, 2000; Halbleib and Ludden, 2000).

1.4. The pathways for the assimilation of NH_4^+ in *R. rubrum*

Ammonium assimilation in *R. rubrum* has been shown to occur via the glutamine synthetase and glutamine: αKG amino-transferase (GS-GOGAT) system (Slater and Morris, 1973):

$$NH_3 + \alpha KG + NADPH + H^+ + ATP \Rightarrow L\text{-}Glu + ADP + P_i + NADP^+ + H_2O \qquad (2)$$

In *R. rubrum* the presence of L-Glu, L-Gln, and L-Asp as the dominant amino acid pools is characteristic of organisms possessing the GS-GOGAT assimilation mechanism (Dharmawardene *et al.*, 1972). GOGAT activity was found to be highest under NH_4^+ limitation in *R. rubrum* and lowest under high NH_4^+ with low to intermediate levels with L-Glu as N-source (Brown and Herbert, 1977). Thus, direct supply of Glu in the medium, decreases the dependence on the GS-GOGAT system. A third enzyme, glutamate dehydrogenase (GDH) can catalyze the reductive amination of αKG to yield L-Glu. Under N-limiting conditions, assimilation is more efficient via the GS reaction than the GDH reaction, since the K_m of NH_3 for GS is only 0.55 mM whereas that for GDH is 11.5 mM (Tempest *et al.*, 1970; Brown and Stanley, 1972). However, in the presence of L-Glu, the GDH reaction rates are very high (Brown and Herbert, 1977) though the reaction equilibrium is heavily displaced in the reverse direction (yielding αKG).

1.5. The role of amino acids in the regulation of N_2 fixation

In H_2-producing cultures of *R. rubrum*, no free NH_4^+ could be assayed and interestingly, when grown in the presence of certain amino acids, some amino acids were found to promote growth as well as supporting H_2 production, whilst some amino acids inhibited H_2 production (Bregoff and Kamen, 1952) (See Table 1.2 and Fig. 1.2). Similarly, in *Rb. capsulatus*, the H_2

evolving function of N_2ase was found to be inhibited by N_2 and NH_4^+ salts and maximally expressed in cells growing with certain amino acids as N_2 source (Hillmer and Gest, 1977). The study of Hillmer and Gest (1977) must be carefully interpreted, as the pre-cultures used for the experiments were not washed prior to the experiment but were all grown in the presence of 7 mM L-Glu (they report Glu was used up completely quite early during growth). The most reliable and recent data on the regulation of N_2ase in *Rb. capsulatus* by means of various amino acids was obtained by Pollock *et al.* (1988). They devised a β- galactosidase based assay for measuring transcription rates from the *nifHDK* promotor in the presence of different amino acids as N_2 source. Using *lac* fusions it was demonstrated that transcription of the *nifHDK* operon was totally repressed when the growth medium was supplemented with ammonia, became fully de-repressed in ammonia-free medium, and proceeded at intermediate levels when other nitrogen sources (amino acids) were used. This result provides the basis for a mechanism which could possibly be used to control and fine- tune the expression levels from the *nif*H promoter, for any gene of interest that could be cloned downstream to it, leading to a novel expression system.

Organism	***R. rubrum***		***Rb. capsulatus***		
Reference	Bregoff and Kamen, 1952		Hillmer and Gest, 1976		Pollock *et al.*, 1988
Preculture	Cells washed in water		Cells directly from cultures with 7 mM L-Glu, (**<u>N_2 containing!</u>**)		Cells washed in water
C- source	**Malate**		**Lactate**		**Malate**
Assay system	H_2 production and detection/absence of NH_3 in culture		H_2 production		β-galactosidase activity of *lacZ* gene, fused downstream of *nif* promotor.
	Amino acids ($+H_2$)	**Amino acids ($-H_2$)**	**Amino acids ($+H_2$)**	**Amino acids ($-H_2$)**	**Amino acids examined (see Fig. 1. 2 for data)**
	Glu Asp Arg Pro *Leu*	Ala Ser His Gly Lys Asn Gln <u>Cys</u>	*Glu* Ser Ala Pro Tyr Gln Asp Asn Arg *Leu*	Lys <u>Cys</u>	<u>Cys</u> Arg *Glu* Gln Thr *Leu*

Table 1.2. A summary of literature for experiments conducted with amino acids as N-source for regulation of the *nif* promotor in *R. rubrum* and *Rb. capsulatus*. The pre- cultures used by Hillmer and Gest (1976) contained 7 mM Glu. The amino acids which showed high H_2 production or *nif* gene expression in all three reports are Glu and Leu (italicized), while the amino acid showing the least *nif* gene expression was Cys (underlined).

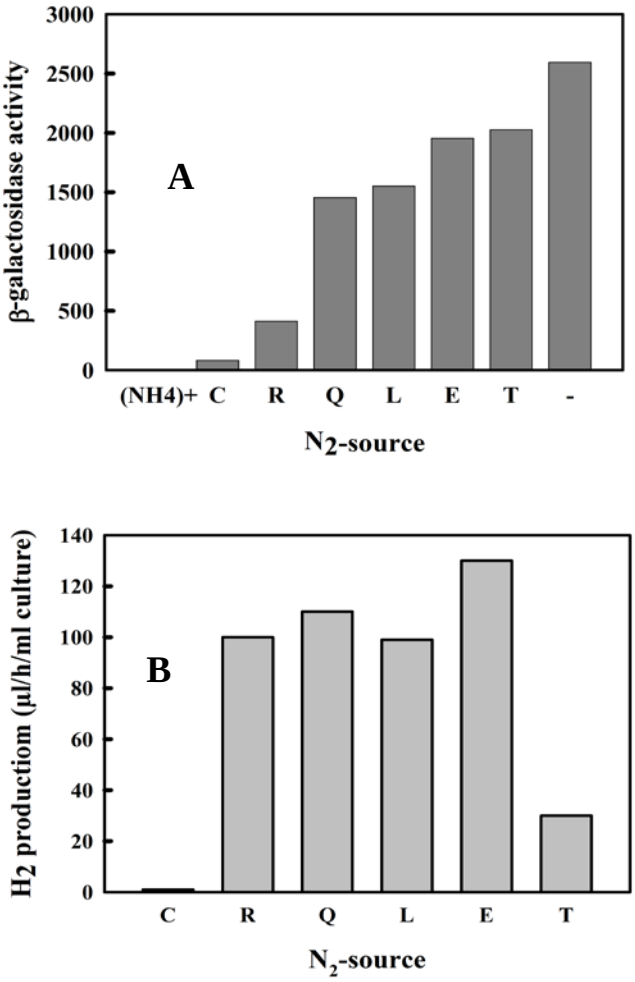

Fig. 1.2. (A) Schematic summary of the results obtained by Pollock *et al.* (1988) for *Rb. capsulatus*. The regulation of *nif* genes with the use of various amino acids (L to R: $(NH_4)_2SO_4$, cysteine, arginine, glutamine, leucine, glutamic acid, threonine, no N_2 source), NH_4^+ and NH_4^+-free medium as N_2 source in *Rb. capsulatus*, measured in terms of β-galactosidase activity. **(B)** Bar chart representation of the results obtained by Hillmer and Gest (1976) for the same amino acids as employed by Pollock *et al.*, (1988). The use of unwashed cells containing 7 mM Glu as pre-culture or the use of a different assay system are probably responsible for the difference in results.

2. MATERIALS AND METHODS (see also Part I Chapter 2)

2.1. Strain purification

Strains were plated out as 3-fold streaks several times or sometimes in sectors, until a single colony was obtained. In general, replated cultures were used to inoculate a slope, incubated aerobically (lid loosely shut) in the dark or anaerobically (lid tightly shut, shifted to light for two days). After about 3 days, the slope was filled up with the appropriate medium, allowed to grow either photosynthetically (preceded by a 24 h dark incubation) or semi-aerobically. About 4 ml of the slope culture was used to obtain a 100 ml culture. Anaerobic cultures were generally obtained after 7 days growth in closed vesssels (slopes, bottles, anaerobic jars). In all cases, the closed vessel was incubated for 24 h in the dark to allow the culture to remove residual O_2 by respiration.

2.2. Vector cloning

2.2.1. Plasmid preparation

For minipreps, the “High Pure Plasmid Isolation Kit” (Roche) was used to isolate plasmid DNA. For large amounts of DNA or for low copy plasmids, Q-20 tips (Qiagen) were used to purify the plasmid DNA.

2.2.2. Restriction enzyme digestion

Restriction enzyme (RE) digestion was performed in 20 µl volumes, with 1× restriction digestion buffer (RB), 10-20 enzyme units (1-2 µl) at 37°C (exceptions, according to the New England Biolabs (NEB) catalog). Enzyme inactivation was performed by either heating to 70°C for 10 min or to 85°C for 30 min, according to the NEB recommendation.

2.2.3. Agarose gel electrophoresis

0.8% agarose analytical gel electrophoresis was used for visualizing fragment sizes after digestion with specific restriction enzymes to confirm the directionality of insert. λ-DNA digested by *Hind*III was used as DNA marker.

2.2.4. Preparative enzyme digestion and preparative gels

1.2 - 2 µg DNA was digested in 1 × RB, 1x BSA and 60-200 U of RE in a 100 µl volume for 1 h at 37°C. Up to 200 U of RE was re- added for a second digestion step. 60 ng DNA was removed for analytical gel electrophoresis. If the DNA had been well digested, 20 µl loading buffer was added and then loaded onto a preparative gel which ran at 15 V for 12h at 4°C.

The desired band was cut out of the preparative gel and placed into a 2 ml Eppendorf tube and weighed. The “QIAquick gel extraction Kit” (Qiagen) was used for DNA extraction.

2.2.5. DNA precipitation

To precipitate DNA, 1/10 volume (vol.) 3M sodium acetate (NaOAc) and 2.5 vol. 100% EtOH were added to 1 vol. DNA, mixed and left at -20°C for 2h or longer. DNA was pelleted by centrifugation at 13,000 rpm (16,700×g) and 4°C for 16 min. The supernatant was removed and the DNA pellet was washed with 200 µl 70% EtOH, recentrifuged again at 13,000 rpm (16,700×g) at 4°C for 12 min. After removal of the supernatant, the DNA pellet was dried in a dessicator for 3 min. Generally, DNA was dissolved in Tris-EDTA buffer (TE) for further use or in H_2O for DNA sequencing.

2.2.6. Phenol/chloroform extraction

To 1 vol. of DNA, 1 vol. of phenol/dichloromethane (DCM)/TE was added, mixed thoroughly by vortexing, the mixture was centrifuged at 13,000 rpm (16,700×g) at RT for 10 min, and the DNA upper phase was washed with 1 vol. of chloroform/TE. After centrifugation, the DNA upper phase was precipitated as described before.

2.2.7. Blunting and polishing

5' restriction enzyme overhangs were blunted with any buffer with 1× dNTPs (0.2 mM each), 5 U Klenow (NEB) for 20 min at 21°C. 3' restriction enzyme overhangs were polished using 3 U of T4 DNA polymerase (NEB) in any buffer with 1× dNTPs for 15 min at 12 °C.

2.2.8. Dephosphorylation

Phenol/chloroform extraction was performed prior to dephosphorylation. DNA was precipitated as described before. The DNA pellet was dried for 3 min and redissolved in 20 µl TE. DNA dephosphorylation was performed with 1×dephosphorylation buffer, 2 U calf intestinal phosphatase (CIP (NEB)) in a 50 µl volume at 37°C for 30 min which was followed by another 30 min at 55°C with the addition of another 2 U CIP.

2.2.9. Ligation

Ligation using 26-30 ng DNA was performed in 20 µl with 1× T4 DNA ligase buffer, 20 U T4 DNA ligase (NEB). For blunt-end ligation, the molar vector-to-insert ratio ranged from 1:1 to 4:1, and the ligation was performed at 23°C overnight. For sticky-end ligation, the molar

vector-to-insert ratio ranged from 1:1 to 1:4, and the ligation was performed at 17°C overnight.

2.3. Preparation of competent cells

Competent cells of the *E. coli* strains XL1 MR, RR28, Top 10 and BL21(DE3)-RP were made by the $CaCl_2$ method. The appropriate strain was plated out directly from the glycerol culture and grown at 37°C overnight. The colonies from the plate were then used to inoculate a 10ml pre-culture which was grown at 37°C for 12h, shaking at 340 rpm. The pre-culture was inoculated into two 100 ml flasks containing 50 ml LB medium and grown at 37°C shaking at 290 rpm. After about 2 h, the cultures achieved an OD around 0.5 at 420 nm (1 cm path-length), 20 ml aliquots were distributed into four sterile polycarbonate tubes. After centrifugation at 1,940×g and 4°C for 10 min, the supernatant was removed and the cell pellet was resuspended with 5 ml cold and sterile 100 mM $CaCl_2$. After 2 h in ice, the resuspended cells were recentrifuged at 1,940×g and 4°C for 10 min. The supernatant was removed and the cell pellet was resuspended in 2 ml cold and sterile 50 mM $CaCl_2$ containing 20% glycerol. 200 µl aliquots of the suspended culture were distributed into cold 1.5 ml Eppendorf tubes and left in ice overnight and transferred to the -80°C freezer. The overnight incubation allows a somewhat higher competence to be achieved.

2.4. Transformation

Competent cells were removed from the -80°C freezer and thawed in ice for 10 min. After mixing and resuspending gently, 20 µl plasmid DNA was added and the cells were incubated in ice for 30 min, after which a 3 min heat shock was performed at 42°C. The samples were cooled at RT for 10 min, 1 ml LB medium was added and the cells were incubated at 37 °C for 1 h. Finally, 50 µl, 200 µl, and the rest of the sample were plated out on three LB agar plates containing 200 µg/ml ampicillin. The number of colonies on a 50 µl plate was counted and the frequency of competence was calculated.

2.5. Conjugation

Calculations were made from OD_{660} of fresh *E. coli* and *R. rubrum* cultures to obtain volumes containing 5 x 10^8 colony-forming units (cfu) for all three strains. For this purpose, the conversion factor 5×10^8 cfu/ml ≡ OD_{660} (1cm) = 1.4. (Sägesser, 1992) was employed. To remove residual antibiotics, *E. coli* and *R. rubrum* strains were washed twice with 1 ml 0.9 % NaCl and 1 ml M-medium, respectively, by centrifugation at 13,000 rpm (16,700×g) for 2 min, and then resuspended in 1 ml 0.9 % NaCl. For triparental mating, the helper strain

pRK2013/RR28 and the target plasmid strain were mixed with *R. rubrum* (adjusted to 5×10^8 cfu), with the ratio of *R. rubrum* to *E. coli* being 100:1. After mixing and centrifugation, the supernatant was removed and the cell pellet was resuspended in 17 µl 0.9 % NaCl. The resuspended cells were pipetted onto a nitrocellulose filter on a LB plate and left in the dark to dry for 15 min at RT, and then transferred to the 30°C oven. After 5 h incubation, the filter was transferred to a 1.5 ml eppendorf tube and washed with 1 ml 0.9 % NaCl. After removal of the filter, 200 µl of the resuspended cells were replated onto plates containing the appropriate antibiotics. The plates were placed in an anaerobic jar after a short period of drying and incubation.

2.6. Solubility of amino acids

The solubility of amino acids in aqueous solvents is an important consideration for the preparation of stock solutions for examining the effects on *nif* gene expression (see Appendix 2.7). Both Bregoff and Kamen (1952) and Hillmer and Gest (1976) used amino acids in a final concentration of 7 mM in their experiments, though stock concentrations have to be many fold higher (10x to 100x). Thus, amino acids were titrated with acid (HCl for basic amino acids) or base (NaOH for acidic amino acids) to achieve up to 100-fold higher stock solutions.

2.7. Fluorescence microscopy

Slides were prepared by diluting cold (4° C) cultures with saline (0.9 % NaCl), pipetting ~ 20 µl of the diluted culture onto the slide and covering with a coverslip such that no air bubbles were visibly trapped within. The sides of the coverslip were sealed with nail-polish (lacquer) and dried in air before mounting on the fluorescence microscope (Axiovert 200M, Zeiss, Germany) stage. The pRed optical filter set AT560 and AT635 (Chroma, Germany) was used to visualize mCherry fluorescence. mCherry has a fluorescence excitation and emission maxima at 587 nm and 610 nm respectively. The range of the optical filter set used is shown in Fig. 3.1. The images were obtained by AxioCam NR_m and processed by the AxioVision software version 4.8.2. Images were obtained with a 100x objective.

2.8. Semi-aerobic and anaerobic growth curve of *R. rubrum*

For quantitative semi-aerobic growth experiments with *R. rubrum*, 4 ml of a culture grown photoheterotrophically with M medium were used to inoculate 100 ml of M2SF or M2NF medium (present in 250 ml baffled Erlenmeyer flasks), and the culture was shaken at 150 rpm (2 cm throw) at 30°C in the dark. The A_{660} (4mm) and A_{882} (4mm) values of the culture at

different time points were measured using a single-beam spectrophotometer with a 4 mm path length cuvette. It has been shown previously (G.S. Wang and R. Ghosh, manuscript in preparation) that the A_{660} (4mm) correlates linearly with the dry weight up to an A_{660} (4mm) of 1.4. Above this value the culture must be diluted as appropriate.

Anaerobic growth curves were performed in 160 ml Schott bottles with a rubber seal and aluminum caps for air-tight sealing in M2NF medium (without fructose), with a magnetic fish for stirring. At least 4 ml of headspace was left in each bottle prior to sealing. Cultures were first incubated in the dark (O_2 consumption phase) for up to 48 hours before transferring to light at 30°C. The time of transfer to the light was considered as the 0 h time point. The initial turbidity measurement was performed after about 12 h growth in the light. Culture samples were taken every 24 h, by using a sterile 1 ml syringe and a 21-gauge needle (Braun, Germany), (with a second, 18-gauge needle (Braun, Germany) acting as air inlet). Measurements were conducted as for semi-aerobic growth curves (see section 4.3.2. for more details). In the figures and results reported within this chapter, the [NH_4^+]s were rounded off for clarity and do not take into account the percent ionization of succinate at the medium pH of 6.8 which determines [NH_4^+]. The actual calculated concentrations are: 1.92 mM, 3.84 mM, 9.6 mM, 13.44 mM, 19.2 mM, 38.4 mM and 76.8 mM [NH_4] and will appear as such in the subsequent publication of this work (manuscript in preparation).

2.9. Construction of the plasmid-borne (pRK290) fluorescent protein mCherry, under control of the *R. rubrum nifH* promotor (the construction of the mCherry-pRK290-derivative was performed by R. Ghosh)

A 720 bp section of DNA, coding for the 240 amino acid-containing mCherry protein (https://www.takarabio.com) downstream to the *R. rubrum nifH* promoter sequence (no structural *nifH* gene, total 1192 b.p.), was designed with codon optimization for the *R. rubrum* host, and constructed by total gene synthesis. This 1192 b.p. *Bam*HI blunt-ended Klenow fragment insert was cloned into the plasmid vector pRK290 (18.613 kb, tetracycline resistant (Tet^R), (Saegesser *et al.*, 1992)) at the *Eco*R1 site within the *telB* region using standard molecular biology methods (Sambrook and Russel, 2001) (See Fig. 2.1). Double restriction digests were performed to confirm that the insert was present in the reverse direction to the *telB* region of the plasmid vector. This construct was transformed into an *E. coli* XL1MR strain and maintained by selecting for the Tet^R phenotype. The *trfA* gene in the pRK290 helps regulate the plasmid and make it a very stable vector in *R. rubrum*. The plasmid pRK290 is a low copy number vector, and does not undergo rearrangements following conjugation

(Saegesser *et al.*, 1992), which is ideal for examining the physiological levels of *nif* gene expression.

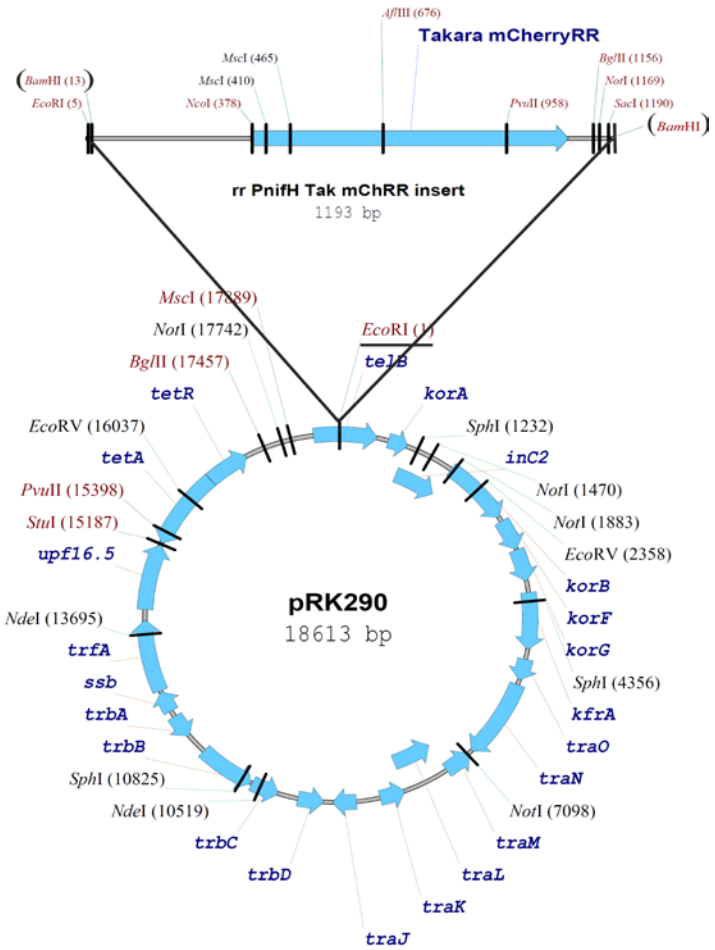

Fig. 2.1. The *Bam*HI blunt-ended Klenow fragment (*Bam*HI site in parentheses indicates blunt ends, and loss of adjacent *Eco*R1(5) site) rr_P_{nifH} Tak mChRR and the pRK290 vector map indicating the *Eco*RI (1) site (underlined) for insertion. The fragment was inserted in the reverse direction.

The transconjugant Tet^R strain pRKTmChRR1/S1 was purified from the conjugation mix under aerobic and anaerobic culture conditions and scaled up to larger culture volumes. A control strain pRK290/S1 containing only the plasmid vector was similarly constructed and maintained under Tet^R selection pressure.

3. RESULTS

3.1. Objective of this work and preliminary considerations

3.1.1. Development of medium for growth and differential expression of *nif* genes in *R. rubrum*

The use of the *nif* promoter (P_{nif}) may yield a useful expression system, where the expression level of recombinant proteins encoded downstream to the promoter can be adjusted by varying the nitrogen source (provided by various amino acids). *R. rubrum* has a high potential for various applications in biotechnology, especially due to the development of the M2SF medium (Ghosh *et al.*, 1994), which allows the formation of intracytoplasmic membranes (ICM) under microaerophilic conditions in the dark, which allows the production of compounds which require a lipophilic compartment (Wang *et al.*, 2012). This high level of dark ICM expression is currently not attainable in any other purple photosynthetic bacterium.

Our present aim is to characterize the response of physiological growth parameters of *R. rubrum* to varying levels of NH_4^+ in anaerobic and semi-aerobic conditions in lab-scale cultures via medium developed solely for this purpose. Along with the standard S1 strain, for which the cell turbidity (A_{660}), the A_{882}/A_{660} ratio and H_2 production was used as an indicator for N_2 fixation and *nif* expression, our experiments also employed a plasmid-borne fluorescent protein mCherry, under the control of the P_{nif} which should allow online-monitoring of the expression level by fluorescence techniques.

3.1.2. Mechanistic basis of the effect of M2SF medium upon photosynthetic gene expression

The standard M medium (Sistrom, 1960) for phototrophic growth of *R. rubrum* contains succinate as a C-source, solubilized by titrating the acid with KOH , and the final medium pH is adjusted to pH 6.8 with 2N NaOH (see Appendix 2). The uptake of succinate by the cells is in the protonated form, which implies that an equivalent amount of H^+ are extracted from the medium, leaving behind an excess of OH^-, which makes the medium progressively alkaline. M2SF medium (Appendix 2, (Ghosh *et al.*, 1994)) employs an improved buffer system and a second substrate, fructose, to overcome these limitations. Succinate is preferentially used until the pO_2 goes below 0.3%, whereupon the genes for anaerobic fermentation and photosynthesis are expressed, and fructose utilization is stimulated. The acidic end products of fructose fermentation are able to counteract the pH rise due to succinate uptake. More impressively, the M2SF medium allows full expression of photosynthetic genes in the dark, and a higher cell density than under anaerobic photosynthetic conditions. ICM expression

requires low O_2 tensions and light (at the molecular level, where light regulation is known to be mediated via a redox based signal). S1 growing in M2SF medium therefore is able to reach low O_2 tensions and an extremely low redox state akin to light conditions, triggering ICM expression in the dark (Grammel and Ghosh, 2008; Grammel *et al.*, 2003). Such low O_2 tensions are ideal to avoid O_2 inhibition of N_2ase.

3.1.3. Development of the M2SN medium (see Appendix 2): a NH_4^+ free variant of the M2SF medium.

In the M2SF medium, the major counterion NH_4^+ replaces Na^+ and the final [NH_4^+] is as high as 80 mM as compared to 8 mM in M medium. Thus, a modification of the medium to replace the NH_4^+ components with other bases such as, the tri-amine base triethylamine (TEA) and the monoamine base methylamine (MEA) becomes essential to overcome N_2ase repression.

By varying the ratios of the succinate-TEA and NH_4^+-succinate in culture, (keeping a constant final [succinate] of 40 mM), the growth physiology of the *R. rubrum* strains could be examined under a range of [NH_4^+]s. Systematic studies on the dependence of growth on [NH_4^+] would allow us to characterize expression from the *nifH* promoter in presence of various amino acids under anaerobic or semi-aerobic growth conditions and allow comparison with the P_{nif} in *Rb. capsulatus* which is regulated by N-source.

Although *R. rubrum* expresses a periplasmic TMAO (trimethylamine N-oxide)/DMSO (dimethyl sulfoxide) reductase constitutively (Sajitz *et al.*, 1993), which enables TMAO to be used as an electron sink under dark anaerobic conditions (Schultz and Weaver, 1982; Madigan and Gest, 1978), there is no evidence to suggest the uptake or utilization of trimethylamine (TMA) or TEA by the TMAO/DMSO reductase or the use of trimethylamine oxide (TEAO) as a substrate. However, the production of TMA during growth on TMAO increases alkalinity and inhibits further growth (Schultz and Weaver, 1982). In our experiments, an attempt to use TMA instead of TEA to neutralize the succinate solution in the M2NF medium, resulted in no growth of *R. rubrum* even at neutral pH values.

3.2. Expression of mCherry in *R. rubrum*

The excitation and emission spectra of mCherry (taken from www.chroma.com) are shown below:

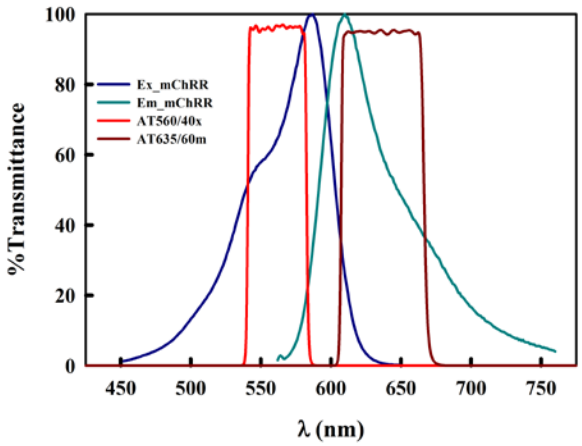

Fig. 3.1. Fluoresence microscopy for detection of mCherry expression: Fluorescence spectrum of mCherry excitation (Ex_mChRR) and emission (Em_mChRR) with the maxima at 587 nm and 610 nm respectively. The band width spectrum of the optical filter set (AT560 and AT635) used to visualize the mCherry fluorescence signal are indicated.

The following images were obtained from experiments with anaerobically grown pRKTmChRR1/S1, as well as with the control strain pUTmChRR1/*E. coli*. The latter expressed mCherry constitutively under control of the *lac* promoter.

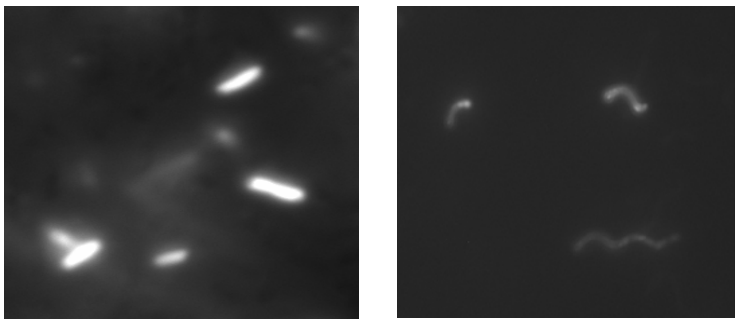

Fig. 3.2. Visualization of expression of the mCherry protein in pUTmChRR1/*E. coli* (R. Ghosh, unpublished) (left panel) and in anaerobically grown pRKTmChRR1/S1 (right panel) by fluorescence microscopy at 1000x magnification. Expression of mCherry under control of the *lac* promotor of pUC57, a high copy number vector, in *E.coli*, accounts for the difference in mCherry intensities of the two images.

3.3. A comparison of the growth of S1 and pRKTmChRR1/S1 strains in standard M2SF medium (high NH_4^+) shows close physiological similarities

The growth physiology of the S1 strain in M2SF medium (measured in triplicates) was compared to the growth of the pRKTmChRR1/S1 strain in M2SF Tet_4 (measured in duplicates).

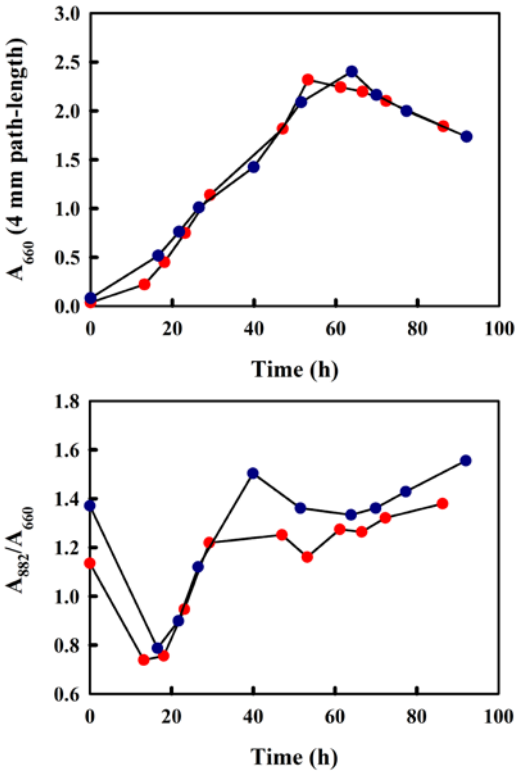

Fig. 3.3. Growth curves of S1 (red) and pRKTmChRR1/S1 (blue) in M2SF and M2SF Tet^4 medium (semi-aerobic growth), respectively. The S1 growth was measured in triplicate, while duplicate measurements were employed for the pRKTmChRR1/S1 strain. Upper panel: growth kinetics: lower panel: A_{882}/A_{660} (ICM /cell).

The growth profiles of the strains were nearly identical. Both strains reached similar maximum turbidities at A_{660} (4 mm) and the amount of ICM per cell (given by the A_{882}/A_{660} ratio) in both strains also shows a similar progression. This shows that presence of the low copy plasmid pRKTmChRR1 in S1 has only a very limited effect upon cell physiology. Note however, that under the growth conditions employed above, with 80 mM NH_4^+ as a N-source for S1, P_{nif} is completely repressed.

3.4. Growth response of *R. rubrum* to variation of the [NH_4^+] under semi-aerobic conditions

3.4.1. A comparison of the growth of pRKTmChRR1/S1 strains in M2SF medium versus the M2NF medium shows physiological differences

The growth physiology of the pRKTmChRR1/S1 strain was compared in M2SF medium and in M2NF medium, respectively:

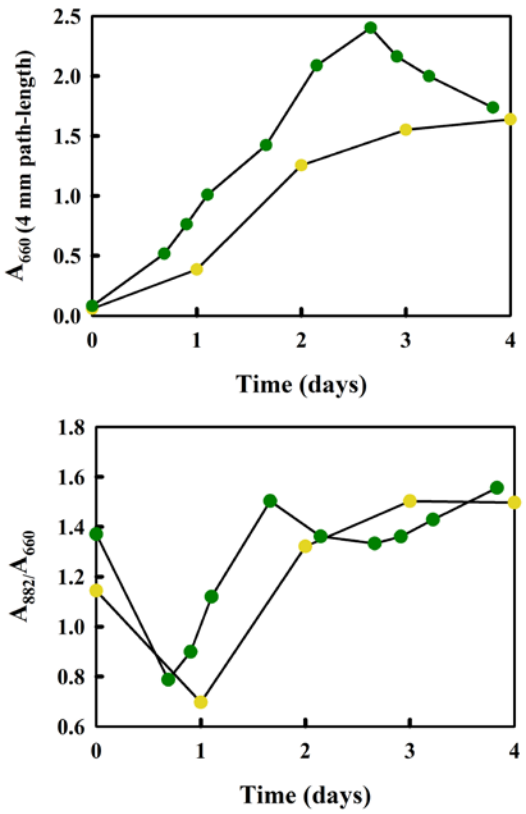

Fig. 3.4. Semi-aerobic growth curve of pRKTmChRR1/S1 in M2SF medium (green, triplicate measurements) and in M2NF medium (yellow, duplicate measurements) at a saturating [NH_4^+] of 80 mM in both experiments. Upper panel: growth kinetics: lower panel: ICM /cell.

The maximum cell density reached in M2NF medium (A_{660} (4 mm) = 1.5) is significantly lower than in M2SF medium (A_{660} (4 mm) = 2.5)) as well as the specific growth rate. Since M2NF medium contains only [NH_4^+]-succinate (80 mM) but no TEA-succinate solution, the only major difference between the media is the use of methylamine for titration of the HEPES buffer stock solution and for titration of the complete medium to pH 6.8. Nevertheless, the final ICM/cell ratio obtained in both media is essentially identical.

3.4.2. Growth dependence upon [NH_4^+] in M2SN medium

The major consideration for establishment of standardized experimental conditions was to eliminate the effect of residual NH_4^+ present in the inoculating volume of the preculture used. Routinely, a 4 ml inoculum was used for a 100 ml culture of *R. rubrum*. For precultures grown in M2S or M2SF medium, it is possible that, the majority of NH_4^+ remains unutilized

following growth and the dilution of 4 ml of preculture into 100 ml fresh medium, results in a low but physiologically significant concentration of NH_4^+, even in the absence of an additional N-source. Assuming that 80 - 90% of NH_4^+ is not utilized, the pre-culture may contribute up to 3 mM [NH_4^+] in the fresh culture. However, pelleting and washing the preinoculum with N-free media obviates this uncertainty, as the residual [NH_4^+] present after washing is almost negligible.

TEA, the counterion for succinate, is highly unlikely to act as an N-source, as the annotated *R. rubrum* genome does not contain any mono- or triamine uptake proteins or dehydrogenases.

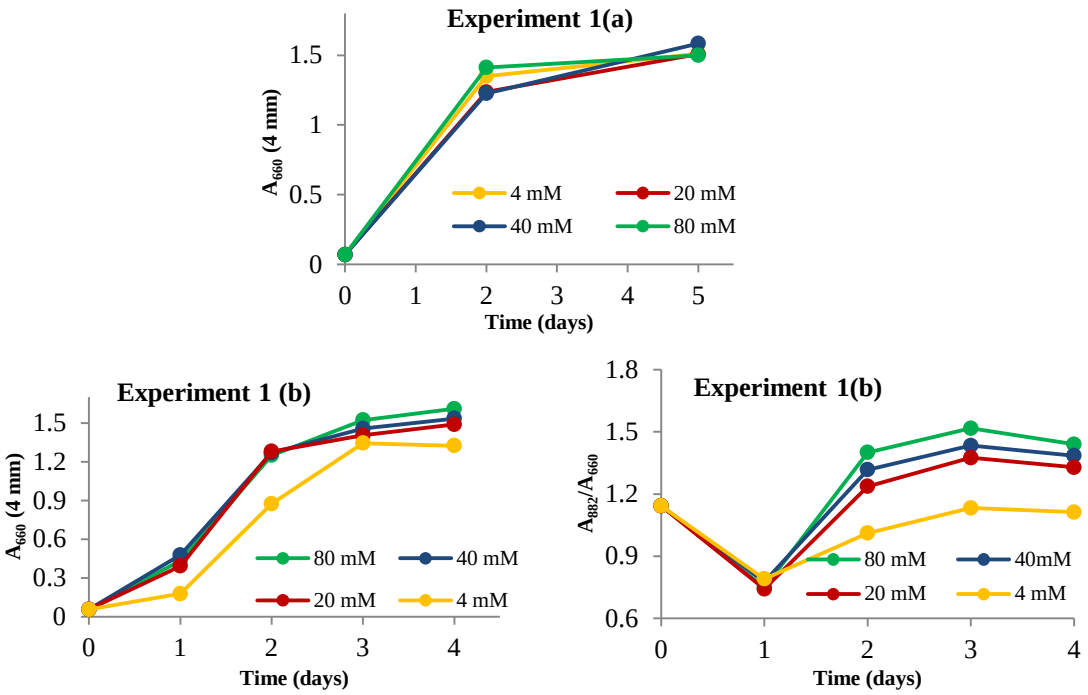

Fig. 3.5. Preliminary growth experiments (**1(a)** and **1(b)**) of pRKTmChRR1/S1 in semi-aerobic M2NF medium containing 7 mM Glu with varying [NH_4^+] in mM (indicated). The ICM/cell ratio (A_{882}/A_{660}) is shown only for expt 1 (b) here. See text for details.

Experiments where the cells were not washed prior to inoculation are shown in Fig. 3.5. The semi-aerobic experiment (1a) showed similar growth and final turbidities for cultures containing from 4 to 80 mM NH_4^+ in the presence of 7 mM Glu, respectively. Thus, 20 mM [NH_4^+] may be considered as non-limiting NH_4^+ conditions (M-medium has 8 mM NH_4^+). However, the similarity of the 4 mM NH_4^+ culture to the others indicates that the 7 mM Glu, along with the residual NH_4^+ from the inoculum (4 ml from standard M2SF culture) contribute to growth.

When this experiment was repeated (experiment 1b), with an inoculum taken from the 4 mM NH_4^+ + 7 mM Glu culture from experiment 1(a) rather than a standard M2SF culture, the 4 mM NH_4^+ curve did not concur with growth at the higher concentrations. It is clear that the true growth physiology in response to [NH_4^+] can be demonstrated only if the residual NH_4^+ and Glu from the inoculum is kept to a minimum or eliminated by washing the cells.

3.4.3. 4 mM NH_4^+ is the limiting concentration for the M2SF effect

The omission of the 7 mM L-Glu finally allowed for differences in growth physiology at limiting concentrations of NH_4^+ (Fig. 3.6). The difference in growth profiles from 0 - 4 mM NH_4^+ shows a steep rise in final turbidity at low NH_4^+ concentrations, which flattens out subsequently at higher concentrations. Growth appears to be saturated at 14 mM NH_4^+ and above. The regulation of growth and *nif* gene expression in *R. rubrum* is therefore controlled at this critical region of the curve, below 20 mM NH_4^+, where minute increments in the [NH_4^+] can lead to very large physiological differences.

However, there does not seem to be just two well defined physiological states of NH_4^+ sufficiency and NH_4^+ deficiency. This is revealed by the A_{882}/A_{660} values of the 14 mM NH_4^+ culture in experiment 1(d). The decrease in the amount of ICM/ cell after 60 h shows how complex the effects of NH_4^+ are to growth and ICM yield. Experiment 1(b) also shows a clear systematic increase in the A_{882}/A_{660} ratios from the 20 to 40 to 80 mM NH_4^+ cultures. ICM content per cell in the 0 - 4 mM cultures remained more or less at a constant level throughout growth and below 4 mM NH_4^+, the growth kinetics indicate that the cells do not conform to the growth phenotype usually observed with M2SF medium i.e. they suffer from low expression of photosynthetic membranes (low A_{882}/A_{660} ratio) and concentrations below 4 mM NH_4^+ are not useful for obtaining real growth curves, though they are quite useful for assessing *nif* gene expression.

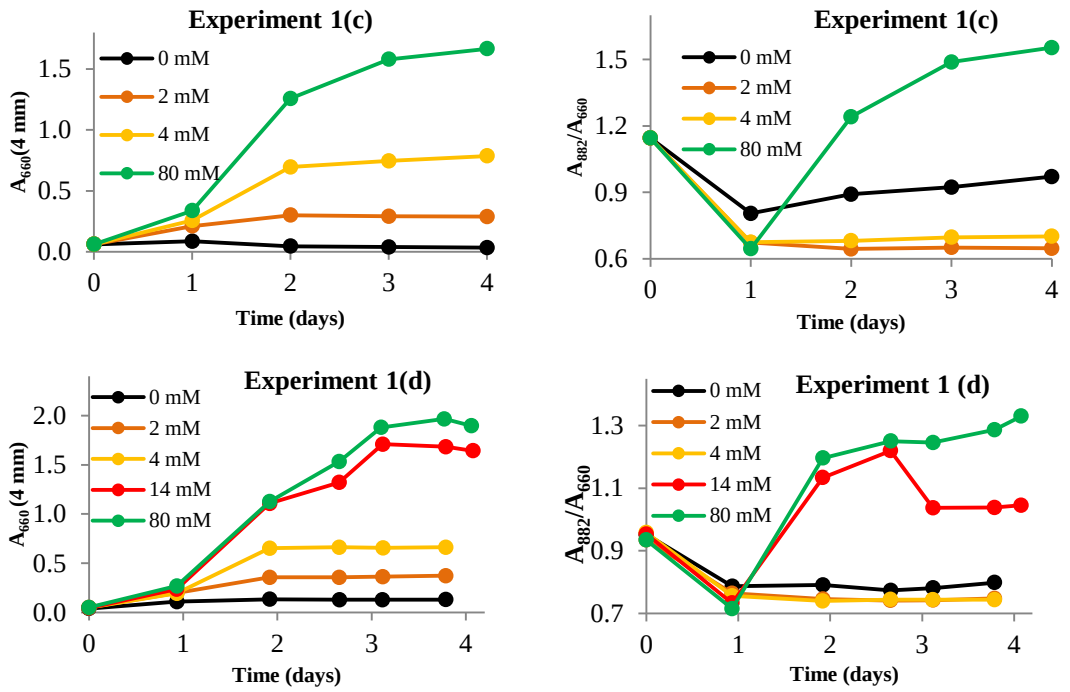

Fig. 3.6. Final set of growth curves and ICM/cells (A_{882}/A_{660}). Experiment **1(c)** and **1(d)** in semi-aerobic M2NF medium for the strain pRKTmChRR1/S1 at varying conc. of NH_4^+ (no Glu). The only difference between the two experiments is that the inoculum used in experiment (1c) was from a 4 mM M2NF culture (no Glu), while in 1(d), cells from 80 mM M2S washed in saline (0.9 % NaCl) were used as inoculum.

Some form of inhibition or negative cooperation between NH_4^+ might explain this effect as well. Indeed, the points of final OD obtained at various [NH_4^+]s could not be fit well with a standard Michaelis-Menten curve, but rather with a sigmoidal curve (simulation not shown). Hence a cooperative effect of NH_4^+ utilization in *R. rubrum* cannot be ruled out.

3.5. The response of *R. rubrum* to NH_4^+ concentration in anaerobic conditions

3.5.1. The use of *R. rubrum* strain S1 for establishing the anaerobic response to NH_4^+

The S1 strain shows close physiological similarities with strain pRKTmChRR1/S1 as discussed in section 3.3 because the low copy number vector, pRK290, has near-physiological levels of *nif* gene expression under N-limitation. The pRKTmChRR1/S1 strain provides the possibility of measuring the levels of fluorescence corresponding to the extent of *nif* gene expression. Since the measurement of growth parameters at 660 nm and 882 nm are sufficient for our purposes, we chose to use the S1 strain for the anaerobic experiments instead. Additionally, we use the presence or absence of evolved H_2 as an indicator of N_2 fixation.

3.5.2. Constant headspace volumes and ratios of NH_4^+-succinate to succinate-TEA across experimental replicates are critical experimental considerations for performing the anaerobic growth curve of S1

The anaerobic NH_4^+ titration series with S1 featured the use of only NH_4^+-succinate as the fixed N_2 source, no Glu was used in any of the experiments and cells were always washed in 0.9 % NaCl prior to inoculation. Special care was taken to measure the volumes of each individual anaerobic culture bottle, which varied by as much as 10 ml from one another. According to the bottle volume and desired [NH_4^+], the volumes of the NH_4^+-sucinate and TEA-succinate were calculated, such that each culture bottle finally had an equal amount of headspace (4 ml) available (equal N_2 amounts for N_2-fixation) to it.

3.5.3. The anaerobic titration curve (like the semi-aerobic curve) shows cooperative effect of [NH_4^+] on growth with H_2 production at 4 mM NH_4^+ and below

The anaerobic growth curves were performed at least once as duplicates measurements and confirmed as a single set during subsequent experiments (Fig. 3.7). Data from these experiments show good overlap between replicates, confirming the importance of calculating the volume of medium components for each culture.

H_2 production was visibly noticeable in cultures containing 0, 2, and 4 mM NH_4^+ as a swelling of the rubber caps of bottles (confirmed by gas chromatography), within a few days of incubation in the light. This indicates the activation of the N_2 fixation pathway. The maximum H_2 was measured at day 6 and 7 after transfer to light and decreased thereafter. The 0 mM, 2 mM and 4 mM NH_4^+ cultures evolved a maximum of around 1 ± 0.2 mM H_2 (for ~155 ml culture volumes), however lower levels were also achieved in different experimental sets. H_2 production was however not observed for all of the replicates of the 0 mM NH_4^+ cultures, or very low levels of H_2 were seen.

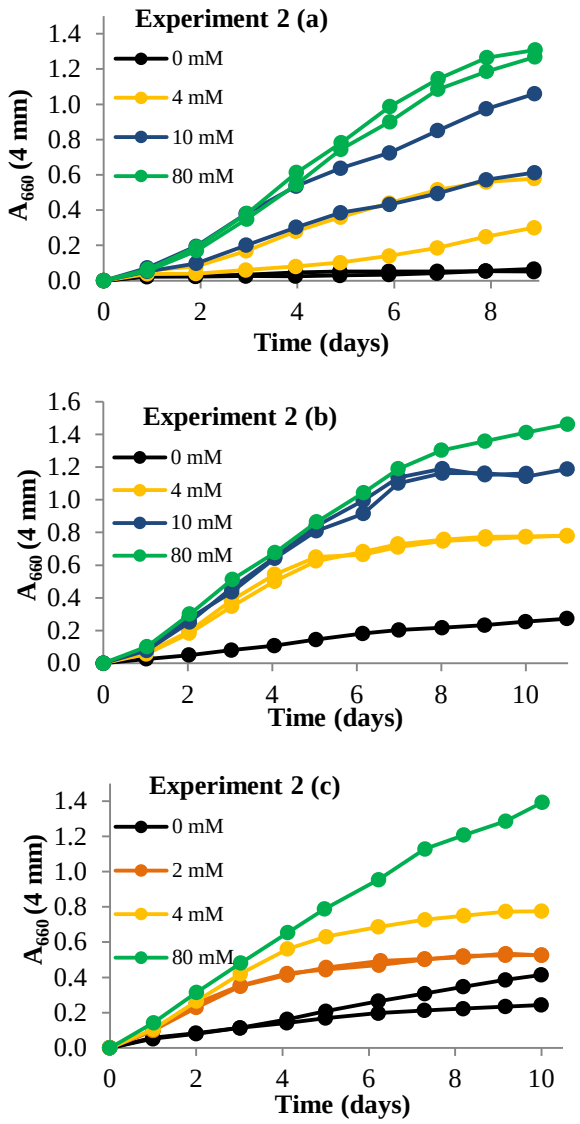

Fig. 3.7. The effect of the [NH_4^+] (concentrations indicated in figure) upon the growth of *R. rubrum*.

2(a): The first set of anaerobic growth curves shows the discrepancy in the replicates of the 4 and 10 mM NH_4^+ curve which probably arise from filling errors of anaerobic bottles.

2(b) and **2(c)**: Duplicates show identical turbidity, when filling errors are eliminated. The mismatch between the duplicate 0 mM NH_4^+ curves in experiment 2(c) results possibly from the differences in the N_2 fixation rates between the two experiments.

The differences in the turbidities reached by the 0 mM NH_4^+ culture across experiments may be attributed to the fixation of the molecular N_2 available, with the extent of *nif* gene activation possibly creating differences between the different final turbidities reached. H_2 production was not observed in 10 mM NH_4^+ cultures or above.

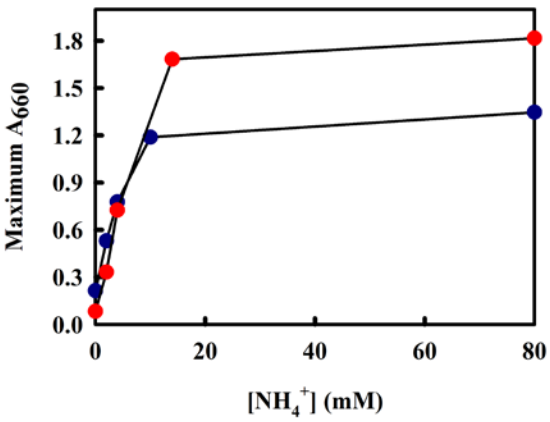

Fig. 3.8. The anaerobic (blue) NH_4^+ dependence curve of S1 in M2NF (no fructose) medium and semi- aerobic (red) NH_4^+ dependence curve of pRKTmChRR1/S1 in M2NF medium respectively. The maximum turbidities of cultures are plotted against their respective [NH_4^+].

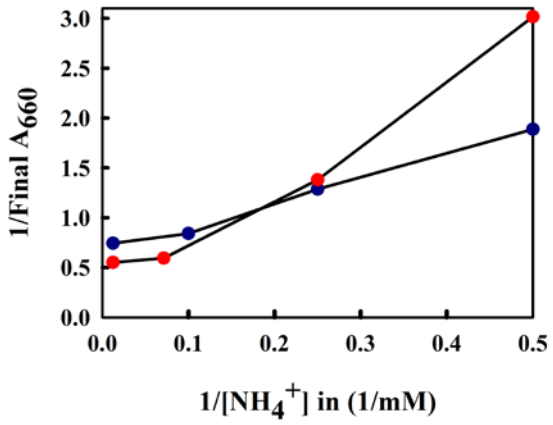

Fig. 3.9. The Lineweaver-Burke plots of the NH_4^+ utilization curves, anaerobic (blue) and semi- aerobic (red) clearly show non-Michaelis-Menten behaviour.

The final anaerobic NH_4^+ utilization curve obtained was quite similar in profile to the semi-aerobic curve, with a steep rise in maximum turbidities at lower [NH_4^+] ranges followed by a flattening of the curve around 10 mM NH_4^+. Beyond that, large increases in concentration have negligible effects on the final turbidity. Higher maximum turbidities were obtained with dark semi-aerobic growth in M2NF medium (A_{660} (4 mm) = 1.8) than with anaerobic growth in M2NF (without fructose) in the light (A_{660} (4 mm) = 1.35). Thus, the "M2SF effect" is clearly preserved at high [NH_4^+] in the modified M2NF.

It was established previously (Fig. 3.5. experiment 1(a) and 1(b)) that at the higher range of [NH_4^+] (20 mM, 40 mM and 80 mM), the cultures reached similar final OD values, but that the growth kinetics at lower [NH_4^+] showed limited reproducibility. Therefore in subsequent experiments, lower ranges were examined more carefully. Only one saturating [NH_4^+] culture (80 mM) was employed as a control in each subsequent experiment.

4. DISCUSSION

We were unable to find literature which systematically studied the concentration dependence of the [NH_4^+] upon the growth of *R. rubrum*. Kanemoto and Ludden (1987) used 20 mM NH_4^+ in medium, to obtain *nif* repressed cultures of *R. rubrum*. Our experiments have shown that concentrations as low as 10 mM NH_4^+ are sufficient to allow high cell densities to be achieved. Cultures of *R. rubrum*, under NH_4^+ limitation, and with N_2 and glutamate as N-sources, respectively, were all found to fix N_2. Munson and Burris (1969), reported that *R. rubrum* grew faster with limited NH_4^+, with a generation time of 5.1 h, than cultures fixing N_2 as the only N-source (generation time of 8.3 h), while cells with only L-Glu as N-source had a generation time of 13.3 h. However, cells grown on L-Glu could fix N_2 at rates slightly higher than that of cells grown with N_2 as a N-source. Overall, NH_4^+ -limited cultures were a better source in terms of cell mass with their rapid growth and higher output, in contrast to L-Glu-or N-limited cultures.

This demonstrates the need for a systematic study of the concentration dependence of NH_4^+ and also various amino acids as N-sources for optimum *nif* gene expression. Ideally, achieving a high culture density would be a goal, as this is important for attaining high levels of recombinant protein expression under control of the *nif* promoter. Preliminary results based on spectrofluorometric measurements of mCherry expression by the pRKTmChRR1/S1 strain obtained by a cooperation partner (Prof. H. Grammel, (HBC) unpublished data) have already indicated that the regulation of *nif* genes of *R. rubrum* by the use of different amino acids is not identical to that reported for *Rb. capsulatus* by Pollock *et al.* (1988) (see Fig. 1.2).

Growth of *R. rubrum* depends upon NH_4^+ transport into cells, and assimilation via the glutamine synthetase-GOGAT reaction. The GS enzyme in *R. rubrum* is composed of 12 equivalent subunits with a molecular mass of 660 kDa (Caballero *et al.*, 1985). Kinetic studies on the GS of *E. coli*, suggests negative cooperative binding of substrate NH_4^+ to GS (Meek and Villafranca, 1980). Negative co-operativity of binding was first predicted from the allosteric model of Koshland *et al.* (1966) and established experimentally for the glyceraldehyde-3-phosphate dehydrogenase present in rabbit muscle (Conway & Koshland, 1968; Meunier and Dalziel, 1978). The flux catalyzed by such enzymes will be insensitive to large changes in the fractional saturation of substrate, but will respond quickly to rapid local fluctuations (Ghosh, 1981). Similarly, in *R. rubrum*, negative cooperativity of NH_4^+ binding, would allow the enzyme to be insensitive to large fluctuations in [NH_4^+] especially at higher substrate concentrations, while maintaining an efficient response at the lower range of [NH_4^+]. This implies that, at higher [NH_4^+] only a small fraction of the NH_4^+ is processed further through the GOGAT reaction, preventing the attainment of high cell densities. This is

precisely what we observed in our studies of the NH_4^+-dependence of growth kinetics. Though the uptake may be insensitive to NH_4^+ fluxes at higher concentration ranges, the cooperative nature of GS may confer a high sensitivity at low [NH_4^+]s.

The NH_4^+ utilization profiles and the H_2 evolution data (measured for anaerobic cultures only) suggests that the window for regulating *nif* gene expression lies between 0 and 10 mM NH_4^+ and that there is a trade-off between high cell densities and high levels of *nif* gene expression, with the goals of the application deciding the optimum concentration to be used. We have been able to characterize the growth of *R. rubrum* in the new modified medium M2NF at different levels of fixed N_2 and provide a foundation for characterizing the growth kinetics using other amino acids as N-source.

The use of the M2NF medium, gives us the advantage of attaining dark N_2-fixation in *R. rubrum*. The potential ability to regulate expression of the N_2ase enzyme makes this medium highly suitable for applications of bio-H_2 production resulting from both the N_2ase and additional hydrogenase pathways in *R. rubrum*. Thus, the need to fine-tune the fixed N_2 levels for achieving optimum cell densities and *nif* expression has significance for the development of novel recombinant protein expression systems under control of the *nif* promoter and for attainment of high levels of H_2 production.

Part III

A modified Kulka micromethod for the rapid and safe analysis of fructose and 1-deoxy-D-xylulose-5-phosphate

(This work has been published in 2018 in "Metabolites", vol. 8, p77-92, and is reproduced here in the form of the final submitted manuscript)

by

Shreya Shaw [1] and Robin Ghosh [1,*]

[1] Department of Bioenergetics, Institute of Biomaterials and Biomolecular Systems, University of Stuttgart, Pfaffenwaldring 57, D-70569 Stuttgart, Germany; robin.ghosh@bio.uni-stuttgart.de; st154798@stud.uni-stuttgart.de

***** Correspondence: robin.ghosh@bio.uni-stuttgart.de; Tel.: +49-711-685-65040

Abstract: The Kulka resorcinol assay (Kulka, R.G., *Biochemistry* 1956, *63*, 542-548.) for ketoses has been widely used in the literature but suffers from two major disadvantages: (a) it employs large amounts of potentially harmful reagents for a general biology laboratory environment; and (b) in its original formulation, is unsuited for modern high throughput applications. Here, we have developed a modified Kulka assay, which contains a safer formulation, employing approx. 5.4 M HCl in 250 µl aliquots, and is suitable for use in high-throughput systems biology or enzymatic applications. The modified assay has been tested extensively for the measurement of two ketoses; fructose (a common substrate in cell growth experiments) and 1-deoxy-D-xylulose-5-phosphate (DXP), the product of the DXP-synthase reaction, which until now has only been assayable using time-consuming HPLC methods or radioactivity. The Kulka microassay has a sensitivity of 0-250 nmol fructose or 0-500 nmol DXP. The assay is suitable for monitoring the consumption of fructose in bacterial growth experiments but is too insensitive to be used directly for the measurement of DXP in *in vitro* enzyme assays. However, we show that after concentration of the DXP-enzyme mix by butanol extraction, the Kulka resorcinol method can be used for enzyme assays.

Keywords: Fructose assay, 1-deoxy-D-xylulose-5-phosphate, resorcinol reagent, micro-method, systems biology, enzyme assay**.**

1. Introduction

The determination of sugars in biological assays is a common task in many areas of biochemistry, fermentation, and more recently, systems biology. The most sophisticated methods for sugar determination usually involve high-performance liquid chromatography (HPLC) techniques [1-6], which allow both sugar identification as well as their precise quantitation. However, HPLC techniques are inherently slow, and also usually require deproteinization of biological samples prior to analysis. An alternative is gas-liquid chromatography [3,4,7], which though precise, requires derivatization procedures, as well as requiring long run times, and is thus cumbersome for a large number of samples.

For studies requiring the rapid analysis of large numbers of sample, e.g. in areas of enzyme kinetics, fermentation or systems biology, colorimetric methods involving usually absorbance or fluorescence measurements, are still of great utility due to their potential for high-throughput as well as being suitable for automated techniques. Many methods for the colorimetric measurements of furanoses and pyranoses exist, some of which involve either direct measurement of extracted samples [8-15], whereas others require prior rapid purification by thin-layer chromatography [16-19]. However, many of these methods are today, in view of laboratory safety regulations, only of historical importance, as they usually involve large quantities of acids or reagents with significant potential as carcinogens. Nevertheless, we show here that, at least for the rapid determination of furanoses, in particular, here, D-fructose, D-xylulose, and 1-deoxy-D-xylulose-5-phosphate (DXP), the historically important Kulka method [10] can be modified as a micromethod, suitable for the determination of nanomolar amounts of fructose or DXP. The method can be adapted for rapid handling of samples using modern techniques, and also provides a much higher level of biological and laboratory safety than the original method. Nevertheless, the modified Kulka method retains its well-known reliability for furanose determination.

The Kulka method [10], an adaptation of the resorcinol method described by Bacon and Bell [11], involves the ferric ammonium sulphate-mediated oxidation of furanose in concentrated HCl acid to form the furfural product from furanose, followed by reaction with the dye resorcinol to form a coloured product, which can then be quantitated by absorption spectroscopy. The basic reaction scheme is shown in Figure 1.

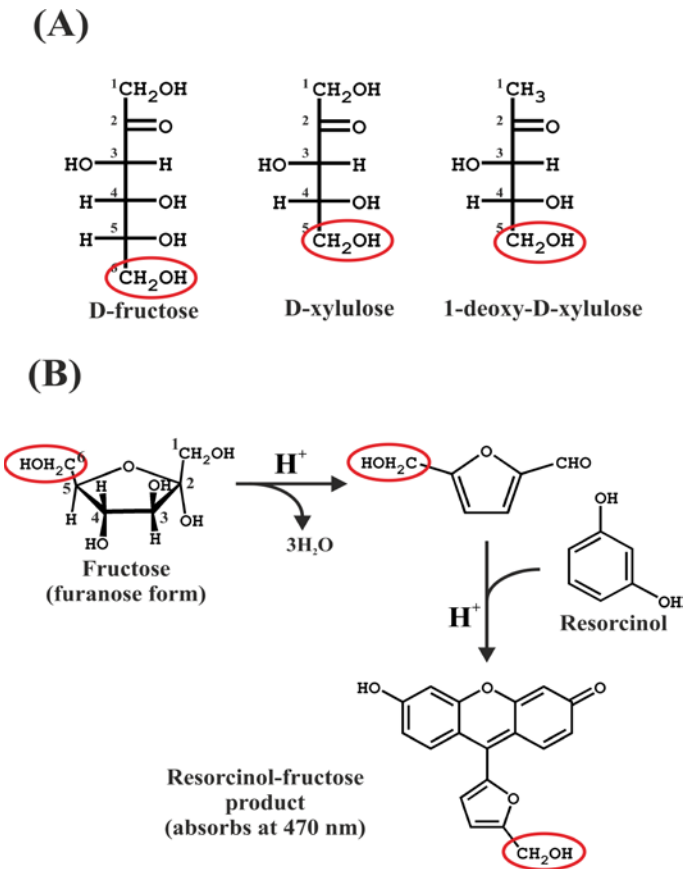

Fig. 1. (A) Fisher projections of the sugars used in this study. The hydroxymethyl groups remaining after furfural formation are indicated by red ellipses. **(B)** Reaction scheme showing the formation of the furfural intermediate which then reacts with resorcinol in the presence of hot concentrated acid.

In the original Kulka procedure [10] the acid step was performed using concentrated HCl (approximately 11.8 M) which must be heated for 30 min. at 80°C in order to form the furfural product. The high HCl concentration not only prohibits the use of normal automatic pipettes but poses a considerable danger to the experimentalist as well as the laboratory environment in case of an accident.

In our study, we show that levels of acid as low as 5.38 M HCl (which can be handled with a normal automatic pipette) are still sufficient to allow efficient furfural formation from furanose, and that once formed, the product can be diluted with water to yield a final acid concentration of about 1.2 M, which presents only minimal risk to the user and laboratory environment. Nevertheless, the new modified Kulka assay is able to reliably determine fructose and DXP in the micromolar range. The final protocol is described in detail in the Materials and Methods section.

2. Results

2.1. General considerations

Although, in the original Kulka method, the whole procedure was carried out in concentrated HCl [10], we show below that the initial formation of furfural is also efficiently performed in the presence of approximately 6 M HCl (the final [HCl] in the assay is 5.38 M), here used in a final volume of only 225-245 µl volumes. As mentioned above, this lower concentration of acid can also be pipetted with automatic pipettes commonly found in most laboratories. In addition, since 6 M HCl is a constant boiling mixture, the Fe(III)-HCl reagent (solution A) is quite stable at room temperature in a closed bottle. We reasoned that, once formed, the furfural-resorcinol product should be stable in water, allowing us to dilute the reaction mixture further to yield a final acid concentration of about 1.2 M, which can be safely handled in the laboratory. However, as we show below, this last dilution leads to some precipitation of non-reacted furfural product, necessitating a centrifugation step prior to measurement, as well an absorption measurement at two wavelengths to ensure calibration reliability. These latter steps contribute only minimally to the total procedural time.

2.2. Spectral analysis of the fructose- and DXP-resorcinol reaction mixtures

In the original work, Kulka [10] showed that the fructose-furfural product reacted with resorcinol to produce a final product exhibiting two characteristic absorption maxima, which were assigned to 415 nm and 480 nm, respectively. When we re-measured the absorption spectrum of the fructose-resorcinol product (here using a modern scanning spectrophotometer) we confirmed the general form of the spectrum, but in 1.2 M HCl, three absorption maxima at 470 nm, 417 nm, and 333 nm, respectively, were observed (Figure 2A).

The absorption spectrum of the fructose-resorcinol product is complex (Figure 2A), containing so far undocumented very weak absorption bands at about 700 nm and 820 nm, respectively. We noted that for higher amounts of fructose (at about 50 nmol fructose) the turbidity of the product rose significantly in the 1.2 M HCl measuring solution, even though the reaction product absorption at 470 nm still increased with the amount of fructose assayed. This problem was eliminated by a 5 min. centrifugation step prior to measurement (see Figure 2A). To eliminate the very small baseline contribution at 700 nm, the absorption difference (A_{470}-A_{700}) proved to be reliable for estimating the concentration dependence.

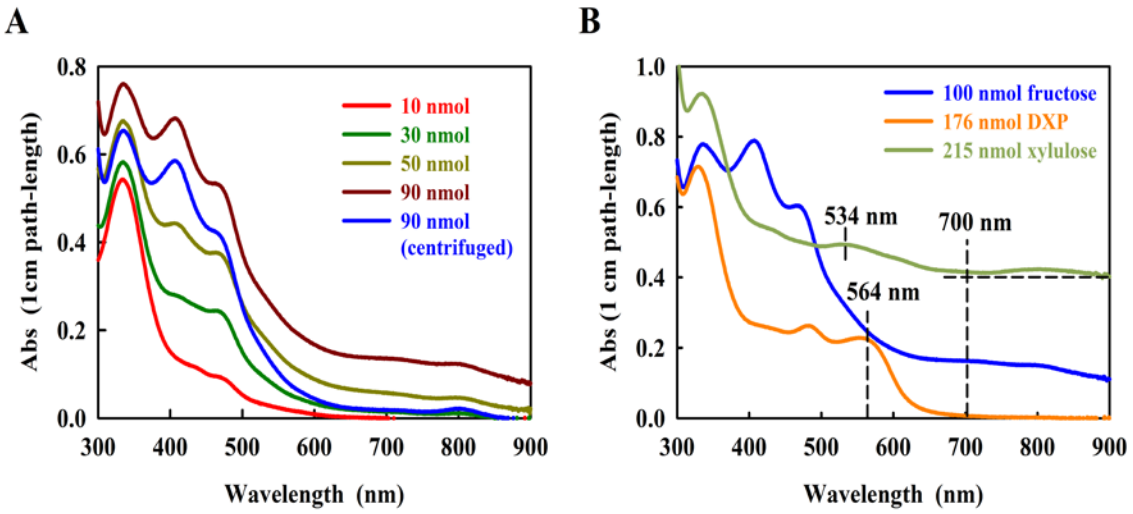

Fig. 2. Absorption spectra of the resorcinol adducts with **(A)** D-fructose; and **(B)** D-xylulose and DXP. Concentrations of sugar are indicated. The relevant measurement wavelengths are indicated by dashed vertical lines. The horizontal dashed line shows the baseline value used to calculate the D-xylulose baseline-corrected spectra.

We have not performed an exhaustive analysis of furanoses, as many of these were reported in the original Kulka [10] publication.

However, in a second step of the work, we chose to focus on the possible use of resorcinol to assay DXP, which to our knowledge has never been reported. Kulka [10] reported that the related furanose, D-xylulose, is still able to react with resorcinol, yielding a green product showing about one tenth of the absorption observed with fructose. The xylulose-furfural derivative still contains a single aldehyde group, derived from the C-1-hydroxymethyl moiety (Figure 1A), and is thus able to form a limited resorcinol product, although the final structure has not been reported. In DXP, the C-1-hydroxymethyl group is absent, which would seem to preclude a reaction with resorcinol. In initial trials, we found that, surprisingly, DXP reacts well with resorcinol, forming a red product with a characteristic absorption at 564 nm (Figure 2B). The absorption intensity of the DXP-resorcinol product is about 5-fold higher than that of the baseline-corrected D-xylulose product at its corresponding characteristic absorption maximum (534 nm, Figure 2B). Although we have not determined the structure of the DXP-resorcinol product, we assume that the acid step is sufficient to remove the phosphate group by hydrolysis, thus allowing the resulting C-4 hydroxymethyl group to become available to react with the C-2 carbonyl, allowing furfural formation. However, the subsequent reaction with resorcinol must be unusual, since the reactive C-1

hydroxymethyl group has now been replaced with an unreactive methyl moiety. Nevertheless, the absorption of the DXP-resorcinol product at 564 nm is distinct, and as an added bonus, shows almost negligible turbidity in 1.2 M HCl.

2.3. Calibration guidelines for fructose and DXP using the modified Kulka method

2.3.1. Calibration with fructose.

In the original Kulka method [10] a calibration curve of 0 - 100 µg/ml sample (fructose) solution was shown. The highest value corresponded to a fructose concentration of 555 µM. In this measurement range, the absorption maximum at 480 nm (the measuring wavelength used by Kulka [10]) appeared to vary almost linearly with the fructose concentration. Our own measurements, using our modified Kulka procedure, shows that the attainable dynamic range is much higher than that originally reported in the original publication. As the data in Figure 3 shows, the modified Kulka method can reliably measure concentrations of 0 - 250 nmol fructose, present in the 20 µl aqueous sample (corresponding to 12.5 mM fructose) added to the resorcinol-HCl reagent.

The assay can tolerate up to 20 µl sample without detrimentally diluting the acid. This range corresponds to the concentrations 0-12.5 mM or 0-2250 µg/ml fructose, respectively. The non-linearity of the large dynamic range (Figure 3A) can be easily addressed by separating the curves into “low” (0-50 nmol fructose (Figure 3B)) and “high” (50-250 nmol fructose (Figure 3C)) measurement regions, respectively. In both cases, the curves can be well fitted by (different) second-order polynomials, of the form $y = y_0 + ax + bx^2$, where x and y are the concentration of fructose and the difference absorption value (A_{470}-A_{700}), respectively, and y_0, a, and b are constants to be determined by curve-fitting procedures (see Figure 3, legend) In the absence of access to curve-fitting software, the concentration dependence of the lower range is almost linear (indicated by the low sum of squares $\Sigma(y_{expt}-y_{calc})^2 = 0.172$) and the values thus obtained by linear regression show only a small deviation from those obtained after polynomial fitting (Figure 3B, residual panel). Although the residual value is a commonly used direction vector for regression algorithms, and is a sufficient fitting criterion for precise measurements, more extensive tests of linearity can be found in the review of Araujo [20].

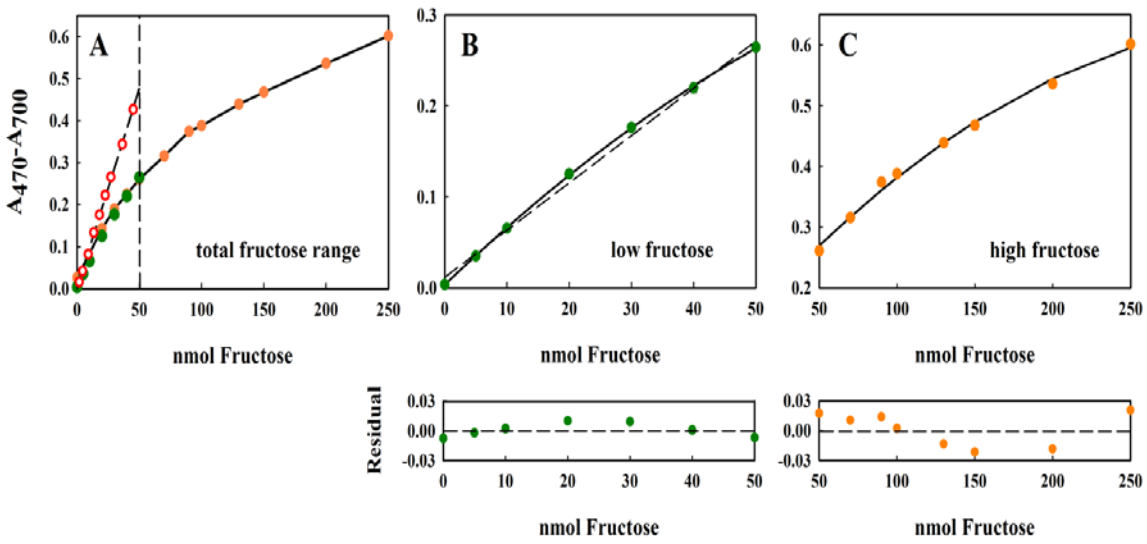

Fig. 3. Standard curve of fructose showing good overlap between the absorption values measured with the 2.5 mM and 10 mM stock solutions. All measurements were performed in triplicate, and the average value is indicated. The error of the measurement is usually about 2% (data not shown). The separated ranges (indicated by the dashed line in panel **(A)**)0 - 50 nmol fructose and 50 - 250 nmol fructose, have been extracted from (A) and plotted separately in panels **(B)** and **(C)**, respectively. For the data in both panels (B) and (C), the solid lines correspond to a polynomial regression to the equation $y = y_o + ax + bx^2$, whereas the dashed line shown in panel B corresponds to a linear regression to the equation: $y = y_o + ax$. For the 0-50 nmol fructose data set, the polynomial constants were: $y_o = 0.0033 \pm 0.0013$; $a = 0.0066 \pm 0.0001$; b = -2.728E-05±2.67E-006. For the linear fit to the same data, the fitted constants were: $y_o = 0.0114 \pm 0.0047$; $a = 0.0052 \pm 0.0002$. For the 50-250 nmol fructose data set, the polynomial constants were: $y_o = 0.0629 \pm 0.136$; $a = 0.004 \pm 0.0004$; and b = -7.71E-0.006±2.73E-008. The quality of the fit has been shown by the residual plot (lower panels under (B) and (C)), defined as $\{(A_{470}\text{-}A_{700})_{exptl} - (A_{470}\text{-}A_{700})_{calc}\}$, where $(A_{470}\text{-}A_{700})_{calc}$ has been calculated from the fitted equation. For the 0-50 nmol fructose range, only the residual derived from the linear fit is shown. In panel A, the original Kulka data [10], recalculated to include the four-fold dilution in our assay, is also shown (red circles, dashed line).

We also examined the stability of the final reaction product. We found, after incubation of the centrifuged and diluted reaction product for a series of time points (data not shown), that the reaction stays completely stable for at least 2 h after reaction, provided that the final cocktail is not mixed. Regular agitation of the final reaction cocktail leads to significant loss of A_{470} product, presumably due to an oxidative side-reaction. However, in the absence of mixing, the A_{470} product decreases by only about 10% after 6 h at room temperature. We emphasize, however, that performance of the reaction as described in the Methods section is extremely reliable and reproducible.

Comparison of the results obtained here for the modified method with those originally reported by Kulka [10] (Figure 4A, red circles, dashed line) show that the original Kulka method is more sensitive at lower concentrations of fructose (note that the A_{480} values reported by Kulka [10] have been reduced 4.08-fold to take the different dilutions employed by the two methods into account). However, our modified method shows a higher dynamic range, thus making high fructose concentrations accessible to the assay. The reason for the discrepancy between the two procedures may be due to the different reaction conditions used.

2.3.2. Effects of interfering substances upon the modified Kulka assay

Biochemical reaction cocktails usually employed in enzyme assays contain a variety of substances which may interfere with the modified Kulka assay. We have analyzed the effects of several commonly used buffers and salts at concentrations typical for their use in enzyme assays, and the results are shown in Table 1.

The effect of interference was quantified by measuring a single, low concentration of fructose (20 nmol) in the presence of the interfering reagent. In the event, commonly used buffers such as TrisHCl, Na-phosphate, HEPES, and MOPS, as well as NaCl, each sampled (20 µl sample) from a 100 mM stock solution, had either negligible or only very minor effects upon the assay. No effect of $MgCl_2$ (taken from a 10 mM stock solution) was also observed.

The effects of proteins on the assay were more complicated. We observed that large concentrations (mg amounts) of the model proteins bovine serum albumin (BSA) and lysozyme in the solutions to be assayed have a significant effect upon the modified Kulka assay (increasing the A_{470} - A_{700}) by up to 165% (for a protein sample concentration of 5 mg/ml) of the control measured in the absence of protein). However, lower protein concentrations (100 µg/ml), typical for the stabilization of enzymes, had only a small (increase to 120%) effect upon the assay (see Table 1).

Compound	Stock soln.[a]	µmol in assay[b]	% of control	Increase /Decrease
TrisHCl	100 mM	2	104	+
Na-Phosphate	100 mM	2	109	+
NaCl	100 mM	2	105	+
$MgCl_2$	10 mM	0.2	105	+
HEPES	100 mM	2	107	+
MOPS	100 mM	2	104	+
TCA	72%	3.4 - 5% (w/v)	96-107	-
BSA	100 µg/ml	2 µg	120[c]	+
BSA/TCA	100 µg/ml	2 µg	99	-
Glucose	2.5 mM	20 nmol	103	+
Glucose only	2.5 mM	20 nmol	15	-
Glucose	111 mM	2.2 µmol	195	+
Glucose only	111 mM	2.2 µmol	142	+

Table 1. The effect of commonly used buffers and salts upon the modified Kulka assay.

[a] The solution to be measured. Routinely, 20 µl of this solution is added to the resorcinol assay mix.

[b] Unless otherwise stated, all assays contained 20 nmol fructose. No fructose was present in the assays indicated as 'Glucose only'.

[c] Average value obtained with a BSA concentration of 100 µg/ ml.

It is known that both BSA (which contains 17 disulphide bridges) and lysozyme retain significant tertiary structure upon acid denaturation [21], which still allows binding of aromatic substances (such as resorcinol and its adducts) to exposed hydrophobic pockets, so the effects at the higher concentrations are to be expected. At the lower concentrations, the molar ratio of BSA/resorcinol (1/152 (mol/mol)) is too low to be significant. Nevertheless, proteins are often present in biochemical assays at higher concentrations, which might limit

the applicability of the modified assay. However, when we performed an initial deproteinization of the protein-containing sample by preincubating with 3.4 % (w/v) trichloroacetic acid (TCA) followed by a 20 min. centrifugation step to remove the protein pellet (see Materials and Method for details), the values obtained for 20 nmol fructose were very close to those obtained in the absence of both protein and TCA. In control assays we could demonstrate that within the range 3.4 - 5 % TCA (which is sufficient for deproteinization), furfural development was only weakly dependent upon the the amount of TCA added (Table 1). We were also able to demonstrate that the form of the fructose calibration curve is unchanged compared to the data shown in Figure 3A. However, routinely, the fructose calibration curve should be performed including the TCA precipitation step to be used in the experiment.

Finally, we have examined the effects of glucose upon the fructose concentrations obtained with the modified assay. At equimolar concentrations of fructose and glucose (20 nmol, respectively), the absorption values A_{470}-A_{700} were increased by only about 1-3% (Table 1) which is consistent with data originally reported by Kulka [10]. However, when the molar ratio of glucose/fructose was set to 110, the A_{470}-A_{700} values were increased by about 90%. A control assay containing high [glucose] alone also showed a high A_{470}-A_{700} value (see Table 1). We have not examined these effects systematically, since our results indicate that fructose measurements in the presence of about 100-fold higher concentrations of glucose will be unreliable, and should be determined by another method. Nevertheless, in situations where the glucose and fructose concentrations are comparable (for example, in a sugar isomerase reaction) the Kulka method will be reliable.

Finally, we could show that the phosphorylated forms of fructose, fructose-6-phosphate (F6P) and fructose-1,6-diphosphate (F1,6diP), could also be determined with the modified Kulka assay, although both sugar phosphates yielded lower A_{470}-A_{700} values (F6P, 74 % of the control (fructose); F1,6diP; 87.5 % of the control) compared to those of non-phosphorylated fructose when incubated for 40 min. at 80°C. However, extension of the 80°C reaction step to 120 min. increased the value for F1,6diP to that of the control, and also increased the value for F6P. The latter value was about 81 % of the control measured after 40 min.

2.3.3. Application of the modified Kulka assay to determine the consumption of fructose in a bacterial growth experiment.

To demonstrate a typical application of the modified Kulka method developed here, we measured the consumption of fructose in a bacterial growth experiment. We have shown previously [22,23] that the purple bacterium *Rhodospirillum rubrum* will grow semi-aerobically in the dark in shake flasks, in the presence of the carbon sources succinate and fructose. In this experiment, succinate rapidly attains a steady-state level, whereas fructose is consumed continuously throughout the major part of the growth experiment. In the final phase of the growth experiment, the fermentation product acetate, produced from fructose metabolism, is then further metabolized by the organism until the end of the growth phase [23].

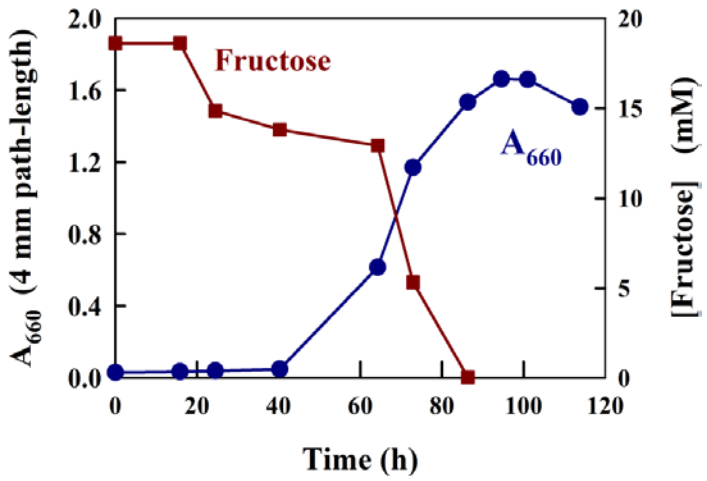

Fig. 4. Growth curve data and fructose measurement for *R. rubrum* growing semi-aerobically on fructose/succinate M2SF medium in a shake flask at 30°C (dark conditions). The cell turbidity (A_{660}) is measured at 660 nm, which contains no contribution from photosynthetic pigments.

A typical growth experiment using the medium, M2SF [22], a modification of Sistrom medium A [24], which contains both 20 mM succinate, and 8 mM ammonium chloride, as C- and N-sources, respectively, as well as a large number of trace elements [24], with the addition of 18 mM fructose as a second carbon source, is shown in Figure 4. Prior to the determination of fructose in this experiment, we tested whether Sistrom medium A reacted with the modified Kulka reagent. In the event, no significant reaction was observed. For the experiment shown in Figure 4, a slightly aged (a stationary phase culture kept at 6°C for two weeks) *R. rubrum* culture was employed as inoculum. As expected, the A_{660} profile indicated that the culture showed an approximately 20 h lag phase, followed by normal growth (the generation time is about 3.5 h for semi-aerobic growth [22]) for about 60 h, finally reaching a

stationary phase with A_{660} (4 mm path-length) values of approximately 1.6. For the determination of fructose in the medium supernatant, we precipitated 1 ml culture samples using 4.6 % (w/v) TCA (see Materials and Methods) and then assayed the fructose present in a 10 or 20 µl aliquot. The determination of fructose consumption with the modified Kulka assay yielded satisfying results, completely consistent with previous experiments where HPLC determination of fructose was employed [23]. Thus, following the initial 20 h lag phase, where no fructose consumption was observed, the early, aerobic growth phase (up to an A_{660} of about 0.5) showed a low rate of fructose consumption. We have shown previously, that under aerobic conditions, succinate is used preferentially before fructose [23]. However, when the cells enter the semi-aerobic growth phase (above an A_{660} of about 0.5), the pathways of anaerobic metabolism are induced, which lead to rapid fructose consumption and exhaustion (at about 82 h). In the final growth phase, the acetate formed by fructose catabolism, induces the ethylmalonyl-CoA pathway [25], allowing acetate to be utilized as a growth substrate [23].

2.3.4. The determination of DXP using the modified Kulka assay

The reaction of DXP with resorcinol was measured at 564 nm. Since the spectral analysis showed no turbidity due to the reaction product, we found it unnecessary to perform a control measurement at 700 nm (see Fig. 2B). The calibration curve A_{564} *vs*. nmol DXP was curved (Figure 5A) and, unlike the fructose calibration curve, could be fitted well by a hyperbolic equation. This naturally leads to the use of an inverse plot for routine calibration purposes (Figure 5B). Absorbance values were stable for up to 1 hour, after which they steadily decreased to 77% of the initial value after 2 hours.

The sensitivity of the modified Kulka assay for DXP is limited to about 2 mM (i.e. 40 nmol DXP/20 µl sample), which is more than sufficient for the determination of DXP in situations where DXP is being overproduced in cells for production purposes.

2.3.5. Application to the assay of DXP synthase (DXS)

To illustrate the problems of DXP determination in a typical DXS assay, we simulated a theoretical progress curve for the consumption of substrate (glyceraldehyde-3-phosphate (G3P)) and the production of product, DXP, using the kinetic constants reported by Eubanks and Poulter [26] for the DXS enzyme from *Rhodobacter capsulatus*, using a typical value of saturating [G3P] (0.5 mM) as a starting point. In this simulation, we assume, for simplicity, that the reaction goes to completion. In reality, an equilibrium [DXP] is reached, significantly below the maximal value shown in Figure 5C. We also assumed that the reaction is performed

in a reaction volume of 200 µl, which could be accommodated into the well of a 96-well plate. Figure 5C indicates that the maximal amount of DXP expected is not more than 10 nmol/20 µl aliquot (the largest volume tolerated in the modified Kulka assay), taken directly from the assay mix which is too low to be estimated reliably by our method (see Figure 5A).

To solve the sensitivity problem we examined two methods for increasing the effective sugar phosphate concentration. First, in a control experiment, we attempted to precipitate the sugar phosphate, fructose-6-phosphate (F6P), with $BaCl_2$, since Ba-phosphate salts are water-insoluble [27, 28]. We found that an [F6P] of 0.2 - 0.5 mM could be precipitated by addition of a 100-fold higher concentration of $BaCl_2$ in the presence of 50% ethanol. However, for higher fructose concentrations, even a 10-fold molar excess of $BaCl_2$ was found to be sufficient for precipitation. We enhanced the efficiency of precipitation by solubilizing F6P in 5 mM Na-phosphate buffer pH 8.0. The buffer not only ensures that the F6P phosphate moiety is ionized, but also acts as a phosphate carrier and, after centrifugation, yields a clearly visibly white precipitate after the addition of $BaCl_2$ to the F6P solution. $BaCl_2$ and 5 mM Na-phosphate were shown to have no effects upon the assay. The Ba^{2+}-F6P precipitate went into solution upon addition of ferric ammonium sulphate-HCl (FAS-HCl) reagent. The resuspended F6P samples yielded A_{564} values that were 90-100% of the control values obtained for 20-50 nmol F6P samples dissolved in H_2O.

The slightly low value for F6P obtained using the Ba^{2+}-precipitation method, may be due to the fact that about 1% of the phosphate moiety is in the singly charged form at pH 8.0, and may precipitate less effectively with Ba^{2+}. Unfortunately, the precipitation of DXP by ethanolic $BaCl_2$ was poor and unreliable, yielding values as low as 60% of the DXP control samples.

Thus, as an alternative, we attempted to concentrate the aqueous phase of large aliquots by repeated extraction with *n*-butanol [29]. In this procedure, the charged DXP should remain in the aqueous phase, thereby increasing its concentration, and hence accessibility in the modified Kulka assay. In the event, we were able to achieve a 4-fold reduction in volume of 100 µl samples, containing 0.05 - 0.5 nmol DXP, by extracting twice with 200 µl *n*-butanol. Smaller volumes of *n*-butanol were used if small reductions in volume were desired. The A_{564} values obtained for the extracted samples were between 85 - 100% of DXP control samples. Routinely, for the determination of an unknown dilute [DXP], a calibration curve obtained from initially dilute, *n*-butanol-extracted samples of known concentration was performed. *n*-butanol alone has no effect upon the modified Kulka assay.

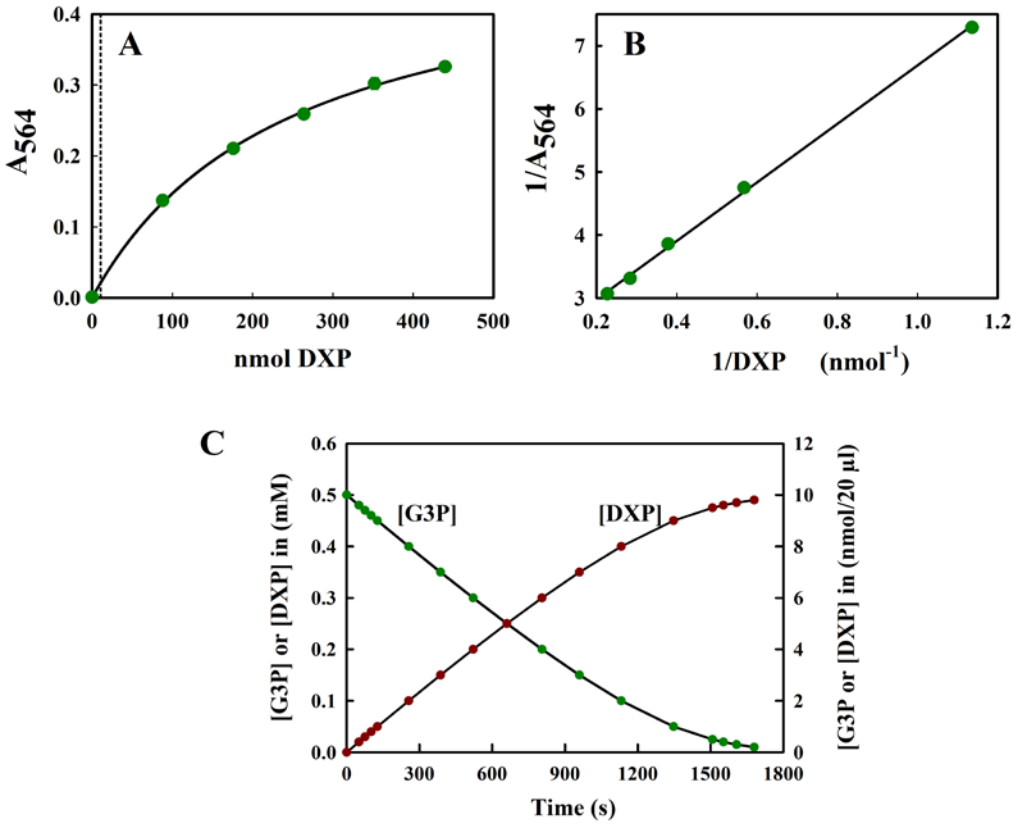

Fig. 5. (A) The standard curve of DXP measured at 564 nm. All measurements were performed in triplicate, and the average value is indicated. The curve could be fitted to the hyperbolic equation y = ax/(b+x), where the fitted constants were: a = 0.507±0.0124 and b = 244.323±12.946. The dotted line indicates the upper limit (10 nmol) of the region relevant for the DXS assay shown in (C); **(B)** the inverse plot of the data shown in (A). **(C)** The theoretical progress curve of the DXS reaction, with pyruvate and G3P as substrates. The pyruvate concentration was assumed to be kept at a saturating level, whilst the G3P concentration steadily decreases as DXP is formed.

2.3.6. Reagent interference in the modified Kulka assay for DXP

Reagents at concentrations commonly used in DXS assays were tested for interference in the modified Kulka estimation of DXP in the DXS assay mix. (1) Dithiothreitol (DTT): 1mM DTT decreased the A_{564} value to 70 - 90% of the control DXP values, with the number rising to 80 to 100% when DTT was used in the presence of 20-fold H_2O_2; (2) thiamine pyrophosphate (TPP): 0.1 mM TPP was not found to interfere with the assay. In the absence of DXP neither reagents contribute to the A_{564}.

2.3.7. Adaptation of the modified Kulka method for a high-throughput format

The modified Kulka method can also be performed in 96-well plates, suitable for high-throughput applications. Since each well can only accommodate a total volume of 200 µl, all

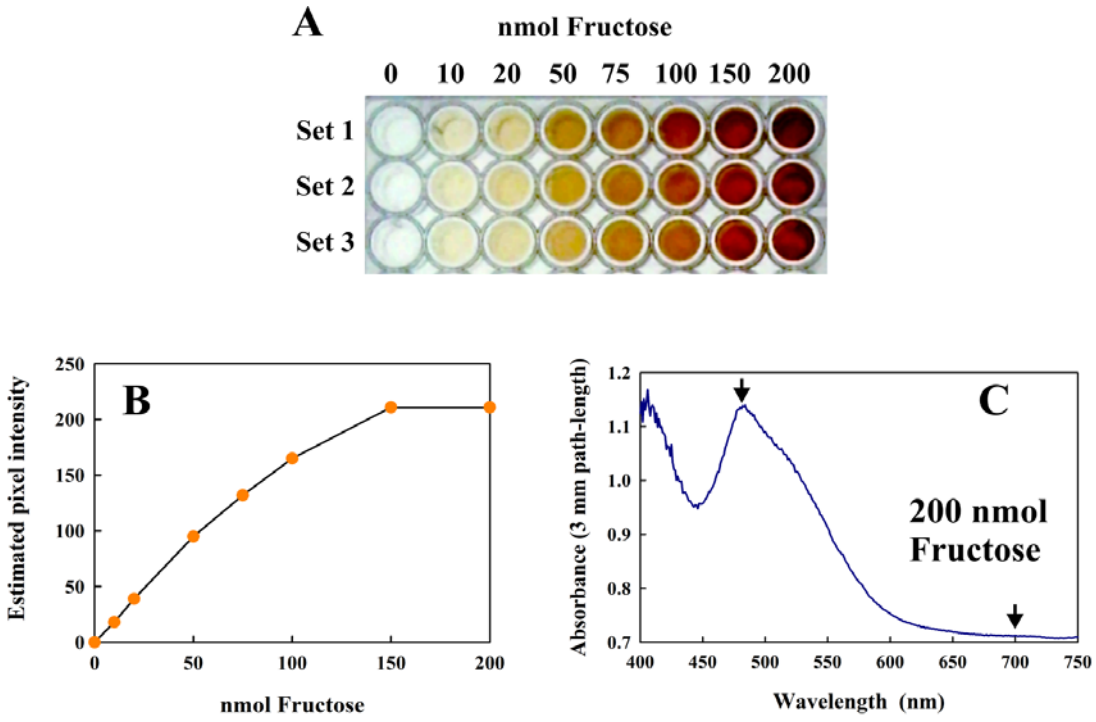

Fig. 6. (A) The modified Kulka assay performed in 96-well plates using increasing amounts of fructose. Three replicates are shown (Sets 1-3) as a 24-bit colour image. **(B)** Plot of the average pixel intensity from the centre of each well in Set 1 of the RGB green channel 8-bit image (obtained from the 24-bit RGB image in (A)) *vs*. the amount of fructose present. **(C)** shows the absorption spectrum obtained from 100 µl of the Set 1 well (centrifuged) reaction mix containing 200 nmol fructose, using a diode array spectrometer. The arrows indicate the measured absorbances.

reagent volumes must be scaled down five-fold (see Materials and Methods for details). Although we have not performed a true high throughput assay in this study, we have successfully performed the reaction in a 96-well plates (Figure 6A) and indicated the results and limitations of different types of analysis (Figure 6B and C).

The calibration curve shown in Figure 6B shows that the assay can successfully be performed in this format, and analyzed by the usual methods of quantitative image processing.

However, at very high concentrations (above 150 nmol fructose), the images are too intense for precise analysis using this method. However, diode-array absorption spectra can be obtained reliably from even the highest values (Figure 6C), and the absorption difference between the visible peak maximum (at about 480 nm in this format) and the “baseline” at 700 nm corresponds well to the data shown in Figure 3 when corrections for the different path-lengths (conventional cuvettes, 1 cm; height of 100 µl sample in a 96-well plate: 3 mm) are made. The only significant limitation of the 96-well format is that the concentration of fructose in the 4 µl sample must be within the detection limits of the assay.

3. Discussion

In this study we have modified the well-known, and very reliable Kulka assay method for the determination of furanoses [10] to use in modern high-throughput applications. Our modified method uses small volumes of reagents which can be handled safely with the usual pipettes and tips found in every biology laboratory. In our study we have only tested two furanoses: fructose, which finds many applications in biological contexts, and DXP, a substrate and product of two enzymes DXS, and DXP reductoisomerase, respectively [30,31], of the methylerythritol phosphate (MEP)-pathway of carotenoid biosynthesis in bacteria. In recent years, both of the latter enzymes have been found to be crucial for the production of precursors in biotechnological applications [32], so that a simple assay for them may often be convenient. DXP is also of interest in that it is a phosphorylated furanose, which has not been reported for use with the Kulka assay so far.

We have shown that the sensitivity and reliability for fructose determination with our modified assay corresponds well with that reported originally [10]. However, commonly observed turbidity effects have prompted us to use a two-wavelength measurement procedure for added reliability. We have also shown, that the phosphorylated fructoses F6P and F1,6diP are also measurable with the method. However, for the diphosphate, an appropriate calibration curve with the pure compound should be performed for additional precision.

We have also demonstrated, that the assay is insensitive to the presence of small amounts of TCA, which is a convenient reagent for rapid deproteinization of samples. Indeed, TCA precipitation and removal of protein prior to resorcinol assay is recommended for biological samples. The assay is also insensitive to many of the salts and buffers commonly used in biological experiments, which has not been reported previously.

The assay proved to be very successful for the determination of DXP, even though the 1´-OH moiety, which is required for cyclic furfural product formation, is absent. However, the useful measurement range is limited for use in DXS assays, and requires a concentration step

prior to measurement. For this purpose, we have found sequential extraction with *n*-butanol to be effective, though this becomes tedious with large numbers of samples. In general, for the DXS assay, the modified Kulka method may be most convenient for a rapid assessment of the presence of enzyme activity. A more precise measurement will usually require a further determination by more advanced (usually HPLC) methods.

For workers wishing to determine other furanoses of interest, our work defines some initial tests that should be performed prior to employing the method. In particular, an absorption spectrum of the resorcinol-furanose adduct should be performed to assess the position of a characteristic absorption maximum, since the appropriate measurement wavelength can vary widely for different furanoses. Also, a displacement of the baseline of the absorption spectrum from that of the control (no reagent) can indicate significant turbidity, which should be treated as shown above (usually employing a two-wavelength measurement).

4. Materials and Methods

4.1. Chemicals

All chemicals were obtained from Sigma-Aldrich (Germany) unless otherwise stated. The purple bacterium, *R. rubrum* S1 (ATCC no. 11170) was obtained from our in-house culture collection, and grown as described previously [22,23].

4.2. The modified Kulka protocol

Since the protocol requires an extended heating step at 80°C, we routinely use 1.5 ml Safe-Lock® tubes (Eppendorf, Germany) for the method. For other 1.5 ml reaction tubes, the stability of the lid at 80°C should be tested for a water-filled tube, and if necessary, every tube should be pierced with a 1.2 x 40 mm needle prior to heating. The latter will cause only very small losses due to evaporation while still ensuring lid stability.

We have reduced the number of reagents to 3 stock solutions: (1) Solution A or FAS-HCl reagent : 6.6 M HCl solution containing 0.9 mM $Fe(III)(NH_4)(SO_4)_2.12\ H_2O$; (2) Solution B: 1% (w/v) resorcinol (Sigma-Aldrich, Germany) dissolved in neat ethanol; (3) solution C: a fructose (or DXP) calibration aqueous solution. For fructose, we have found that fructose calibration solutions of 2.5 mM and 10 mM allow comfortable pipetting schemes for the ranges 0-100 nmol and 100-250 mmol fructose, respectively. Solution A remains stable in a tightly-closed bottle for at least two months at room temperature, the resorcinol solution has an even longer life (up to one year) at 4-6°C, and fructose calibration solutions are stable for at least months as frozen aliquots at -20°C. For the calibration with DXP, a 44 mM and a 2 mM stock solution in water was prepared and stored at -20°C.

The modified Kulka protocol consists of two steps: (a) colour development of the resorcinol-furfural adduct: the appropriate amount (not more than 20 µl volume) of either Solution C or unknown sample is added to 200 µl of solution A in a 1.5 ml SafeLock^{TM} tube, followed by the addition of 25 µl resorcinol reagent (solution B). The closed tube is then vortexed briefly, then incubated at 80°C for 40 min, followed by a 3 min. cooling period in ice. (b) The spectrophotometric step: to the cooled sample (at room temperature) 0.8 ml H_2O is added to stop the reaction, mixed by vortexing and then centrifuged for 5 min. at 13,000 rpm (11,000 x g) at room temperature. Subsequently, supernatant is transferred to a fresh tube and the absorption measured at the wavelengths 470 nm (fructose) or 564 nm (DXP) and also at 700 nm (fructose only) using a 1 cm path-length cuvette. The calibration curve is calculated from the A_{470}-A_{700} vs. [fructose] or the A_{564} vs. [DXP]. Since the DXP reaction product was not turbid, no centrifugation step is required for the DXP measurements and only a single measurement, A_{564}, is sufficient for reliable determinations. For the initial part of the work, involving the assessment of the accuracy of the calibration assay, all measurements were performed in triplicate. Thereafter, for the model experiments described, only duplicate measurements were performed.

4.3. Deproteinization of samples prior to fructose determination.

For samples containing significant amounts of protein, deproteinization of the sample prior to assay with modified Kulka method was performed as follows. TCA from a 72% (w/v) stock solution was added to the appropriate sample to yield a final concentration of 3.4 % (w/v) (for samples containing only low amounts of protein) - 4.6 % (w/v) (for analysis of cell cultures samples). After a 30 min. incubation at room temperature, the sample was centrifuged in a desktop centrifuge for 20 min, at 11,000 x g, then the supernatant (containing the deproteinized fructose solution) was removed to a separate tube and immediately used to perform the assay using a 20 µl aliquot therefrom.

4.4. Absorption spectroscopy

Routinely, absorption spectra (using 1 cm path-length quartz cuvettes (Starna, U.K.) and also single absorption measurements (using plastic 1 cm path-length cuvettes (Roth, Germany)) were performed using a Jasco V-560 spectrophotometer (Jasco Corporation, Japan). However, 4 mm path-length plastic cuvettes were employed for turbidity measurements of *R. rubrum* cell cultures.

For 100 µl reaction volumes in 96-well plates, absorption spectra were obtained in transmission mode using a J&M TIDAS diode array spectrometer (J&M Analytik AG, Germany), using the procedure recommended by the manufacturer.

4.5. Simulation of a progress curve for DXS enzyme reaction

DXS catalyzes the TPP-dependent condensation of pyruvate and G3P to yield DXP. To simulate the progress curve, the integrated rate equation (1) for a single-substrate irreversible reaction [33,34] was used:

$$t = \frac{K_m}{V_{max}} * \left(ln\left(\frac{[S_0]}{[S_o]-[P]}\right)\right) + \frac{[P]}{V_{max}} \qquad (1)$$

where K_m and V_{max} are the kinetic constants of the calculated reaction direction, $[S_o]$ is the initial concentration of one substrate S, and [P] is the calculated concentration of product at a given time t.

Experimentally, this equation may be held valid when one of the substrates (e.g. pyruvate) is held at a saturating concentration, whereas the other substrate (e.g. G3P) is non-saturating. The kinetic constants for DXS as reported by Eubanks and Poulter [26] were used: K_m^{G3P} = 0.068 mM, $K_m^{pyruvate}$ = 0.44 mM, and a V_{max} (at saturating pyruvate concentration) = 0.45 µM/s was assumed throughout the reaction. The curve was calculated for the consumption of an initial $[S_0]$ or [G3P] of 0.5 mM together with concomitant, stoichiometric production of [DXP].

4.6. Procedures for concentration of sugar phosphate samples using $BaCl_2$ or n-butanol

Aqueous samples of F6P (100 µl of 0.2-0.5 mM), dissolved in 5 mM Na-phosphate buffer at pH 8.0, were precipitated with the addition of 10 µl 500 mM $BaCl_2$ solution ($[BaCl_2]$/[F6P] = 100) dissolved in 50 mM TrisHCl and addition of 100 µl of 100 % ethanol. For higher concentrations of F6P, a 10-fold molar excess of $BaCl_2$ can be used for precipitation. The samples were incubated at 4°C for 30 min, centrifuged at room temperature in a benchtop centrifuge at 11,000 x g (13,000 rpm) for 5 min., and then the supernatant was removed. The assay was performed routinely in duplicates by the addition of FAS-HCl reagent, which immediately dissolves the Ba^{2+}-F6P precipitate, and resorcinol added to complete the assay cocktail.

To the aqueous DXP solution (100 µl aliquot, containing between 5-50 nmol DXP dissolved in H_2O), 200 µl *n*-butanol was added, with pipettes and tips suitable for use with

organic solvents and vortexed for 30 seconds, centrifuged at 11,000 x g for 5 min at room temperature. The lower, aqueous layer was removed from the bottom of the tube and transferred to a fresh tube and extracted further with *n*-butanol as required. Two extraction steps with 200 µl *n*-butanol reduced the volume of 100 µl DXP sample to approximately 25 µl. A smaller volume of *n*-butanol (25-100 µl) was used for finer reductions in sample volume if required. Prior to addition of FAS-HCl reagent, samples were air dried inside a fume cupboard to remove traces of *n*-butanol. All dilute samples extracted by this method must be assayed in triplicates.

4.7. Adaptation of the assay for high-throughput measurements using 96-well plates

The assay can be adapted for 200 µl volumes, commonly used in plastic 96-well plates as follows. The initial reaction mixture in each well contains 40 µl FAS reagent and 5 µl resorcinol, to which 4 µl of fructose-containing sample is added. Since the sensitivity of the reaction remains unchanged in small volumes, the sample should be subjected to a concentration step prior to measurement. However, this requirement is also true for many other assays in metabolic studies, so we do not consider it explicitly here. The 96-well plate (with closed lid) is then incubated for 40 min. at 80°C, and then water is added to a final volume of 200 µl. The absorption measurement can then be performed using a plate reader or diode array spectrometer.

Acknowledgments: We thank the German Ministry for Education and Research (BMBF grant nos. 031A171A and 031B0135) and the Vector MINT Stiftung (grant no. P2015-0059) for generous financing. We also thank Gerasimoula Gerasimidou for expert technical assistance, and Dr. Caroline Autenrieth for proof-reading the manuscript and for stimulating discussions. We also acknowledge the suggestion by a referee to extend the reaction time for the sugar phosphates, which proved to be effective.

Author Contributions: S.S. and R.G. conceived and designed the experiments; S.S. performed the experiments; S.S. and R.G. analyzed the data; R.G and S.S. wrote the paper.

Conflicts of Interest: The authors declare no conflict of interest.

References

1. **Anumula, K.R. and Du, P.** (1999) *Anal. Biochem.* 275, 236-242. Characterization of carbohydrates using highly fluorescent 2-aminobenzoic acid tag following gel electrophoresis of glycoproteins.
2. **Han, Y., Sabbioni, C., Heijden, R.V.D. and Verpoort, R.** (2003) *J. Chromatog. A* 986, 291-296. High-performance liquid chromatography assay for 1-deoxy-D-xylulose 5-phosphate synthase activity using fluorescence detection.
3. **Li, B.W., Schuhmann, P.J. and Wolf, W.R.** (1985) *J. Agric. Food Chem.* 33, 531-536. Chromatographic determinations of sugars and starch in a diet composite reference material.
4. **Kametani, S., Shiga, Y. and Akanuma, H.** (1996). *Eur. J. Biochem.* 242, 832–838. Hepatic production of 1,5-anhydrofructose and 1,5-anhydroglucitol in rat by the third glycogenolytic pathway.
5. **Langmeier, J.M. and Rogers, D.E.** (1995) *Cereal Chem.* 72, 349-351. Rapid method for sugar analysis of doughs and baked products.
6. **Sprenger, G.A., Schörken, U., Wiegert, T., Grolle, S., Graff, A.A.D., Taylor, S.V., Begley, T.P. Bringer-Meyer, S. and Sahm, H.** (1997) *Proc. Natl. Acad. Sci. USA* 94, 12857–12862. Identification of a thiamin-dependent synthase in *Escherichia coli* required for the formation of the 1-deoxy-D-xylulose 5-phosphate precursor to isoprenoids, thiamin, and pyridoxal.
7. **Zhou, X., Yuan, X., Shi, Z., Meng, D., Jiang, W., Wu, L., Chen, J. and Chen, G.** (2012) *Microb. Cell Factories* 11, 54. Hyperproduction of poly (4-hydroxybutyrate) from glucose by recombinant *Escherichia coli*.
8. **Bartos, J. and Pesez, M.** (1979) *Pure and Appl. Chem.* 51, 1803-1814. Colorimetric and fluorimetric determination of aldehydes and ketones.
9. **Jue, C.K. and Lipke, P.N.** (1985) *J. Biochem. Biophys. Meth.* 11, 109-115. Determination of reducing sugars in the nanomole range with tetrazolium blue.
10. **Kulka, R.G.** (1956) *Biochemistry* 63, 542-548. Colorimetric estimation of ketopentoses and ketohexoses
11. **Bacon, J.S.D. and Bell, D.J.** (1948) *Biochem. J.* 42, 397-405. Fructose and glucose in the blood of the foetal sheep.
12. **Lauretin, A. and Edwards, C.A.** (2002) *Anal. Biochem.* 315, 143-145. A microtiter modification of the anthrone-sulfuric acid colorimetric assay for glucose-based carbohydrates.

13. **Monsigny, M., Petit, C. and Roche, A.** (1988) *Anal. Biochem.* 175, 525-530. Colorimetric determination of neutral sugars by a resorcinol sulfuric acid micromethod.
14. **Somani, B.L., Khanade, J. and Sinha, R.** (1987) *Anal. Biochem.* 167, 327-330. A modified anthrone-sulfuric acid method for the determination of fructose in the presence of certain proteins.
15. **Waffenschmidt, S. and Jaenicke, L.** (1987) *Anal. Biochem.* 165, 337-340. Assay of reducing sugars in the nanomole range with 2,2'-bicinchoninate.
16. **Dietrich, C.P., Dietrich, S.M.C. and Pontis, H.G.** (1964) *J. Chromatog. A*, 15, 277-278. Separation of sugar phosphates and sugar nucleotides by thin-layer chromatography.
17. **Moczar, E., Moczar, M., Schillinger, G. and Robert, L.** (1967) *J. Chromatog. A,* 31, 561-564. A rapid micro-determination of neutral sugars and aminosugars in glycopeptides by thin-layer chromatography.
18. **Raadsveld, C.W. and Klomp, H.** (1971) *J. Chromatog. A* 57, 99-106. Thin-layer chromatographic analysis of sugar mixtures.
19. **Waring, P.P. and Ziporin, Z.Z.** (1964) *J. Chromatog.* A, 15, 168-172. The separation of hexosephosphates and triosephosphates by thin-layer chromatography.
20. **Araujo, P.** (2009) *J. Chromatog. B,* 877, 2224-2234. Key aspects of analytical method validation and linearity evaluation.
21. **Harrington, W.F., Johnson, P. and Ottewill, R.H.** (1956) *J. Biochem.* 62, 569-582. Bovine serum albumin and its behavior in acid solution.
22. **Ghosh, R., Hardmeyer, A., Thoenen, I. and Bachofen, R.** (1994) *Appl. Environ. Microbiol.* 60, 1698-1700. Optimization of the Sistrom culture medium for large-scale batch cultivation of Rhodospirillum rubrum under semiaerobic conditions with maximal yield of photosynthetic membranes.
23. **Grammel, H., Gilles, E.D. and Ghosh, R.** (2003) *Appl. Environ. Microbiol.* 69, 6577-6586. Microaerophilic cooperation of reductive and oxidative pathways allows maximal photosynthetic membrane biosynthesis in *Rhodospirillum rubrum*.
24. **Sistrom, W.R.** (1960) *J. Gen. Microbiol.* 22, 778-785. A requirement for sodium in the growth of *Rhodopseudomonas spheroides.*
25. **Erb, T.J., Berg, I.A., Brecht, V., Müller, M., Fuchs, G. and Alber, B.E.** (2007) *Proc. Natl. Acad. Sci. USA,* 104, 10631-10636. Synthesis of C5-dicarboxylic acids from C2-units involving crotonyl-CoA carboxylase/reductase: the ethylmalonyl-CoA pathway.
26. **Eubanks, L.M. and Poulter, C.** (2003) *Biochemistry*, 42, 1140-1149. *Rhodobacter capsulatus* 1-deoxy-D-xylulose 5-phosphate synthase: steady-state kinetics and substrate binding.

27. **LePage, A.G.** (1948) *Cancer Res.* 8, 197-200. Phosphorylated intermediates in tumor glycolysis. II. Isolation of phosphate esters from tumors.
28. **McGeown, G.M. and Malpress, H.F.** (1952) *J. Biochem.* 52, 606–611. Studies on the synthesis of lactose by the mammary gland 2. The sugar phosphate esters of milk.
29. **Sambrook, J., Fritsch, E.F. and Maniatis, T.** (1989) Molecular cloning: A laboratory manual, 2nd ed. Cold Spring Harbor Laboratory Press, Cold Spring Harbor, New York, USA.
30. **Lois, L.M., Campos, N., Putra, S.R., Danielsen, K., Rohmer, M. and Boronat, A.** (1998) *Proc. Natl. Acad. Sci. USA* 95, 2105-2110. Cloning and characterization of a gene from *Escherichia coli* encoding a transketolase-like enzyme that catalyzes the synthesis of D-1-deoxyxylulose 5-phosphate, a common precursor for isoprenoid, thiamin, and pyridoxol biosynthesis.
31. **Hoeffler, J.F., Tritsch, D., Grosdemange-Billiard, C. and Rohmer, M.** (2002) *Eur. J. Biochem.* 269, 4446–4457. Isoprenoid biosynthesis via the methylerythritol phosphate pathway- Mechanistic investigations of the 1-deoxy-D-xylulose 5-phosphate reductoisomerase.
32. **Ajikumar, P.K., Xiao, W.H., Tyo, K., Wang, Y., Simeon, F., Leonard, E., Mucha, O., Phon, T.H., Pfeiffer, B. and Stephanopoulos, G.** (2010) *Science* 330, 70-74. Isoprenoid pathway optimization for taxol precursor overproduction in *Escherichia coli*.
33. **Dixon, M. and Webb, E.C.** (1964) Enzymes 2nd ed., Longmans Green, London, England, pp. 114-116.
34. **Atkins, G.L. and Nimmo, I.** (1973) *Biochem. J.* 135, 779-784. The reliability of Michaelis constants and maximal velocities estimated using the integrated Michaelis-Menten equation.

Appendix 1. Bacterial and algal strains used in this study

Organism and Strain	Genotype	Reference
C. reinhardtii strain SAG 18.79 or CC-1418	Standard laboratory strain *mt*$^{-}$ *	The SAG Culture Collection of Algae, University of Göttingen.
R. rubrum strain S1	wild-type, ps^{+}, crt^{+}	Cohen-Bazire *et al.*, 1998
R. rubrum pRK290/S1	S1 strain containing the low copy number plasmid pRK290, Tet^{R}	R. Ghosh, unpublished
R. rubrum pRKTmChRR1/S1	S1 containing the Takara®* mCherry gene under control of the *R. rubrum nifH* promoter, in the plasmid pRK290, Tet^{R}	R. Ghosh, unpublished
E. coli XL1 MR	Δ(*mcrA*)183 Δ(*mcrCB-hsdSMR-mrr*)173 *endA1 supE44 thi-1 recA1 gyrA*96 *relA1 lac*.	Stratagene (now, Agilent)
E. coli XL1 MRF'	Δ(*mcrA*)*183* Δ(*mcrCB-hsdSMR-mrr*)173 *endA1 supE44 thi-1 recA1 gyr*A96 *rel*A1 *lac*.F': *proAB*$^{+}$ *lacZ* Δ*M15* Tn*10*(Tet ^{R})	Stratagene (now, Agilent)
E. coli RR28	F*supE44 lac*Y1 *ara*14 *gal*K2 *xyl*5 *mtl*1 *leu*B6 *pro*A2 *phe*S12 *hsd*S20 *recA rps*L20 *thi*1 *mcrB* lambda	Hennecke *et al.*, 1982

*The *C. reinhardtii* strain SAG 18.79 listed as 'Red tide, Florida, Provasoli' has a chloroplast DNA indistinguishable from that of CC-125 wild type 137c and genetic features (a Gulliver transposon pattern) like other laboratory strains (Ferris, 1989).

*® The native mCherry gene commercially available from Takara® (Japan) has been codon-optimized here for expression in *R. rubrum*.

Appendix 2. Culture media used in this study

2.1. Luria-Bertani (LB) medium (see Sambrook and Russell, 2001)

10g Tryptone
5g Yeast extract
10g NaCl

Dissolved in 1 litre H_2O obtained from the Millipore® water purification apparatus, autoclaved at 121°C for 20 min.

2.2. Hutner´s supplement for Sistrom medium A (Sistrom, 1960)

Chemical	Conc. (g/litre)
EDTA	50
$ZnSO_4.7H_2O$	22
H_3BO_3	11.4
$MnCl_3.4H_2O$	5.1
$FeSO_4.7H_2O$	5
$CoCl_2.6H_2O$	1.6
$CuSO_4.5H_2O$	1.1
$(NH_4)_6Mo_7O_{24}.4H_2O$	1.1

2.3. Sistrom Medium A (Sistrom, 1960) and M2SF medium (Ghosh *et al.*, 1994)

Composition		Conc. (g/litre or ml/litre)	M-medium (ml/litre)	ml/litre M2S-medium	ml/litre M2SF-medium
M1	KH_2PO_4/ K_2HPO_4	148 222	10 ml	20 ml	20 ml
M2	Succinate KOH	236 224	10 ml	_	_
NH_4-succinate	Adjust pH with 25% NH_4OH	236	_	20 ml	20 ml
M3	NH_4Cl	214	2 ml	_	_
M4	Nitrilotriacetic acid Aspartic acid Glutamic acid KOH $MgSO_4.7H_2O$ $FeSO_4.7H_2O$ Nicotinic acid Thiamine Biotin $CaCl_2{\cdot}2H_2O$ Hutner´s supplement	20 4 10 22 28.8 0.2 0.1 0.05 0.002 6.6 20 ml	10 ml	10 ml	10 ml
HEPES	2M HEPES (adjust with NH_4OH to pH 6.8)	_	_	20 ml	20 ml
M5	NaCl	120	1ml	1ml	1ml
M6	*p*-Aminobenzoic acid	2.85	1ml	1ml	1ml
Fructose	30% Fructose (sterile) added after autoclaving.	_	_	_	10 ml

Before autoclaving adjust pH to 6.8 with 2N NaOH or 25% NH_4OH for M medium and M2S/ M2SF medium, respectively.

2.4. TAP medium (Gorman and Levine, 1965) and Tris-citrate-phosphate medium (this study)

Composition		Conc. g/litre	ml/litre TAP medium	ml/litre Tris-citrate-phosphate medium	Final conc. in TAP medium (mM)
1M Tris base	Tris Base	121.14	20 ml	20 ml	20
Phosphate Buffer II	$K_2HPO_4.3H_2O$ KH_2PO4	108 56	1 ml	1 ml	0.47 0.41
Solution A	NH_4Cl $MgSO_4.7H_2O$ $CaCl_2.2H_2O$	40 10 5	10 ml	10 ml	7.478 0.406 0.340
Hutner's trace elements	EDTA disodium salt $ZnSO_4.7H_2O$ H_3BO_3 $MnCl_2.4H_2O$ $CoCl_2.6H_2O$ $CuSO_4.5H_2O$ $(NH_4)6Mo_7O_{24}.4H_2O$ $FeCl_2.4H_20$	50 22 11.4 5.06 1.61 1.57 1.1 3.6	1 ml	1 ml	0.134 0.077 0.184 0.026 0.007 0.006 0.001 0.018
Glacial acetic acid	Glacial acetic acid		1 ml	-	17.4
1M citric acid	Titrate with citric acid to pH 7.0	-	-	Titrate with citric acid to pH 7.0	-
Na-acetate	Na-acetate(solid), add after titration of medium	0.66/ 0.98/ 1.23	-	Na-acetate (solid)	8/ 12/ 15

2.5. Sulphur-depleted TAP medium (Melis *et al.*, 2000)

Composition		Conc. g/litre	ml/litre S-depleted TAP medium	Final conc. in TAP medium (mM)
1M Tris base	Tris base	121.14	20 ml	20
Phosphate Buffer II	$K_2HPO_4.3H_2O$ KH_2PO4	108 56	1 ml	0.47 0.41
Solution A	NH_4Cl $MgCl_2.6H_2O$ $CaCl_2.2H_2O$	40 8.13 5	10 ml	7.478 0.406 0.340
Hutner's trace elements	EDTA disodium salt $ZnCl_2$ H_3BO_3 $MnCl_2.4H_2O$ $CoCl_2.6H_2O$ $CuCl_2.2H_2O$ $(NH_4)_6Mo_7O_{24}.4H_2O$ $FeCl_2.4H_20$	50 10 11.4 5.06 1.61 1 1.1 3.6	1 ml	0.134 0.077 0.184 0.026 0.007 0.006 0.001 0.018
Glacial acetic acid	Glacial acetic acid		1 ml	17.4

2.6. Modified M2SF medium for *nif* gene expression: M2SN medium (this work)

M2SN medium for *nifH* expression with controlled N- sources							
Soln.	**Substance**	**Mol. Wt.**	**Amount g/l**	**Amount g/100 ml**	**[conc.] in stock solution**	**[conc.] in final medium**	**Amt. (ml)/ l medium**
M1	KH_2PO_4 K_2HPO_4		148 222	**14.8** **22.2**	**1.088** **0.97**	20 mM 20 mM	**20**
M2N	Succinate Triethylamine (added after autoclaving)		236 pH 6.8	**23.6**	**2 M**	40 mM	**20**
M4N	Nitrilotriacetic acid KOH (5M) $MgSO_4.7H_2O$ $FeSO_4.7H_2O$ Nicotinic Acid Thiamine Biotin HutnersN* $CaCl_2.2H_20$ (separate)		20 adj. to pH ~7 28.8 200 mg/l 100 mg/l 50 mg/l 2 mg/l 20 ml 6.6	**2** **~2.6 ml** **2.88** **20 mg** **10 mg** **5 mg** **0.2 mg** **2 ml** **0.66**			**10**
M5	NaCl		120	**12**	**2 M**	2 mM	**1**
M6	*p*-aminobenzoic acid	137.14	2.85	**0.285**	**20 mM**	20 µM	**1**
HEPES	HEPES-Methylamine (to pH 6.8)	238.3	476.62	**47.662**	**2 M**	40 mM	**20**
Fructose	30% Fruct. (sterile) (after autoclaving)	180.16	300	30	**1.7 M** or **30%**	17 mM or 0.3%	**10**

* Substituted with an NH_4^+ free molybdate salt.

M1, M4N, M5, M6 and HEPES containing medium was adjusted to pH 6.8 with methylamine and autoclaved.

By varying the ratios of the succinate-TEA (M2N) and NH_4^+-succinate (from Appendix 2.3) in culture, (keeping a constant final [succinate] of 40 mM), a range of [NH_4^+] of the M2NF culture can be achieved as desired. Both solutions are added through sterile filters, into autoclaved and cooled medium containing M1, M4N, M5, M6 and HEPES solutions, prior to inoculation.

2.7. Solubility of amino acids in H_2O

		AnaSpec® (USA) data*			Dunn *et al.*, 1933; Nozaki and Tanford, 1970		
Amino acid	**Mol. mass**	**Solubility (25°C)**			**Solubility (25°C)**		
		g/100 ml	**g/l**	**Molarity**	**g/100 ml**	**g/l**	**Molarity**
Lys	146.19	v. soluble	v. soluble	v. soluble			
Arg	174.20	15.00	150.00	0.86			
His	155.16	4.19	41.90	0.27			
DL-Asp	133.00	0.78	7.78	0.06	0.82	8.16	0.06
L-Asp	133.00				0.54	5.39	0.04
D,L-Glu*	147.00	*0.86*	*8.64*	*0.06*	2.64	26.43	0.18
D-Glu	147.00				0.89	8.88	0.06
Ser	105.09	5.02	50.23	0.48			
Thr	119.12	v. soluble	v. soluble	v. soluble			
Met	149.21	3.38	33.81	0.23	5.60	56.00	0.38
Cys	121.15	v. soluble	v. soluble	v. soluble			
Pro	115.13	162.30	1623.00	14.10			
Asn	132.12	3.53	35.30	0.27	2.51	25.10	0.19
Gln	146.15	2.50	25.00	0.17	4.38	43.80	0.30
Gly	75.07	24.99	249.90	3.33	25.31	253.10	3.37
DLAla	89.09	16.65	166.50	1.87	16.58	165.80	1.86
DL-Val	117.15	8.85	88.50	0.76	7.44	74.41	0.64
DLLeu	131.17	2.43	24.26	0.18	1.18	11.81	0.09
DL-Ile	131.17	4.12	41.17	0.31	2.19	21.88	0.17
L-Tyr	181.19	0.05	0.45	0.00	0.05	0.48	0.00
Trp	204.23	1.14	11.36	0.06			
DL-Phe	165.19	2.97	29.65	0.18	1.42	14.18	0.09
***For 0°C*							

***https://www.anaspec.com/html/amino_acids_properties.html**

Appendix 3. Description of Bola components used for the screw cap assembly in this study (All images except for 'Universal Coupling' have been taken from the official BOLA website (www.bola.de))

BOLA Product name	Material	Image
Multiple Distributors for Bottles	Green screw cap made of PP (polypropylene) for bottle thread GL 45 and body made of PP. Distributors with GL-14 threaded necks.	
2-way Stopcocks	Conductive PTFE (polytetrafluoroethylene) -EX (explosion) proof with straight bore and two connections with GL-14 thread.	
Screw Cap with gasket	Screw cap with handy knurl made of PPS (polyphenylsiloxan), with integrated PTFE (lower surface) /silicone (upper surface) gasket. After assembly, the product is only exposed to PTFE.	
Laboratory Screw Joints Ex	Screw cap made of conductive black PPS-EX reinforced with glass fibres. Inner parts- sealing, tapered and V ring made of conductive PTFE-EX.	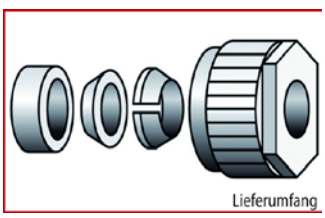

BOLA Product	Material	Image
GL Tube fittings EX, straight- 2 way GL thread connector	Made of PTFE-EX, two connections with GL thread. For connection of tubing or tube with BOLA Laboratory Screw Joints EX	
Zebra Explosion-Proof Tubing	Transparent PFA (Perfluoralkoxy Copolymer) tubing with black longitudinal conductive stripes on the outer surface.	
Universal Coupling	PTFE. For connecting GL 14 to G ¼ inch Swagelok assembly.	

Appendix 4. The enzymatic assay of glucose

Principle:

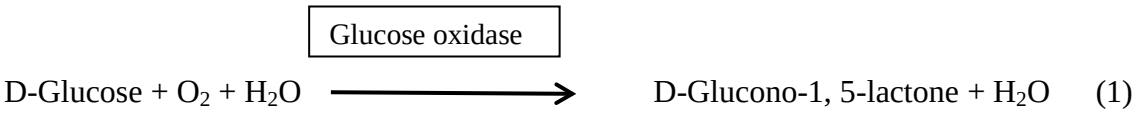

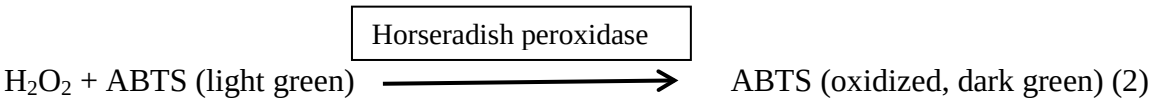

(ABTS: 2,2'-azino-bis(3-ethylbenzthiazoline-6-sulfonic acid))

(Only reaction (1) is used for O_2 consumption in *C. reinhardtii* S-depletion in Setup II)

Stock solutions:

Assay buffer:

(1) 125 mM Na-phosphate, pH 7 (125NaP7)

25 ml of 0.5 M NaP7 + 75 ml H_2O

(2) 25 mM ABTS solution: Mol. wt.: 548.7 g/mol

Dissolve 27.43 mg in 2 ml of 125NaP7.

(3) Glucose oxidase: 200 U/mg

Primary stock (PS): 1000 U/ml = 5mg/ml in 125NaP7

Working solution 1 (WS1): 100 U/ml i.e. a 10-fold dilution of PS = 10µl PS + 90µl NaP7

Working solution 2 (WS2): 10 U/ml or 0.01 U/µl i.e. a 10-fold dilution of WS1 = 5µl WS1 + 45 µl NaP7

[Per assay = 2.5 µl of WS2 =0.025 U]

(4) Horseradish peroxidase: 6.1 mg~ 2000U

Primary Stock: 2000 U/100 µl or 20 U/µl. Added 100 µl 125 mM NaP7 to entire contents of HRP bottle

Working solution 1: 2 U/µl or a 10-fold dilution of PS=1 µl PS+ 9 µl NaP7

Working solution 2: 0.1U/µl or a 20-fold dilution of WS1= 10 µl WS1+190 µl NaP7

[Per assay= 12.5 µl of WS2= 1.25 U]

(5). Glucose stock: (For plotting standard Michaelis-Menten curve)

1 M solution or 18 % (w/v) 18 g in 100 ml H_2O

Appendix 5. Development of the $NaBH_4$ experiment for calibration of H_2

A5.1. Additional experimental factors relevant to the $NaBH_4$-H_2 evolution experiment

Large variations were observed in the final amount of H_2 evolved (peak areas) in the experiments shown in Fig A5.1 (A) and (B). They both represent experiments conducted with 20 ml water and 1 pellet of $NaBH_4$. Though a small variation in the amount of H_2 produced is expected due to daily temperature and air pressure differences, this does not satisfactorily explain the large differences in the value of their final peak areas. This experimental variation was resolved in Fig. A5.1 (C) by using 40 ml H_2O and a magnetic stirrer to ensure homogenous mixing conditions.

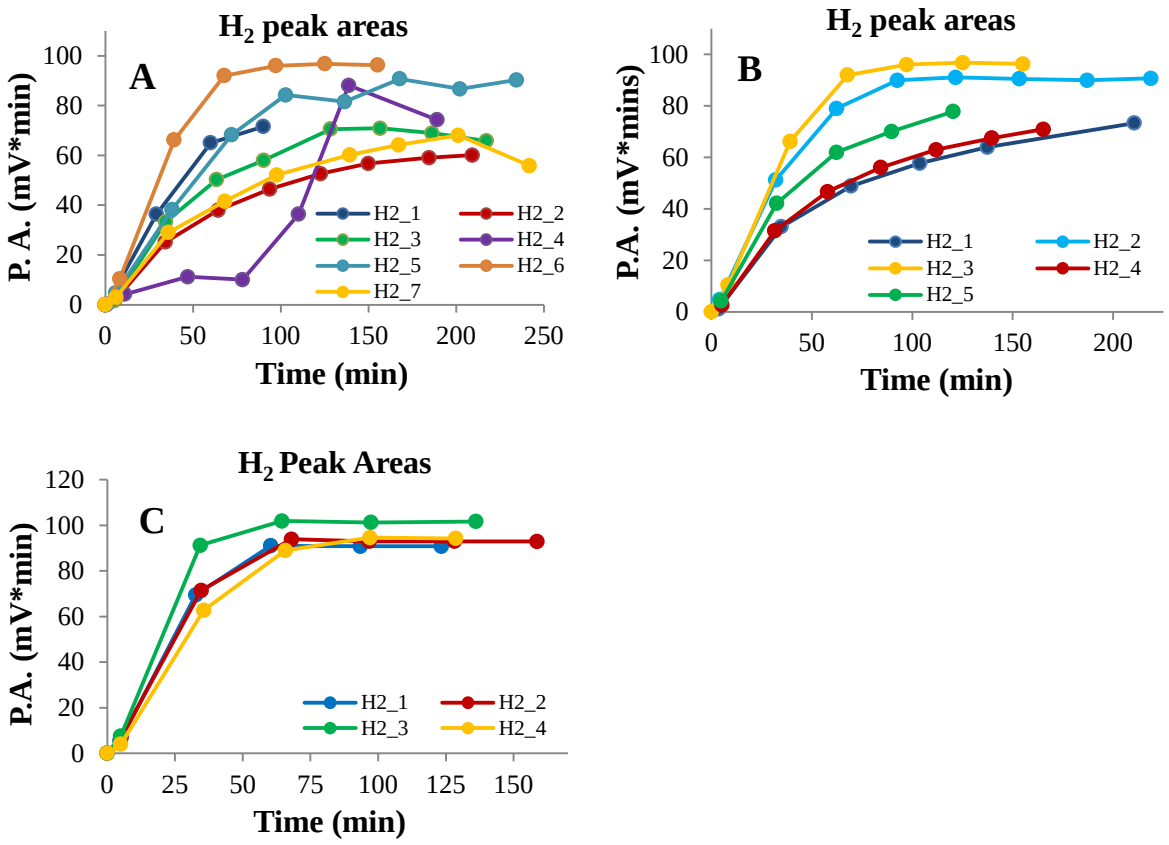

Fig. A5.1. The progression of the $NaBH_4$ experiment towards development of the final experimental protocol. **(A)**, **(B)** and **(C)** show the H_2 evolution peaks vs. time for different experiments in chronological order of the experiments (the use of colours and numbers are arbitrary, plots in same colours are not indicative of the same experiment). The measurement at time 0 mins indicates the initial air measurement, just before the reaction is started and the bottle is sealed. **(A)** and **(B)** show the plots of experiments conducted with 20 ml H_2O (no stirring) **(C)** shows the reactions of the pellet with 40 ml H_2O with mechanical stirring for proper mixing.

The irregular features of the H_2 evolution in Fig. A5.1 (A) and (B) were a result of:

(1) clogging of the front port of the needle due to coring of the rubber septa of the BOLA gas sampling port and the GC sample injection port (plots 4 and 5 in (A)) and

(2) the lack of mechanical mixing, which prevents H_2 levels from reaching similar maximum levels in Fig. A5.1 (B).

The smoothening of the H_2 evolution profile seen from Fig. A5.1 (A) to (B) and to (C) was attributed to:

(1) the use of the point style 5 conical side port Hamilton needles (Reno, USA) over front port ones which prevented coring and resolved experimental problems related to needle blockage,

(2) H_2 tightness of the BOLA connections and bottle by use of the Snoop® (Swagelok, Germany) leak detector which ensured that the reactor bottle held the maximum constant value of the evolved H_2 over a long period of time (tested overnight) and

(3) the use of mechanical stirring along with use of 40 ml H_2O for the reaction results in almost identical H_2 evolution curves amongst replicates in Fig. A5.1 (C). The higher amount of water ensured that the pellet and magnetic stirrer remained submerged throughout the experiment.

Having minimized the factors leading to experimental heterogeneity, we noted that the pellets have a standard deviation of 0.01 g in their weight and along with daily changes in temperature and pressure, small variations in the final H_2 peak area cannot be eliminated as seen in Fig. A5.1 (C).

The established experimental protocol included the following steps:

(1) The temperature of the reaction vessel and the GC sample loop was recorded for every measurement.
(2) The bottle must be placed inside of a fume hood, in a room with near constant temperature conditions throughout the day.
(3) Since, the most crucial experimental value for the purpose of this experiment is the difference between the initial and final O_2 peak sizes, it was essential to make three air

measurements in the beginning of each experiment with the bottle equilibrated with fresh air, prior to starting the $NaBH_4$ reaction by dropping in the pellet and sealing the reaction bottle.

An important indicator for the success of these experiments is that the progression of depression of the O_2 peak areas should match exactly the rise of the H_2 peak such that the plot of the latter against the former is always a straight line (Fig. A5.2 (C)).

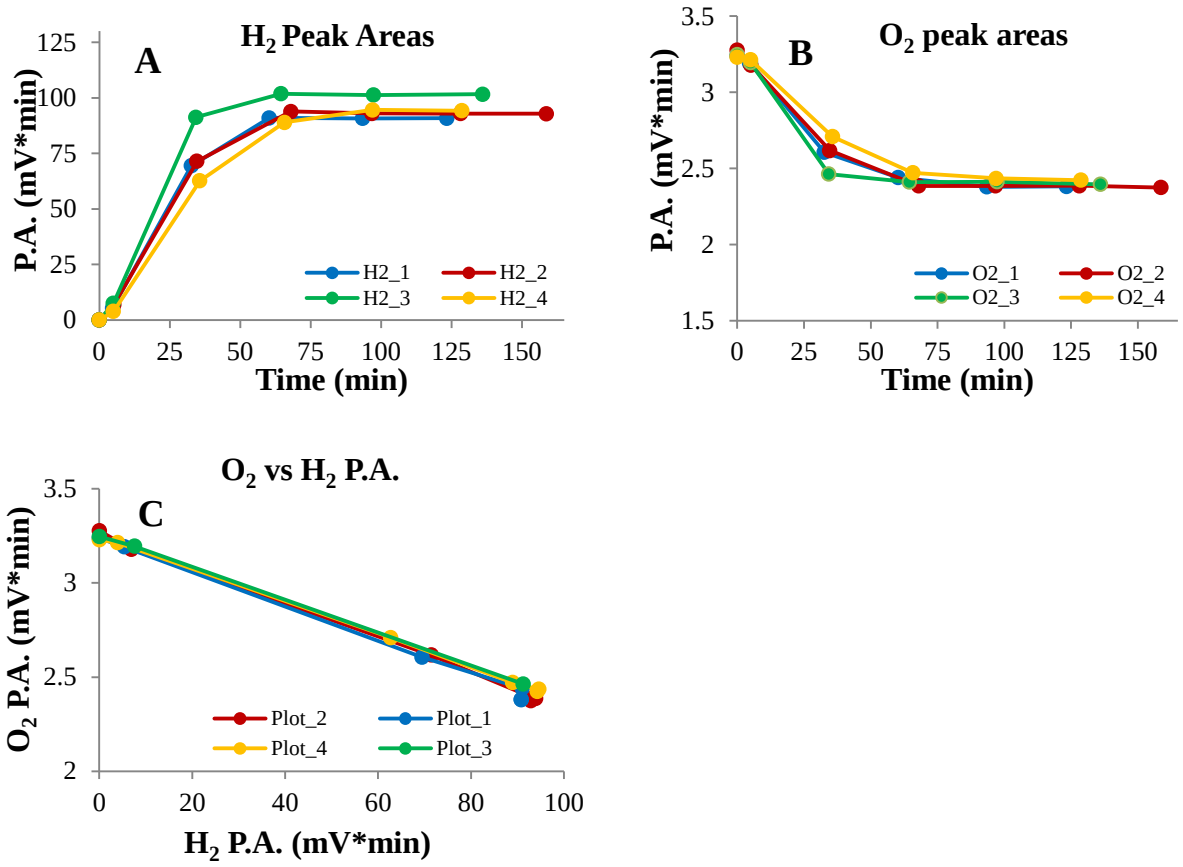

Fig. A5.2. **(A)**, **(B)** and **(C)** show the H_2 and O_2 profiles of 4 experiments (same colours are used to indicate data from the same experiments) performed according to the final protocol of 1 pellet $NaBH_4$ in 40 ml H_2O with mechanical stirring. **(A)** is the same as Fig. A5.1 (C). The linear correlation shown between the H_2 and O_2 levels at every time point of the experiments **(C)** indicates a successful experiment and confirms that the decrease in size of the O_2 peak relates quantitatively to the increase in size of the H_2 peak.

A5.2. Dilution of H_2 evolved from $NaBH_4$ experiments into SubaSeal(ed) dilution bottles

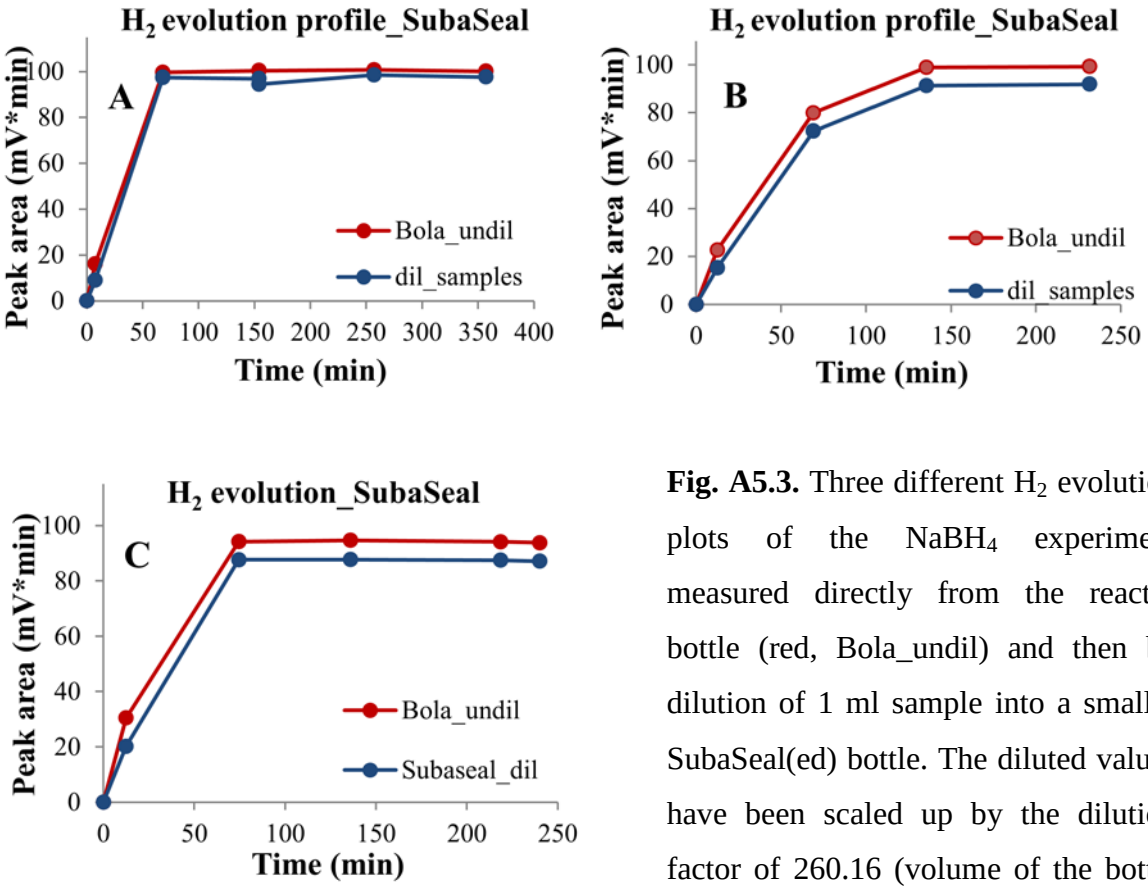

Fig. A5.3. Three different H_2 evolution plots of the $NaBH_4$ experiment measured directly from the reactor bottle (red, Bola_undil) and then by dilution of 1 ml sample into a smaller SubaSeal(ed) bottle. The diluted values have been scaled up by the dilution factor of 260.16 (volume of the bottle in ml) (blue, Subaseal_dil).

The average error of dilution at saturating H_2 levels for the three experiments (A) to (C) were 3.1 %, 7.4 % and 7.1 % respectively. 1 ml H_2-containing gas from the calibration bottle, diluted 260.16 -fold into SubaSeal dilution bottle, contributes only 1.8 x 10^{-3} atm. in excess pressure, which was therefore considered to be negligible.

A5.3. Final H_2 liberated (peak area) as a direct function of pellet weight.

As an additional validation of the robustness of our experimental protocol, several rounds of experiments with varying weights of $NaBH_4$ pellets were performed and their gas profile examined by GC. They showed a similar pattern of rise in H_2 levels and depression in their O_2 levels with a linear correlation between the H_2 and O_2 peak areas. A maximum saturating level of H_2 evolution was reached in all experiments as seen in Fig. A5.4.

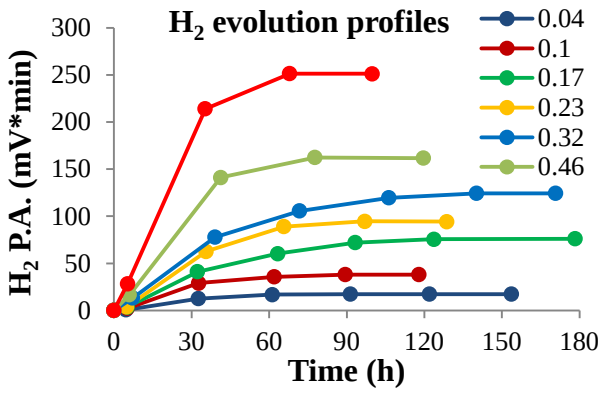

Fig. A5.4. The H_2 evolution profile for reactions carried out with various weights in (g) of the $NaBH_4$ pellet. The final H_2 peak sizes correspond well to the weight of the pellet and they all reach a stationary maximum value.

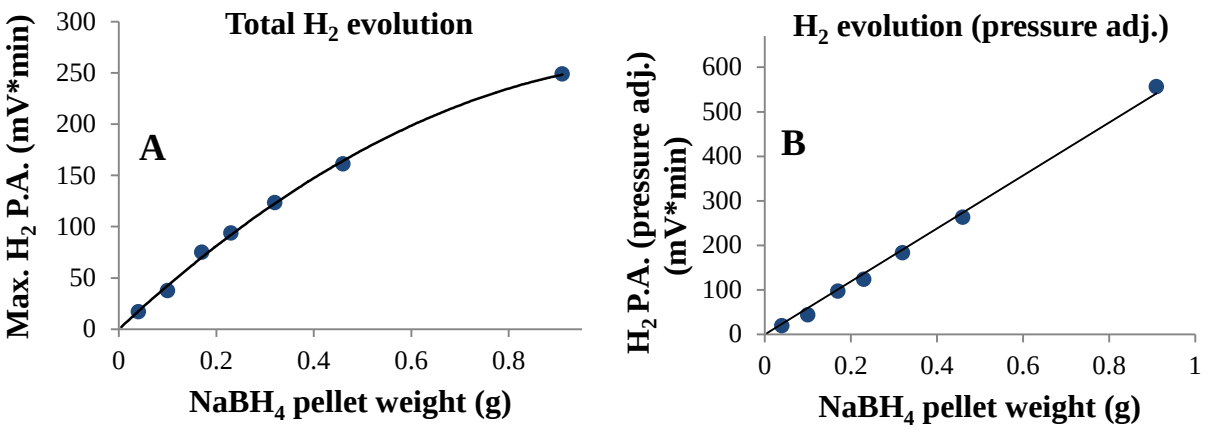

Fig. A5.5. **(A)** The maximum H_2 peak area as measured by the GC plotted against the respective weight of $NaBH_4$ pellet used fits well to a second order polynomial curve; **(B)** when the peak areas are multiplied by their respective γ factors, generated inside the bottle, the plot assumes a linear correlation to pellet weight.

The straightening of the curve obtained as seen in A5.5 (B) when the maximum peak areas obtained by GC measurements were multiplied by their respective calculated γ factors (see Part 1 Results section 3.1.1.6 for mathematical explanation of γ factor), confirms that, when a pressurized gas sample is injected into the GC, significant loss of molecules occurs at

the GC sample loop, and that the actual number of molecules of a gas are much higher inside the pressurized vessel (by a factor of γ). This implies that the shape of the first plot is a function of the pressure-equalizing effect of the GC sample loop, and when multiplied by their respective γ factors, the resultant linear curve reflects the actual number of gas molecules in the starting sample, in this case the actual number of H_2 molecules evolved by the pellets of different weights. Theoretically, the amount of H_2 liberated must be directly proportional to pellet weight, and has been demonstrated here by us experimentally.

Appendix 6. *C. reinhardtii* strains reportedly used in literature to study H_2 production.

Reference	Strain and Genotype	*Chlamydomonas* Culture Collection strain designation	Source
Ben-Amotz and Gibbs, 1975	No strain name mentioned	-	Indiana Culture Collection
Greenbaum, 1979	137c (mt^+)	CC-125	-
Melis *et al.*, 2000	137c (mt^+)	CC-125	-
Kosourov *et al.*, 2003	137c (mt^-)	CC-124	Affiliated with NREL, USA
Hemschemeier, 2005 (dissertation)	137c (mt^+)	CC-125	*Chlamydomonas* Culture Collection, Duke University, USA
Hemschemeier *et al.*, 2009	137c (mt^-)	CC-124	-
Tortillo *et al.*, 2008	wt (SAG 11/32b) (mt^+)	CC-409	-
	L159I-N230Y	-	Constructed by Tortillo *et al.*, 2008
	137c (mt^-)	CC-124	Dr. Siebert, NREL, USA
Oncel and Sukan, 2011	137c (mt^-)	CC-124	Dr. Giuseppe Torzillo, CNR, Italy
This study	SAG 18.79 (mt^-)	CC-1418	The SAG Culture Collection of Algae, University of Göttingen

(mt^+ and mt^- indicate the two mating types of *C. reinhardtii*)

References

Abeles, F.B. (1964) *Plant Physiol.* 39, 169-176. Cell-free hydrogenase from *Chlamydomonas*.

Adams, M.W.W. (1990) *FEMS Microbiol.* Rev. 75, 219-238. The metabolism of hydrogen by extremely thermophilic sulphur-dependent bacteria.

Adams, M.W.W. and Hall, D.O. (1977) *Biochem. Biophys. Res. Commun.* 77, 730–737. Isolation of the membrane-bound hydrogenase from *Rhodospirillum rubrum*.

Adams, M.W.W. and Hall, D.O. (1979) *Arch. Biochem. Biophys.* 195, 288–299. Properties of the solubilized membrane-bound hydrogenase from the photosynthetic bacterium *Rhodospirillum rubrum*.

Adams, M.W.W., Mortenson, L.E. and Chen, J.S. (1981) *Biochim. Biophys. Acta.* 594, 105–176. Hydrogenase.

Arnold, W., Rump, A., Klipp, W., Priefer, U.B. and Puhler, A. (1988) *J. Mol. Biol.* 203, 715-738. Nucleotide sequence of a 24,206-base-pair DNA fragment carrying the entire nitrogen fixation gene cluster of *Klebsiella pneumoniae*.

Arnon, D.I., Mitsui, A. and Paneque, A. (1961) *Science* 134, 1425-1425. Photoproduction of hydrogen gas coupled with photosynthetic phosphorylation.

Assael, M.J., Antoniadis, K.D. and Wakeham, W.A. (2010) *Int. J. Thermophys.* 31, 1051-1072. Historical evolution of the transient hot-wire technique.

Ausubel, F.M. (1984) *Cell* 37, 5-6. Regulation of nitrogen fixation genes.

Ausubel, F.M. and Cannon, F.C. (1981) *Cold Spring Harb. Symp. Quant. Biol.* 45, 487-499. Molecular genetic analysis of *Klebsiella pneumoniae* nitrogen-fixation (*nif*) genes.

Avtges, P., Scolnik, P.A. and Haselkorn, R. (1983) *J. Bacteriol.* 156, 251-256. Genetic and physical map of the structural genes (*nifH,D,K*) coding for the N_2ase complex of *Rhodopseudomonas capsulata*.

Bandyopadhyay, A., Stöckel, J. Min, H., Sherman, L.A. and Pakrasi, H. B. (2010) *Nature Commun.* 1, 1-7. High rates of photobiological H_2 production by a cyanobacterium under aerobic conditions**.**

Baroukh, C., Turon, V. and Bernard, O. (2017) *PLoS Comput. Biol.* 13, e1005590. Dynamic metabolic modeling of heterotrophic and mixotrophic microalgal growth on fermentative wastes.

Bateman, R.C. and Evans, J.A. (1995) *J. Chem. Edu.* 72, A240. Using the glucose oxidase/peroxidase system in enzyme kinetics.

Ben-Amotz, A. and Gibbs, M. (1975) *Biochem. Biophys. Res. Commun.* 64, 355-359. H_2 metabolism in photosynthetic organisms 2: Light-dependent H_2 evolution by preparations from *Chlamydomonas* , *Scenedesmus*, and spinach.

Benemann, J.R. and Weare, N.M. (1974) *Science* 184, 174-175. Hydrogen evolution by Nitrogen-fixing *Anabaena cylindrica* cultures.

Bennoun, P. (1982) *Proc. Natl. Acad. Sci. USA* 79, 4352–4356. Evidence for a respiratory chain in the chloroplast.

Berggren, G., Adamska, A., Lambertz, C., Simmons, T., Esselborn, J., Atta, M., Gambarelli, S., Mouesca, J. M., Reijerse, E. J., Lubitz, W., Happe, T., Artero, V., and Fontecave, M. (2013) *Nature* 499, 66-69. Biomimetic assembly and activation of [FeFe]-hydrogenases.

Berman, H.M., Westbrook, J., Feng, Z., Gilliland, G., Bhat, T. N., Weissig, H., Shindyalov, I.N. and Bourne, P.E. (2000) *Nucleic Acids Res.* 28, 235-242. The protein data bank.

Bollman, R.C. and Robinson, G.G. (1977) *J. Phycol.*, 13, 1-5. The kinetics of organic acid uptake by three chlorophyta in axenic culture.

Bonam, D., Murrell, S. A. and Ludden, P. W. (1984) *J. Bacteriol.* 159, 693-699. Carbon monoxide dehydrogenase from *Rhodospirillum rubrum.*

Bregoff, H.M. and Kamen, M.D. (1952) *Arch. Biochem. Biophys.* 36, 202-220. Studies on the metabolism of photosynthetic bacteria. XIV. Quantitative relations between malate dissimilation, photoproduction of hydrogen, and nitrogen metabolism in *Rhodospirillum rubrum.*

Brigle, K.E., Newton, W.E. and Dean, D.R. (1985). *Gene* 37, 37-44. Complete nucleotide sequence of the *Azotobacter vinelandii* nitrogenase structural gene cluster.

Brill, W. (1980). *Microbiol. Rev*. 44, 449-467. Biochemical genetics of nitrogen fixation.

Brown, C.M. and Herbert, R.A. (1977) *FEMS Lett.* 1, 43-46. Ammonia assimilation in members of the *Rhodospirillaceae.*

Brown, C.M. and Stanley, S.O. (1972) *J. Appl. Chem. Biotechnol.* 22, 368-389. Environment-mediated changes in the cellular content of the “pool” constitutes and their associated changes in cell physiology.

Buchanan-Wollaston, V. and Cannon F. (1984) Regulation of *nif* Transcription in *Klebsiella pneumoniae*. In: Veeger C., Newton W.E. (eds) Advances in Nitrogen Fixation Research. Advances in Agricultural Biotechnology, vol 4, Springer, Dordrecht, Netherlands.

Buchanan-Wollaston, V., Cannon, M.C., Beynon, J.L. and Cannon, F.C. (1981) *Nature* 294, 776–778**.** Role of the *nifA* gene product in the regulation of *nif* expression in *Klebsiella pneumoniae*.

Burns, R.C. and Bulen, W.A. (1965) *Biochim. Biophys. Acta.* Enzymology and biological oxidation 105, 437-445. ATP-dependent hydrogen evolution by cell-free preparations of *Azotobacter vinelandii*.

Burris, R.H. (1991) *J. Biol. Chem.* 266, 9339-9342. Nitrogenases.

Caballero, F.J., Cejudo, F.J., Florencio, F.J., Cardenas, J. and Castillo, F. (1985) *J. Bacteriol.* 162, 804-809. Molecular and regulatory properties of glutamine synthetase from the phototrophic bacterium *Rhodopseudomonas capsulata* E1F1.

Chalima, A., Oliver, L., Fernández de Castro, L., Karnaouri, A., Dietrich, T. and Topakas, E. (2017) *Fermentation* 3, 54-71. Utilization of volatile fatty acids from microalgae for the production of high added value compounds.

Chen, C., and Gibbs, M. (1992) *Plant Physiol.* 100, 1361–1365. Coupling of carbon dioxide fixation to the oxyhydrogen reaction in the isolated chloroplast of *Chlamydomonas reinhardtii*.

Chisnell, J., Premakumar, R. and Bishop, P. (1988) *J. Bacteriol.* 170, 27–33. Purification of a second alternative N_2ase from a *nifHDK* deletion strain of *Azotobacter vinelandii*.

Cohen-Bazire, G., Sistrom, W.R. and Stanier, R.Y. (1957) *J. Cell Comp. Physiol.* 49, 25–68. Kinetic studies of pigment synthesis by non-sulfur purple bacteria.

Conway, A. and Koshland, D.E. (1968) *Biochemistry* **7,** 4011-4023**.** Negative cooperativity in enzyme action. Binding of diphosphopyridine nucleotide to glyceraldehyde-3-phosphate dehydrogenase.

Davis, R., Lehman, L., Petrovich, R., Shah, V.K., Roberts, G.P. and Ludden, P.W. (1996) *J. Bacteriol.* 178, 1445–1450. Purification and characterization of the alternative N_2ase from the photosynthetic bacterium *Rhodospirillum rubrum*.

Dharmawardene, M.W.N., Stewart, W.D.P. and Stanley, S.O. (1972) *Planta*. 108, 133-145. N_2ase activity, amino acid pool patterns and amination in blue-green algae.

Doebbe, A., Rupprecht, J., Beckmann, J., Mussgnug, J.H., Hallmann, A., Hankamer, B. and Kruse, O. (2007) *J. Biotechnol.* 131, 27–33. Functional integration of the HUP1 hexose symporter gene into the genome of *C. reinhardtii*: impacts on biological H_2 production.

Dunn, M.S., Ross, F.J. and Read, L.S. (1933) *J. Biol. Chem.* 103, 579-595. The solubility of the amino acids in water.

Earth System Research Laboratory, National Oceanic and Atmospheric Administration, U.S. Department of Commerce. (https://www.esrl.noaa.gov).

Edgren, T. and Nordlund, S. (2006) *FEMS Microbiol. Lett.* 260, 30–35. Two pathways of electron transport to N_2ase in *Rhodospirillum rubrum*: the major pathway is dependent on the *fix* gene products.

Engel, B.D., Schaffer, M., Cuellar, L.K., Villa, E., Plitzko, J.M., Baumeister, W. (2015) *eLife,* 4, e04889. Native architecture of the *Chlamydomonas* chloroplast revealed by *in situ* cryo-electron tomography.

Erbes, D.L., King, D. and Gibbs, M. (1979) *Plant Physiol.* 63, 1138-1142. Inactivation of hydrogenase in cell-free extracts and whole cells of *Chlamydomonas reinhardtii* by oxygen.

Esquivel, M.G., Amaro, H.M., Pinto, T.S., Fevereiro, P.S. and Malcata, F.X. (2011) *Trends Biotechnol.* 29, 595–600. Efficient H_2 production via *Chlamydomonas reinhardtii*.

Esselborn, J., Lambertz, C., Adamska-Venkatesh, A., Simmons, T., Berggren, G., Noth, J., Siebel, J.F., Hemschemeier, A., Artero, V., Reijerse, E.J., Fontecave, M., Lubitz, W. and Happe, T. (2013) *Nat. Chem. Biol.* 9, 607-609. Spontaneous activation of [FeFe]-hydrogenases by an inorganic [2Fe] active site mimic.

Ferris, P.J. (1989) *Genetics* 122, 363-377. Characterization of a *Chlamydomonas* transposon, Gulliver, resembling those in higher plants.

Frey, M. (2002) *Chem. Bio. Chem.* 3, 153-160. Hydrogenases: hydrogen-activating enzymes.

Fritsch, J., Lenz, O., and Friedrich, B. (2013) *Nat. Rev. Microbiol.* 11, 106-114. Structure, function and biosynthesis of O_2-tolerant hydrogenases.

Gaffron, H. (1939) *Nature* 143, 204–205. Reduction of CO_2 with H_2 in green plants.

Gaffron, H. (1942) *J. Gen. Physiol.* 26, 241–267. Reduction of carbon dioxide coupled with the oxyhydrogen reaction in algae.

Gaffron, H. and Rubin, J. (1942) *J. Gen. Physiol.* 26, 219–240. Fermentative and photochemical production of hydrogen in algae.

Gaffron, H. (1944) *Biol. Rev. Cambridge Philos. Soc.* 19, 1–20. Photosynthesis, photoreduction and dark reduction of carbon dioxide in certain algae.

Gallaher, S.D., Fitz-Gibbon, S.T., Glaesener, A.G., Pellegrini, M. and Merchant, S.S. (2015) *The Plant Cell* 27, 2335-2352. *Chlamydomonas* genome resource for laboratory strains reveals a mosaic of sequence variation, identifies true strain histories, and enables strain-specific studies.

Gans, P. and Rebeille, F. (1990) *Biochim. Biophys. Acta* 1015, 150-155. Control in the dark of the plastoquinone redox state by mitochondrial activity in *Chlamydomonas reinhardtii.*

Gest, H. and Kamen, M. D. (1949a) *Science* 109, 558–559. Photoproduction of molecular hydrogen by *Rhodospirillum rubrum*.

Gest, H., Ormerod, J.G. and Ormerod, K.S. (1962) *Arch. Biochem. Biophys.* 97, 21-33. Photometabolism of *Rhodospirillum rubrum*. Light-dependent dissimilation of organic compounds to carbon dioxide and molecular hydrogen by an anaerobic citric acid cycle.

Geierstanger, B.H., Prasch, T., Griesinger, C., Hartmann, G., Buurman, G. and Thauer, R.K. (1998) *Angew. Chem. Int. Ed.* 37, 3300-3303. Catalytic mechanism of the metal-free hydrogenase from methanogenic archaea: reversed stereospecificity of the catalytic and noncatalytic reaction.

Gfeller, R.P. and Gibbs, M. (1984) *Plant Physiol.* 75, 212–218. Fermentative metabolism of *Chlamydomonas reinhardtii*. I: analysis of fermentative products from starch in dark and light.

Glick, R.E. and Melis, A. (1988) *Biochim. Biophys. Acta* 934, 151–55. Minimum photosynthetic unit size in system-I and system-II of barley chloroplasts.

Gorman, D.S. and Levine, R.P. (1965) *Proc. Natl. Acad. Sci. USA* 54, 1665-1669. Cytochrome f and plastocyanin: their sequence in the photosynthetic electron transport chain of *Chlamydomonas reinhardtii*.

Ghirardi, M.L., Togasaki, R.K. and Seibert, M. (1997) *Appl. Biochem. Biotechnol.* 63, 141-151. Oxygen sensitivity of algal H_2- production.

Ghosh, R. (1981) *J. Theor. Biol.* 93, 395-401. On the physiological significance of positive and negative co-operativity.

Ghosh, R., Hardmeyer, A., Thoenen, I. and Bachofen, R. (1994) *Appl. Environ. Microbiol.* 60, 1698-1700. Optimization of the Sistrom culture medium for large-scale batch cultivation of *Rhodospirillum rubrum* under semi-aerobic conditions with maximal yield of photosynthetic membranes.

Ghysels. B., Godaux, D., Matagne, R. F., Cardol, P. and Franck. F. (2013) *Plos One* 8, e64161. Function of the chloroplast hydrogenase in the microalga *Chlamydomonas:* The role of hydrogenase and state transitions during photosynthetic activation in anaerobiosis.

Gibbs, M., Gfeller, R.P. and Chen, C. (1986) *Plant Physiol.* 82, 160–166. Fermentative metabolism of *Chlamydomonas reinhardtii*. III: photoassimilation of acetate.

Gogotov, I.N. (1984) *Arch. Microbiol.* 140, 86–90. Hydrogenase of purple bacteria: properties and regulation of synthesis.

Golden, J.W., Carrasco, C.D., Mulligan, M.E., Schneider, G.J., and Haselkorn, R. (1988) *J. Bacteriol.* 170, 5034-5041. Deletion of a 55-kilobase-pair DNA element from the chromosome during heterocyst differentiation of *Anabaena sp*. strain PCC 7120.

Gorrell, T.E. and Uffen, R.L. (1977) *J. Bacteriol.* 131, 533–543. Fermentative metabolism of pyruvate by *Rhodospirillum rubrum* after anaerobic growth in darkness.

Graham, D. (1980) Effects of light and “dark” respiration. In: Davies, D.D. ed, “The Biochemistry of Plants. A Comprehensive Treatise, Vol 2”. Academic Press, New York, 525-579.

Grammel, H. and Ghosh, R. (2008) *J. Bacteriol.* 190, 4912-4921. Redox-State Dynamics of ubiquinone-10 imply cooperative regulation of photosynthetic membrane expression in *Rhodospirillum rubrum*.

Grammel, H., Gilles, E.D. and Ghosh, R. (2003). *Appl. Environ. Microbiol.* 69, 6577-6586. Microaerophilic cooperation of reductive and oxidative pathways allows maximal photosynthetic membrane biosynthesis in *Rhodospirillum rubrum*.

Gray, M.W. and Boer, P.H. (1988) *Philos. Trans. R. Soc. Lond. B Biol. Sci.* 319, 135-47. Organization and expression of algal (*Chlamydomonas reinhardtii*) mitochondrial DNA.

Greenbaum, E. (1979) Simultaneous photoproduction of hydrogen and oxygen by photosynthesis. United States: N. p. https://www.osti.gov/servlets/purl/5393013.

Gussin, G.N., Ronson, C.W. and Ausubel, F.M. (1986) *Ann. Rev. Genet.* 20, 567-591. Regulation of nitrogen fixation genes.

Hahn, J.J., Ghirardi, M.L., and Jacoby, W.A. (2004) *Biotechnol. Progr.* 20, 989-991. Effect of process variables on photosynthetic algal hydrogen production.

Halbleib, C.M. and Ludden, P.W. (2000) *J. Nutr.* 130, 1081–1084. Regulation of biological nitrogen fixation.

Halbleib, C.M., Zhang, Y. and Ludden, P.W. (2000) *J. Biol. Chem.* 275, 3493–3500. Regulation of diN_2ase reductase ADP-ribosyltransferase and diN_2ase reductase-activating glycohydrolase by a redox-dependent conformational change of N_2ase Fe protein.

Happe, T. and Naber, J.D. (1993) *Eur. J. Biochem.* 214, 475-481. Isolation, characterization and N-terminal amino acid sequence of hydrogenase from the green alga *Chlamydomonas reinhardtii*.

Happe, T. and Kaminski, A. (2002) *Eur. J. Biochem.* 269, 1022-1032. Differential regulation of the Fe-hydrogenase during anaerobic adaptation in the green alga *Chlamydomonas reinhardtii.*

Happe, T., Mosler, B. and Naber, J.D. (1994) *Eur. J. Biochem.* 222,769-774. Induction, localization and metal content of hydrogenase in the green alga *Chlamydomonas reinhardtii.*

Harris, E.H. (1989) The *Chlamydomonas* Sourcebook. Academic Press, San Diego.

Harris, E.H. (2001) *Ann. Rev. Plant Physiol. Plant Mol. Biol.* 52, 363-406. *Chlamydomonas* as a model organism.

Hemschemeier A. (2002) Der H_2-Metabolismus von *Chlamydomonas reinhardtii* unter Schwefelmangel: eine physiologische und molekularbiologische Studie. *Diploma thesis, Friedrich-Wilhelms University, Bonn, Germany*.

Hemschemeier A. (2005) The anaerobic life of the photosynthetic alga *Chlamydomonas reinhardtii*. Photofermentation and hydrogen production upon sulphur deprivation. *PhD thesis, Ruhr-University Bochum, Germany.*

Hemschemeier, A., Melis, A. and Happe, T. (2009) *Photosynth. Res.* 102, 523–540. Analytical approaches to photobiological hydrogen production in unicellular green algae of *Chlamydomonas reinhardtii*.

Hendriks, J.H.M., Kolbe, A., Gibon, Y., Stitt, M. and Geigenberger, P. (2003) *Plant Physiol.* 133, 838–849. ADP-glucose pyrophosphorylase is activated by posttranslational redox-modification in response to light and to sugars in leaves of *Arabidopsis* and other plant species.

Hennecke, H., Günther, I. and Binder, F. (1982) *Gene* 19, 231-234. A novel cloning vector for the direct selection of recombinant DNA in *E. coli*.

Hill, S. (1988) *FEMS Microbiol. Rev.* 4, 111-129. How is N_2ase regulated by oxygen?

Hillmer, P. and Gest, H. (1977) *J. Bacteriol.* 129, 724-731. H_2 metabolism in the photosynthetic bacterium *Rhodopseudomonas capsulata*: H_2 production by growing cultures.

Hoover, T.R., Santero, E. Porter, S. and Kustu, S. (1990) *Cell* 63, 11-22. The integration host factor stimulates interaction of RNA polymerase with NIFA, the transcriptional activator for nitrogen fixation operons.

Houille-Vernes, L., Rappaport, F., Wollman, F.A., Alric, J. and Johnson, X. (2011) *Proc. Natl. Acad. Sci. U.S.A.* 108, 20820-20825. Plastid terminal oxidase 2 (PTOX2) is the major oxidase involved in chlororespiration in *Chlamydomonas*.

Huang, J.J., Heiniger, E.K., McKinlay, J.B., and Harwood, C.S. (2010) *Appl. Environ. Microbiol.* 76, 7717–7722. Production of hydrogen gas from light and the inorganic electron donor thiosulfate by *Rhodopseudomonas palustris*.

Hummel, E., Guttmann, P., Werner, S., Tarek, B., Schneider, G., Kunz, G., Frangakis, A. S. and Westermann, B. (2012) *Plos One* 7, 1-9.3D Ultrastructural organization of whole *Chlamydomonas reinhardtii* cells studied by nanoscale soft X-ray tomography.

Hutner, S.H. (1946) *J. Bacteriol.* 52, 213-221. Organic growth essentials of the aerobic nonsulfur photosynthetic bacteria.

Jacobs, J., Pudollek, S., Hemschemeier, A. and Happe, T. (2009) *FEBS Lett*. 583, 325–329. A novel, anaerobically induced ferredoxin in *Chlamydomonas reinhardtii*.

Jans, F., Mignolet, E., Houyoux, P.A., Cardol, P., Ghysels, B., Cuiné, S., Cournac, L., Peltier, G., Remacle, C. and Franck, F. (2008) *Proc. Natl. Acad. Sci. USA* 105, 20546–20551. A type II NAD(P)H dehydrogenase mediates light-independent plastoquinone reduction in the chloroplast of *Chlamydomonas*.

Joerger, R.D., Bishop. P.E. and Evans, H.J. (1988) *Crit. Rev. Microbiol.* 16, 1–14. Bacterial alternative nitrogen fixation systems.

Joerger, R.D., Jacobson, M.R., Premakumar, R., Wolfinger, E.D. and Bishop, P.E. (1989). *J. Bacteriol.* 171, 1075-1086. Nucleotide sequence and mutational analysis of structural genes (*anfHDGK*) for the second alternative nitrogenase from *Azotobacter vinelandii*.

Joerger, R.D., Loveless, T.M., Pau, R.N., Mitchenall, L.A., Simon, B.H. and Bishop, P.E. (1990) *J. Bacteriol.* 3400-3408. Nucleotide sequences and mutational analysis of the structural genes for nitrogenase 2 of *Azotobacter vinelandii.*

Johnson, X. and Alric, J. (2013) *Eukaryotic Cell* 12, 776-793. Central carbon metabolism and electron transport in *Chlamydomonas reinhardtii*: metabolic constraints for carbon partitioning between oil and starch.

Kamen, M.D. and Gest, H. (1949) *Science* 109, 560-561. Evidence for a N_2ase system in the photosynthetic bacterium *Rhodospirillum rubrum*.

Kanemoto, R.H. and Ludden, P.W. (1987) *J. Bacteriol*. 169, 3035-3043. Amino acid concentrations in *Rhodospirillum rubrum* during expression and switch-off of N_2ase activity.

Kessler, E. (1966) *Biochim. Biophys. Acta.* 112, 173–175. The effect of glucose on hydrogenase activity in *Chlorella*.

Kessler, E. (1974) Hydrogenase, photoreduction and anaerobic growth of algae. In: "Algal Physiology and Biochemistry" Vol 10. Blackwell Scientific Publications Ltd, Berkley and Los Angeles, California, 454–473.

Klein, U. (1986) *Planta.* 167, 81–86. Compartmentation of glycolysis and of the oxidative pentosephosphate pathway in *Chlamydomonas reinhardtii*.

Klipp, W. (1990) Organization and regulation of nitrogen fixation genes in *Rhodobacter capsulatus*. In: Gresshoff, P.M., Roth, L.E., Stacey, G. and Newton, W.E. (eds) "Nitrogen Fixation". Springer, Boston, MA.

Kim, E.J., Lee, M.K., Kim, M.S. and Lee, J.K. (2008) *Int. J. Hydrog. En.* 33, 1516- 1521. Molecular hydrogen production by nitrogenase of *Rhodobacter sphaeroides* and by Fe-only hydrogenase of *Rhodospirillum rubrum*.

Kong, Q., Li, L., Martinez, B., Chen, P. and Ruan, R. (2010) *Appl. Biochem. Biotechnol.* 160, 9–18. Culture of microalgae *Chlamydomonas reinhardtii* in wastewater for biomass feedstock production.

Koshland, Jr. D.E., Nemethy, G. & Filmer, D. (1966). *Biochemistry* 5, 365-385. Comparison of experimental binding data and theoretical models in proteins containing subunits.

Kosourov, S., Tsygankov, A.A., Ghirardi, M.L. (2002) *Biotechnol. Bioeng.* 78, 731-740. Parameters affecting algal hydrogen photoproduction.

Kosourov, S., Seibert, M., and Ghirardi, M.L. (2003) *Plant and Cell Physiol.* 44, 146–155. Effects of extra-cellular pH on the metabolic pathways in sulfur-deprived, H_2-producing *Chlamydomonas reinhardtii* cultures.

Kosourov, S., Patrusheva, E., Ghirardi, M.L., Seibert, M., and Tsygankov, A. (2007) *J. Biotechnol.* 128, 776–787. A comparison of hydrogen photoproduction by sulfur-deprived *Chlamydomonas reinhardtii* under different growth conditions.

Kosourov, S.N., Batyrova, K.A., Petushkova, E.P., Tsygankov, A.A., Ghirardi, M.L. and Seibert, M. (2012) *Int. J. Hydrog. Energy* 37, 8850–8858. Maximizing the hydrogen photoproduction yields in *Chlamydomonas reinhardtii* cultures: the effect of the H_2 partial pressure.

Kosourov, S., Jokel, M., Aro, E.M. and Allahverdiyeva, Y. (2018*) Energy Environ. Sci.*, 11, 1431-1436. A new approach for sustained and efficient H_2 photoproduction by *Chlamydomonas reinhardtii*.

Kranz, R.G. and Foster-Hartnett, D. (1990). *Mol. Microbiol.* 4, 1793–1800. Transcriptional regulatory cascade of nitrogen-fixation genes in anoxygenic photosynthetic bacteria: Oxygen- and nitrogen-responsive factors.

Kranz, R.G. and Haselkorn, R. (1986) *Proc. Natl. Acad. Sci. USA* 83, 6805-6809. Anaerobic regulation of nitrogen-fixation genes in *Rhodopseudomonas capsulata*.

Kranz, R.G., Pace, V.M. and Caldicott, I.M. (1990) *J. Bacteriol.* 172, 53-62. Inactivation, sequence, and lacZ fusion analysis of a regulatory locus required for repression of nitrogen fixation genes in *Rhodobacter capsulatus*.

Krasna, A.I. (1979) *Enzyme Microb. Technol.*, 165-173. Hydrogenase: properties and applications.

Kropat, J., Hong-Hermesdorf, A., Casero, D., Ent, P., Castruita, M., Pellegrini, M., Merchant, S.S. and Malasarn, D. (2011) *Plant J.* 66, 770-780. A revised mineral nutrient supplement increases biomass and growth rate in *Chlamydomonas reinhardtii*.

Kruse, O., Rupprecht, J., Bader, K.P., Thomas-Hall, S., Schenk, P.M., Finazzi, G. and Hankamer, B. (2005a) *J. Biol. Chem.* 280, 34170–34177. Improved photobiological H_2 production in engineered green algal cells.

Kustu, S., Santero, E., Keener, J., Popham, D. and Weiss, D. (1989) *Microbiol. Rev.* 53, 367–376. Expression of sigma 54 (*ntrA*)-dependent genes is probably united by a common mechanism.

Laurinavichene, T.V., Fedorov, A.S., Ghirardi, M.L. Seibert, M. and Tsygankov, A.A. (2006) *Int. J. Hydrog. Energy* 31, 659-667. Demonstration of sustained photoproduction by immobilized, sulphur deprived *Chlamydomonas reinhardtii* cells.

Laurinavichene, T., Tolstygina, I. and Tsygankov, A. (2004) *J. Biotechnol.* 114, 143–151. The effect of light intensity on hydrogen production by sulfur-deprived *Chlamydomonas reinhardtii.*

Lee, D.Y. and Fiehn, O. (2008) *Plant Methods* 4. High quality metabolomic data for *Chlamydomonas reinhardtii*.

Llama, M.J., Serra, J.L., Rao, K.K. and Hall, D.O. (1981) *Eur. J. Biochem.* 114, 89–96. Isolation of two hydrogenase activities in *Chromatium*.

Lien, T. and Schreiner, O. (1975) *Biochim. Biophys. Acta* 384, 168–179. Purification of a derepressible arylsulfatase from *Chlamydomonas reinhardtii*.

Lindstrom, E.S., Burris, R.H. and Wilson, P.W. (1949) *J. Bacteriol.* 58, 313–316. Nitrogen fixation by photosynthetic bacteria.

Lubitz, W., Hideaki Ogata, H., Rüdiger, O. and Reijerse, E. (2014) *Chem. Rev.* 114, 4081-4148. Hydrogenases.

Ludden, P.W. and Roberts, G.P. (1989) *Curr. Top. Cell. Regul.* 30, 23–56. Regulation of N_2ase activity by reversible ADP ribosylation.

Madigan, M.T. and Gest, H. (1978). *Arch. Microbiol.* 117, 119-122. Growth of a photosynthetic bacterium anaerobically in darkness, supported by “oxidant-dependent” sugar fermentation.

Maione, T.E. and Gibbs, M. (1986) *Plant Physiol.* 80, 360-363. Hydrogenase-mediated activities in isolated chloroplasts of *Chlamydomonas reinhardtii*.

Maione, T.E. and Gibbs, M. (1986) *Plant Physiol.* 80, 364-368. Association of the chloroplastic respiratory and photosynthetic electron transport chains of *Chlamydomonas reinhardtii* with photoreduction and the oxyhydrogen reaction.

Malnoë, P., Mayfield, S.P. and Rochaix, J.D. (1988) *J. Cell Biol.* 106, 609-616. Comparative analysis of the biogenesis of photosystem II in the wild-type and Y-1 mutant of *Chlamydomonas reinhardtii.*

Maness, P.C. and Weaver, P. (2001) *Appl. Microbiol. Biotechnol.* 57, 751-756. Evidence for three distinct hydrogenase activities in *Rhodospirillum rubrum*.

Matthew, T., Zhou, W., Rupprecht, J., Lim, L., Thomas-Hall, S.R., Doebbe A., Kruse O., Hankamer, B., Marx, U.C., Smith, S.M. and Schenk, P.M. (2009) *J. Biol. Chem.* 284, 23415–23425. The metabolome of *Chlamydomonas reinhardtii* following induction of anaerobic H_2 production by sulfur depletion.

Margulies, M.M. (1991) *Photosynth Res.* 29, 133-47. Sequence similarity between Photosystems I and II. Identification of a Photosystem I reaction center transmembrane helix that is similar to transmembrane helix IV of the D2 subunit of Photosystem II and the M subunit of the non-sulfur purple and flexible green bacteria.

Masepohl, B., Klipp, W. and Pühler, A. (1988) *Molec. Gen. Genet.* 212, 27-37. Genetic characterization and sequence analysis of the duplicated nifA/nifB gene region of *Rhodobacter capsulatus.*

Maul, J.E., Lilly, J.W., Cui, L., dePamphilis, C.W., Miller, W., Harris, E.H. and Stern, D.B. (2002) *Plant Cell.* 14, 2659–2679. The *Chlamydomonas reinhardtii* plastid chromosome islands of genes in a sea of repeats.

McBride, C., Lien, S., Togasaki, R.K. and Pietro A.S. (1977) Mutational analysis of *Chlamydomas reinhardtii*: application to biological solar energy conversion. In: Mitsui, A., Miyachi, S., San Pietro, A. and Tamura, S. (eds.) “Biological solar energy conversion”. Academic press, New York, New York, 77–86.

Meek, T.D. and Villafranca, J.J. (1980) *Biochemistry* 19, 5513-5519. Kinetic mechanism of *Escherichia coli* glutamine synthetase.

Melis, A. (1991) *Biochim. Biophys. Acta* 1058, 87-106. Dynamics of photosynthetic membrane composition and function.

Melis, A. (2007) *Planta* 226, 1075–1086. Photosynthetic H_2 metabolism in *Chlamydomonas reinhardtii* (unicellular green algae).

Melis, A. and Anderson, J.M. (1983) *Biochim. Biophys. Acta* 724, 473-484. Structural and functional organization of the photosystems in spinach chloroplasts. Antenna size, relative electron-transport capacity, and the chlorophyll composition.

Melis, A. and Happe, T. (2001) *Plant Physiol.* 127, 740-748. Hydrogen production: Green algae as a source of energy.

Melis, A., Zhang, L.P., Forestier, M., Ghirardi, M.L. and Seibert, M. (2000) *Plant Physiol.* 122, 127–135. Sustained photobiological hydrogen gas production upon reversible inactivation of oxygen evolution in the green alga *Chlamydomonas reinhardtii.*

Merchant, S.S., Prochnik, S.E., Vallon, O., Harris, E.H., Karpowicz, S.J,, Witman, G.B., Terry, A., Salamov, A., Fritz-Laylin, L.K., Maréchal-Drouard, L., Marshall, W.F., Qu, L.H., Nelson, D.R., Sanderfoot, A.A., Spalding, M.H., Kapitonov, V.V., Ren, Q., Ferris, P., Lindquist, E., Shapiro, H., Lucas, S.M., Grimwood, J., Schmutz, J., Cardol, P., Cerutti, H., Chanfreau, G., Chen, C.L., Cognat, V., Croft, M.T., Dent, R., Dutcher, S., Fernández, E., Fukuzawa, H., González-Ballester, D., González-Halphen, D., Hallmann, A., Hanikenne, M., Hippler, M., Inwood, W., Jabbari, K., Kalanon, M., Kuras, R., Lefebvre, P.A., Lemaire, S.D., Lobanov, A.V., Lohr, M., Manuell, A., Meier, I., Mets, L., Mittag, M., Mittelmeier, T., Moroney,. J.V., Moseley, J., Napoli, C., Nedelcu, A.M., Niyogi, K., Novoselov, S.V., Paulsen, I.T., Pazour, G., Purton, S., Ral, J.P., Riaño-Pachón, D.M, Riekhof, W., Rymarquis, L., Schroda, M., Stern, D., Umen, J., Willows, R., Wilson, N., Zimmer, S.L., Allmer, J., Balk, J., Bisova, K., Chen, C.J., Elias, M., Gendler, K., Hauser, C., Lamb, M.R., Ledford, H., Long, J.C., Minagawa, J., Page, M.D., Pan, J., Pootakham, W., Roje, S., Rose, A., Stahlberg, E., Terauchi, A.M., Yang, P., Ball, S., Bowler, C., Dieckmann, C.L., Gladyshev, V.N., Green, P., Jorgensen, R., Mayfield, S., Mueller-Roeber, B., Rajamani, S., Sayre, R.T, Brokstein, P., Dubchak, I., Goodstein, D., Hornick, L., Huang, Y.W., Jhaveri, J., Luo, Y., Martínez, D., Ngau, W.C., Otillar, B., Poliakov, A., Porter, A., Szajkowski, L., Werner, G., Zhou, K., Grigoriev, I.V., Rokhsar, D.S. and Grossman, A.R. (2007) *Science* 318, 245-50. The *Chlamydomonas* genome reveals the evolution of key animal and plant functions.

Mettler, T., Mühlhaus, T., Hemme, D., Schöttler, M.A., Rupprecht, J., Idoine, A., Veyel, D., Pal, S.K., Yaneva-Roder, L., Winck, F.V., Sommer, F., Vosloh, D., Seiwert, B., Erban, A., Burgos, A., Arvidsson, S., Schönfelder, S., Arnold, A., Günther, M., Krause, U., Lohse, M., Kopka, J., Nikoloski, Z., Mueller-Roeber, B., Willmitzer, L., Bock, R., Schroda, M. and Stitt, M. (2014) *The Plant Cell* 26, 2310-2350. Systems analysis of the response of photosynthesis, metabolism, and growth to an increase in irradiance in the photosynthetic model organism *Chlamydomonas reinhardtii*.

Merrick, M., Hill, S., Hennecke, H., Hahn, M., Dixon, R. and Kennedy, C. (1982) *Molec. Gen. Genet.* 185, 75-81. Repressor properties of the *nifL* gene product in *Klebsiella pneumoniae*.

Meunier, J.C. and Dalziel, **K.** (1978). *Eur. J. Biochem.* 82, 483-492. Kinetic studies of glyceraldehyde-3-phosphate dehydrogenase from rabbit muscle.

Meuser, J.E., Adamo, S.D., Jinkerson, R.E., Mus, F., Yang, W., Ghirardi, M.L., Seibert, M. Grossman, A.R. and Posewitz, M.C. (2012) *Biochem. Biophys. Res. Commun.* 417, 704–

709. Genetic disruption of both *Chlamydomonas reinhardtii* [FeFe]-hydrogenases: Insight into the role of HYDA2 in H_2 production.

Meyer, J. (2007) *Cell. Mol. Life Sci.* 64, 1063–1084. [FeFe] hydrogenases and their evolution: a genomic perspective.

Morett, E. and Buck, M. (1989) *J. Mol. Biol.* 210, 65-77. *In vivo* studies on the interaction of RNA polymerase-σ^{54} with the *Klebsiella pneumoniae* and *Rhizobium meliloti nifH* promoters: the role of NifA in the formation of an open promoter complex.

Mortenson, L.E. and Thorneley, R.N.F. (1979) *Ann. Rev. Biochem.* 48, 387-418. Structure and function of nitrogenase.

Munson, T.O. and Burris, R.H. (1969) *J. Bacteriol.* 97, 1093-1098. Nitrogen fixation by *Rhodospirillum rubrum* grown in nitrogen-limited continuous culture.

Mus, F., Dubini, A., Seibert, M., Posewitz, M.C. and Grossman, A.R. (2007) *J. Biol. Chem.* 282, 25475–25486. Anaerobic adaptation in *Chlamydomonas reinhardtii*: anoxic gene expression, hydrogenase induction and metabolic pathways.

Mus, F., Cournac, L., Cardettini, W., Caruana, A. and Peltier, G. (2005) *Biochim. Biophys. Acta.* 1708, 322–332. Inhibitor studies on non-photochemical plastoquinone reduction and H_2 photoproduction in *Chlamydomonas reinhardtii*.

Nash, H.A. and Robertson, C.A. (1981) *J. Biol. Chem.* 256, 9246-9253. Purification and properties of the *Escherichia coli* protein factor required for λ integrative recombination.

Nguyen, A.V., Thomas-Hall, S.R., Malnoe, A., Timmins, M., Mussgnug, J.H., Rupprecht, J., Kruse, O., Hankamer, B. and Schenk, P.M. (2008) *Eukaryot. Cell.* 7, 1965-1979. Transcriptome for photobiological hydrogen production induced by sulfur deprivation in the green alga *Chlamydomonas reinhardtii*.

Nozaki, Y. and Tanford, C. (1970) *J. Biol. Chem.* 245, 1648-1652. The solubility of amino acids, diglycine, and triglycine in aqueous guanidine hydrochloride solutions.

Ohta, S., Miyamoto, K. and Miura, Y. (1987) *Plant Physiol.* 83, 1022–1026. Hydrogen evolution as a consumption mode of reducing equivalents in green algal fermentation.

Oncel, S. and Sukan, F.V. (2011) *Biomass Bioenerg.* 35, 1066-1074. Effect of light intensity and the light: dark cycles on the long term hydrogen production of *Chlamydomonas reinhardtii* by batch cultures.

Ormerod, J.G. and Gest, H. (1962) *Bacteriol. Rev.* 26, 51–66. Symposium on metabolism of inorganic compounds. IV-Hydrogen photosynthesis and alternative metabolic pathways in photosynthetic bacteria.

Peterson, G.L. (1979) *Anal. Biochem.* 100, 201-220. Review of the Folin phenol protein quantitation method of Lowry, Rosebrough, Farr and Randall.

Porra, R.J., Thompson, W.A. and Kriedemann, P.E. (1989) *Biochim. Biophys. Acta* 975, 384–394. Determination of accurate extinction coefficients and simultaneous equations for assaying chlorophylls a and b extracted with four different solvents: verification of the concentration of chlorophyll standards by atomic absorption spectroscopy.

Pröschold, T., Harris, E.H., Coleman, A.W. (2005) *Genetics* 170, 1601-1610. Portrait of a species: *Chlamydomonas reinhardtii*.

Raghavendra, A.S. and Padmasree, K. (2003) *Trends Plant Sci.* 11, 546-53. Beneficial interactions of mitochondrial metabolism with photosynthetic carbon assimilation.

Rochaix, J.D. (1995) *Ann. Rev. Genet.* 29, 209–30. *Chlamydomonas reinhardtii* as the photosynthetic yeast.

Rochaix, J.D. (1996) *Plant Mol. Biol.* 32, 327-341. Post-transcriptional regulation of chloroplast gene expression in *Chlamydomonas reinhardtii*.

Rubio, L.M. and Ludden, P.W. (2005) *J. Bacteriol.* 187, 405-414. Maturation of N_2ase: a biochemical puzzle.

Rumpel, S., Siebel, J.F., Diallo, M., Fares, C., Reijerse, E.J. and Lubitz, W. (2015) *Chembiochem* 16, 1663-1669. Structural insight into the complex of ferredoxin and [FeFe] hydrogenase from *Chlamydomonas reinhardtii*.

Russel, G.K. and Gibbs, M. (1968) *Plant Physiol.* 43, 649-652. Evidence for the participation of the reductive pentose phosphate cycle in photoreduction and the oxyhydrogen reaction.

Ruvkun, G.B. and Ausubel, F.M. (1980) *Proc. Natl. Acad. Sci. USA* 77, 191-195. Interspecies homology of N_2ase genes.

Saegesser, R., Ghosh, R. and Bachofen, R. (1992) *FEMS Microbiol. Lett.* 95, 7-11. Stability of broad host range cloning vectors in the phototrophic bacterium *Rhodospirillum rubrum*.

Sajitz, P., Klemme, J.H., Koch, H.G. and Molitor, M. (1993) *Z. Naturforsch.* 48, 812-814. Isolation and properties of trimethylamine N-oxide/dimethylsulfoxide reductase from the purple bacterium *Rhodospirillum rubrum*.

Sambrook, J. and Russell, D.W. (2001) "Molecular cloning: a laboratory manual", 3rd ed. Cold Spring Harbor Press, Cold Spring Harbor, N.Y.

Sayle, R. and Milner-White, E.J. (1995) *Trends Biochem. Sci.* 20, 374-376. RasMol: Biomolecular graphics for all.

Schneider, K., Muller, A., Schramm, U. and Klipp, W. (1991) *Eur. J. Biochem.* 195, 653-661. Demonstration of a molybdenum- and vanadium-independent nitrogenase in a *nifHDK*-deletion mutant of *Rhodobacter capsulatus*.

Schön, G. and Voelskow, H. (1976) *Arch. Microbiol.* 107, 87-92. Pyruvate fermentation in *Rhodospirillum rubrum* and after transfer from aerobic to anaerobic conditions in the dark.

Schultz, J.E. and Weaver, P.F. (1982) *J. Bacteriol.* 149, 181-190. Fermentation and anaerobic respiration by *Rhodospirillum rubrum* and *Rhodopseudomonas capsulata*.

Scomaa, A. and Hemschemeier, A. (2017) *Algal Res.* 26, 341–347. The hydrogen metabolism of sulfur deprived *Chlamydomonas reinhardtii* cells involves hydrogen uptake activities.

Shafaat, H.S., Rüdiger, O., Ogata, H. and Lubitz, W. (2013) *Biochim. Biophys. Acta, Bioenerg.* 1827, 986-1002. [NiFe] hydrogenases: a common active site for hydrogen metabolism under diverse conditions.

Shapira, M., Lers, A., Heifetz, P.B. Irihimovitz, V., Osmond, C.B., Gillham, N.W. and Boynton, J.E. (1997) *Plant Mol. Biol.* 33, 1001-1011. Differential regulation of chloroplast expression in *Chlamydomonas reinhardtii* during photoacclimation: light stress transiently suppresses synthesis of the Rubisco LSU protein while enhancing synthesis of the PSII D1 protein.

Sistrom, W.R. (1960) *J. Gen. Microbiol.* 22, 778-785. A requirement for sodium in the growth of *Rhodopseudomonas sphaeroides*.

Slater, J.H. and Morris, I. (1974) *Arch. Microbiol.* 95, 337-346. Light-dependent synthesis of glutamate in *Rhodospirillum rubrum*. Physiological evidence for ammonia assimilation via the glutamine synthetase and glutamine: 2-oxoglutarate amino-transferase system.

Smith, B.M., Morrissey, P.J., Guenther, J.E., Nemson, J.A., Harrison, M.A., Allen, J.F. and Melis, A. (1990) *Plant physiol.* 93, 1433-1440. Response of the photosynthetic apparatus in *Dunaliella salina* (green alage) to irradiance stress.

Stephenson, M. and Stickland, L.H. (1931), *Biochem. J.* 25, 205-214. Hydrogenase: A bacterial enzyme activating molecular hydrogen.

Stirnberg, M. and Happe T. (2004) Identification of a cis-acting element controlling anaerobic expression of the *hydA*-gene from *Chlamydomonas reinhardtii*. In: "Biohydrogen III" (Miyake, J., Igarashi, Y. and Roegner, M., eds), Elsevier Science, Oxford, 117-127.

Swanson, K.D. Ratzloff, M.W., Mulder, D.W., Artz. J.H., Ghose, S., Hoffman, A., White, S., Zadvornyy, O.A. Broderick, J.B., Bothner, B. King, P.W. and Peters, J.W. (2015) *J. Am. Chem. Soc.* 137, 1809–1816. [FeFe]-hydrogenase oxygen inactivation is initiated at the H cluster 2Fe subcluster.

Tempest, D.W., Meers, J.L. and Brown, C.M. (1970). *Biochem. J.* 117, 405-407. Synthesis of glutamate in *Aerobacter aerogenes* by a hitherto unknown route.

Teramoto, H., Nakamori, A., Minagawa, J. and Ono, T. (2002) *Plant Physiol*. 130, 325-333. Light-intensity-dependent expression of Lhc gene family encoding light-harvesting chlorophyll-a/b proteins of photosystem II in *Chlamydomonas reinhardtii*.

Thauer, R.K, Klein, A.R. and Hartmann, G.C. (1996) *Chem. Rev.* 96, 3031-3042. Reactions with molecular hydrogen in microorganisms: evidence for a purely organic hydrogenation catalyst.

Torzillo, G., Scomaa, A., Faralonia, C., Ena, A. and Johanningmeier, U. (2009) *Int. J. Hydrog. Energy* 34, 4529-4536. Increased hydrogen photoproduction by means of a sulfur-deprived *Chlamydomonas reinhardtii* D1 protein mutant.

Turpin, D.H., and Weger, H. G. (1990) Interactions between photosynthesis, respiration and N assimilation. In: Dennis, D.T. and Turpin, D.H. eds, "Plant Physiology, Biochemistry and Molecular Biology." Longman Scientific and Technical, Harlow, UK. 422-433.

Uffen, R.L. (1981) *Enzyme Microb Technol.* 3, 197–206. Metabolism of carbon monoxide.

Vignais, P.M., Billoud, B. and Meyer, J. (2001) *FEMS Microbiol. Rev.* 25, 455–501. Classification and phylogeny of hydrogenases.

Vijayaraghavan, K., Karthik, R. and Kamala Nalini, S.P. (2010). *J. Plant Sci.* 5, 1-19. Hydrogen generation from algae: A review.

Villar, R., Held, A.A., Merino, J. (1995) *Plant Physiol.* 107, 421-427. Dark leaf respiration in light and darkness of an evergreen and a deciduous plant species.

Voelskow, H. and Schön, G. (1980) *Arch. Microbiol.* 125, 245–249. H_2 production of *Rhodospirillum rubrum* during adaptation to anaerobic dark conditions.

Volgusheva, A., Styring, S. and Mamedov, F. (2013) *Proc. Natl. Acad. Sci. U.S.A.* 110, 7223–7228. Increased photosystem II stability promotes H_2 production in sulfur-deprived *Chlamydomonas reinhardtii.*

Volgusheva, A., Kukarskikh, G., Krendeleva, T., Rubin, A. and Mamedov, F. (2015) *RSC Adv.* 5, 5633–5637. Hydrogen photoproduction in green algae *Chlamydomonas reinhardtii* under magnesium deprivation.

Wang, B., Wang, J., Zhang, W. and Meldrum, D.R. (2012) *Front. Microbiol.* 3, 344-359. Application of synthetic biology in cyanobacteria and algae.

Wang, G.S., Grammel, H., Abou-Aisha, K., Sagesser, R., and Ghosh, R. (2012). *Appl. Environ. Microbiol.* 78, 7205-7215. High-level production of the industrial product, lycopene, using the photosynthetic bacterium, *Rhodospirillum rubrum*.

Warakont, J., Tsai, C., Michel, E.J., Murphy, G.R., Hsueh, P.Y., Roston, R.L., Sears, B.B. and Benning, C. (2015) *Plant J.* 84, 1005-1020. Chloroplast lipid transfer processes in *Chlamydomonas reinhardtii* involving a trigalactosyldiacylglycerol 2 (TGD2) orthologue.

Weger, H.G. and Dasgupta, R. (1993), *J. Phycol.* 29, 300-308. Regulation of alternative pathway respiration in *Chlamydomonas reinhardtii* (chlorophyceae).

Weissman, J.C. and Benemann, J.R. (1977) *Appl. Environ. Microbiol.* 33, 123-129. Hydrogen production by nitrogen starved cultures of *Anabaena cylindrical.*

Wientjes, E., Philippi, J., Borst, J.W. and van Amerongen, H. (2017) *Biochim. Biophys. Acta.* 1858, 259-265. Imaging the photosystem I/photosystem II chlorophyll ratio inside the leaf.

Winkler, M., Hemschemeier, A., Gotor, C., Melis, A. and Happe, T. (2002) *Int. J. Hydrog Energy* 27, 1431–1439. [Fe]-hydrogenases in green algae: photo-fermentation and hydrogen evolution under sulfur-deprivation.

Wykoff, D.D., Davies, J.P., Melis, A. and Grossman, A.R. (1998) *Plant Physiol.* 117, 129–139. The regulation of photosynthetic electron-transport during nutrient deprivation in *Chlamydomonas reinhardtii*.

Xie, Q., Michaeli, S., Peled-Zehavi, H. and Galili, G. (2015) *Trends Plant Sci.* 20, 264-265. Chloroplast degradation: one organelle, multiple degradation pathways.

Zhang, L., Happe, T. and Melis, A. (2002) *Planta* 214, 552–561. Biochemical and morphological characterization of sulfur-deprived and H_2-producing *Chlamydomonas reinhardtii* (green alga).

Zhang, Z., Shrager, J., Jain, M., Chang, C.W., Vallon, O. and Grossman, A.R. (2004). *Eukaryot. Cell* 3, 1331–48. Insights into the survival of *Chlamydomonas reinhardtii* during sulfur starvation based on microarray analysis of gene expression.

Zienkiewicz, K., Du, Z.Y., Ma, W., Vollheyde, K. And Benning, C. (2016) *Biochim. Biophys. Acta* 186, 1269-1281. Stress-induced neutral lipid biosynthesis in microalgae: molecular, cellular and physiological insights.

Zouni, A., Witt, H.T., Kern, J., Fromme, P., Krauss, N., Saenger, W. And Orth, P. (2001) *Nature* 409, 739-743. Crystal structure of photosystem II from *Synechoccus elongatus* at 3.8 Å resolution.

Zürrer, H. and Bachofen, R. (1982) *Biomass* 2, 165- 174. Aspects of growth and hydrogen production of the photosynthetic bacterium *Rhodospirillum rubrum* in continuous cultures.

Acknowledgements

First, I want to sincerely thank my supervisor Prof. Dr. Robin Ghosh for giving me the opportunity to become a member of his group. I am thankful for the excellent training he imparted in all aspects of performing and presenting a body of scientific work. His mentorship, encouragement and patience over the last four years have been invaluable for this thesis and for the development of my scientific interests and temper.

I also want to thank our group member, Dr. Caroline Autenrieth for her teaching and her friendly unvaried support and mentorship in the laboratory. Additionally, her help with critical proofreading of several manuscripts as well as this thesis has been tremendous.

I would like to thank Prof. Dr. Ch. Venkata Ramana for his support during my Master's thesis in Hyderabad, India. The independent scientific work I carried out under his mentorship, encouraged me to further pursue a doctoral degree.

I want to thank Prof. Dr. Arnd Heyer for providing the *Chlamydomonas reinhardtii* strain SAG 18.79 and for use of his department facilities. I would like to extend my thanks to Dr. Simon Stutz and other lab members for their kind help.

Many thanks to PD Dr. Mike Schweikert for his help in performing microscopy and for the use of his department facilities.

I would like to thank our lab member Gerasimoula Gerasimidou for the friendly working atmosphere, for the expert technical guidance and for frequently being my German interlocutor.

I acknowledge the BMBF (grant no. 031A171A) and the Vector Mint foundation (grant no. P2015-0059) for generous financial support over the last four years. I also want to thank Prof. Dr. Ingrid Weiss for financial support for a short period of my PhD.

Lastly, I would like to thank my parents for their constant support and for always setting a high bar for academic expectation and achievement. And a big thanks to all my friends here as well as in India, for always keeping me in good humour.